UAB
Universitat Autònoma de Barcelona

Characterization of neurodegeneration and small vessel disease through neuroimaging techniques in Down syndrome

Alejandra O. Morcillo-Nieto

ADVERTIMENT. L'accés als continguts d'aquesta tesi queda condicionat a l'acceptació de les condicions d'ús establertes per la següent llicència Creative Commons: https://creativecommons.org/licenses/?lang=ca

ADVERTENCIA. El acceso a los contenidos de esta tesis queda condicionado a la aceptación de las condiciones de uso establecidas por la siguiente licencia Creative Commons: https://creativecommons.org/licenses/?lang=es

WARNING. The access to the contents of this doctoral thesis it is limited to the acceptance of the use conditions set by the following Creative Commons license: https://creativecommons.org/licenses/?lang=en

Doctoral thesis

Characterization of neurodegeneration and small vessel disease through neuroimaging techniques in Down syndrome

Alejandra O. Morcillo-Nieto

Supervisor:

Dr. Alexandre Bejanin

Tutor:

Dr. Alberto Lleó Bisa

Neurobiology of Dementia Unit
Sant Pau Memory Unit
Institut de Recerca Sant Pau

Doctoral Program in Neuroscience
Institut de Neurociències
Universitat Autònoma de Barcelona
Barcelona, 2026

CERTIFICATE OF DIRECTION

Dr. Alexandre Bejanin, who obtained his PhD in Psychology in the University of Caen-Lower Normandy (France), head of the Brain ImAgeing research group at the Institut de Recerca Sant Pau, Barcelona. Dr. Alberto Lleó Bisa, who obtained his PhD in Medicine in the Universitat of Barcelona, Head of the Neurology Department in Hospital de la Santa Creu i Sant Pau and associate professor in the Universitat Autònoma de Barcelona.

Certify:

That the work "Characterization of neurodegeneration and small vessel disease through neuroimaging techniques in Down syndrome", presenting by Alejandra O. Morcillo Nieto to qualify for Doctor in Neurociènces for the Universitat Autònoma de Barcelona, has been done under our direction and meets all the requirements to be presented and defended in the presence of the corresponding Thesis Committee.

Dr. Alexandre Bejanin, Memory Unit IR Sant Pau

Dr. Alberto Lleó Bisa, Neurology Department Hospital de la Santa Creu i Sant Pau

Signatures,

Dr. Alexandre Bejanin

Alejandra O. Morcillo-Nieto

LIST OF ABBREVIATIONS

AD	Alzheimer's disease
ADAD	Autosomal dominant Alzheimer's disease
aDS	Asymptomatic Down syndrome
APOE	Apolipoprotein E
APP	Amyloid precursor protein
APPdup	Amyloid precursor protein duplication
ARIA	Amyloid-related imaging abnormalities
ASHS	Automatic Segmentation of Hippocampal Subfields
Aβ	Amyloid-β
BACE2	Beta-site APP cleaving enzyme 2
Br35	Brodmann area 35
Br36	Brodmann area 36
CAA	Cerebral amyloid angiopathy
CAMCOG-DS	Cambridge Cognitive Examination for Older Adults with Down Syndrome
CAT12	Computational Anatomy Toolbox 12
CDR	Clinical Dementia Rating
CRASHS	Cortical Reconstruction for Automatic Segmentation of Hippocampal Subfields
CSF	Cerebrospinal fluid
DABNI	Down Alzheimer Barcelona Neuroimaging Initiative
dDS	Down syndrome with Alzheimer's disease dementia
DS	Down syndrome
DSAD	Down syndrome-associated Alzheimer's disease
DTI	Diffusion tensor imaging
DWI	Diffusion weighted imaging
DYRK1A	Dual-specificity tyrosine phosphorylation-regulated kinase 1A
ePVS	Enlarged perivascular spaces
ERC	Entorhinal cortex
EYO	Estimated years to symptom onset
FA	Fractional anisotropy
FDG-PET	Fluorodeoxyglucose-positron emission tomography
FLAIR	Fluid-attenuated inversion recovery
GDS-FAST	Global Deterioration Scale - Functional Assessment Staging
GFAP	Glial fibrillary acidic protein.
GM	Grey matter
ICH	Intracerebral hemorrhage
ID	Intellectual disability
IQR	Image quality rating
LPA	Lesion prediction algorithm
LST	Lesion Segmentation Toolbox
MB	Microbleeds
MCI	Mild cognitive impairment
mCRT	Modified Cued Recall Test
MD	Mean diffusivity
MMSE	Mini-Mental State Examination
MRI	Magnetic resonance imaging
MTL	Medial temporal lobe

NfL	Neurofilament light chain
NFT	Neurofibrillary tangles
pDS	Down syndrome with prodromal Alzheimer's disease
PET	Positron emission tomography
PHC	Parahipocampal cortex
PSEN1	Presenilin-1
PSEN2	Presenilin-2
PSMD	Peak width of skeletonized mean diffusivity
pTau	Phosphorylated tau
sAD	Sporadic Alzheimer's disease
SOD1	Superoxide dismutase 1
SPM12	Statistical Parametric Mapping 12
SUVr	Standardized uptake value ratio
SVD	Small vessel disease
SWI	Susceptibility-weighted imaging
T1w	T1-weighted
TIV	Total intracranial volume
uDS	Down syndrome with an uncertain diagnosis of neurodegenerative disease
WM	White matter
WMH	White matter hyperintensities
YKL-40	Chitinase-3-like protein 1

TABLE OF CONTENTS

LIST OF FIGURES AND TABLES

ABSTRACT

Down syndrome (DS), caused by trisomy of chromosome 21, represents the most common genetically determined form of Alzheimer's disease (AD). The triplication of the *amyloid precursor protein* (*APP*) gene results in lifelong overproduction of amyloid-β (Aβ), leading to near-universal AD neuropathology by the fourth decade of life. In parallel, vascular deposition of Aβ gives rise to cerebral amyloid angiopathy (CAA), which typically emerges by the fifth decade. This biological context provides a unique model to investigate the interplay between neurodegeneration and cerebral small vessel disease (SVD) across the AD continuum.

This doctoral thesis aimed to comprehensively characterize changes in grey matter (GM) and white matter (WM) in adults with DS using a multimodal neuroimaging framework integrated with demographic, genetic, clinical, and fluid biomarker data. First, we examined medial temporal lobe (MTL) atrophy across the AD continuum in DS. We identified a non-linear trajectory characterized by an early phase of cortical thickening followed by progressive atrophy. Notably, the entorhinal cortex and posterior hippocampus were among the earliest affected regions, with detectable structural changes occurring up to 15 years before the estimated onset of clinical symptoms. Second, we investigated the spatial distribution of WM hyperintensities (WMH) in DS. WMH burden increased with age, following a steeper trajectory in DS than in euploid individuals. Lesions initially predominated in periventricular regions and progressively extended into subcortical areas as AD clinical severity advanced. WMH were associated with fluid biomarkers of AD pathology, neurodegeneration, and neuroinflammation, supporting a multifactorial origin of WM injury in DS. Third, to extend these cross-sectional findings, we assessed the evolution of WMH over time. Longitudinal trajectories were variable and non-

monotonic, with a pronounced reduction in lesion burden at the symptomatic stage. This heterogeneous pattern likely reflects distinct processes, including lesion accumulation, progressive tissue degeneration, and inflammatory resolution. Finally, we investigated microstructural WM injury using the peak width of skeletonized mean diffusivity (PSMD). PSMD alterations were detectable up to 15 years before the estimated symptom onset and increased steadily with advancing AD severity. Moreover, PSMD correlated with both neurodegenerative and SVD-related markers, highlighting its sensitivity as an early indicator of WM injury in DS.

Overall, this thesis provides comprehensive evidence that SVD and neurodegeneration in DS are closely interconnected processes that evolve across the AD continuum. Early and progressive changes in both GM and WM constitute a core feature of DS-associated AD, with potential implications for biomarker development and clinical trial design.

RESUMEN

El síndrome de Down (SD), causado por la trisomía del cromosoma 21, representa la forma genéticamente determinada más común de la enfermedad de Alzheimer (EA). La triplicación del gen de la *proteína precursora amiloide* (*APP*) provoca una sobreproducción a lo largo de la vida de β-amiloide (Aβ), lo que da lugar a la aparición de neuropatología de EA de forma prácticamente universal hacia la cuarta década de vida. En paralelo, el depósito vascular de Aβ origina la angiopatía amiloide cerebral (AAC), que suele aparecer hacia la quinta década. Este contexto biológico proporciona un modelo único para investigar la interacción entre la neurodegeneración y la enfermedad cerebrovascular de pequeño vaso (EPV) a lo largo del continuo de la EA.

Esta tesis doctoral tuvo como objetivo caracterizar los cambios en la sustancia gris (SG) y la sustancia blanca (SB) en adultos con SD mediante un enfoque de neuroimagen multimodal integrado con datos demográficos, genéticos, clínicos y de biomarcadores en fluidos. En primer lugar, examinamos la atrofia del lóbulo temporal medial (LTM) a lo largo del continuo de la EA en el SD. Identificamos una trayectoria no lineal caracterizada por una fase temprana de engrosamiento cortical seguida de una atrofia progresiva. Cabe destacar que la corteza entorrinal y el hipocampo posterior fueron las primeras regiones afectadas, con cambios estructurales detectables hasta 15 años antes del inicio estimado de los síntomas clínicos. En segundo lugar, investigamos la distribución espacial de las hiperintensidades de la SB (HSB) en el SD. La carga de HSB aumentó con la edad, siguiendo una trayectoria más pronunciada en el SD que en los individuos euploides. Las lesiones predominaron inicialmente en regiones periventriculares y se extendieron progresivamente hacia áreas subcorticales a medida que avanzaba la gravedad clínica de la EA. Las HSB se asociaron con biomarcadores de patología de la EA, neurodegeneración y neuroinflamación, lo que respalda

un origen multifactorial del daño de la SB en el SD. En tercer lugar, para profundizar en estos hallazgos transversales, evaluamos la evolución de las HSB a lo largo del tiempo. Las trayectorias longitudinales fueron variables y no monotónicas, con una reducción marcada de las HSB en la fase sintomática. Este patrón heterogéneo probablemente refleja distintos procesos, como la acumulación de lesiones, la degeneración tisular progresiva y la resolución inflamatoria. Finalmente, investigamos el daño microestructural de la SB mediante la métrica *peak width of skeletonized mean diffusivity* (PSMD). Las alteraciones de PSMD fueron detectables hasta 15 años antes del inicio estimado de los síntomas y mostraron un aumento gradual con la progresión de la gravedad de la EA. Además, el PSMD se correlacionó tanto con marcadores de neurodegeneración como con marcadores relacionados con la EPV, destacando su sensibilidad como indicador precoz del daño de la SB en el SD.

En conjunto, esta tesis aporta evidencia sólida de que la EPV y la neurodegeneración en el SD son procesos estrechamente interrelacionados que evolucionan a lo largo del continuo de la EA. Los cambios tempranos y progresivos tanto en la SG como en la SB constituyen una característica central de la EA asociada al SD, con posibles implicaciones para el desarrollo de biomarcadores y el diseño de ensayos clínicos.

RESUM

La síndrome de Down (SD), causada per la trisomia del cromosoma 21, representa la forma genèticament determinada més comuna de la malaltia d'Alzheimer (MA). La triplicació del gen de la *proteïna precursora amiloide* (*APP*) provoca una sobreproducció de β-amiloide (Aβ) al llarg de la vida, la qual cosa dona lloc a l'aparició de neuropatologia de MA de forma pràcticament universal cap a la quarta dècada de vida. En paral·lel, el dipòsit vascular d'Aβ origina l'angiopatia amiloide cerebral (AAC), que sol aparèixer cap a la cinquena dècada. Aquest context biològic proporciona un model únic per investigar la interacció entre la neurodegeneració i la malaltia de petit vas (MPV) al llarg del continu de la MA.

Aquesta tesi doctoral va tenir com a objectiu caracteritzar de manera integral els canvis en la substància grisa (SG) i la substància blanca (SB) en adults amb SD mitjançant un enfocament de neuroimatge multimodal integrat amb dades demogràfiques, genètiques, clíniques i de biomarcadors en fluids. En primer lloc, vam examinar l'atròfia del lòbul temporal medial (LTM) al llarg del continu de la MA en la SD. Vam identificar una trajectòria no lineal caracteritzada per una fase primerenca d'engrossiment cortical seguida d'una atròfia progressiva. Cal destacar que el còrtex entorrinal i l'hipocamp posterior van ser les primeres regions afectades, amb canvis estructurals detectables fins a 15 anys abans de l'inici estimat dels símptomes clínics. En segon lloc, vam investigar la distribució espacial de les hiperintensitats de la SB (HSB) en la SD. Les HSB van augmentar amb l'edat, seguint una trajectòria més pronunciada en la SD que en els individus euploides. Les lesions van predominar inicialment en regions periventriculars i es van estendre progressivament cap a àrees subcorticals a mesura que avançava la gravetat clínica de la MA. Les HSB es van associar amb biomarcadors de patologia de la MA, neurodegeneració i neuroinflamació, la qual cosa dona

suport a un origen multifactorial del dany de la SB en la SD. En tercer lloc, per aprofundir en aquestes troballes transversals, vam avaluar l'evolució de les HSB al llarg del temps. Les trajectòries longitudinals van ser variables i no monòtones, amb una reducció marcada de les HSB en la fase simptomàtica. Aquest patró heterogeni probablement reflecteix diferents processos com l'acumulació de lesions, la degeneració tissular progressiva i la resolució inflamatòria. Finalment, vam investigar el dany microestructural de la SB mitjançant la mètrica *peak width of skeletonized mean diffusivity* (PSMD). Les alteracions del PSMD van ser detectables fins a 15 anys abans de l'inici estimat dels símptomes i van mostrar un augment gradual amb la progressió de la gravetat de la MA. A més, el PSMD es va correlacionar tant amb marcadors de neurodegeneració com amb marcadors relacionats amb la MPV, destacant la seva sensibilitat com a indicador precoç del dany de la SB en la SD.

En conjunt, aquesta tesi aporta evidència sòlida que la MPV i la neurodegeneració en la SD són processos estretament interrelacionats que evolucionen al llarg del continu de la MA. Els canvis primerencs i progressius tant en la SG com en la SB constitueixen una característica central de la MA associada a la SD, amb possibles implicacions per al desenvolupament de biomarcadors i el disseny d'assaigs clínics.

PREFACE

Individuals with Down syndrome (DS) represent the most common genetically determined form of Alzheimer's disease (AD). Driven by the triplication of the *amyloid precursor protein* (*APP)* gene on chromosome 21, this population experiences a lifelong overproduction of amyloid-β (Aβ) peptides. This culminates not only in the near-universal development of AD neuropathology by their fourth decade of life, but also in a parallel, severe accumulation of vascular amyloid, manifesting as cerebral amyloid angiopathy (CAA).

Crucially, adults with DS present a striking vascular paradox. They are remarkably protected from traditional cardiovascular risk factors, such as hypertension and arteriolosclerosis, which typically drive small vessel disease (SVD) in the general aging population. Yet a remarkable burden of neuroimaging markers classically associated with SVD. Consequently, DS provides an unparalleled, "pure" AD model for investigating amyloid-driven SVD, largely unconfounded by typical age-related comorbidities.

Despite recent advances in delineating the temporal sequence of AD biomarkers in DS, including the establishment of hippocampal volume as a core neuroimaging metric, the structural trajectories of medial temporal lobe (MTL) subregions beyond the hippocampus across the full AD clinical continuum remain underexplored. Moreover, significant gaps remain in our understanding of cerebrovascular disease in DS. While post-mortem studies have established the high prevalence of CAA, and prior cross-sectional neuroimaging studies have identified an increased burden of SVD markers, such as white matter hyperintensities (WMH), the dynamic evolution of these lesions and their specific associations with fluid biomarkers remain poorly characterized. Finally, there remains a lack of comprehensive, multimodal neuroimaging data tracking both

the macrostructural and microstructural white matter (WM) injury associated with SVD across the AD continuum in DS.

Therefore, this thesis addresses these fundamental gaps by rigorously characterizing the spatial patterns and temporal trajectories of neurodegeneration and SVD-related brain lesions in adults with DS. By integrating structural MRI, diffusion-weighted imaging, and multimodal fluid biomarkers, this work aims to advance our understanding of how MTL atrophy, WM microstructural injury, and cerebrovascular pathology interact across the lifespan and the AD continuum in DS. Ultimately, this research seeks to inform disease modeling, refine *in vivo* imaging biomarkers, and guide future therapeutic strategies for this genetically determined form of AD.

This PhD research has yielded four first-authored papers peer-reviewed publications, all published in first decile journals (*Alzheimer's and Dementia* [Impact Factor, IF, 2024=11.1, Rank=6/202 in Clinical Neurology, D1] and *Brain* [IF 2024=11.7, Rank=5/202 in *Clinical Neurology*, D1]*)*.

1. INTRODUCTION

1.1 DOWN SYNDROME

Down syndrome (DS) is a genetic condition caused by the trisomy of chromosome 21. The DS phenotype encompasses manifestations in the musculoskeletal, neurological, and cardiovascular systems.[1]

Clinically, the syndrome is characterized by a well-defined physical phenotype including a flattened facial profile, almond-shaped eyes with epicanthal folds, a small nose with a flat nasal bridge, low-set ears, and macroglossia within a relatively small mouth. Musculoskeletal and structural alterations are equally prominent, manifesting as generalized hypotonia, atlantoaxial instability, brachycephaly, short stature, a shortened neck with redundant nuchal skin, clinodactyly of the fifth digit, a single transverse palmar crease, and a sandal gap deformity.[2,3] Neurologically, individuals with DS present a divergent developmental blueprint expressed through varying degrees of intellectual disability (ID), cerebellar hypoplasia, and a widespread reduction in neuronal density.[1]

Beyond these structural and developmental manifestations, people with DS exhibit an increased susceptibility to a wide range of lifelong comorbid medical conditions. These include congenital heart defects, hypothyroidism, autoimmune disorders, obstructive sleep apnea, and epilepsy.[1,4] Crucially, as medical care has advanced over the last decades, DS is no longer viewed solely as a developmental disorder but rather as a complex lifespan condition with prominent neurological involvement culminating in highly penetrant, early-onset Alzheimer's disease (AD).[1]

1.1.1 Epidemiology

DS is the most common genetic cause of ID, affecting approximately 1 in 700 live births worldwide.[5] Advanced maternal age at conception remains the principal known risk factor for trisomy 21.[6]

Over the last few decades, the epidemiology of DS in Europe has been shaped by two opposing phenomena. Based on EUROCAT registry data, an increasing proportion of mothers aged 35 and older has driven a rise in the estimated incidence of DS conceptions, increasing from 16 to 23 per 10,000 births by 2015.[7] Conversely, the widespread implementation of prenatal genetic screening programs has led to a parallel increase in the rates of elective termination of pregnancy for fetal anomalies. Consequently, while the absolute number of DS conceptions has risen across Europe, the overall prevalence of live births has remained relatively stable or decreased.[7,8]

This dynamic is particularly pronounced in Spain, where universal access to prenatal screening has resulted in termination rates of approximately 84% to 90% following a prenatal diagnosis of DS.[8] Accordingly, the incidence of DS live births has declined drastically over the past 50 years. From an incidence of 15 per 10,000 births between 1976 and 1980, the rate dropped to 5.51 between 2011 and 2012, and reached a low of 4.01 per 10,000 births by 2023 (Figure 1A, B). As a result, the absolute population size of individuals with DS in Spain has reached its historical maximum in 2015, and since then, natural demographic growth has become consistently negative.[9]

Despite declining birth rates, advances in medical, educational, and social care over the past five decades have resulted in a dramatic increase in life expectancy among individuals with DS, with current estimates approaching 60 years of age and a global population exceeding six million individuals.[1] In Spain, the

demographic profile strongly reflects this aging trend: of the approximately 35,000 individuals currently living with DS, 83.5% are over 16 years old, and more than half (51.3%) fall within the 35–49 age range;[9] a distribution perfectly reflected in our Down Alzheimer Barcelona Neuroimaging Initiative (DABNI) cohort, exhibiting a high prevalence of individuals aged 30 to 60 (Figure 1C). As a consequence, there is a need to address emerging age-related conditions in people with DS, with AD being the major clinical challenge.

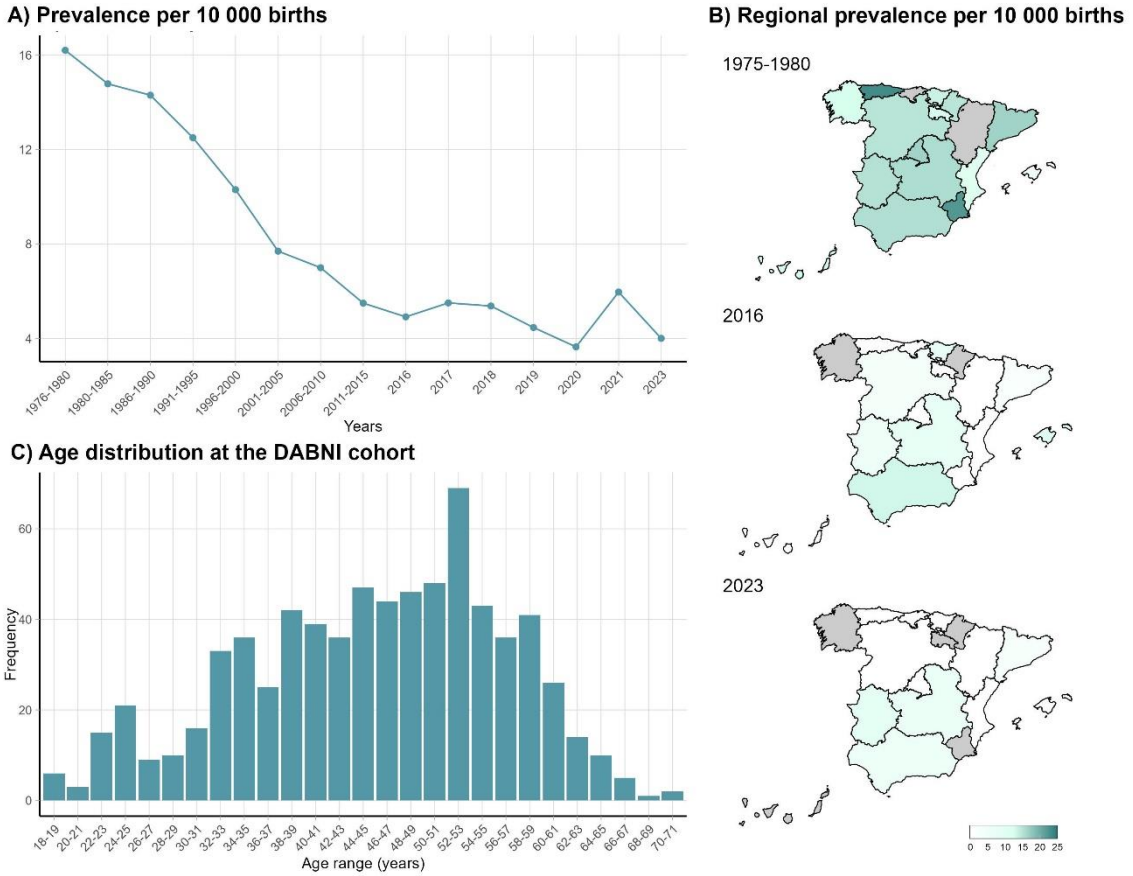

Figure 1. ***Demographic trends of DS in Spain and the DABNI study cohort.*** *A) National and B) regional prevalence of DS live births per 10,000 births in Spain from 1976 to 2023. Data are sourced from the Base de Datos Estatal de Personas con Discapacidad (BDEP, 2012), the Encuesta de Discapacidad, Autonomía Personal y Situaciones de Dependencia (EDAD, 2008), and the bulletins of the Estudio Colaborativo Español de Malformaciones Congénitas (ECEMC). C) Age distribution of the Down Alzheimer Barcelona Neuroimaging Initiative (DABNI) cohort as of 2024. The distribution highlights a pronounced representation of individuals with DS aged between 30 to 60 years, effectively illustrating the current aging demographic profile of this population.*

1.1.2 Genetics

Genetically, DS is caused by the presence of an additional copy of chromosome 21. Complete trisomy 21 accounts for approximately 95% cases, whereas translocations (4%), in which a portion of an extra chromosome 21 attaches to another chromosome, and mosaicism (1%), where only a subset of cells carry three copies of chromosome, occur less frequently.[10]

The biological perturbations driving the complex DS phenotype have traditionally been conceptualized through two primary, non-exclusive frameworks. The *gene-dosage effect hypothesis* attributes the phenotype to the direct, proportional overexpression of specific chromosome 21 genes and the subsequent dysregulation of their downstream signalling networks. The *developmental instability hypothesis* posits that the extra genetic material induces a global disturbance in gene expression beyond chromosome 21, thereby disrupting overall biological homeostasis.[1] Furthermore, this genetic imbalance is accompanied by a distinct epigenetic signature, characterized by specific DNA methylation patterns that correlate with both developmental defects and a premature aging phenotype.[11]

Chromosome 21 contains numerous genes encoding proteins with highly diverse biological functions, regulating pathways involved in neurodevelopment, neurogenesis, synaptic function, neuroinflammation, immune response, and oxidative stress.[12,13] The triplication of this chromosome in DS therefore results in systematic overdosage of these gene products, disrupting multiple biological cascades and profoundly impacting brain development, metabolic homeostasis, and the functional organization of neuronal networks.[1] Of particular relevance to this thesis, several of these overexpressed genes, such as a*myloid precursor protein* (*APP*) and *dual-specificity tyrosine phosphorylation-regulated kinase 1A*

(*DYRK1A*), have been directly implicated in the early onset of AD in this population.[1]

1.1.3 Neuroanatomy

Individuals with DS exhibit distinctive neuroanatomical features that persist across the lifespan. Disruptions in neurogenesis, synaptogenesis, and myelination are evident as early as 21 weeks of gestation,[14] leading to a reduction in total cell number and lower neuronal density.[15]

Macroscopically, DS is characterized by an overall reduction in total brain volume, accompanied by brachycephaly and ventriculomegaly.[16–18] However, this reduced brain size is not driven by a uniform global shrinkage, but rather by a specific topographic pattern of regional vulnerabilities. Volume reductions are most prominent in the frontal and temporal lobes, the brainstem, and the cerebellum[16,17,19,20] (Figure 2 C, D). The profound cerebellar hypoplasia, in particular, is a consistent hallmark across the literature in DS[16,21,22] (Figure 2 C, D). Conversely, other brain structures appear relatively preserved, including parietal and occipital lobes.[19,20,22,23]

Among the most vulnerable structures, the hippocampus is significantly smaller from an early age.[18,24,25] Microstructural and pathological studies attribute this to reduced cell proliferation and decreased volume in specific subfields, notably the dentate gyrus.[15,26] In contrast to this marked reduction in hippocampal volume, individuals with DS have shown an increased volume of the adjacent parahippocampal gyrus.[18,25,27] Furthermore, morphological variants are highly prevalent; individuals with DS characteristically exhibit a higher rate of incomplete hippocampal inversion[28] (Figure 2 E F).

In addition to grey matter (GM) alterations, the white matter (WM) in DS is fundamentally altered. Neurodevelopment is characterized by myelination

deficits, including reduced and delayed myelin formation.[29] Consistent with these early disruptions, neuroimaging techniques reveal structural differences in WM integrity across the lifespan, particularly within the frontal tracts.[30]

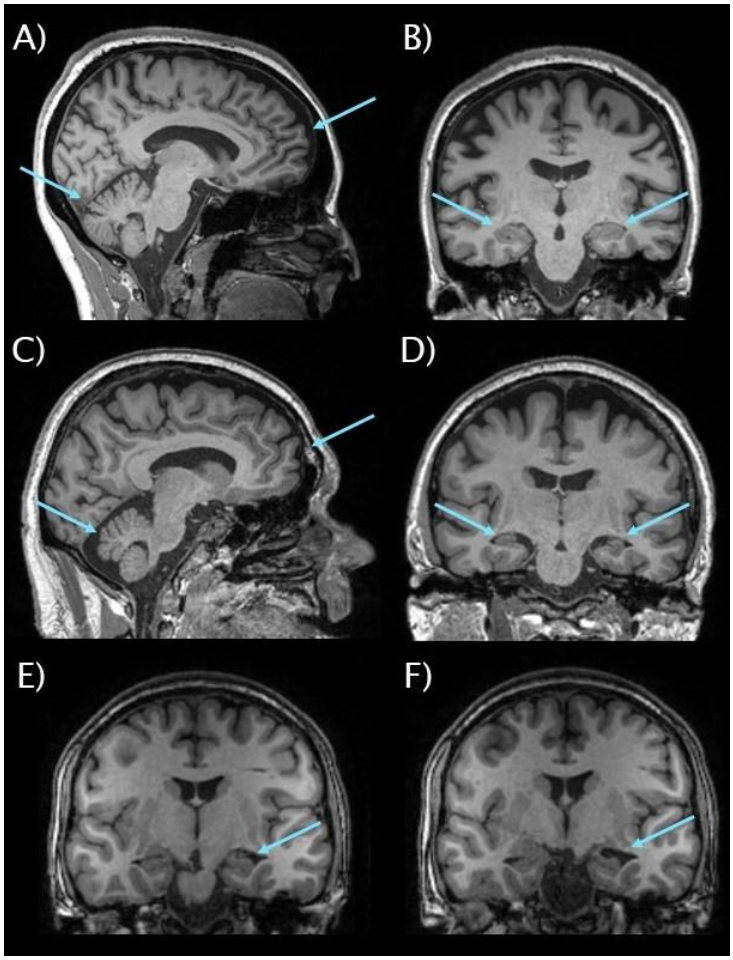

Figure 2. ***Structural brain changes in DS.*** *Representative T1-weighted MRI sagittal (A, C) and coronal (B, D-F) sections. A, B) a 44-year-old euploid control and C, D) a 45-year-old individual with DS without dementia. Arrowheads highlight differences in the frontal cortex, cerebellum, and hippocampus. E, F) a 36-year-old individual with DS without dementia, Arrowheads highlight the presence of a left incomplete hippocampal inversion.*

1.2 ALZHEIMER'S DISEASE

1.2.1 Definition and general concepts

AD is the leading cause of dementia globally, accounting for an estimated 60% to 80% of all dementia cases.[31] The global prevalence of dementia represents a major health challenge, with projections indicating that by the year 2050, approximately 130 million people worldwide will be affected.[32] In Spain, it is estimated that over 800,000 individuals, representing 3–4% of the population over 75 years of age, currently suffer from AD, which is projected to double and surpass 1.5 million cases by 2050.[33] Driven by the profound social and economic burden of the disease and the limited efficacy of current treatments, AD research has become an urgent global priority, shifting scientific and clinical focus heavily toward prevention and early intervention.

Clinically, AD is a neurodegenerative disorder characterized by a progressive deterioration of cognitive functions, including memory, language, executive functioning, and visuospatial skills, culminating in a profound loss of autonomy and functional independence.[34] The disease is now robustly conceptualized as a biological continuum that begins with a prolonged preclinical phase, defined by silent pathophysiological alterations in the brain up to 20 years before the manifestation of any clinical symptoms.[35] It then progresses gradually through mild cognitive impairment (MCI) before advancing to clinical dementia.[36,37]

1.2.2 Neuropathology

Neuropathologically, AD is the only neurodegenerative disease defined by two proteinopathies.[38] These main hallmarks are the presence of extracellular amyloid-β (Aβ) plaques, mainly composed of Aβ1–42 (Aβ42) peptides, and the intracellular accumulation of hyperphosphorylated tau proteins forming

neurofibrillary tangles (NFT)[38] (Figure 3). Amyloid plaque deposition follows a specific spatial trajectory, commencing in neocortical regions, particularly the temporal lobe (Thal phase 1), before spreading to allocortical (phase 2), subcortical (phase 3), brainstem (phase 4), and cerebellar regions (phase 5).[39] In contrast, tau pathology initially affects the entorhinal cortex (ERC) and transentorhinal regions (stages I–II), subsequently spreading to limbic and neocortical regions (stages III–VI).[40]

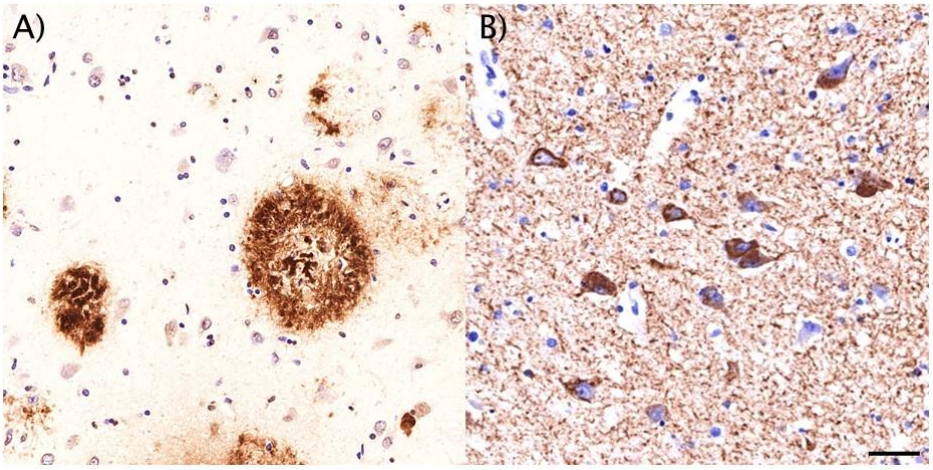

Figure 3. ***Histopathological hallmarks of AD.*** *Representative immunohistochemical staining in the temporal cortex of a 61-year-old male demonstrating A) Aβ plaques and B) NFT. Courtesy of Borja Moya-Llamas.*

The exact relationship between Aβ plaques and tau NFT is still poorly understood. According to the amyloid cascade hypothesis, the abnormal aggregation of Aβ peptides represents the initial event in AD pathophysiology,[41] subsequently triggering tau hyperphosphorylation, synaptic dysfunction, neurodegeneration, and cognitive decline. While Aβ accumulation is considered an early and necessary process, converging evidence indicates that tau pathology correlates more closely with neuronal loss, brain atrophy, and clinical symptom severity.[42–44] Beyond these core proteinopathies, the complexity of AD is reflected by a spectrum of concomitant, non-specific pathological events that

are critical to disease pathogenesis, including synaptic dysfunction, gliosis, neuroinflammation, and vascular dysregulation.[34,45]

1.2.3 Forms of Alzheimer's disease

AD can be broadly categorized into sporadic and genetic forms. Sporadic AD (sAD) accounts for over 95% of cases, with clinical symptoms typically detected after the seventh decade of life.[46] It is considered a multifactorial disorder driven by a complex interplay of genetic, environmental, and lifestyle factors.[46] Advanced age remains the strongest primary risk factor for sAD, with incidence rates doubling approximately every five years after the age of 65.[31] Alongside aging, genetic susceptibility plays a role, with the *Apolipoprotein E* (*APOE*) ϵ4 allele being the greatest genetic risk factor.[46,47] Heterozygous carriers exhibit a markedly increased risk for developing AD, while homozygous carriers (ϵ4/ϵ4) face a 14-fold increased risk compared to ϵ3/ϵ3 carriers, with evidence now suggesting that *APOE4* homozygotes should be considered as a genetic form of AD.[48]

In contrast to sAD, autosomal dominant AD (ADAD) accounts for less than 1% of all AD cases and is driven by *APP* missense mutations, *APP* duplication (*APP*dup), or mutations, *presenilin-1* (*PSEN1*), and *presenilin-2* (*PSEN2*) genes.[49,50] These mutations drive rapid amyloid accumulation, resulting in an early-onset presentation typically developing before the age of 65.[31] Investigating these genetic, early-onset forms provides a unique window into the pure pathophysiological cascade of AD.

1.2.4 Alzheimer's disease in Down syndrome

1.2.4.1 Genetic Basis and *APP* Triplication

As previously mentioned, individuals with DS have an extra copy of chromosome 21, which encodes the *APP* gene. This triplication triggers a lifelong overproduction of Aβ peptides that begins during adolescence, and by their 40s, nearly all individuals with DS exhibit the core neuropathological hallmarks of AD.[51] The central role of the *APP* gene in the AD pathogenesis is robustly supported by rare autopsy cases of individuals with partial trisomy 21; when *APP* was not triplicated, AD neuropathology was absent even at the relatively advanced ages of 72 or 78 years for people with DS.[52,53] Thus, the triplication of *APP* has been proposed to be both sufficient and necessary to drive AD pathogenesis, establishing DS-associated AD (DSAD) as the most common genetically determined form of the disease.[51] Reflecting this biological certainty, the latest revised diagnostic criteria from both the International Working Group and the Alzheimer's Association classify asymptomatic individuals with DS as being in a presymptomatic stage, or Stage 0, denoting the presence of a genetic determinant of AD prior to the onset of clinical symptoms.[54,55]

While *APP* triplication is the central driver, other genes on chromosome 21 also contribute to the underlying pathogenesis and modulate the age of AD onset.[1] Among these, *DYRK1A* is particularly significant: already strongly linked to ID, it contributes significantly to AD pathogenesis.[13,56–58] by hyperphosphorylating tau protein at key residues, thereby priming it for aggregation into NFT.[13] Other notable genetic modifiers include the *Beta-site APP cleaving enzyme 2* (*BACE2*), which further influences *APP* processing and the amyloidogenic cascade,[59] and *superoxide dismutase 1* (*SOD1*), whose overexpression drives mitochondrial dysfunction and oxidative stress linked to premature aging in DS.[60]

Finally, alongside chromosome 21–specific mechanisms, genome-wide risk factors, may also modulate disease onset, progression, and clinical presentation of AD in the DS population.[56,61] Notably, the major genetic risk factor for sAD, the *APOE* gene, has been associated with an earlier age of symptom onset in adults with DS.[16,51,59] The presence of the *APOE* ϵ4 allele in DS was further shown to accelerate amyloid deposition and advance the onset of symptomatic disease by approximately two years,[62] even though this result has not been replicated across all cohorts.[63,64]

1.2.4.2 Clinical presentation and trajectory

Clinically, the trajectory of DSAD is strikingly age-dependent. Dementia is rare in individuals with DS before the age of 40; however, its incidence and prevalence rise exponentially thereafter, reaching 88–100% in those older than 65 years.[65] On average, the median age of prodromal AD diagnosis in DS is approximately 51 years, typically progressing to AD dementia between 53 and 55 years, with death occurring between 57 and 60 years of age.[51,66,67] When symptoms emerge after age 40, the clinical presentation closely mimics sAD, initially characterized by deficits in episodic memory and receptive language.[59,68] Conversely, when dementia emerges in younger individuals (aged 30–40 years), it frequently presents with changes in behaviour, personality, and executive function.[59,68] Some atypical presentations, including cases with posterior cortical atrophy, have also been described.[69,70] These cases are characterized by early deficits in the visual domain with significant occipital involvement, underscoring the clinicopathological heterogeneity that can occur even within this genetically determined form of AD.

1.2.4.3 Neuropathology

Post-mortem studies demonstrate that the hallmark neuropathological features of AD are nearly universal in the brains of adults with DS by the age of 40 years, although pathological changes begin decades earlier.[16,71] Specifically, the neuropathology of AD, alongside associated gross neuroanatomical change, is present in 80% of individuals with DS by the fourth decade, reaching 100% in those over 60 years of age.[72]

The overexpression of the *APP* gene results in intraneuronal Aβ accumulation detectable as early as 21 weeks of gestation, primarily within endosomal-lysosomal compartments implicated in *APP* processing.[16,73,74] During childhood and adolescence, Aβ pathology begins to accumulate in the brain,[75–77] yielding substantial amounts of diffuse extracellular Aβ plaques by 20 years of age.[71] By the third and fourth decades of life, Aβ accumulation accelerates exponentially, indicating a phase of accelerated deposition at this age,[78,79] as diffuse deposits transition into compact neuritic plaques.[51]

The spatial distribution of Aβ in DS broadly recapitulates the Thal phases established in sAD.[39] Deposition initiates in the temporal neocortex before rapidly involving other neocortical regions.[39] Subsequently, it extends into allocortical areas, including the entorhinal region, the CA1 sector of the hippocampus, and the insular cortex. It is not until individuals reach their 40s that the amyloid burden extends to subcortical regions, the brainstem, and the cerebellum.[71]

Following the initial amyloid cascade, tau pathology emerges chronologically later, typically becoming evident around 35 years of age.[51] The spatial spreading of NFTs in DS adheres closely to the Braak staging system.[40] Initial tau accumulation is observed in the ERC and transentorhinal cortex, as well as the

hippocampal molecular layer, before spreading to the CA1 region and subiculum.[80,81] Subsequently, tau pathology extends to limbic and neocortical regions, achieving full neocortical coverage by the mid-50s.[71] Crucially, it is this progressive accumulation and topographical spread of tau that most strongly correlates with the onset of clinical dementia and overall disease severity in DSAD.[82]

1.2.4.4 Fluid Biomarkers

Over the past two decades, the conceptualization of AD has undergone a profound paradigm shift, evolving from a clinicopathological entity defined at autopsy to a biological continuum that can be precisely tracked *in vivo*.[36,37] This transformation has been driven by the validation of fluid and neuroimaging biomarkers, which allow researchers and clinicians to detect the underlying pathophysiological cascade decades before the onset of cognitive decline. In DS, the temporal sequence and progression of biomarker patterns are highly similar to those observed in both sAD and ADAD[83] (Figure 4).

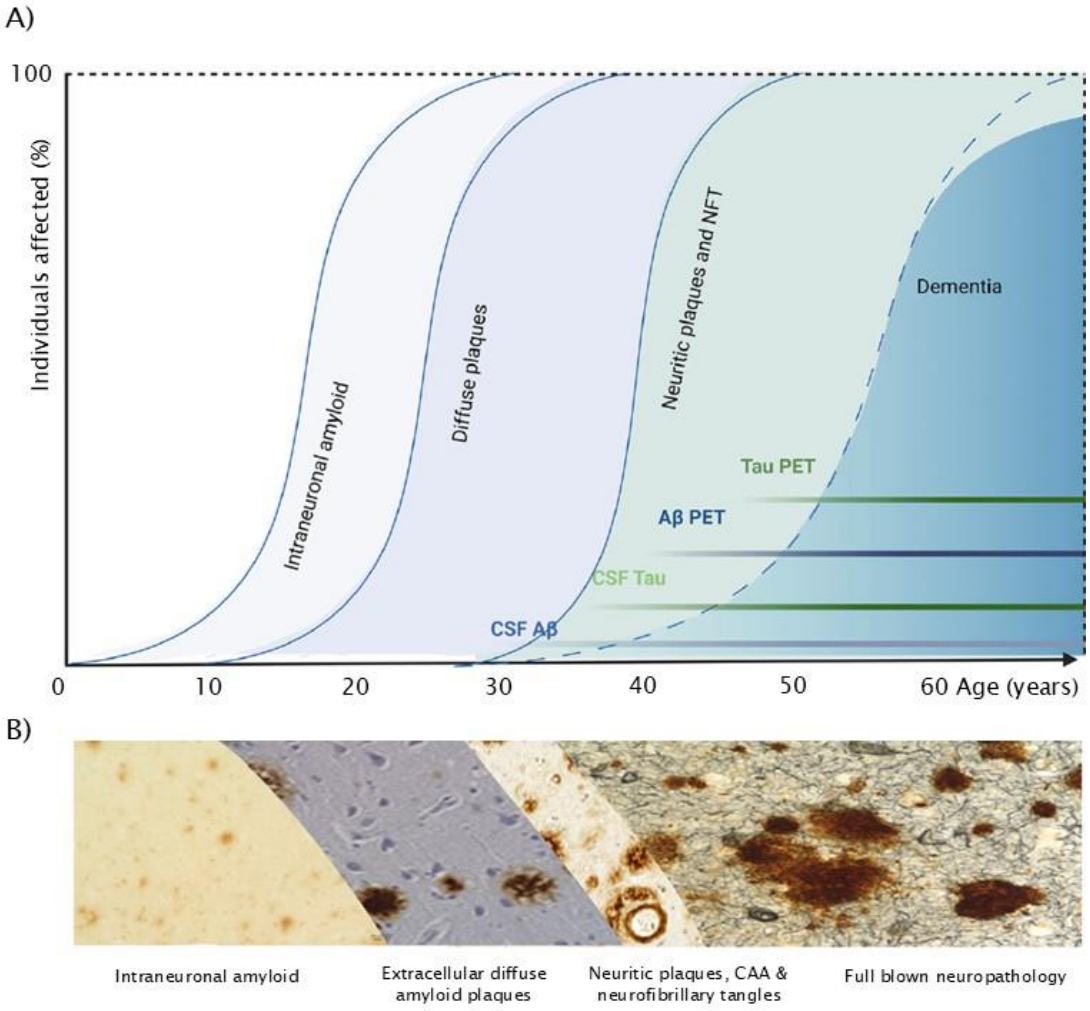

Figure 4. ***Natural history of DSAD.*** *A) Chronological trajectory of pathophysiological changes across the lifespan and their detection via fluid and neuroimaging biomarkers, and B) Histopathological samples reflecting the neuropathological hallmarks corresponding to the different stages of disease progression. Adapted from Maure-Blesa et al. (2025).*

- ## Cerebrospinal fluid biomarkers

Cerebrospinal fluid (CSF) studies consistently demonstrate the core AD biomarker profile in symptomatic individuals with DS, including a marked reduction in the Aβ42/Aβ40 ratio and significant elevations in total tau and phosphorylated tau (pTau) concentrations.[84–87] Specifically, both CSF Aβ42 and Aβ40 are elevated in early childhood due to the *APP* gene dose effect. These levels subsequently decrease, entering a period of pseudo-normalization until the late 20s.[51] Approximately two decades before the onset of dementia, absolute Aβ42 levels drop below normative thresholds, ultimately reaching floor

effects during the prodromal stages of the disease.[51] The CSF Aβ42/Aβ40 ratio provides a robust index of amyloid,[86] demonstrating a significant decrease approximately 26 years prior to clinical diagnosis.[83,88]

Following the alterations of amyloid markers, CSF pTau181 concentrations begin to rise approximately 15 years before dementia onset, tightly coinciding with the initial increases in amyloid PET standardized uptake value ratios (SUVr).[83,85] While pTau181 is well-characterized, there is currently a notable lack of studies specifically examining the temporal dynamics of other phosphorylated tau isoforms in CSF in the DS population.[87]

Beyond amyloid and tau, markers reflecting axonal damage, synaptic dysfunction, and neuroinflammation are highly relevant, given their early presence across the AD continuum. Neurofilament light chain (NfL), a marker of axonal injury, increases early in the preclinical stage, even preceding amyloid PET positivity, and shows strong diagnostic and prognostic value in DSAD.[83,85]. Furthermore, neuroinflammatory markers, specifically the astroglial activation markers glial fibrillary acidic protein (GFAP) and YKL-40 (also known as chitinase-3-like protein 1), have shown age-dependent and disease-severity associations.[86,89–91]

- ### Blood-based biomarkers

Unlike CSF, plasma concentrations of Aβ42 and Aβ40 are consistently elevated throughout the lifespan in AD due to peripheral Aβ production. Because of this confounding peripheral amyloid pool, current immunoassays for plasma Aβ lack the diagnostic utility to reliably detect symptomatic AD.[85,87]

In contrast, plasma tau isoforms have emerged as exceptionally powerful diagnostic and prognostic tools. Plasma pTau species (including pTau181, and pTau217) begin to increase in the mid-30s in DS. Specifically, pTau217 starts to

rise between 36 and 40 years of age,[63,92] while pTau181 diverges from euploid trajectories age 40.[93] Both markers accurately discriminate symptomatic from asymptomatic individuals and correlate robustly with core CSF biomarkers, neurodegeneration, and cognitive decline.[83,87,93,94]

Similar to its CSF counterpart, plasma NfL rises non-linearly from early adulthood and accelerates profoundly as the disease advances, serving as an excellent prognostic marker for clinical conversion.[83,95] Finally, plasma GFAP elevations begin in the mid-to-late 20s and rise continuously into symptomatic stages, discriminating clinical status more effectively than CSF GFAP.[90]

1.2.4.5 Neuroimaging

Neuroimaging modalities, encompassing positron emission tomography (PET) and magnetic resonance imaging (MRI), have revolutionized the study of AD by enabling the *in vivo* visualization of its underlying pathophysiological substrates. In sAD, hallmark neuroimaging biomarkers capture a sequence of medial temporal lobe (MTL) atrophy and posterior-predominant cortical thinning on MRI, alongside temporoparietal hypometabolism on fluorodeoxyglucose-PET (^{18}F-FDG-PET), and cortical Aβ deposition on amyloid-PET.[34] Similarly, in the DS population, these modalities delineate the onset of neuroimaging alterations decades before clinical dementia (Figure 5).

- **Positron Emission Tomography**

In DS, amyloid PET signal increases decades before symptom onset, typically emerging in the late 30s.[63,88,96] This early accumulation involves prominent deposition in the striatum and precuneus,[97] extending to frontal lobe areas before reaching medial temporal and subcortical structures.[63,64,97,98] Notably, striatal amyloid signal precedes cortical amyloid deposition by approximately

three years,[99,100] with widespread cortical positivity typically reached by the mid-40s.[101]

Following the amyloid deposition, tau PET signal in DS notably escalates between ages 37 and 41.[88] Tau PET positivity occurs almost exclusively in amyloid-positive individuals, often within two years of conversion to amyloid positivity.[102] The spatial progression of tau PET broadly follows Braak staging,[103,104] beginning in the MTL, notably in the ERC and hippocampus, before spreading posteriorly and dorsally into the parietal cortices.[105] In DS, however, early signal is also seen in subcortical structures such as the amygdala and pallidum, before spreading to the neocortical regions.[88]

Concurrently, ^{18}F-FDG-PET captures the metabolic dysfunction emerging characteristically in the parietal cortex, precuneus, and posterior cingulate,[106-108] mirroring the metabolic signature of sAD.[109] Interestingly, early regional hypermetabolism has been reported in young, asymptomatic individuals with DS, which may reflect transient compensatory mechanisms or fundamentally altered baseline glucose utilization linked to neurodevelopmental differences.[106,108,110]

- Magnetic Resonance Imaging

With the emergence of AD pathology, structural MRI reveals a classic AD-like pattern of atrophy characterized by profound MTL loss and posterior-predominant cortical thinning.[17,111] The hippocampus and ERC, regions highly susceptible to early tau pathology,[81] exhibit measurable volume loss 5 to 10 years prior to symptom onset.[83] Compared to non-demented individuals with DS, those with symptomatic DSAD show severe reductions in the MTL,[112] notably in the volume of the hippocampus and amygdala.[27,113-116] This volume loss extends to striatal structures, including the putamen and caudate,[114] and is

coupled with significant enlargement of ventricular CSF spaces, a cardinal feature of global brain shrinkage.[117]

Beyond these GM alterations, diffusion tensor imaging (DTI) unveils early vulnerabilities in the WM architecture of individuals with DS, including reduced fractional anisotropy (FA) and increased mean diffusivity (MD) compared to the euploid population.[118–122] As Aβ burden increases and AD progresses, these microstructural alterations become profoundly exacerbated, reflecting the widespread degradation of the neural tracts.[30,123,124]

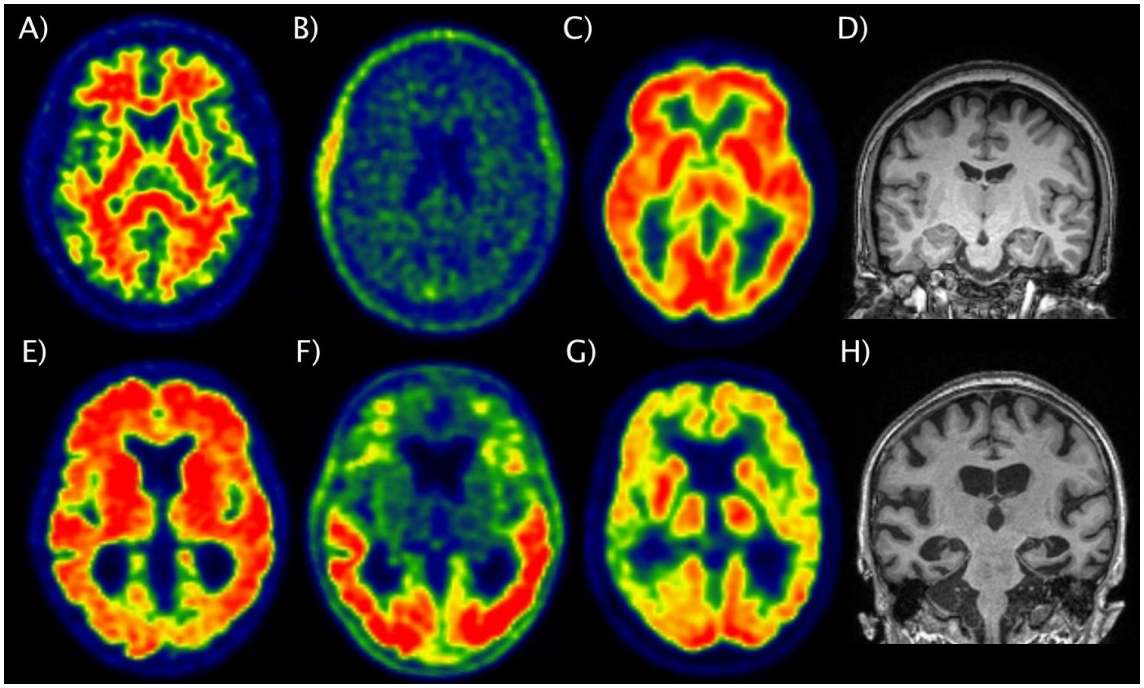

Figure 5. ***Multimodal neuroimaging hallmarks of DSAD.*** *Representative images encompassing amyloid-PET (A, E), tau-PET (B, F), ^{18}F-FDG-PET (C, G), and structural MRI (D, H). A-D) depicts a 46-year-old cognitively stable individual with DS, demonstrating negative amyloid and tau burden, and preserved cerebral glucose metabolism and structural integrity. E-H) presents a 66-year-old individual with DS and AD dementia, characterized by widespread amyloid and tau positivity (with prominent parieto-temporal tau accumulation), reduced glucose uptake indicative of hypometabolism, and pronounced cortical and MTL atrophy.*

1.3 CEREBROVASCULAR DISEASE

1.3.1 Definition and general concepts

Cerebrovascular disease encompasses a heterogeneous spectrum of pathological processes affecting the cerebral blood vessels[125] and is widely recognized as the most common cause of dementia after AD.[126] Vascular disease is strongly associated with systemic risk factors such as hypertension, atherosclerosis, hypercholesterolemia, and diabetes mellitus,[125] and its most prevalent manifestation in the context of cognitive impairment is cerebral small vessel disease (SVD).[127] SVD is an umbrella term describing pathological alterations in the brain's smallest vessels, including perforating arterioles, capillaries, and venules.[127,128] Evidence consistently demonstrates that SVD is a critical comorbidity that lowers the threshold for the clinical expression of dementia.[129,130] Furthermore, the presence of SVD accelerates the age of clinical onset[131] and drives a more rapid cognitive decline for any given burden of underlying AD pathology.[130]

1.3.2 Subtypes of small vessel disease

Pathologically, SVD is broadly categorized into distinct subtypes that, despite their divergent etiologies, converge into a shared spectrum of macroscopic brain damage. Among these, arteriolosclerosis (Type 1 SVD) and cerebral amyloid angiopathy (CAA; Type 2 SVD) are the most prevalent forms.[128] Arteriolosclerosis is predominantly driven by aging and traditional vascular risk factors, particularly hypertension and diabetes.[132] Morphologically, it is characterized by thickened, dysmorphic vessel walls and increased arteriolar tortuosity, without the formation of atheroma[132] (Figure 6 A, B). CAA is defined by the progressive deposition of Aβ peptides, predominantly in its Aβ40 isoform, within the walls of cortical and leptomeningeal arterioles, and occasionally capillaries[133,134]

(Figure 6 C, D). Advanced age and the presence of AD pathology are established risk factors for CAA.[135]

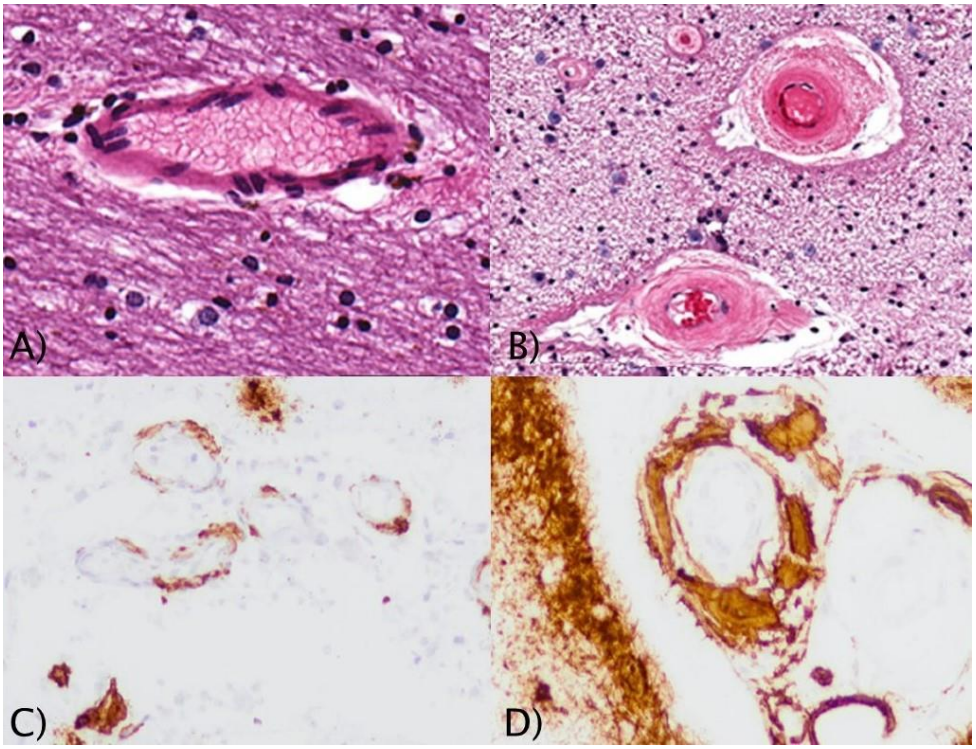

Figure 6. ***Histopathological features of SVD.*** *Representative immunohistochemical staining of leptomeningeal arterioles demonstrating arteriolosclerosis (A, B) and CAA (C, D). A, C) exhibit minimal structural changes, whereas B, D) demonstrate severe pathological involvement. Adapted from Blevins et al. (2021) and Carmona-Iragui et al. (2019).*

1.3.3 Neuroimaging markers of small vessel disease

Although direct *in vivo* visualization of cerebral small vessels remains elusive,[128] MRI biomarkers of brain structural and vascular functional impairments allow us to reliably identify the parenchymal sequelae of SVD. To harmonize research and clinical assessment, the International Standards for Reporting Vascular Changes on Neuroimaging (STRIVE-1)[136] and its recent update, STRIVE-2,[137] were established to standardize the definitions of SVD features on neuroimaging and encourage the consistent, unbiased use of terminology. Guided by these frameworks, the main imaging hallmarks of SVD are defined as follows (Figure 7):

- White matter hyperintensities (WMH): Signal abnormalities appearing as hyperintense lesions on T2-weighted fluid-attenuated inversion recovery (FLAIR) sequences, typically presenting symmetrically across the cerebral hemispheres.
- Microbleeds (MB): Small areas of signal void with associated blooming artifacts on T2*-weighted or susceptibility-weighted imaging (SWI), reflecting focal hemosiderin deposition from prior microhemorrhages or vascular leakage.
- Cortical Superficial Siderosis: Thin areas of hypointensity on T2*-weighted or SWI sequences located within or overlying the superficial cortex, indicative of hemosiderin deposition in the subarachnoid space or superficial cortical layers.
- Enlarged Perivascular Spaces (ePVS): Small, fluid-filled spaces following the typical course of perforating vessels, appearing isointense to CSF on both T1-weighted (T1w), and T2-weighted MRI.
- Lacunes: Round or ovoid subcortical fluid-filled cavities that mark the territory of prior deep infarcts, identifiable across FLAIR, T1w, and T2-weighted.
- Recent subcortical infarct: A recent infarction in the territory of a single perforating arteriole, typically occurring within the previous few weeks (up to ~3 weeks), detected on T1w, FLAIR, and presenting as hyperintense lesions on diffusion weighted imaging (DWI).
- Cortical microinfarct: Small ischemic lesions appearing hypointense on T1w and hyperintense on T2-weighted, FLAIR, or DWI.
- Brain atrophy: Global or regional brain volume loss that is not attributable to a specific macroscopic focal injury, such as trauma or a territorial infarction.

- DTI-derived metrics: Using DWI, DTI models the magnitude and spatial anisotropy of water diffusion to assess microstructural integrity. Indices such as free water fraction and peak width of skeletonized mean diffusivity (PSMD)[138] have recently been validated as highly sensitive markers that often outperform conventional SVD metrics.[139]

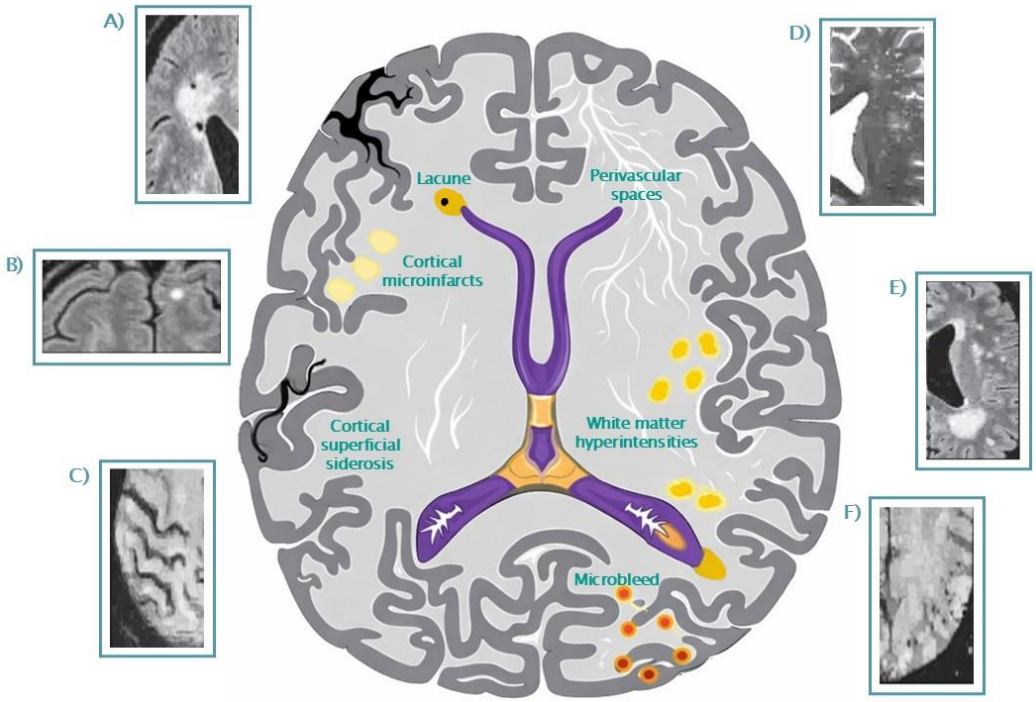

Figure 7. ***Neuroimaging spectrum of SVD.*** *Representative MRI findings demonstrating the macroscopic sequelae of SVD: A) Lacunes on FLAIR; B) Cortical microinfarcts on T1w, C) Cortical superficial siderosis on SWI, (D) ePVS on T2-weighted, E) WMH on FLAIR, and (F) Cerebral MB on SWI. Modified from Carmona-Iragui et al. (2019) and Duering et al. (2023).*

1.3.4 Relationship between small vessel disease and Alzheimer's disease

Epidemiological evidence robustly demonstrates that AD and SVD share a wide range of vascular and lifestyle risk factors.[140,141] These include advancing age, midlife hypertension, diabetes mellitus, smoking, hypercholesterolemia, obesity, hyperhomocysteinemia, sleep apnea, and psychiatric symptoms such as anxiety and depression. Moreover, both conditions are characterized by overlapping pathophysiological mechanisms, including mitochondrial

disruption, oxidative stress, chronic neuroinflammation, and metabolic dysfunction.[140,141]

Post-mortem and epidemiological studies reveal the distinct prevalence of specific SVD subtypes. Specifically, arteriolosclerosis has been observed in over 80% of autopsied individuals beyond 80 years of age.[142] Crucially, pure arteriolosclerosis independently accounts for between 5%[143] and 17%[129] of the risk for AD dementia, a contribution that rises to 35% when concomitant atherosclerosis is present.[129] Conversely, CAA exhibits an estimated prevalence of 25% in the general population over the age of 70[144] and yet is found in over 85–90% of AD brains at autopsy.[145,146] Thus, CAA is not merely a comorbidity of AD; rather, both are intrinsically linked manifestations within the broader cerebral amyloidosis spectrum.[147,148]

1.3.5 Small vessel disease in Down syndrome

1.3.5.1 Vascular profile

Individuals with DS present a striking paradox regarding cerebrovascular disease. Despite a high incidence of factors that would conventionally predict elevated cardiovascular risk, including obesity, a sedentary lifestyle, and obstructive sleep apnea,[149] adults with DS show a remarkably low prevalence of traditional vascular risk factors.[4,150] This dissociation is most dramatic for arterial hypertension: whereas approximately 31.1% of adults worldwide are affected,[151] prevalence in the DS population is virtually absent at 0–1%,[4,149] with blood pressure and heart rate values typically maintained in the low-normal range, or even exhibiting hypotension.[149] Similarly, the rates of diabetes mellitus (1%) and metabolic syndrome (5%) are remarkably diminished.[149] Dyslipidemia also affects only 10–21% of adults with DS, with lipid levels typically remaining within normal clinical ranges, contrasting sharply with the 25–40% prevalence

seen in the general aging population. However, this vascular protection does not extend to all systemic conditions: hypothyroidism, for instance, is highly prevalent, affecting 43–61% of adults across their lifespan.[4,149]

1.3.5.2 Neuropathology

In the DS population, neuropathological studies reveal a highly specific cerebrovascular signature. Consistent with the near-absence of hypertension and other traditional vascular risk factors, age-related vasculopathies, such as atherosclerosis and arteriolosclerosis, are significantly less frequent in individuals with DS compared to healthy controls and those with sAD.[152,153] Consequently, the cerebrovascular landscape in DS is almost exclusively defined by CAA.

The susceptibility to CAA in DS is driven, at least partially, by the triplication of the *APP* gene on chromosome 21, which leads to the lifelong overproduction of Aβ peptides.[152,154] The most compelling evidence for a direct mechanistic role of *APP* overexpression comes from the rare cases of partial trisomy 21 discussed previously: individuals lacking *APP* triplication exhibit not only an absence of AD neuropathology but also a complete absence of CAA, even at advanced ages.[52,53] This gene-dosage relationship extends beyond DS: across genetically determined forms of AD, including DS, ADAD with *APP* missense mutations, and *APPdup*, the frequency and severity of CAA are significantly higher than in both early- and late-onset sAD,[155] reinforcing that *APP* overdosage and mutations directly drive severe vascular amyloid pathology.

Interestingly, pathophysiological divergences emerge within *APP*-driven phenotypes. Specifically, in euploid *APPdup* carriers, massive Aβ deposition occurs early and predominantly in blood vessels, involving both arteries and capillaries, preferentially localizing to the visual cortex,[155] even when

parenchymal Aβ burden is low.[156] Clinically, this severe vascular phenotype renders *APPdup* carriers highly prone to intracerebral hemorrhages.[155]

In contrast, CAA in DS exhibits a more diffuse distribution across cortical and leptomeningeal vessels throughout the brain.[155] Temporally, CAA typically emerges in the fifth decade of life, occurring decades after the initial deposition of parenchymal Aβ plaques.[71,152,157,158] This chronological delay suggests that a specific threshold of Aβ accumulation in the brain parenchyma must be reached before vascular deposition initiates. This is in line with post-mortem assessments showing low levels of parenchymal Aβ deposits with an absence of vascular involvement in individuals with DS without dementia, compared to extensive Aβ deposition in both parenchyma and blood vessels in advanced DSAD cases.[156]

1.3.5.3 Neuroimaging

Over recent years, *in vivo* MRI has demonstrated that SVD pathology is a core, early feature of the AD continuum in DS. Pioneering work applied the modified Boston criteria[159] to assess the neuroimaging hallmarks of CAA, specifically lobar MB, cortical superficial siderosis and lobar intracerebral hemorrhage (ICH) in DS and ADAD compared to euploid controls.[112] This study revealed that individuals with DS exhibit a high frequency of CAA-related neuroimaging features, with lobar MB being particularly prominent in symptomatic stages. Remarkably, despite the high prevalence of CAA pathology, cerebral MB were not significantly more frequent in DS than in other AD forms,[160] although lobar ICH occurred at a higher frequency.[112] Additionally, the degree of WMH, visually assessed using the Fazekas scale, increased significantly with both age and advancing clinical stages of AD in DS.[112]

Expanding these initial findings, a comprehensive multimodal MRI investigation further characterized SVD in individuals with DS along the AD continuum, extending the focus to a broader spectrum of SVD markers, encompassing WMH, MB, ePVS, and infarcts.[161] This study robustly linked the burden of global and regional WMH, ePVS, and infarcts to both age and AD clinical stages. Recent neuroimaging studies have further characterized the SVD burden, revealing that cortical microinfarcts and MB are significantly more prevalent in DS compared to euploid controls. Both lesions increase with age and AD clinical diagnosis, exhibiting a posterior spatial predominance involving parieto-temporo-occipital areas.[162,163] Furthermore, WMH burden was highly correlated with other SVD markers, particularly ePVS, infarcts and MB, suggesting a shared pathophysiological etiology.[161,163]

The pathophysiological overlap between SVD and AD in DS is supported by recent fluid biomarker relationships. The presence of MB is significantly associated with core AD fluid biomarkers in CSF, such as Aβ42/ Aβ40, pTau181 and NFL.[163] Similarly, the severity of WMH strongly correlates with plasma levels of pTau217, NfL and GFAP,[164,165] reinforcing the intrinsic link between SVD and AD in DS.

A recent trajectory model has begun to delineate the chronological cascade of these SVD markers, mapping a temporal sequence in which ePVS and covert infarcts emerge by the early 30s, followed by overt WMH and MBs in the mid-to-late 30s. Crucially, this vascular timeline evolves in tandem with the accumulation of AD pathology.[166] However, the longitudinal dynamics of SVD in DS remain largely understudied. To date, the only longitudinal analysis revealed that the rate of WMH expansion accelerates significantly with clinical AD progression in DS.[167]

1.4 IDENTIFIED KNOWLEDGE GAPS

While the triplication of the *APP* gene establishes DS as an unparalleled biological model for unraveling the interplay between AD, neurodegeneration, and cerebrovascular pathology, a critical review of the current literature reveals several fundamental gaps. Addressing these gaps is essential for characterizing the AD continuum in DS and for developing sensitive biomarkers for future therapeutic interventions.

Specifically, this thesis identifies the following core knowledge gaps:

1.4.1 Topography and dynamics of medial temporal lobe atrophy

While the hippocampus and ERC are well-established targets of early AD pathology, no studies to date have assessed the volumetry of MTL subregions beyond these core areas across the full AD clinical continuum in DS. A thorough characterization of the progressive involvement of these distinct subregions is required to identify early structural biomarkers and provide deeper insights into the spatiotemporal dynamics of neurodegeneration. Furthermore, mapping these topographic changes is essential for establishing sensitive metrics of neurodegeneration as outcome measures in clinical trials.

1.4.2 Spatial distribution and longitudinal evolution of white matter hyperintensities

Although an increased burden of WMH has been recognized in adults with DS, the precise spatial distribution of these lesions, which could provide crucial anatomical clues regarding their underlying etiology, remains poorly understood. Furthermore, despite the links between amyloidosis and SVD, no study to date has systematically assessed the relationships between regional

WMH and established fluid and neuroimaging biomarkers of AD in the DS population. Moreover, the longitudinal evolution of WMH in DS and their dynamic association with advancing AD pathology remain poorly unexplored. A comprehensive understanding of their natural history and pathophysiological trajectory is strictly necessary to provide insight into their etiology.

1.4.3 Early microstructural white matter degradation

While markers like WMH capture macroscopic tissue damage, there is a critical lack of neuroimaging data tracking early, microstructural WM injury associated with SVD across the AD continuum in DS. Beyond traditional DTI metrics, the PSMD, a dispersion-based measure that quantifies heterogeneity in water diffusion along the WM skeleton, has emerged as a highly promising biomarker for SVD. However, its performance and trajectory in DS remain uninvestigated. Deep characterization using PSMD holds profound potential to yield novel insights and serve as a sensitive, clinically relevant metric for detecting early WM changes in AD.

2. HYPOTHESIS AND OBJECTIVES

2.1 GENERAL HYPOTHESIS

We hypothesize that, in adults with DS, AD-related neurodegeneration and SVD emerge early, and progress in parallel along the AD continuum. Neuroimaging markers, including MTL atrophy, WMH, and PSMD, will be associated with fluid biomarkers of amyloid and tau pathology, neurodegeneration, and neuroinflammation, providing complementary insights into the convergent mechanisms underlying DSAD.

2.1.1 Specific hypothesis

1. MTL structures in DS will exhibit a progressive, non-linear, and region-specific pattern of atrophy along the AD continuum, with decline emerging prior to the expected age of symptom onset and following a topography consistent with established AD neuropathological staging.

2. WMH burden in DS will increase with age and advancing clinical stage of AD, following a steeper age-related trajectory than in euploid individuals and emerging years before the expected onset of AD symptoms. WMH will be strongly associated with biomarkers of neurodegeneration.

3. WMH will accumulate longitudinally in DS, with faster rates of progression in individuals presenting clinical AD symptoms, greater neurodegeneration, and higher SVD burden.

4. PSMD will detect microstructural WM damage earlier in DS than in euploid individuals, emerging before symptom onset and increasing with advancing clinical stage of AD. PSMD will be associated with neurodegeneration and other SVD markers, and will precede WMH.

2.2 GENERAL OBJECTIVE

To characterize the neuroimaging signatures of AD-related neurodegeneration and SVD across the AD continuum in DS, focusing on MTL atrophy, WMH, and PSMD, and to assess their associations with age, estimated years to symptom onset (EYO), clinical stage, and fluid biomarkers of amyloid, tau, neurodegeneration, and neuroinflammation, in order to clarify the temporal emergence, regional topography, and interplay between neurodegenerative and cerebrovascular processes in DSAD.

2.2.1 Specific objectives

1. To map the regional pattern of MTL atrophy across the AD continuum in DS and to determine its associations with EYO, clinical stage and fluid biomarkers of amyloid, tau, and neurodegeneration.

2. To characterize the prevalence, burden, and spatial distribution of WMH across age and clinical stages of AD in adults with DS, and to evaluate their relationship with biomarkers of AD pathology, neurodegeneration and neuroinflammation.

3. To examine annual longitudinal changes in global and regional WMH volumes in adults with DS and to identify the demographic, genetic, clinical, and biomarker determinants of WMH trajectories across the AD continuum.

4. To evaluate PSMD across age and clinical stages of AD in DS, to assess its associations with biomarkers of AD, neurodegeneration and SVD, and to determine its temporal relationship with WMH.

3. METHODS

The specific materials and methods employed in each individual study included in this thesis are described in detail within their corresponding articles. The present section provides a consolidated overview of the cohorts analyzed across the four studies, along with a concise summary of the common methodological approaches shared among them.

3.1 STUDY DESIGN

This thesis is based on a single-center study conducted in adults with DS from the DABNI cohort,[168] as well as euploid, cognitively unimpaired controls, and individuals with sAD from the Sant Pau Initiative on Neurodegeneration (SPIN) cohort.[169]

3.1.1 DABNI cohort

The Alzheimer-Down Unit was established in 2012 as a collaborative initiative between the Hospital de la Santa Creu i Sant Pau and the Catalan Down Syndrome Foundation. Its primary clinical objective is the prevention, early detection, and treatment of AD in adults with DS. To this end, a structured health plan for adults with DS was developed, incorporating comprehensive annual medical and neuropsychological evaluations as part of routine clinical screening. For individuals with symptomatic AD, assessments are conducted every six months or more frequently as clinically indicated, with visit frequency individually adapted according to each participant's needs.

Building upon this clinical foundation, the DABNI cohort was launched in 2014 through a joint effort between the aforementioned institutions. All adults (≥18 years of age) attending the Alzheimer-Down Unit are initially enrolled in the routine health plan and subsequently invited to participate voluntarily in the

DABNI research cohort, provided they or their legally authorized representatives give informed consent or assent.

DABNI is a population-based, longitudinal cohort that employs a comprehensive research protocol extending well beyond standard clinical care. Participants undergo structured annual or semiannual neurological, neuropsychological, and nursing assessments conducted by experienced clinicians. Furthermore, the protocol incorporates a comprehensive and optional multimodal biomarker program, encompassing neuroimaging, fluid biomarker collection (plasma and CSF), and genetic profiling. By comprehensively integrating clinical, cognitive, and biomarker data, DABNI not only advances basic and translational research into the natural history of DSAD, but also contributes to the development of therapeutic strategies by facilitating participation in clinical trials for adults with DS.

Between its inception in 2012 and 2025, the overarching initiative successfully recruited 1,232 participants with DS, yielding an unparalleled repository comprising 2,223 plasma samples, 403 CSF samples, and 590 MRI studies.

3.1.2 SPIN cohort

The SPIN cohort study was initiated in 2011 as an umbrella project designed to harmonize and integrate individual observational clinical studies conducted at the Sant Pau Memory Unit (Hospital de la Santa Creu i Sant Pau, Barcelona, Spain). The primary objective of the SPIN cohort is the discovery and validation of fluid (plasma and CSF) and neuroimaging biomarkers across the spectrum of neurodegenerative diseases.

To achieve this, the SPIN cohort captures a wide clinical population, encompassing cognitively unimpaired controls, individuals with subjective cognitive decline and MCI, as well as patients presenting with sAD,

frontotemporal lobar degeneration-related syndromes, and dementia with Lewy bodies. Crucially, the SPIN framework also integrates the DABNI cohort, providing a unique infrastructure for comparative analyses.

Participant enrolment requires written informed consent for the collection of multimodal clinical, biological, and imaging data. Inclusion criteria mandate a detailed neurological and neuropsychological assessment, the acquisition of biofluid samples, and a structural brain MRI. During the baseline visit, a multidisciplinary team, comprising a neurologist and a neuropsychologist, conducts a thorough review of the participant's medical history, a full physical examination, and standardized cognitive testing. This clinical evaluation is typically followed by venipuncture and lumbar puncture for biofluid collection and neuroimaging acquisitions may be scheduled on separate days. Additionally, specific participant subgroups undergo advanced phenotyping, including video-polysomnography and/or molecular neuroimaging with radiotracers such as ^{18}F-FDG, amyloid PET, or Tau PET. The SPIN protocol employs a robust longitudinal design: participants undergo annual clinical follow-ups for a minimum of four years and are offered the opportunity to repeat neuroimaging and CSF biomarker assessments every two years.

Between 2011 and 2025, the SPIN cohort has included 4,859 participants, and gathered 3,327 CSF samples, 5,278 plasma samples and 1,493 MRI studies.

3.2 CLINICAL ASSESSMENT

3.2.1 Adults with Down syndrome

The routine neurological visit consisted of a structured anamnesis with both the DS participant and their caregiver, and a physical examination performed by expert neurologists. This clinical evaluation incorporated the Dementia

Questionnaire for Persons with Mental Retardation, the Neuropsychiatric Inventory, and the Cambridge Examination for Mental Disorders of the Elderly with Down Syndrome interview, which leverages caregiver reports to detect functional and cognitive changes relative to the individual's best-ever level of functioning.

Participants also underwent a specialized neuropsychological protocol specifically adapted for this population. This included the Spanish version of Cambridge Cognitive Examination for Older Adults with Down Syndrome (CAMCOG-DS),[170] the modified Cued Recall Test (mCRT),[171] the Cats&Dogs test and a cancellation task. The CAMCOG-DS is a comprehensive cognitive battery yielding a maximum total score of 109 (where higher scores indicate better cognitive performance), comprising seven subscales that assess orientation, language (comprehension and expression), memory (new learning, remote, and recent), attention, praxis (visoconstruction and motor), abstract thinking, and visoperception. The mCRT was utilized as a two-phase paradigm specifically adapted to evaluate episodic memory in individuals with ID.

At baseline, the individual’s level of ID was categorized as mild, moderate, or severe/profound based on the Diagnostic and Statistical Manual of Mental Disorders, Fifth Edition,[172] and the caregiver’s report of the individual’s best-ever level of functioning. To further support the ID classification, the intelligence quotient is assessed using the Spanish version of Kaufman Brief Intelligence Test,[173] administered only when there was no clinical suspicion of cognitive decline, to avoid biased intelligence estimations.

The diagnostic workflow was structured sequentially, to avoid circularity in the research studies. Initially, the neurologist and neuropsychologist conducted independent evaluations, and established a diagnosis strictly blinded to each other's findings and to all biomarker data. Following these independent

assessments, there is a clinical consensus meeting between both professionals to determine a joint clinical diagnosis based solely on clinical and neuropsychological data. Finally, to establish the definitive diagnosis for a given visit, this consensus was retrospectively revisited by integrating available biomarker profiles and longitudinal follow-up data.

Based on this comprehensive procedure, participants were classified into one of four diagnostic categories: (1) asymptomatic (aDS, i.e., no clinical or neuropsychological suspicion of AD-related cognitive decline), (2) prodromal AD (pDS, i.e., evidence of cognitive decline due to AD, but no significant impact on baseline activities of daily living), (3) AD dementia (dDS, i.e., when the cognitive decline impaired daily activities) and (4) uncertain (uDS, i.e., when there were medical, pharmacological, and/or psychiatric conditions interfering with cognition or daily activities, but no suspicion of neurodegenerative origin).

Moreover, longitudinal progression along the AD continuum was defined as a change in clinical and cognitive status after carefully excluding other medical and psychosocial confounders. Progression from aDS to pDS was established when relevant cognitive or behavioural changes emerged without additional interference in daily functioning, whereas progression from pDS to dDS was defined when these changes began to compromise the patient's premorbid personal autonomy.

3.2.2 Euploid controls and sporadic Alzheimer's disease

Participants in the SPIN cohort underwent a standardized neurological and neuropsychological assessment to evaluate global cognitive impairment, functional impact, and neuropsychiatric symptoms across multiple cognitive domains.[174] For clinical diagnostic staging, we used the Clinical Dementia Rating

(CDR) global scale, Global Deterioration Scale – Functional Assessment Staging (GDS-FAST) and the Mini-Mental State Examination (MMSE).

The clinical diagnosis of sAD, identifying individuals in both the MCI and dementia stages of AD, was established following the National Institute on Aging-Alzheimer's Association criteria.[175,176] In a subset of participants with available fluid biomarkers, AD diagnosis was further confirmed according to a previously validated CSF biomarker cutoff (Aβ42/Aβ40 ratio < 0.062),[177] indicating the presence of amyloid pathology.

The cognitively unimpaired controls were volunteers, usually spouses or children of patients from the Sant Pau Memory Unit, who were informed about our studies at the outpatient clinics. They exhibited no cognitive complaints, scored 0 on the CDR global scale, and/or 1 on the GDS-FAST. Their neuropsychological evaluation was within the normal range for their respective normative groups regarding age and education. Furthermore, none of the participants in the control group reported any neurological or psychiatric disorders or other major medical illnesses.

3.3 MRI ACQUISITION

All participants underwent MRI scanning at one of two institutions in Barcelona, Spain: Hospital del Mar, using a 3 T Philips-Achieva scanner; or Hospital Clinic, with a 3 T Siemens-Prisma scanner. MRI protocols include high-resolution three-dimensional T1w, FLAIR, DWI and SWI. The specific acquisition parameters for each sequence are detailed in Table 1.

Table 1. 3T T1w, DWI, FLAIR, and SWI acquisition protocols.

	3T Philips – Achieva (Hospital del Mar – Barcelona, Spain)			
	Protocol 1			
	T1w	**DWI**	**FLAIR**	**SWI**
Echo Time (ms)	3.8	78	140	24
Repetition Time (ms)	8.2	10800	10000	17
Flip Angle (°)	8	90	90	15
Number of Slices	160	80	140	130
Slice Thickness (mm)	1	2	1	1
Field of View (mm²)	256x256	256x256	256x256	512x512
Voxel Resolution (mm)	0.94x0.94x1	2x2x2	0.9x0.9x1	0.45x0.45x1
b-value		0;100		
N. Directions		32		
	3T Siemens-Prisma (Hospital Clinic- Barcelona, Spain)			
	Protocol 2			
Echo Time (ms)	2.98	89	128	20
Repetition Time (ms)	2300	7700	9000	26
Flip Angle (°)	9	90	150	15
Number of Slices	240	60	45	192
Slice Thickness (mm)	1	2	1	0.75
Field of View (mm²)	256x256	250x250	220x220	240x240
Voxel Resolution (mm)	1x1x1	2x2x2	0.9x0.9x3	0.75x0.75x0.75
b-value		30		
N. Directions		0;1000		
	Protocol 3			
Echo Time (ms)	2.96	71	397	20
Repetition Time (ms)	2300	3700	6000	26
Flip Angle (°)	9	90	120	15
Number of Slices	208	60	160	192
Slice Thickness (mm)	1	2	1	0.75
Field of View (mm²)	256x256	232x232	256x256	240x240
Voxel Resolution (mm)	1x1x1	2x2x2	1x1x1	0.75x0.75x0.75
b-value		127		
N. Directions		0;500; 1000; 2000		

3.4 MRI PROCESSING

All MRI scans underwent visual quality control, and those with unsatisfactory raw quality were excluded.

3.4.1 T1w preprocessing

Structural T1w images were preprocessed using the Computational Anatomy Toolbox 12 version 8 (CAT12v8)[178] toolbox of Statistical Parametric Mapping 12 (SPM12, Wellcome Centre for Human Neuroimaging, University College London, Queen Square Institute of Neurology). CAT12 computed the image quality rating (IQR), a weighted average image quality metric based on noise contrast ratio, inhomogeneity contrast ratio, and resolution. For each participant, CAT12 was used to segment probability maps for GM, WM, and CSF, as well as to extract total intracranial volume (TIV) and the corresponding tissue volumes. Furthermore, the Hammers atlas was also coregistered into the native T1w space at each visit.

3.4.2 DWI preprocessing

DWI acquisition consisted of either single-shell protocol (b-value=1000 s/mm^2) or multi-shell (b-values=0,500,1000, and 2000 s/mm^2). To harmonize the data across the cohort and follow the PSMD developers' guidance that b-values between 700 and 1200 s/mm2 are required,[138] we retained only the b-value = 1000 s/mm^2 volume, which was extracted using *fslsplit* and reassembled with *fslmerge* in FSL (v6.0.7.1).[179]

Preprocessing was performed with an in-house Python pipeline using Diffusion Imaging in Python (DIPY).[180] First, DWI images were denoised using Marchenko-Pastur principal component analysis with *dipy_denoise_mppca*. Although a subset of participants had additional reverse phase-encoded b=0 images

enabling susceptibility distortion correction with FSL *TOPUP*, this step was not applied in order to maintain a uniform processing pipeline across the full cohort. Exploratory analyses indicated that applying TOPUP did not significantly affect the resulting PSMD values. Finally, for all participants, eddy-current and motion correction were then applied with FSL *EDDY*.

3.4.3 WM parcellation

WM was parcellated for each subject using an in-house pipeline inspired by the bullseye classification system previously developed by Sudre and colleagues.[181] Specifically, two distinct sets of parcellations were created: concentric layers and lobar regions (for details, see Annex 2). For the concentric layers, we adapted the approach proposed by Jiménez-Balado and colleagues[182] and to compute a normalized distance map, which reflects the distance of each WM voxel to the lateral and third ventricles. For the lobar segmentation, we used the anatomical Hammers atlas to label the WM according to the lobes (frontal, parietal, temporal, occipital, and basal ganglia). The normalized distance map was then applied to each lobar region, which were subsequently divided into four concentric layers of similar volume. These layers spanned from the periventricular regions to juxtacortical areas.

3.4.4 MTL structures

For individuals with multiple available MRI scans, the highest-quality T1w image was automatically selected based on the IQR generated by CAT12. These T1w images then underwent automated segmentation of the MTL using the Automatic Segmentation of Hippocampal Subfields (ASHS)-T1 pipeline, a method validated in older adults and patients with AD.[183] This pipeline automatically segments the whole hippocampus (anterior and posterior) and extrahippocampal MTL subregions including ERC, Brodmann areas 35 (Br35,

which approximates the transentorhinal cortex) and 36 (Br36), and parahippocampal cortex (PHC), together with regional WM and the dura mater, and accounts for some confounds of conventional approaches, such as dura mater mis-segmentation.[184,185] Following this, we applied a surface-based modelling and groupwise registration pipeline, called CRASHS (Cortical Reconstruction for ASHS; GitHub script (https://github.com/pyushkevich/crashs),[185,186] to compute the surfaces of the ERC, Br35, Br36 and PHC. CRASHS integrates the detailed cortical reconstruction capabilities of NighRes/CRUISE[187,188] with the precise MTL boundary definitions of ASHS, enhancing the topographical accuracy of the segmentations. The corresponding regional volumes were reported in cubic millimetres, and regional cortical thickness was reported in millimetres. In Study 1, we assessed GM regions relevant to AD: the anterior and posterior hippocampus, for which we focused on volumes, in addition to the ERC, Br35, Br36 and the PHC, for which we assessed cortical thickness. For these latter regions, we also present sensitivity analyses using the volumes from ASHS-T1 (for details, see Annex 1).

To ensure the quality of ASHS-T1 segmentation, trained raters visually assessed each segmentation and graded errors on a four-point scale (0 coded for no error, and a severity level 1–3) based on the rater's estimate of the percentage of area affected.[189] Minor deviations (<10% over- or under- estimation) were classified as level 1, moderate errors (10%–25%) as level 2, and severe errors (>25%) were categorized as level 3. Level 3 errors resulted in automatic exclusion, whereas level 2 errors underwent consensus review by two independent raters to determine the final exclusion or inclusion of the subject.

3.4.5 WMH segmentation

In Study 2, for the segmentation of WMH, raw FLAIR images were first coregistered onto their corresponding T1w scan using Advanced Normalization Tools (ANTs).[190] Then, WMH were segmented in the MRI-native space using the lesion prediction algorithm (LPA)[191] implemented in the Lesion Segmentation Toolbox (LST v3.0.0) for SPM12. Specifically, the LPA method computed a WMH probability map for each participant based on a logistic regression algorithm to classify each voxel as either a lesion or non-lesion. These probability maps were then binarized by applying a threshold of 0.3 (for details, see Annex 2).

In Study 3, to accurately quantify WMH evolution across multiple time points, we employed the longitudinal pipeline implemented in LST for SPM12.[192] This pipeline is specifically designed to compare lesion probability maps previously generated by the LPA across multiple time points. First, the longitudinal pipeline of LST performed a rigid between-time-point coregistration of each participant's FLAIR images. The resulting space transforms were subsequently applied to the lesion probability maps, ensuring that for each participant, all FLAIR images and corresponding lesion maps were aligned in a common space. Finally, relative changes in FLAIR signal intensity were computed for all voxels that were labeled as a lesion in at least one time point. Through an iterative procedure, the pipeline distinguishes true lesion change from natural variability in FLAIR signal across time points. This yielded refined and binarized lesion maps for each time point that were jointly informed by the full longitudinal series.

3.4.5.1 Extraction of WMH volumes

Total WMH volumes were obtained as the intersection between the LPA-derived lesion maps and the WM masks generated by CAT12v8. Regional WMH volumes

were computed from the overlap between the binarized WMH maps and the WM parcellation templates.

In Study 3, annualized changes in total and regional WMH volumes were computed as the difference between the last follow-up and the baseline values, divided by the corresponding time interval between visits, expressed in years. Positive values indicate increases in WMH volume between the two time points, while negative values indicate decreases in WMH volume.

3.4.6 PSMD computation

In Study 4, PSMD was automatically computed using the freely available script developed by Baykara and colleagues (2016).[138] Briefly, eddy-corrected DWI scans were processed with the standard Tract-Based Spatial Statistics pipeline in FSL. First, FA volumes were registered to the FMRIB 1 mm FA template in standard space. Second, a WM skeleton was derived from the mean FA image and thresholded at FA $\geq$ 0.2 to exclude predominantly non-WM voxels. Third, MD maps were projected onto the FA skeleton and further masked using the WM skeleton mask, provided by Baykara and colleagues, with an FA threshold of $>$ 0.3 to mitigate CSF partial volume effects. Finally, PSMD was calculated as the difference between the 95th and 5th percentile values of the MD histogram within the entire skeleton mask, representing a global WM diffusion metric.

3.4.7 MB segmentation

SWI scans were N4 bias field corrected using ANTs and coregistered to their corresponding T1w image. Cerebral microbleeds were manually segmented in ITK-SNAP (v3.8.0),[193] as previously described.[163] Participants were classified according to the presence of microbleed (MB- and MB+).

3.5 BIOFLUID COLLECTION AND PROCESSING

A subset of participants underwent a lumbar puncture and/or blood extraction. Blood samples were drawn at the time of the lumbar puncture or during a routine clinical visit for participants who declined the lumbar puncture. While fasting was not mandatory, the time elapsed since the participant's last meal was systematically recorded.

CSF and blood samples were collected and processed in polypropylene tubes following international recommendations.[194,195] For the lumbar puncture, a total of 15–20 mL of CSF was collected. The first 2 mL were immediately routed to the general laboratory for standard cell count, glucose, and protein analyses. The remaining volume, along with the collected blood samples, was transferred to our research laboratory, where it was centrifuged (for blood), processed, and aliquoted within two hours of collection. All aliquots were subsequently stored at −80 °C until analysis.

3.5.1 Fluid biomarkers

CSF concentration levels of Aβ40, Aβ42 and pTau181 were quantified using a commercially available immunoassay in a fully automated platform (Lumipulse; Fujirebio-Europe), following a previously published protocol.[169] CSF and plasma GFAP concentrations were measured using the SR-X single-molecule array (Quanterix). CSF NfL and YKL-40 levels were measured with enzyme-linked immunosorbent assay (NF-Light Assay, UmanDiagnostics and MicroVue EIA, Quidel, respectively) according to the manufacturer's recommendations.

To define the presence of AD pathology, participants were stratified into amyloid-positive (A+) and tau-positive (T+) groups based on previously established clinical cut-off values.[177] Specifically, an abnormal CSF Aβ42/Aβ40

ratio (<0.062) was utilized to define amyloid positivity, while elevated CSF pTau181 (>63 pg/mL) was used to define tau positivity.

3.6 ETHICAL ASPECTS

All studies were approved by the Sant Pau Ethics Committee based on the international ethical guidelines for medical research in humans, following standards contained in the Declaration of Helsinki and Spanish law. All participants, or their legally authorized representative, gave written consent before enrolment.

3.7 STATISTICAL ANALYSES

Statistical analyses were conducted using R software (https://www.r-projrct.org/) and the statistical significance threshold was set at p=0.05. Specific statistical procedures are described within each study; here, we outline the general statistical framework applied across studies.

Given that different MRI acquisition protocols were used, key neuroimaging metrics were harmonized using the ComBat method,[196] implemented in the *neuroCombat* R library. In addition, W-scores were computed for each MTL region to reduce the effects of age, sex, and TIV (see for details, Study 1).

Baseline demographic and clinical differences among groups were assessed using the *compareGroups* R library.[197] Chi-squared tests were applied to categorical variables and Mann-Whitney or Kruskall-Wallis tests for non-normally distributed continuous variables. Logarithmic transformation was applied to variables exhibiting skewness.

Associations with age were examined using Spearman rank correlation or robust linear regression models (*robustbase* R library). To represent the data, we

performed locally estimated scatterplot smoothing (LOESS) curves with a tricubic weight function and a span parameter of 0.75. The effects of sex, *APOE* ϵ4 status, ID level, and AD clinical stage on neuroimaging metrics were evaluated using Mann–Whitney or t-tests for two-group comparisons, and Kruskal–Wallis or ANOVA followed by Dunn's or Tukey's post hoc tests for multi-group comparisons, depending on data distribution. Participants classified as uDS were excluded only from analyses stratified by AD clinical diagnosis.

Finally, associations between neuroimaging markers and fluid biomarkers were assessed using robust linear regression models and Spearman rank correlations.

4. RESULTS

Study 1: Medial Temporal Lobe Atrophy in Down Syndrome Along the Alzheimer's Disease Continuum

Benjamin J. Buehner[1,†]; Alejandra O. Morcillo-Nieto[1,2,†]; Sara E. Zsadanyi[1,2]; Mateus Rozalem Aranha[1,2]; José Enrique Arriola-Infante[1,2]; Lídia Vaqué-Alcázar[1,3,4]; Javier Arranz[1]; Íñigo Rodríguez-Baz[1,2]; Lucia Maure Blesa[1]; Laura Videla[1,2,5]; Isabel Barroeta[1,2]; Laura Del Hoyo Soriano[1]; Bessy Benejam[1,5]; Susana Fernández[5]; Aida Sanjuan Hernandez[1,5]; Nuria Bargalló6,7; Sofía González-Ortiz[6,7]; Sandra Giménez[1,2,8]; Robin de Flores[9]; Paul A Yushkevich[10]; Daniel Alcolea[1,2]; Olivia Belbin[1,2]; Alberto Lleó[1,2]; Maria Carmona-Iragui[1,2,5]; Juan Fortea[1,2,5] and Alexandre Bejanin[1,2]

†These authors contributed equally to this work

[1]Sant Pau Memory Unit, Department of Neurology, Hospital de la Santa Creu i Sant Pau, Biomedical Research Institute Sant Pau, Universitat Autònoma de Barcelona, Barcelona, Spain. [2]Center of Biomedical Investigation Network for Neurodegenerative Diseases (CIBERNED), Madrid, Spain. [3]Department of Medicine, Faculty of Medicine and Health Sciences, Institute of Neurosciences, University of Barcelona, Barcelona, Spain. [4]Institut d'Investigacions Biomèdiques August Pi i Sunyer (IDIBAPS), Barcelona, Spain. [5]Barcelona Down Medical Center, Fundació Catalana de Síndrome de Down, Barcelona, Spain. [6]Nuclear Medicine Department, Hospital de la Santa Creu i Sant Pau, Universitat Autònoma de Barcelona, Barcelona, Spain. [7]Neuroradiology Section, Radiology Department, Diagnostic Image Center, Hospital Clínic de Barcelona, Universitat de Barcelona, Barcelona, Spain. [8]Multidisciplinary Sleep Unit, Respiratory Department, Hospital de la Santa Creu i Sant Pau, Institut d'Investigació Biomèdica Sant Pau (IIB SANT PAU), Barcelona, Spain. [9]Normandie Univ, UNICAEN, INSERM, U1237, PhIND 'Physiopathology and Imaging of Neurological Disorders', NeuroPresage Team, Caen, France. [10]Department of Radiology, University of Pennsylvania, Philadelphia, PA, USA.

Brain (2025) 148(7):2509-2521 doi: 10.1093/brain/awaf133
IF (2024) = 11.7, Rank = 5/202 in Clinical Neurology, D1

BRAIN
ORIGINAL ARTICLE

Medial temporal lobe atrophy in Down syndrome along the Alzheimer's disease continuum

Benjamin J. Buehner,[1,†] Alejandra O. Morcillo-Nieto,[1,2,†] Sara E. Zsadanyi,[1,2] Mateus Rozalem Aranha,[1,2] José Enrique Arriola-Infante,[1,2] Lídia Vaqué-Alcázar,[1,3,4] Javier Arranz,[1] Íñigo Rodríguez-Baz,[1,2] Lucia Maure Blesa,[1] Laura Videla,[1,2,5] Isabel Barroeta,[1,2] Laura Del Hoyo Soriano,[1] Bessy Benejam,[1,5] Susana Fernández,[5] Aida Sanjuan Hernandez,[1,5] Nuria Bargalló,[6,7] Sofía González-Ortiz,[6,7] Sandra Giménez,[1,2,8] Robin de Flores,[9] Paul A Yushkevich,[10] Daniel Alcolea,[1,2] Olivia Belbin,[1,2] Alberto Lleó,[1,2] Maria Carmona-Iragui,[1,2,5] Juan Fortea[1,2,5] and Alexandre Bejanin[1,2]

[†]These authors contributed equally to this work.

Medial temporal lobe structures are among the first areas impacted by neurofibrillary tangle pathology, making volumetric changes of these areas promising biomarkers for Alzheimer's disease. To date, little is known about the integrity of these regions in individuals with Down syndrome, a population that almost invariably develops Alzheimer's disease and thus offers a unique opportunity to determine the earliest structural changes related to the disease. We aimed to characterize the sequential involvement of medial temporal lobe structures with Alzheimer's disease progression, explore associations with fluid biomarkers of Alzheimer's pathology and assess the utility of regional volumes and cortical thickness in distinguishing Alzheimer's disease clinical stages in Down's syndrome.

One hundred and thirty-eight euploid controls and 259 adults with Down syndrome underwent clinical assessment and MRI scanning, followed by automated segmentation of the medial temporal lobe on T1-weighted images. Parametric statistical tests and local regression models were used to assess the cross-sectional association between regional volumes/cortical thickness and Alzheimer's disease clinical stage, estimated years of onset, and CSF biomarkers. Additionally, markers were assessed in their ability to distinguish clinical stages using area under the receiver-operating characteristic curves.

Results showed a progressive loss of volume and cortical thickness in the medial temporal lobe with advancing Alzheimer's disease stage, showing reduced volume/thickness at the dementia stage in all subregions. The asymptomatic and prodromal groups showed significant differences in the anterior and posterior hippocampus. We identified the entorhinal cortex and posterior hippocampus as the regions showing the earliest loss in Down syndrome, starting 13–15 years before Alzheimer's disease symptom onset. We observed non-linear structural changes with disease progression, with certain structures (e.g. the parahippocampal cortex) characterized by an initial increase in cortical thickness followed by subsequent thinning. Of all subregions, the hippocampal volumes showed the closest correlation with CSF amyloid-$\beta_{42/40}$, tau phosphorylated at threonine 181 and neurofilament light chain levels. Further analyses demonstrated a high predictive value, similar to CSF biomarkers, of the hippocampus in differentiating between individuals with asymptomatic versus prodromal/dementia Alzheimer's disease in Down syndrome.

This study provides a novel understanding of the progressive, non-linear volumetric changes of medial temporal lobe structures in relationship to Alzheimer's disease pathology in Down syndrome, which can have important implications

Received September 28, 2024. Revised February 19, 2025. Accepted March 29, 2025. Advance access publication April 17, 2025
© The Author(s) 2025. Published by Oxford University Press on behalf of the Guarantors of Brain. All rights reserved. For commercial re-use, please contact reprints@oup.com for reprints and translation rights for reprints. All other permissions can be obtained through our RightsLink service via the Permissions link on the article page on our site—for further information please contact journals.permissions@oup.com.

Downloaded from https://academic.oup.com/brain/advance-article/doi/10.1093/brain/awaf133/8115454 by guest on 16 May 2025

for clinical trials monitoring neurodegeneration using MRI. We also show that MRI information can refine the prediction of clinical status in Down syndrome. This is particularly relevant in Down syndrome, where early clinical stages can be challenging to detect owing to neurodevelopmental intellectual disability.

1 Sant Pau Memory Unit, Department of Neurology, Hospital de la Santa Creu i Sant Pau, Biomedical Research Institute Sant Pau, Universitat Autònoma de Barcelona, Barcelona 08041, Spain
2 Center of Biomedical Investigation Network for Neurodegenerative Diseases (CIBERNED), Madrid 28029, Spain
3 Department of Medicine, Faculty of Medicine and Health Sciences, Institute of Neurosciences, University of Barcelona, Barcelona 08036, Spain
4 Institut d'Investigacions Biomèdiques August Pi i Sunyer (IDIBAPS), Barcelona 08036, Spain
5 Barcelona Down Medical Center, Fundació Catalana de Síndrome de Down, Entresòl 08029, Barcelona, Spain
6 Nuclear Medicine Department, Hospital de la Santa Creu i Sant Pau, Universitat Autònoma de Barcelona, Barcelona 08041, Spain
7 Neuroradiology Section, Radiology Department, Diagnostic Image Center, Hospital Clínic de Barcelona, Universitat de Barcelona, Barcelona 08036, Spain
8 Multidisciplinary Sleep Unit, Respiratory Department, Hospital de la Santa Creu i Sant Pau, Institut d'Investigació Biomèdica Sant Pau (IIB SANT PAU), Barcelona 08041, Spain
9 Normandie Univ, UNICAEN, INSERM, U1237, PhIND 'Physiopathology and Imaging of Neurological Disorders', NeuroPresage Team, Caen 14074, France
10 Department of Radiology, University of Pennsylvania, Philadelphia, PA 19104, USA

Correspondence to: Alexandre Bejanin, PhD
Sant Pau Memory Unit, Department of Neurology
Institut de Recerca Sant Pau, Sant Quintí 77–79, Barcelona 08041, Barcelona, Spain
E-mail: ABejanin@santpau.cat

Keywords: Alzheimer's disease; Down syndrome; magnetic resonance imaging; neuroimaging; medial temporal lobe; grey matter atrophy

Introduction

Down syndrome is caused by the trisomy of chromosome 21, which results in an extra copy of the *APP* (amyloid precursor protein) gene.[1] This triplication is both sufficient and necessary to produce early-onset Alzheimer's disease pathology in Down syndrome,[2] such that dementia is the leading cause of death in this population.[3]

Alzheimer's disease is associated with the presence of intracellular tau neurofibrillary tangles and extracellular amyloid-β (Aβ) plaques,[4] which accumulate in a very similar pattern in Down syndrome to that observed in euploid individuals with Alzheimer's disease.[5-7] The amyloid pathology in Down syndrome initially manifests in the form of diffuse plaques in the temporal neocortex of individuals in their late teens and it involves the hippocampus and other neocortical regions at a relatively early stage.[8,9] Tau-associated pathological changes can be observed in the medial temporal lobe (MTL) of individuals with Down syndrome in their early thirties, starting in the transentorhinal cortex and the entorhinal cortex (ERC), with subsequent spread throughout the hippocampus and, later, the neocortex.[8,9]

Tau pathology has been associated with grey matter atrophy as measured with *in vivo* MRI[10] and is closely related to neurodegeneration and cognitive decline.[11-13] Previous studies demonstrated that atrophy in Alzheimer's disease is first detected in the anterior MTL, a key site of early tau build-up,[14,15] with accelerated rates of atrophy of MTL subregions in preclinical Alzheimer's disease in the presence of tau pathology.[16] These findings make MTL volumes and cortical thickness promising biomarkers to detect early Alzheimer's disease stages and monitor its progression.

Identifying reliable biomarkers of early detection and disease progression is especially crucial in Down syndrome, because the symptoms of dementia are sometimes confounded with premorbid intellectual disabilities or medical comorbidities.[17] Based on a visual scale, subjects with Down syndrome and Alzheimer's disease were found to have a more severe MTL atrophy when compared with euploid individuals with Alzheimer's disease.[18] Global MTL atrophy, in addition to hippocampal atrophy, has been observed and correlated with dementia in Down syndrome, establishing the utility of MTL assessments in this population.[18-20] However, to date, no studies have assessed the volumetry of MTL subregions beyond the hippocampus and ERC across the full Alzheimer's disease clinical continuum in Down syndrome. Yet, a thorough characterization of the progressive involvement of these subregions could help to identify early biomarkers of Alzheimer's disease and provide new insights into the dynamics and topography of structural changes with disease progression. This, in turn, might be essential for clinical trials that use metrics of neurodegeneration as outcomes of interest. Employing a novel multiatlas segmentation software, Automatic Segmentation of Hippocampal Subfields (T1-ASHS),[21] the aim of this study was to explore the effect of Alzheimer's disease on MTL volumes and thickness in a large cohort of adults with Down syndrome. Specifically, to identify regions of early volumetric changes, we assessed the integrity of substructures of the MTL in relationship to both clinical stages of Alzheimer's disease and estimated years from symptom onset (EYO). We further explored associations with fluid biomarkers of Alzheimer's disease pathology and tested the reliability of MTL volumes and thickness in distinguishing clinical stages of Alzheimer's disease.

Downloaded from https://academic.oup.com/brain/advance-article/doi/10.1093/brain/awaf133/8115454 by guest on 16 May 2025

Materials and methods

Study design and participants

This single-centre cross-sectional study involved 259 adults with Down's syndrome, who were recruited from the population-based Down–Alzheimer Barcelona Neuroimaging Initiative (DABNI),[5] and 138 cognitively unimpaired euploid adults [i.e. healthy controls (HC)] derived from the Sant Pau Initiative on Neurodegeneration (SPIN) cohort,[22] in Barcelona, Spain. The study included participants of both sexes aged ≥18 years with available T1-weighted (T1w) MRI scans and complete neurological and neuropsychological assessments.[23,24] The study was approved by the Sant Pau Ethics Committee based on the standards for medical research in humans recommended by the Declaration of Helsinki. All participants, or their legally authorized representative, gave written consent before enrolment.

Clinical assessment

Participants with Down syndrome were screened for apolipoprotein E (*APOE*) haplotype and underwent comprehensive neurological and neuropsychological evaluation. Global cognition was assessed using a Spanish version of the Cambridge Cognitive Examination for Older Adults with Down syndrome (CAMCOG-DS). CAMCOG-DS is a cognitive battery designed to evaluate language, orientation, memory, attention, praxis, abstract thinking and perception.[25] Additionally, the Diagnostic and Statistical Manual of Mental Disorders, Fifth Edition (DSM-5) was used to categorize the level of intellectual disability into mild, moderate or severe/profound,[26] on the basis of the individual's best ever level of functioning, as determined from carers' reports.

Participants were clinically classified into four groups in a consensus meeting between a neurologist and neuropsychologist. The classification was conducted after independent visits, with both specialists masked from biomarker data. Individuals were categorized as: (i) asymptomatic (aDS), when there was no clinical or neuropsychological suspicion of symptomatic Alzheimer's disease; (ii) prodromal Alzheimer's disease (pDS), when there was a suspicion of cognitive impairment related to Alzheimer's disease, but symptoms did not fulfil criteria for dementia; (iii) Alzheimer's disease dementia (dDS), when there was evidence of cognitive impairment that interfered with everyday activities beyond the basal functioning; and (iv) uncertain or non-degenerative neurocognitive disorder (i.e. when there were medical, pharmacological or psychiatric conditions interfering with cognition or daily living activities, but no suspicion of neurodegenerative origin).

The HC group were volunteers, usually spouses or children of patients from the Sant Pau Memory Unit, who were informed about our studies at the outpatient clinics. They exhibited no cognitive complaints, scoring zero on the Clinical Dementia Rating scale,[27] and their neuropsychological evaluation was within the normal range for their respective normative groups regarding age and education. None of the participants in the HC group reported any neurological or psychiatric disorders or other major medical illnesses.[22] We selected only HC within the same age range as the Down syndrome group, 18–65 years.

MRI acquisition

Subjects underwent MRI scanning at one of two institutions in Barcelona, Spain: Hospital del Mar, using a 3 T Philips-Achieva scanner; and Hospital Clinic, with a 3 T Siemens-Prisma scanner. The acquisition protocols are detailed in Supplementary Table 1.

MRI processing and quality control

T1w images were first pre-processed using the Computational Anatomy Toolbox (CAT12) implemented in SPM12 Software. CAT12 computes a weighted average image quality metric (image quality rating), based on noise contrast ratio, inhomogeneity contrast ratio and resolution.[28] Based on this scoring, we automatically selected the highest-quality T1w image for those individuals for whom we had multiple MRI scans available. CAT12 was also used to extract the total intracranial volume (ICV) for each individual.

The T1w images then underwent automated segmentation of the MTL performed by ASHS-T1, a segmentation pipeline for MTL validated in older adults and patients with Alzheimer's Disease.[29] This pipeline automatically segments the whole hippocampus (anterior and posterior) and extrahippocampal MTL subregions including ERC, Brodmann areas 35 (Br35, which approximates the transentorhinal cortex) and 36 (Br36), and parahippocampal cortex (PHC), together with regional white matter and the dura mater (Supplementary Fig. 1), and accounts for some confounds of conventional approaches, such as dura mater mis-segmentation.[21,30] Following this, we applied a *GitHub* script (https://github.com/pyushkevich/crashs) to compute the surfaces of the ERC, Br35, Br36 and PHC using a surface-based modelling and groupwise registration pipeline called CRASHS.[30,31] CRASHS (Cortical Reconstruction for ASHS) integrates the detailed cortical reconstruction capabilities of NighRes/CRUISE[32,33] with the precise MTL segmentation of ASHS, enhancing the accuracy of segmentations. The corresponding regional volumes of regions of interest (ROIs) were reported in cubic millimetres, and regional cortical thickness was reported in millimetres. In this study, we assessed grey matter regions relevant to Alzheimer's disease: the anterior and posterior hippocampus, for which we focused on volumes, in addition to the ERC, Br35, Br36 and the PHC, for which we assessed cortical thickness. For these latter regions, we also present sensitivity analyses using the volumes from ASHS-T1. Given that different MRI acquisition protocols were used to acquire the data, we harmonized regional volumes and cortical thickness using the ComBat harmonization method as implemented in the R library *neuroCombat*.[34]

The quality of the raw T1w images was assessed using the image quality rating metric automatically generated by the CAT12 pipeline. Additionally, to ensure the quality of ASHS-T1 segmentation, trained raters visually assessed each segmentation and rated segmentation errors on a four-point scale (0 coded for no error, and a severity level 1–3) based on the rater's estimate of the percentage of area affected.[35] Minor deviations (<10% over- or under-estimation) were rated as level 1, an estimated error of 10%–25% as level 2, and errors that caused >25% mis-segmentation were categorized as level 3 errors. Level 3 errors resulted in an automatic exclusion, whereas level 2 errors were assessed by two independent raters to determine the exclusion or inclusion of the subject.

Volume normalization

To isolate the effects of Alzheimer's disease pathology, we computed W-scores for each regional volume and thickness of the MTL.[14] Specifically, a linear regression analysis including age, sex and ICV (in the case of regional volumes), as independent variables, was performed for each ROI in the euploid control group aged 18–65 years. The coefficients (betas) and intercept of this regression were

Downloaded from https://academic.oup.com/brain/advance-article/doi/10.1093/brain/awaf133/8115454 by guest on 16 May 2025

used to calculate, for each subject, a predicted regional volume and thickness of the ROI based on the subject's independent variables. The W-score was then computed by subtracting this predicted value from the subject's raw ROI volume/thickness and subsequently dividing it by the standard deviation (SD) of the residuals of the model, as seen in the equation below:

$$\text{W-score}(i) = \frac{\text{ROI raw volume/thickness}(i) - \text{ROI predicted volume/thickness}(i)}{\text{SD residuals}} \quad (1)$$

Thus, the W-scores reflect measures of regional volumes and cortical thickness without the confounding effects of individual age, sex and ICV (for volumes), based on a reference euploid population. This previously validated technique minimizes confounding variables and preserves biologically relevant information.[36-38]

Fluid biomarkers

CSF biomarkers were acquired in 243 participants via lumbar puncture, as previously described.[39] Fluid concentrations of Aβ peptide 1–40 ($A\beta_{40}$), Aβ peptide 1–42 ($A\beta_{42}$) and tau phosphorylated at threonine 181 (pTau181) were quantified using commercially available immunoassay in a fully automated platform (Lumipulse G600II, Fujirebio), following the previously described protocol.[22] CSF neurofilament light chain (NfL) levels were assessed using an enzyme-linked immunosorbent assay (UmanDiagnostics) based on the manufacturer's recommendations. To reduce skewness, concentrations of CSF biomarkers were logarithmically scaled. Finally, the CSF $A\beta_{42}/A\beta_{40}$ ratio was used to stratify individuals according to the presence of amyloid using previously established cut-off values (i.e. CSF $A\beta_{42}/A\beta_{40} < 0.062$).[40]

Statistical analysis

All statistical analyses were performed with R v.4.3.2 (R Foundation for Statistical Computing). Between-group differences in baseline demographic characteristics were assessed using the *compareGroups* library, which uses χ^2 tests for categorical variables and Mann–Whitney and Kruskal–Wallis tests for continuous variables not following a normal distribution.[41] To assess the effect of Alzheimer's disease clinical stages on MTL volume/thickness (computed as W-scores), we performed separate ANOVA testing for each subregion, followed by Tukey's HSD *post hoc* analysis, because they follow normality. Associations between regional W-scores and EYO were performed using locally estimated scatterplot smoothing (LOESS) curves with a tricubic weight function and a span parameter of 0.75. Consistent with previous studies,[6,7] the EYO was obtained for every individual with Down syndrome, regardless of clinical grouping, by subtracting 53.8, the mean age of Alzheimer's disease diagnosis in this population based on previous literature,[3] from the age of each subject. A piecewise linear regression model was fitted to the data using the R *Segmented* package[42] to identify a singular inflection point for each ROI, i.e. a change in the linear relationship between age and volume/thickness. Spearman's correlation tests were performed to assess the association between volume/thickness and CSF biomarker concentrations.

Finally, we derived an optimal multivariate model to differentiate symptomatic Down syndrome (sDS; comprising pDS and dDS) from aDS, based on the best trade-off between fit and model complexity. Model fit and complexity were evaluated using the Akaike information criterion. This model was created initially using the volume/thickness for all ROIs and relevant demographics (age, sex, *APOE* ε4 status, intellectual disability and CSF biomarkers). We then performed a backward stepwise regression to reduce model complexity while maintaining similar model performance until reaching the multivariate model with the lowest Akaike information criterion. The area under the receiver-operating characteristic curve (AUC) was then used to compare the optimal multivariate model with individual MTL regions and CSF biomarkers in their ability to predict the emergence of Alzheimer's disease clinical symptoms by differentiating aDS patients from sDS. DeLong statistics were used to compare the different AUC models directly in their ability to predict Alzheimer's disease staging.

A bilateral *P*-value of ≤0.05 was considered significant for all testing, and Bonferroni corrections were applied in regional volume/thickness analyses to account for multiple comparisons.

Results

Demographics

A total of 413 participants met the inclusion criteria and had the necessary T1w MRI scans and cognitive testing. Fifteen participants with Down syndrome were excluded owing to insufficient T1w image quality or unsatisfactory ASHS segmentation, resulting in the final inclusion of 259 individuals with Down syndrome and 138 healthy controls (see demographics in Table 1; for details on sample size for each biomarker, see Supplementary Table 2).

Participants with Down syndrome were significantly younger [median (IQR) age, 46.97 (12.28) years] than HCs [54.87 (7.99) years, $P < 0.001$] and presented a lower proportion of females (40.93% versus 71.01%, $P < 0.001$). The HC had a higher frequency of *APOE* ε4 carriers than individuals with Down syndrome ($P = 0.04$). As expected, individuals with Down syndrome demonstrated lower values in CSF for the $A\beta_{42}/A\beta_{40}$ ratio and higher concentrations of pTau181 and NfL (all $P < 0.001$). Among individuals with Down syndrome, 149 were classified as aDS, 41 as pDS and 69 as dDS. As expected, there were significant between-group differences in age, CAMCOG-DS scores and CSF biomarkers ($P < 0.001$). However, the distribution of participants by sex, *APOE* ε4 status and intellectual disability did not differ significantly across groups. The quality of raw T1w MRI images, as assessed by the image quality rating metric generated by CAT12, was slightly better in the euploid control group [2.01 (0.24)] compared with the Down syndrome group [2.11 (0.48), $P < 0.001$], but did not differ among subgroups within the Down syndrome cohort ($P = 0.36$). It is worth mentioning, however, that 99.25% of scans had at least a satisfactory quality according to the CAT12 metric, and we visually ensured sufficient quality of MTL structures for segmentation for all participants.

MTL volume and cortical thickness along the Alzheimer's disease clinical continuum

Regional volume/cortical thickness increased progressively with the clinical staging of Alzheimer's disease in Down syndrome, with a significant group effect for all ROIs ($P < 0.001$; Fig. 1 and Supplementary Table 3 for detailed statistical values). Specifically, individuals in the dDS group presented significantly lower volume/thickness than aDS ($P < 0.001$) and pDS (*P*-values between $P = 0.033$ and $P < 0.001$) for all MTL regions. pDS presented lower volume than aDS in the anterior ($P = 0.045$) and posterior ($P < 0.001$) hippocampus, but no significant differences in thickness were found in the ERC ($P = 0.657$), PHC ($P = 0.857$), Br35 ($P = 0.396$) or Br36 ($P = 0.284$). Finally, in comparison to HC, the aDS group

Downloaded from https://academic.oup.com/brain/advance-article/doi/10.1093/brain/awaf133/8115454 by guest on 16 May 2025

Table 1 Participant demographics with neuropsychological assessment and CSF data

Parameter	HC ($n = 138$)	DOWN ($n = 259$)	P-value	aDS ($n = 149$)	pDS ($n = 41$)	dDS ($n = 69$)	P-value*
Age, years, median [IQR]	54.87 [50.79;58.78]	46.97 [39.86;52.14]	<0.001	40.96 [32.25;46.52]	50.53 [47.91;53.17]	53.21 [48.79;56.93]	<0.001[a]
Sex, female	98 (71.01%)	106 (40.93%)	<0.001	56 (37.58%)	19 (46.34%)	31 (44.93%)	0.440
APOE ε4 carriers	39 (28.47%)	46 (18.70%)	0.038	23 (16.08%)	11 (28.21%)	12 (18.75%)	0.227
Intellectual disability							0.082
Mild	–	70 (27.45%)		49 (33.33%)	10 (25.64%)	11 (15.94%)	–
Moderate	–	145 (56.86%)		74 (50.34%)	24 (61.54%)	47 (68.12%)	–
Severe/profound	–	40 (15.69%)		24 (16.33%)	5 (12.82%)	11 (15.94%)	–
CAMCOG-DS, median [IQR]	–	65.50 [47.00;82.00]		75.00 [59.00;85.50]	63.00 [58.00;80.00]	46.00 [33.00;57.00]	<0.001[b]
CSF $A\beta_{42}/A\beta_{40}$ positivity	0 (0.00%)	82 (53.25%)	<0.001	15 (19.23%)	24 (77.42%)	43 (95.56%)	<0.001[a]
CSF biomarkers, pg/ml, median [IQR]							
$A\beta_{42}/A\beta_{40}$ ($n = 243$)	0.11 [0.10;0.11]	0.06 [0.04;0.08]	<0.001	0.08 [0.07;0.10]	0.04 [0.04;0.06]	0.04 [0.04;0.05]	<0.001[c]
pTau181 ($n = 243$)	33.40 [26.00;43.70]	59.35 [24.52;133.55]	<0.001	27.90 [16.62;44.38]	96.30 [59.40;198.75]	142.50 [94.80;199.40]	<0.001[c]
NfL ($n = 240$)	363.78 [299.34;470.26]	580.75 [363.10;946.82]	<0.001	371.58 [208.35;541.12]	705.05 [573.65;932.93]	1246.27 [757.32;1866.00]	<0.001[a]

Data are *n* (%) or median [interquartile range (IQR)]. *APOE* ε4 carriers are defined by the presence of a homozygous or heterozygous ε4 allele. Between-group differences were assessed using χ^2 tests for categorical variables and Mann–Whitney or Kruskal–Wallis tests for continuous variables not following a normal distribution. *P*-value obtained from Mann–Whitney test comparing healthy/euploid controls (HC) and people with Down syndrome (DS); *P*-value* obtained from Kruskal–Wallis tests comparing people with asymptomatic DS (aDS), prodromal DS and DS with Alzheimer's dementia (dDS). $A\beta_{42}/A\beta_{40}$: concentration ratio between amyloid-β peptide 1–42 and amyloid-β peptide 1–40 (pg/ml); APOE = apolipoprotein E; CAMCOG-DS = Cambridge Cognitive Examination for Older Adults with Down Syndrome; NfL = neurofilament light chain concentration (pg/ml); pTau181 = Tau phosphorylated at threonine 181 concentration (pg/ml).

[a]aDS < pDS < dDS.

[b]aDS = pDS < dDS.

[c]aDS < pDS = dDS.

demonstrated a decreased anterior and posterior hippocampal volume ($P < 0.001$), and an increased cortical thickness in the ERC, PHC and Br35 (all $P < 0.001$), but not Br36 ($P = 0.929$). The increased cortical thickness in comparison to HC was also visible at the prodromal and dementia stages in the PHC ($P < 0.001$) and Br35 ($P = 0.049$). Results using volume rather than cortical thickness were overall very similar (Supplementary Fig. 2 and Supplementary Table 3), except for Br36, where a reduction of volume was evident in aDS and pDS compared with HC ($P < 0.001$ for both), and in pDS compared with aDS ($P = 0.03$). We observed increased cortical volume in the ERC, PHC and Br35 in aDS compared with HC (all $P < 0.001$).

MTL volume and cortical thickness changes with EYO

A decrease in volume and cortical thickness with EYO of Alzheimer's disease was detected across all MTL regions and started years before onset of symptoms (Fig. 2). Using piecewise linear regression models, we determined a change in the linear relationship between EYO and ERC thickness 15.7 years before the mean age of Alzheimer's disease dementia in Down syndrome (53.8 years), followed by the posterior hippocampal volume (EYO = −13.5), Br35 thickness (EYO = −13), the anterior hippocampal volume (EYO = −11.5) and, finally, the PHC (EYO = −9.8) and Br36 (EYO = −9). The morphology of the association varied across ROIs. The posterior hippocampus showed a continuous decrease in volume with EYO, whereas the ERC and PHC first showed an increase, and then a decrease in cortical thickness with EYO. The anterior hippocampus, Br35 and Br36 had an intermediate profile, with limited changes for many years, followed by a steep decline. The pattern of results was similar when using volume rather than thickness for ERC, PHC, Br35 and Br36, with only minor differences for the inflection points (Supplementary Fig. 3). Importantly, the relationship between MTL and EYO was minimally influenced by the W-score transformation. Indeed, results were highly consistent across multiple models, including using raw values, or W-score adjusted or not by age, age squares or *APOE* ε4 status (Supplementary Fig. 4). Inflection points were also remarkably stable across conditions, except for the PHC and Br36 for the model with *APOE* ε4 status.

Relationship of regional volumes and cortical thickness to CSF biomarkers of Alzheimer's disease

CSF $A\beta_{42}/A\beta_{40}$ showed a significant positive correlation with both anterior and posterior hippocampal volumes (anterior hippocampus, $\rho = 0.34$; posterior hippocampus, $\rho = 0.55$, $P < 0.001$), but no other structures (Fig. 3). There was a negative correlation between CSF pTau181 and both hippocampal volumes (anterior hippocampus, $\rho = -0.34$; posterior hippocampus, $\rho = -0.54$, $P < 0.001$) and ERC thickness ($\rho = -0.17$, $P = 0.034$). Finally, CSF NfL showed negative correlations with anterior and posterior hippocampal volumes (anterior hippocampus, $\rho = -0.34$; posterior hippocampus, $\rho = -0.5$, $P < 0.001$) and Br36 thickness ($\rho = -0.23$, $P = 0.006$; Fig. 3). See Supplementary Table 4 for full details of all correlation coefficients and their corresponding *P*-values. When using volume instead of thickness (Supplementary Fig. 5), additional significant associations were found. Specifically, pTau181 showed a significant negative association with PHC ($\rho = -0.16$, $P > 0.001$), Br35 ($\rho = -0.19$, $P = 0.018$) and Br36 ($\rho = -0.18$, $P = 0.027$). Likewise, NfL was negatively correlated with ERC ($\rho = -0.17$, $P = 0.045$), PHC ($\rho = -0.17$, $P = 0.041$) and Br35 ($\rho = -0.19$, $P = 0.024$).

Downloaded from https://academic.oup.com/brain/advance-article/doi/10.1093/brain/awaf133/8115454 by guest on 16 May 2025

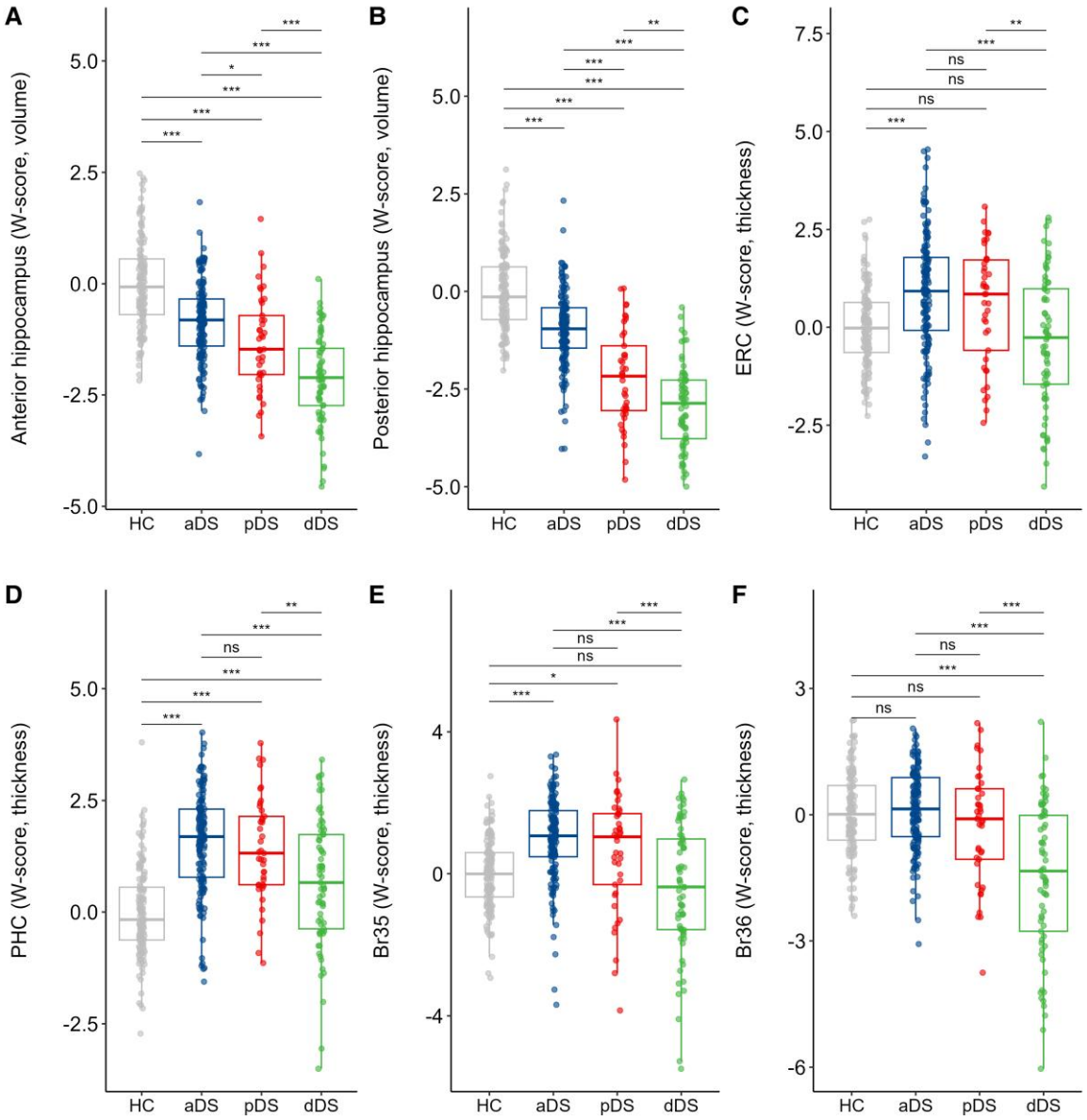

Figure 1 Regional volume and cortical thickness of medial temporal lobe structures across the Alzheimer's disease continuum. Box plots represent the effect of clinical groups on the W-score (age-, sex- and ICV-adjusted volume or thickness) of the anterior (**A**) and posterior (**B**) hippocampus, ERC (**C**), PHC (**D**), Br35 (**E**) and Br36 (**F**). For each boxplot, the box represents the interquartile range, the band represents the median value, and the dots represent individual values. Significance is set at $P < 0.05$ using the Bonferroni correction. *$P < 0.05$; **$P < 0.01$ and ***$P < 0.001$. aDS = asymptomatic DS; Br = Brodmann area; dDS = DS with Alzheimer's dementia; DS = Down syndrome; ERC = entorhinal cortex; HC = healthy/euploid controls; ICV = total intracranial volume; ns = no significance; pDS = prodromal DS; PHC = parahippocampal cortex.

Predicting clinical Alzheimer's disease staging using regional MTL volumes and cortical thickness

Among regional volumes and cortical thickness of the MTL, the posterior hippocampus [AUC 86.32, 95% confidence interval (CI) 79.93, 92.71] showed the highest accuracy to differentiate between asymptomatic ($n = 73$) and symptomatic ($n = 65$) individuals, followed by the anterior hippocampus (AUC 74.96, 95%CI 66.62, 83.30), Br36 (AUC 66.98, 95%CI 57.75, 76.21) and Br35 (AUC 66.34, 95%CI 57.12, 75.57) (Fig. 4; for more details, see Supplementary Table 5). Backward stepwise regression showed that the optimal multivariate model to differentiate aDS from sDS, based on a trade-off between fit and model complexity, included the posterior hippocampus, age, CSF pTau181 and the PHC (AUC 96.38, 95%CI 93.64, 99.11) (Fig. 4). This optimal model outperformed the models including the posterior hippocampus (AUC 96.38 versus AUC 86.32, $P = 0.005$), CSF pTau181 (AUC 96.38 versus AUC 89.88, $P = 0.032$) or NfL (AUC 96.38 versus AUC 88.77, $P = 0.015$) and presented a trend for significantly better performances compared with CSF $A\beta_{42}/A\beta_{40}$ (AUC 96.38 versus AUC 90.41, $P = 0.056$; Supplementary Table 6).

Discussion

In the present study, we used a novel segmentation approach in a large, well-characterized cohort to address the knowledge gap

Downloaded from https://academic.oup.com/brain/advance-article/doi/10.1093/brain/awaf133/8115454 by guest on 16 May 2025

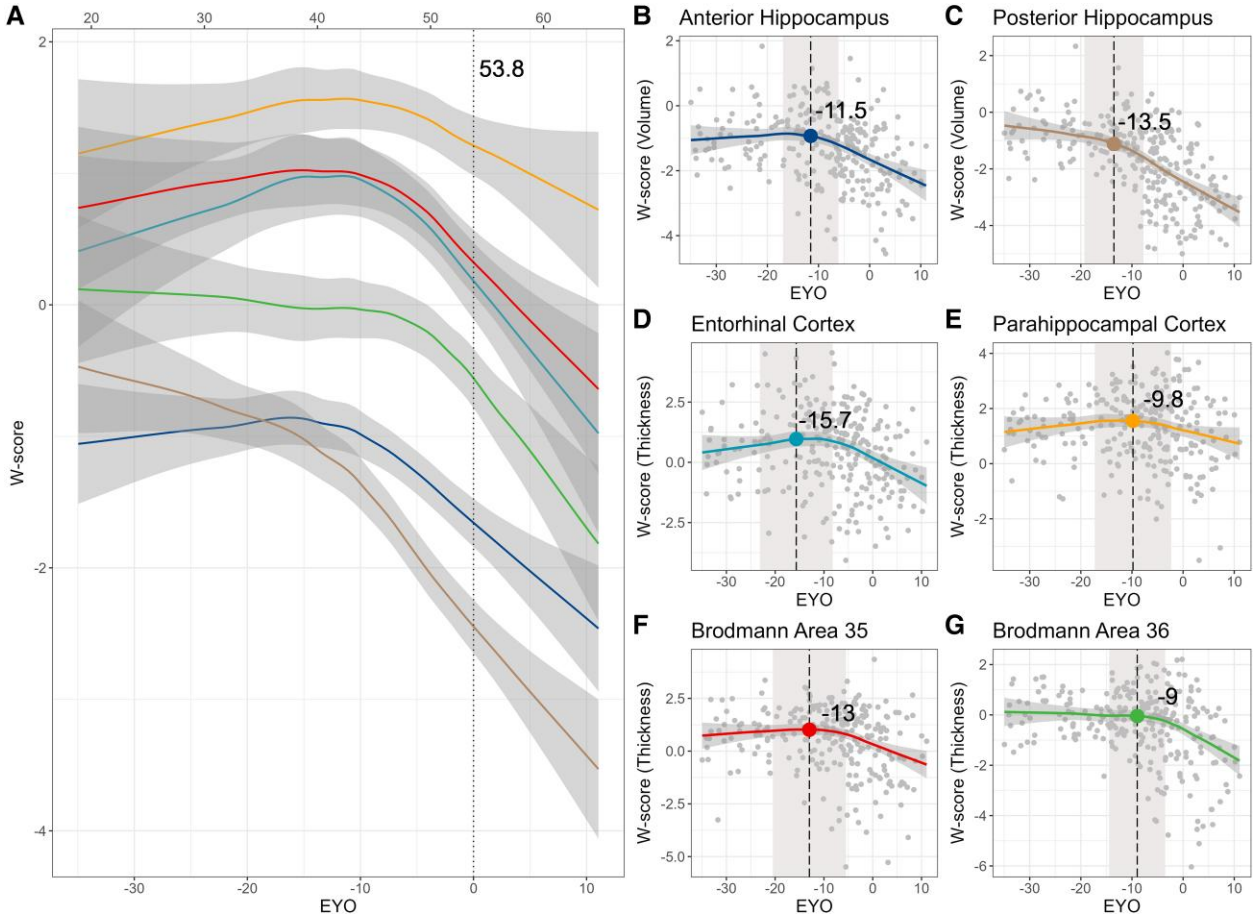

Figure 2 Regional volume and cortical thickness of medial temporal lobe structures along EYO in individuals with Down syndrome. (**A**) Line plots represent the relationship between W-scores (age-, sex- and ICV-adjusted volume or thickness) against the estimated age of onset (EYO: 53.8 years) of Alzheimer's disease in Down syndrome. The anterior (**B**) and posterior (**C**) hippocampus, entorhinal cortex (**D**), parahippocampal cortex (**E**), Brodmann area 35 (**F**) and Brodmann area 36 (**G**) are depicted individually. Lines were computed using estimated scatterplot smoothing (LOESS) curves. Shaded areas represent the 95% confidence interval. Points represent linear model inflection values, computed against EYO. Colour indicates each region of the medial temporal lobe. EYO = estimated years from symptom onset; ICV = total intracranial volume.

surrounding the evolution of volumes and cortical thickness of the MTL, a key site of early Alzheimer's disease neuropathology, in Down syndrome. We found that MTL volumes and cortical thickness decreased with EYO and advancing Alzheimer's disease stages in Down syndrome. Specifically, we identified the ERC and posterior hippocampus as the regions showing the earliest structural loss in Down syndrome, with a decrease in volumes and cortical thickness starting at ages 38–40 years, 15–13 years before onset of Alzheimer's symptoms. We also demonstrated the utility of posterior hippocampal volume in differentiating between asymptomatic individuals and those with symptomatic Alzheimer's disease in Down syndrome. Posterior hippocampal volume demonstrated a similar performance to CSF biomarkers of Alzheimer's disease pathology to detect symptomatic Down syndrome, and it presented a very high predictive value to detect symptomatic Down syndrome when combined with CSF pTau181, PHC thickness and age. Finally, our results indicated non-linear structural changes with EYO, with some MTL structures showing an initial period of increased cortical thickness before their subsequent thinning. Taken together, this study is the first to characterize the progressive non-linear involvement of the MTL across all clinical stages of Alzheimer's disease in the context of Down syndrome and helps to establish the utility of MTL subregions, including the posterior hippocampus, as reliable early biomarkers of disease progression.

We observed a progressive loss of volume/thickness of all MTL regions with advancing Alzheimer's disease stage. Individuals with Alzheimer's dementia showed significantly lower volumes/thickness than prodromal and asymptomatic adults with Down syndrome, and the prodromal group presented an intermediate profile of atrophy, with significant differences from the aDS in the anterior and posterior hippocampus. Our results are consistent with and expand on previous studies showing the specific vulnerability of MTL structures in autosomal dominant Alzheimer's disease[43,44] and Alzheimer's disease in Down syndrome[18-20,45] by including a large cohort of Down syndrome covering all clinical stages of Alzheimer's disease and assessing multiple MTL subregions. Very few studies have previously examined the integrity of MTL regions, beyond the hippocampus, in the pDS group.[5,46] One study reported thickening in the left but not the right ERC in a small sample of pDS ($n = 18$).[47] Here, we assessed the thickness bilaterally, and we did not find differences in volume or thickness in ERC between pDS and aDS. Differences were also not found when considering the left and right ERC separately ($P > 0.05$, data not shown). This discrepancy might be explained by the methods

Downloaded from https://academic.oup.com/brain/advance-article/doi/10.1093/brain/awaf133/8115454 by guest on 16 May 2025

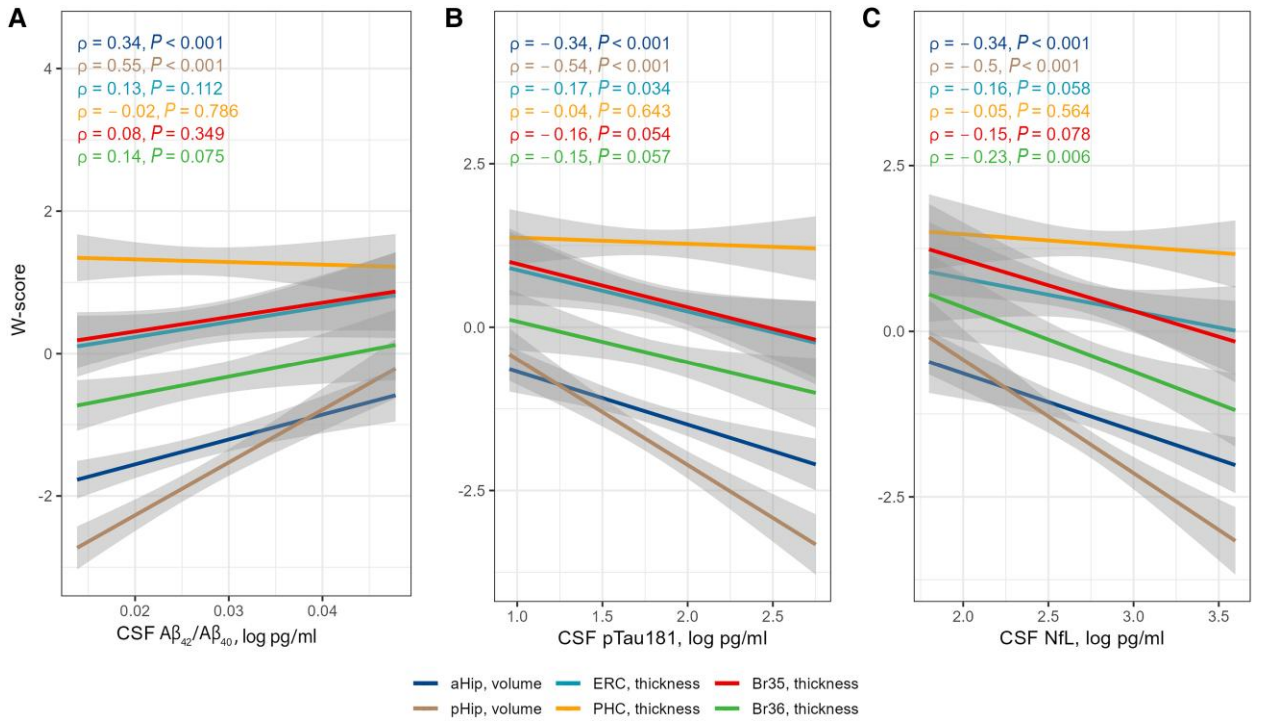

Figure 3 Associations between regional volume and cortical thickness of the medial temporal lobe and CSF biomarkers of Alzheimer's disease. Plots show the association between W-scores (age-, sex- and ICV-adjusted volume or thickness) of the medial temporal lobe and CSF $A\beta_{42}/A\beta_{40}$ (**A**), CSF pTau181 (**B**) and CSF NfL (**C**). The ρ and *P*-values were obtained using Spearman correlation. Colour indicates each region of the medial temporal lobe. Shaded areas represent the 95% confidence interval. CSF markers are log10 scaled. ρ = Spearman correlation coefficient; $A\beta_{42}/A\beta_{40}$ = concentration ratio between amyloid-β peptide 1–42 and amyloid-β peptide 1–40 (in pg/ml); aHip = anterior hippocampus; Br = Brodmann area; ERC = entorhinal cortex; ICV = total intracranial volume; NfL = neurofilament light chain concentration (in pg/ml); PHC = parahippocampal cortex; pHip = posterior hippocampus; pTau181 = tau phosphorylated at threonine 181 concentration (in pg/ml).

used to segment this structure (Freesurfer versus ASHS) and adjust confounding variables or by the clinical stage of the prodromal cases (i.e. early versus late prodromal stage).

To characterize the trajectory of the volume/thickness further, we used a continuous measure of Alzheimer's disease stage, the EYO. Individuals with Down syndrome display a reliable accumulation of pathology across their lives,[2] and the EYO for Alzheimer's disease symptoms presents the same variability in Down syndrome as in autosomal dominant Alzheimer's disease.[3] Therefore, EYO is considered a valid estimator of Alzheimer's disease-related processes and has been used successfully to assess the dynamic of brain and fluid biomarkers along the Alzheimer's disease course in Down syndrome.[6,7] The results confirmed a decreased integrity with advancing EYO across all regions of the MTL in Down syndrome, despite regional differences in trend morphology. Importantly, we established the ERC to be the first region to show a linear changepoint towards an accelerated rate of atrophy, ∼15 years before the mean age of Alzheimer's disease diagnosis in Down syndrome (i.e. 53.8 years),[3] followed by the posterior hippocampus and Br35, the anterior hippocampus and, finally, the PHC and Br36 at ∼45 years of age, ∼9 years before mean onset. This pattern is largely in line with staging in prior longitudinal studies in sporadic Alzheimer's disease, which also show early volume loss in the posterior hippocampus and ERC,[16,48] and studies in autosomal dominant Alzheimer's disease that demonstrated a decrease in hippocampal volumes at −5 to −15 EYO.[49-53] Our results are also in agreement with the sequential pattern of tau deposition,[6,9,54] which begins in the ERC and transentorhinal regions at around −20 EYO (∼30 years of age) in Down syndrome, before spreading into the hippocampus and temporal cortex. Tau pathology is tightly related to neurodegeneration at post-mortem examination and to grey matter atrophy *in vivo*.[10,12,13] Thus, our results suggest that structural MRI, many years before symptom onset, can detect changes in volume/thickness in Down syndrome likely to be related to the early tau deposition.

Using LOESS curves and piecewise linear regression, we modelled the non-linear association with EYO to identify different trajectory types. The posterior hippocampus presented a progressively decreased volume with EYO, whereas the anterior hippocampus, Br35 and Br36 showed limited structural changes for many years, followed by a steep decline. Previous literature concerning the effect of age on MTL atrophy has reported relatively contradictory results in Down syndrome. Beacher *et al.*[55] found a lack of age-related atrophy of the hippocampus in non-demented individuals with Down syndrome, whereas other studies have found evidence for hippocampal and parahippocampal atrophy preceding symptom onset[56-58] and diffuse cortical atrophy starting at an early age.[59] These conflicting results might be explained, in part, by the non-linear trajectory of changes in MTL regions and the initial increased volume/thickness in some structures. Indeed, in the ERC and PHC, we found initial age-related increases in cortical thickness until roughly −10 to −15 EYO, after which the thickness trended steeply downwards. This result mirrors previous findings in autosomal dominant Alzheimer's disease[49,60,61] and sporadic Alzheimer's disease,[48,62,63] arguing for a non-linear model of structural changes in Alzheimer's disease, with initial increases of regional cortical thickness, and not the hippocampus, at the preclinical stages, followed by a decreased integrity.[64] Although the

Downloaded from https://academic.oup.com/brain/advance-article/doi/10.1093/brain/awaf133/8115454 by guest on 16 May 2025

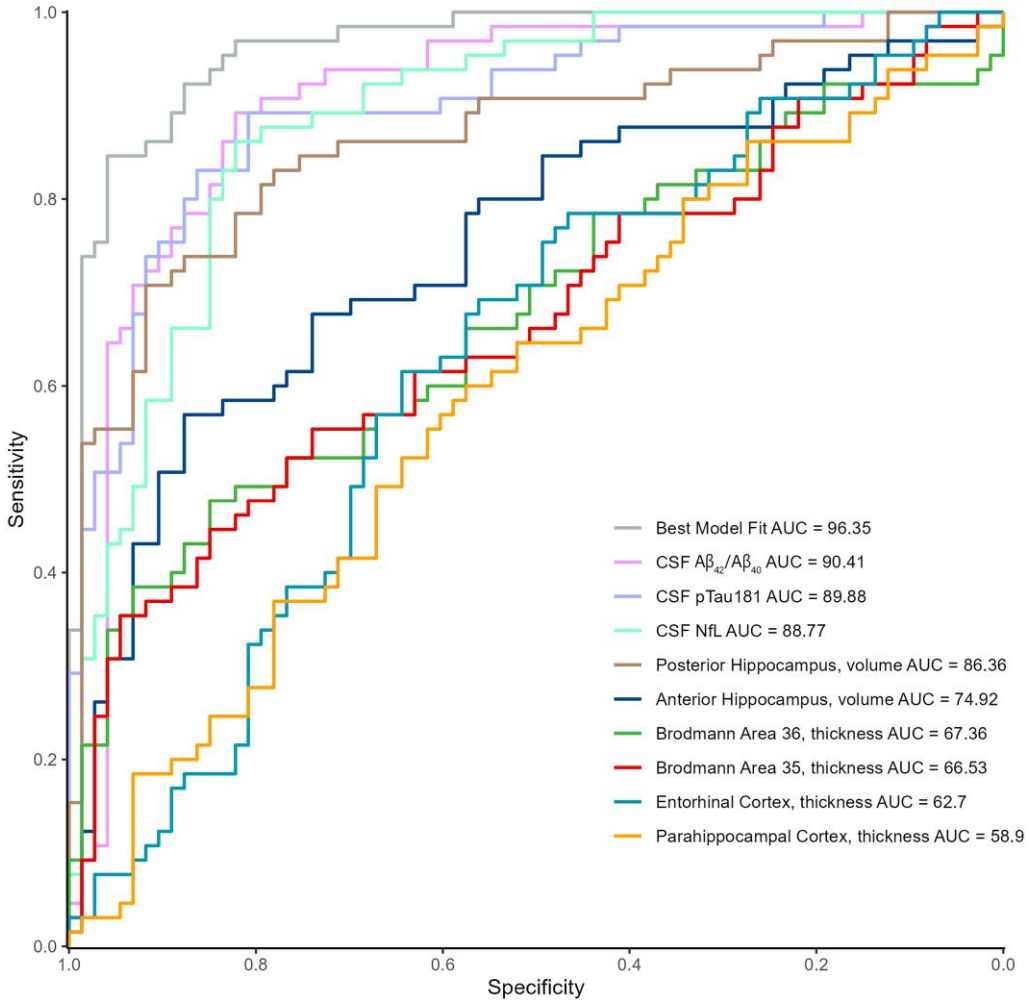

Figure 4 Receiver-operating characteristic curves comparing the multivariate model, CSF biomarkers and medial temporal lobe cortical thickness and volumes in staging Alzheimer's disease. The curves illustrate the performance of each model in distinguishing between asymptomatic ($n = 73$) and symptomatic (prodromal + dementia, $n = 65$) individuals with Down syndrome. The best model fit includes age, pTau181, posterior hippocampus and parahippocampal cortex. Colour indicates different models/biomarkers. $A\beta_{42}/A\beta_{40}$ = concentration ratio between amyloid-β peptide 1–42 and amyloid-β peptide 1–40 (in pg/ml); AUC = area under the curve; NfL = neurofilament light chain concentration (in pg/ml); pTau181 = tau phosphorylated at threonine 181 concentration (in pg/ml).

biological substrate of this initial increase remains uncertain, it has been proposed to be related to the build-up of Aβ and neuroinflammatory changes.[65] In support of this notion, clinical trials of Aβ-lowering therapies have shown cortical thinning as Aβ burden is lowered.[66,67] Neuroinflammation has been found to peak in younger adults with Down syndrome and begins to wane in adults >39 years of age.[68] In our study, this initial increase occurs at a time (approximately −20 EYO, age ∼30 years) when middle-aged individuals with Down syndrome can present with Aβ pathology, oxidative damage and neuroinflammation in the ERC and PHC.[5,9] This timing aligns well with the increased cortical thickness found in autosomal dominant Alzheimer's disease.[1,61] Additional studies are needed to further establish this trend morphology and its biological underpinnings. Of note, the non-linear trajectory of Br35 and ERC, and their changes at the preclinical stage, are likely to explain the lack of significant differences between aDS and pDS groups.

Prior literature has shown hippocampal volume to be useful in categorizing individuals with Down syndrome as having dementia.[69] Moreover, both the hippocampus[20] and global MTL atrophy[19] have been correlated with memory scores in adults with Down syndrome. Our group also reported a steepening decline in hippocampal volumes at roughly −13 EYO.[5] Using a larger sample of adults with Down syndrome ($n = 260$ compared with the previous 170, with <50% overlap in cohorts), we replicated our earlier findings and additionally revealed that structural changes in the posterior hippocampus occur before those in the anterior part. We also demonstrated that, among all subregions of the MTL, the posterior hippocampus showed the best ability to predict aDS versus sDS grouping, followed by the anterior hippocampus and Br36. The posterior hippocampus also performed in a similar manner to established CSF biomarkers in categorizing sDS, with an AUC of 86. The higher predictive value of this structure might be explained, in part, by the early decline and relatively linear associations with EYO. In the euploid population, Xie *et al.*[16] found the posterior hippocampus among the areas to demonstrate the largest longitudinal atrophy in preclinical Alzheimer's disease. Other studies have also found the area including the posterior hippocampus

Downloaded from https://academic.oup.com/brain/advance-article/doi/10.1093/brain/awaf133/8115454 by guest on 16 May 2025

to be atrophied in early prodromal stages.[70] It is also possible that the segmentation quality contributed to the high performances of the posterior hippocampus volume, because this region is typically well and reliably segmented.[29]

We also derived an optimized multivariate model, which included age, CSF pTau181, the volume of the posterior hippocampus and the thickness of the PHC. This multivariate model showed a superior performance in comparison to individual ROIs and traditional CSF biomarkers. These findings suggest that the inclusion of MRI-derived markers can be useful to improve the prediction of Alzheimer's disease clinical status in adults with Down syndrome. These metrics provide a snapshot of the degenerative process in the MTL and are therefore complementary to CSF biomarkers reflecting ongoing biochemical and pathological changes. To date, this is the first time that a study has compared the diagnostic value of MRI versus CSF biomarkers for Alzheimer's disease clinical status in the context of Down syndrome. Previous investigations combining neuroimaging and fluid biomarkers in the euploid population have reported that the best model to predict Alzheimer's dementia onset within 4 years includes plasma biomarkers, *APOE* ε4 status, clinical variables and the cortical thickness in the Alzheimer's disease signature regions, yielding superior diagnostic prediction of Alzheimer's dementia compared with memory clinic physicians.[71] Thus, incorporating topographic information related to neurodegeneration can fine-tune the prediction of cognitive status and cognitive decline in Alzheimer's disease. These findings remain to be validated in the Down syndrome population, but a multifactorial prediction model would presumably provide even greater value in a population where symptoms of dementia are often confounded with concurrent intellectual disabilities or medical comorbidities.

The CSF ratio of $A\beta_{42}/A\beta_{40}$ is an important established marker of Alzheimer's disease that can be detected early in disease progression, before dementia onset.[72] As expected, significant positive correlations were found between CSF $A\beta_{42}/A\beta_{40}$ and hippocampal volumes in adults with Down syndrome. CSF pTau181 and CSF NfL, two markers of tau intracellular neurofibrillary tangle pathology and neurodegeneration, were likewise negatively correlated with hippocampal volumes. Thus, our results further confirm that hippocampal volume is a reliable biomarker of Alzheimer's disease pathological processes in Down syndrome. Additionally, CSF NfL was closely correlated with Br36 thickness ($P = 0.008$), while Br35 and the ERC trended towards significance ($P = 0.088$ and $P = 0.061$, respectively). Prior research in Down syndrome has found a close association between plasma NfL, MTL grey matter and memory scores.[47] CSF pTau181 was found to be more closely tied to MTL volumes and cortical thickness than CSF $A\beta_{42}/A\beta_{40}$. This is in line with literature that has demonstrated a closer relationship between tau and neurodegeneration than between amyloid and neurodegeneration.[10,73,74] Interestingly, despite other subregions trending towards significance, ERC thickness ($P = 0.036$) was the only non-hippocampal area significantly correlated with CSF pTau181, while Aβ showed no significant correlations beyond the hippocampus. This might be attributable to the non-linear nature of atrophy in this population and to the synergistic effect of tau and Aβ pathology[75] on MTL integrity.

In comparison to the euploid control group, individuals with Down syndrome at the asymptomatic stages demonstrated lower adjusted hippocampal volumes, which corroborates previous studies on Down syndrome and suggests a neurodevelopmental abnormality linked to trisomy 21.[18,20,69,76,77] Additionally, aDS showed increased ERC, PHC and Br35 thickness compared with HC. Although few studies have specifically assessed the integrity of MTL structures in Down syndrome, a general increase in cortical thickness and decrease in surface area were described previously in this population.[76,78,79] Some studies have also reported a larger PHC in Down syndrome compared with the euploid population.[80-82] Among other hypotheses, it was proposed that this increased thickness reflects abnormalities in pruning and grey–white matter contrast, which is altered in Down syndrome.[83] Notably, a recent study using 7 T MRI scans found no differences in ERC volumes between young asymptomatic individuals with Down syndrome and HC.[76] However, the young age of this cohort (mean age 24.5 ± 6.5 years) might explain the differences from our results, because ERC volume and thickness increased with age until ~40 years.

The main strength of this study is its large, well-characterized population, with a wide age range and multimodal assessments, allowing us to assess MTL volumetric changes alongside CSF biomarkers. By using W-scores, we took a robust volumetric normalization approach to account for relevant confounding variables, allowing for isolation of Alzheimer's disease pathological effects. Additionally, we explored and compared key MTL subregions, such as Br35 and Br36, in the context of Down syndrome. The usage of ASHS-T1 as a segmentation pipeline helped to overcome various confounds associated with commonly used pipelines, such as Freesurfer, including the common mis-segmentation of the dura mater.[21,29]

Limitations of the study include its cross-sectional design, which prevents testing the sequence of brain changes in the MTL over time and confirming that volume/thickness loss reflects atrophy. Although the uniform development of Alzheimer's disease pathology in Down syndrome[3,84] allows for consistency in large cohorts and helps to ablate some of the limitations inherent to a cross-sectional design, it would be important for longitudinal studies to confirm the progressive pattern of volume/thickness loss over time, in addition to the initial increase observed in some regions. Moreover, we did not use an MTL template specific to the Down syndrome population, and the MTL segmentation was performed on a standard 3 T T1w image. Although visual assessment confirmed appropriate MTL segmentation, studies using higher MRI resolution, as done by Koenig *et al.*,[76] and accounting for the brain morphology in Down syndrome, are necessary to verify our results. Finally, the multivariate predictive model computed in this study should be tested in a validation cohort, because the statistical normalizations risk overfitting the results to one cohort.

Conclusion

In summary, using one of the largest multimodal cohorts worldwide, we demonstrated volume/thickness loss of MTL structures starting ~15 years before onset of Alzheimer's symptoms. The changes in relationship to EYO were not linear and varied in morphology according to the MTL structures. We also reported a progressive decreased integrity of MTL regions with advancing Alzheimer's clinical stages and established a powerful combination of biomarkers to predict the presence of Alzheimer's dementia symptoms in this population. Altogether, our findings underscore the promise of MTL neuroimaging biomarkers to detect early Alzheimer's disease pathological processes in Down syndrome and track disease progression. Longitudinal studies are necessary to assess the effectiveness of these biomarkers in detecting neurodegeneration over time in this population.

Downloaded from https://academic.oup.com/brain/advance-article/doi/10.1093/brain/awaf133/8115454 by guest on 16 May 2025

Data availability

The authors may share de-identified data that underlie the results reported in this article. Data will be available upon receipt of a request detailing the study hypothesis and statistical analysis plan. All requests should be sent to the corresponding authors. The steering committee of this study will discuss all requests and decide, based on the novelty and scientific rigour of the proposal, whether data sharing is appropriate. All applicants will be asked to sign a data access agreement.

Acknowledgements

The authors would like to thank all study participants, their families, and caregivers from the DABNI and SPIN cohorts for their support of, and dedication to, this research. We also acknowledge the Fundació Catalana Síndrome de Down (https://fcsd.org/) for global support.

Funding

This study was funded by the Fondo de Investigaciones Sanitario, Instituto de Salud Carlos III and co-funded by the European Union (PI18/00335 and PI22/00758 to M.C.-I., PI18/00435 and PI22/00611 to D.A., PI14/1561 and PI20/01330 to A.L., PI20/01473 to J.F., PI22/00307 to A.B.), the CIBERNED Program 1, the National Institutes of Health (NIH) (1R01AG056850-01A1; 3RF1AG056850-01S1; AG056850, R21AG056974 and R01AG061566 to J.F.), the Departament de Salut, Generalitat de Catalunya, Fundación Tatiana Pérez de Guzmán el Bueno (IIBSP-DOW-2020-151 to J.F.), the European Union's Horizon 2020, 'MES-CoBraD' (H2020-SC1-BHC-2018-2020/GA 965422 to J.F.), Brightfocus, and Life Molecular Imaging (LMI) to J.F. J.E.A.-I. was supported by Instituto de Salud Carlos III through the Río Hortega Fellowship 'CM22/00219' and co-funded by the European Union. M.C.-I. acknowledges support from the Alzheimer's Association (AARG-22-973966) and Global Brain Health Institute (GBHI_ALZ-18-543740), the Fondation Jérôme Lejeune (#1913 Cycle 2019B), the Societat Catalana de Neurologia (Premi Beca Fundació SCN 2020). M.R.A. acknowledges support from an Alzheimer's Association Research Fellowship to Promote Diversity (AARFD-21-852492). M.R.A. has provided paid consultancy for Veranex. M.R.A. is a partner and director of production at Masima—Soluções em Imagens Médicas LTDA. L.V.-A. was supported by Instituto de Salud Carlos III through the Sara Borrell Fellowship 'CD23/00235'. J.A. was supported by Instituto de Salud Carlos III through the Río Hortega Fellowship 'CM21/00243' and co-funded by the European Union. I.R.-B. was supported by Instituto de Salud Carlos III through the Río Hortega Fellowship 'CM22/00052' and co-funded by the European Union. L.M.B. was supported by Instituto de Salut Carlos III through the Río Hortega Fellowhip 'CM23/00291' and co-funded by the European Union. A.B. acknowledges support from Instituto de Salud Carlos III through the Miguel Servet grant 'CP20/00038' and co-funded by the European Union, and the Alzheimer's Association 'AARG-22-923680'. The sponsors had no role in the design and conduct of the study; collection, management, analysis and interpretation of the data; preparation, review or approval of the manuscript; or decision to submit for publication.

Competing interests

M.R.A. has provided paid consultancy for Veranex and is a partner and director of production at Masima—Soluções em Imagens Médicas LTDA. D.A. reported receiving personal fees for advisory board services and/or speaker honoraria from Fujirebio-Europe, Roche, Nutricia, Krka Farmacéutica, Lilly, Zambon S.A.U., Grifols and Esteve, outside the submitted work. A.L. has served as a consultant or on advisory boards for Fujirebio-Europe, NovoNordisk, Roche, Biogen, Grifols, Novartis, Eisai, Lilly and Nutricia, outside the submitted work. J.F. reported serving on the advisory boards, adjudication committees or receiving speaker honoraria from Roche, NovoNordisk, Esteve, Biogen, Laboratorios Carnot, Adamed, LMI, Novartis, Lundbeck, Roche, AC Immune, Alzheon, Zambon, Lilly, Spanish Neurological Society, T21 Research Society, Lumind Foundation, Jérôme-Lejeune Foundation, Alzheimer's Association, USA National Institutes of Health, and Instituto de Salud Carlos III. D.A., A.L. and J.F. report holding a patent for markers of synaptopathy in neurodegenerative disease (licensed to ADx, EPI8382175.0). The other authors report no competing interests.

Supplementary material

Supplementary material is available at *Brain* online.

References

1. Antonarakis SE, Skotko BG, Rafii MS, et al. Down syndrome. *Nat Rev Dis Primers*. 2020;6:9.
2. Fortea J, Zaman SH, Hartley S, Rafii MS, Head E, Carmona-Iragui M. Alzheimer's disease associated with Down syndrome: A genetic form of dementia. *Lancet Neurol*. 2021;20:930-942.
3. Iulita MF, Chavez DG, Christensen MK, et al. Association of Alzheimer disease with life expectancy in people with Down syndrome. *JAMA Netw Open*. 2022;5:e2212910.
4. Knopman DS, Amieva H, Petersen RC, et al. Alzheimer disease. *Nat Rev Dis Primers*. 2021;7:33.
5. Fortea J, Vilaplana E, Carmona-Iragui M, et al. Clinical and biomarker changes of Alzheimer's disease in adults with Down syndrome: A cross-sectional study. *The Lancet*. 2020;395:1988-1997.
6. Wisch JK, McKay NS, Boerwinkle AH, et al. Comparison of tau spread in people with Down syndrome versus autosomal-dominant Alzheimer's disease: A cross-sectional study. *Lancet Neurol*. 2024;23:500-510.
7. Boerwinkle AH, Gordon BA, Wisch J, et al. Comparison of amyloid burden in individuals with Down syndrome versus autosomal dominant Alzheimer's disease: A cross-sectional study. *Lancet Neurol*. 2023;22:55-65.
8. Head E, Lott IT, Wilcock DM, Lemere CA. Aging in Down syndrome and the development of Alzheimer's disease neuropathology. *Curr Alzheimer Res*. 2015;13:18-29.
9. Davidson YS, Robinson A, Prasher VP, Mann DM. The age of onset and evolution of Braak tangle stage and Thal amyloid pathology of Alzheimer's disease in individuals with Down syndrome. *Acta Neuropathol Commun*. 2018;6:56.
10. La Joie R, Visani AV, Baker SL, et al. Prospective longitudinal atrophy in Alzheimer's disease correlates with the intensity and topography of baseline tau-PET. *Sci Transl Med*. 2020;12:eaau5732.
11. Bejanin A, Schonhaut DR, La Joie R, et al. Tau pathology and neurodegeneration contribute to cognitive impairment in Alzheimer's disease. *Brain*. 2017;140:3286-3300.
12. Nelson PT, Alafuzoff I, Bigio EH, et al. Correlation of Alzheimer disease neuropathologic changes with cognitive status: A review of the literature. *J Neuropathol Exp Neurol*. 2012;71:362-381.
13. Schöll M, Lockhart SN, Schonhaut DR, et al. PET imaging of tau deposition in the aging human brain. *Neuron*. 2016;89:971-982.

Downloaded from https://academic.oup.com/brain/advance-article/doi/10.1093/brain/awaf133/8115454 by guest on 16 May 2025

14. Jack CR, Petersen RC, Xu YC, et al. Medial temporal atrophy on MRI in normal aging and very mild Alzheimer's disease. *Neurology*. 1997;49:786-794.
15. Whitwell JL, Przybelski SA, Weigand SD, et al. 3D maps from multiple MRI illustrate changing atrophy patterns as subjects progress from mild cognitive impairment to Alzheimer's disease. *Brain*. 2007;130:1777-1786.
16. Xie L, Wisse LE, Das SR, et al. Longitudinal atrophy in early Braak regions in preclinical Alzheimer's disease. *Hum Brain Mapp*. 2020;41:4704-4717.
17. Nieuwenhuis-Mark RE. Diagnosing Alzheimer's dementia in Down syndrome: Problems and possible solutions. *Res Dev Disabil*. 2009;30:827-838.
18. Carmona-Iragui M, Balasa M, Benejam B, et al. Cerebral amyloid angiopathy in Down syndrome and sporadic and autosomal-dominant Alzheimer's disease. *Alzheimers Dement*. 2017;13: 1251-1260 .
19. Benejam B, Aranha MR, Videla L, et al. Neural correlates of episodic memory in adults with Down syndrome and Alzheimer's disease. *Alzheimers Res Ther*. 2022;14:123.
20. Pujol J, Fenoll R, Ribas-Vidal N, et al. A longitudinal study of brain anatomy changes preceding dementia in Down syndrome. *Neuroimage Clin*. 2018;18:160-166.
21. Xie L, Wisse LEM, Das SR, et al. Accounting for the confound of meninges in segmenting entorhinal and perirhinal cortices in T1-weighted MRI. *Med Image Comput Comput Assist Interv*. 2016; 9901:564-571.
22. Alcolea D, Clarimón J, Carmona-Iragui M, et al. The Sant Pau initiative on neurodegeneration (SPIN) cohort: A data set for biomarker discovery and validation in neurodegenerative disorders. *Alzheimers Dement (N Y)*. 2019;5:597-609.
23. Devenny DA, Zimmerli EJ, Kittler P, Krinsky-McHale SJ. Cued recall in early-stage dementia in adults with Down's syndrome. *J Intellect Disabil Res*. 2002;46:472-483.
24. Rojas Gil AM, Sánchez Arenas RL. Validez y confiabilidad de una prueba para evaluar comportamientos lingüísticos en población con discapacidad cognitiva. *Revista de Logopedia, Foniatria y Audiologia*. 2016;36:117-126.
25. Esteba-Castillo S, Dalmau-Bueno A, Ribas-Vidal N, Vilà-Alsina M, Novell-Alsina R, García-Alba J. Adaptation and validation of CAMDEX-DS (Cambridge examination for mental disorders of older people with Down's syndrome and others with intellectual disabilities) in Spanish population with intellectual disabilities. *Revista de Neurología*. 2013;57:337-346.
26. Regier DA, Kuhl EA, Kupfer DJ. The DSM-5: Classification and criteria changes. *World Psychiatry*. 2013;12:92-98.
27. Morris JC. The clinical dementia rating (CDR) current version and scoring rules. *Neurology*. 1993;43:2412-2414.
28. Dahnke R, Ziegler G, Grosskreutz J, Gaser C. Retrospective quality assurance of MR images. In: Poster presented at: 19th Annual Meeting of the Organization for Human Brain Mapping, 2013 June.
29. Xie L, Wisse LEM, Pluta J, et al. Automated segmentation of medial temporal lobe subregions on in vivo T1-weighted MRI in early stages of Alzheimer's disease. *Hum Brain Mapp*. 2019;40:3431-3451.
30. Yushkevich P, Xie L, Wisse L, et al. Mapping medial temporal lobe longitudinal change in preclinical Alzheimer's disease. *Alzheimers Dement*. 2023; 19:e081898.
31. Yushkevich PA, Ittyerah R, Li Y, et al. Morphometry of medial temporal lobe subregions using high-resolution T2-weighted MRI in ADNI3: Why, how, and what's next? *Alzheimers Dement*. 2024;20:8113-8128.
32. Huntenburg JM, Steele CJ, Bazin P-L. Nighres: Processing tools for high-resolution neuroimaging. *GigaScience*. 2018;7:giy082.
33. Han X, Pham DL, Tosun D, Rettmann ME, Xu C, Prince JL. CRUISE: Cortical reconstruction using implicit surface evolution. *NeuroImage*. 2004;23:997-1012.
34. Orlhac F, Eertink JJ, Cottereau A-S, et al. A guide to ComBat harmonization of imaging biomarkers in multicenter studies. *J Nucl Med*. 2022;63:172-179.
35. Canada KL, Saifullah S, Gardner JC, et al. Development and validation of a quality control procedure for automatic segmentation of hippocampal subfields. *Hippocampus*. 2023;33: 1048-1057.
36. Chung J, Yoo K, Lee P, et al. Normalization of cortical thickness measurements across different T1 magnetic resonance imaging protocols by novel W-score standardization. *Neuroimage*. 2017; 159:224-235.
37. Bejanin A, Murray ME, Martin P, et al. Antemortem volume loss mirrors TDP-43 staging in older adults with non-frontotemporal lobar degeneration. *Brain*. 2019;142:3621-3635.
38. Montal V, Vilaplana E, Pegueroles J, et al. Biphasic cortical macro- and microstructural changes in autosomal dominant Alzheimer's disease. *Alzheimers Dement*. 2021;17:618-628.
39. Fortea J, Carmona-Iragui M, Benejam B, et al. Plasma and CSF biomarkers for the diagnosis of Alzheimer's disease in adults with Down syndrome: A cross-sectional study. *Lancet Neurol*. 2018;17:860-869.
40. Alcolea D, Pegueroles J, Munoz L, et al. Agreement of amyloid PET and CSF biomarkers for Alzheimer's disease on lumipulse. *Ann Clin Transl Neurol*. 2019;6:1815-1824.
41. Subirana I, Sanz H, Vila J. Building bivariate tables: The compareGroups package for R. *J Stat Softw*. 2014;57:1-16.
42. Muggeo VM. Segmented: An R package to fit regression models with broken-line relationships. *R News*. 2008;8:20-25.
43. Benzinger TLS, Blazey T, Jack CR, et al. Regional variability of imaging biomarkers in autosomal dominant Alzheimer's disease. *Proc Natl Acad Sci U S A*. 2013;110:E4502-E4509.
44. Fleisher AS, Chen K, Quiroz YT, et al. Associations between biomarkers and age in the presenilin 1 E280A autosomal dominant Alzheimer disease kindred: A cross-sectional study. *JAMA Neurol*. 2015;72:316-324.
45. Mullins D, Daly E, Simmons A, et al. Dementia in Down's syndrome: An MRI comparison with Alzheimer's disease in the general population. *J Neurodev Disord*. 2013;5:19.
46. Rozalem Aranha M, Iulita MF, Montal V, et al. Basal forebrain atrophy along the Alzheimer's disease continuum in adults with Down syndrome. *Alzheimers Dement*. 2023;19:4817-4827.
47. DiProspero N, Sathishkumar M, Janecek J, et al. Neurofilament light chain concentration mediates the association between regional medial temporal lobe structure and memory in adults with Down syndrome. *Alzheimers Dement (Amst)*. 2024;16:e12542.
48. Chauveau L, Kuhn E, Palix C, et al. Medial temporal lobe subregional atrophy in aging and Alzheimer's disease: A longitudinal study. *Front Aging Neurosci*. 2021;13:750154.
49. Kinnunen KM, Cash DM, Poole T, et al. Presymptomatic atrophy in autosomal dominant Alzheimer's disease: A serial magnetic resonance imaging study. *Alzheimers Dement*. 2018;14:43-53.
50. McDade E, Wang G, Gordon BA, et al. Longitudinal cognitive and biomarker changes in dominantly inherited Alzheimer disease. *Neurology*. 2018;91:e1295-e1306.
51. Sanchez JS, Hanseeuw BJ, Lopera F, et al. Longitudinal amyloid and tau accumulation in autosomal dominant Alzheimer's disease: Findings from the Colombia-Boston (COLBOS) biomarker study. *Alzheimers Res Ther*. 2021;13:27.
52. Bateman RJ, Xiong C, Benzinger TL, et al. Clinical and biomarker changes in dominantly inherited Alzheimer's disease. *N Engl J Med*. 2012;367:795-804.

Downloaded from https://academic.oup.com/brain/advance-article/doi/10.1093/brain/awaf133/8115454 by guest on 16 May 2025

53. Gordon BA, Blazey TM, Su Y, et al. Spatial patterns of neuroimaging biomarker change in individuals from families with autosomal dominant Alzheimer's disease: A longitudinal study. *Lancet Neurol*. 2018;17:241-250.
54. Braak H, Thal DR, Ghebremedhin E, Del Tredici K. Stages of the pathologic process in Alzheimer disease: Age categories from 1 to 100 years. *J Neuropathol Exp Neurol*. 2011;70:960-969.
55. Beacher F, Daly E, Simmons A, et al. Brain anatomy and ageing in non-demented adults with Down's syndrome: An *in vivo* MRI study. *Psychol Med*. 2010;40:611-619.
56. Teipel SJ, Alexander GE, Schapiro MB, Möller HJ, Rapoport SI, Hampel H. Age-related cortical grey matter reductions in non-demented Down's syndrome adults determined by MRI with voxel-based morphometry. *Brain*. 2004;127:811-824.
57. Teipel SJ, Schapiro MB, Alexander GE, et al. Relation of corpus callosum and hippocampal size to age in nondemented adults with Down's syndrome. *Am J Psychiatry*. 2003;160:1870-1878.
58. Krasuski JS, Alexander GE, Horwitz B, Rapoport SI, Schapiro MB. Relation of medial temporal lobe volumes to age and memory function in nondemented adults with Down's syndrome: Implications for the prodromal phase of Alzheimer's disease. *Am J Psychiatry*. 2002;159:74-81.
59. Romano A, Cornia R, Moraschi M, et al. Age-related cortical thickness reduction in non-demented Down's syndrome subjects. *J Neuroimaging*. 2016;26:95-102.
60. Fortea J, Sala-Llonch R, Bartrés-Faz D, et al. Increased cortical thickness and caudate volume precede atrophy in PSEN1 mutation carriers. *J Alzheimers Dis*. 2010;22:909-922.
61. Montal V, Barroeta I, Bejanin A, et al. Metabolite signature of Alzheimer's disease in adults with Down syndrome. *Ann Neurol*. 2021;90:407-416.
62. Pegueroles J, Vilaplana E, Montal V, et al. Longitudinal brain structural changes in preclinical Alzheimer's disease. *Alzheimers Dement*. 2017;13:499-509.
63. Montal V, Vilaplana E, Alcolea D, et al. Cortical microstructural changes along the Alzheimer's disease continuum. *Alzheimers Dement*. 2018;14:340-351.
64. Harrison TM, Du R, Klencklen G, Baker SL, Jagust WJ. Distinct effects of beta-amyloid and tau on cortical thickness in cognitively healthy older adults. *Alzheimers Dement*. 2021;17:1085-1096.
65. Vilaplana E, Rodriguez-Vieitez E, Ferreira D, et al. Cortical microstructural correlates of astrocytosis in autosomal-dominant Alzheimer disease. *Neurology*. 2020;94:e2026-e2036.
66. Fox N, Black R, Gilman S, et al. Effects of Aβ immunization (AN1792) on MRI measures of cerebral volume in Alzheimer disease. *Neurology*. 2005;64:1563-1572.
67. Alves F, Kalinowski P, Ayton S. Accelerated brain volume loss caused by anti-β-amyloid drugs: A systematic review and meta-analysis. *Neurology*. 2023;100:e2114-e2124.
68. Flores-Aguilar L, Iulita MF, Kovecses O, et al. Evolution of neuroinflammation across the lifespan of individuals with Down syndrome. *Brain*. 2020;143:3653-3671.
69. Beacher F, Daly E, Simmons A, et al. Alzheimer's disease and Down's syndrome: An *in vivo* MRI study. *Psychol Med*. 2009;39:675-684.
70. Das SR, Mancuso L, Olson IR, Arnold SE, Wolk DA. Short-term memory depends on dissociable medial temporal lobe regions in amnestic mild cognitive impairment. *Cerebral Cortex*. 2016;26:2006-2017.
71. Palmqvist S, Tideman P, Cullen N, et al. Prediction of future Alzheimer's disease dementia using plasma phospho-tau combined with other accessible measures. *Alzheimers Dement*. 2021;27:1034-1042.
72. Jagust W. Imaging the evolution and pathophysiology of Alzheimer disease. *Nat Rev Neurosci*. 2018;19:687-700.
73. Mitchell TW, Mufson EJ, Schneider JA, et al. Parahippocampal tau pathology in healthy aging, mild cognitive impairment, and early Alzheimer's disease. *Ann Neurol*. 2002;51:182-189.
74. Biel D, Brendel M, Rubinski A, et al. Tau-PET and in vivo Braak-staging as prognostic markers of future cognitive decline in cognitively normal to demented individuals. *Alzheimers Res Ther*. 2021;13:137.
75. Busche MA, Hyman BT. Synergy between amyloid-β and tau in Alzheimer's disease. *Nat Neurosci*. 2020;23:1183-1193.
76. Koenig KA, Oh S-H, Stasko MR, et al. High resolution structural and functional MRI of the hippocampus in young adults with Down syndrome. *Brain Commun*. 2021;3:fcab088.
77. Aylward EH, Li Q, Honeycutt NA, et al. MRI volumes of the hippocampus and amygdala in adults with Down's syndrome with and without dementia. *Am J Psychiatry*. 1999;156:564-568.
78. Levman J, MacDonald A, Baumer N, et al. Structural magnetic resonance imaging demonstrates abnormal cortical thickness in Down syndrome: Newborns to young adults. *Neuroimage Clin*. 2019;23:101874.
79. Lee NR, Adeyemi EI, Lin A, et al. Dissociations in cortical morphometry in youth with Down syndrome: Evidence for reduced surface area but increased thickness. *Cerebral Cortex*. 2015;26:2982-2990.
80. Raz N, Torres IJ, Briggs SD, et al. Selective neuroanatornic abnormalities in Down's syndrome and their cognitive correlates: Evidence from MRI morphometry. *Neurology*. 1995;45:356-366.
81. White NS, Alkire MT, Haier RJ. A voxel-based morphometric study of nondemented adults with Down syndrome. *Neuroimage*. 2003;20:393-403.
82. Kesslak J, Nagata S, Lott I, Nalcioglu O. Magnetic resonance imaging analysis of age-related changes in the brains of individuals with Down's syndrome. *Neurology*. 1994;44:1039-1039.
83. Bletsch A, Mann C, Andrews DS, et al. Down syndrome is accompanied by significantly reduced cortical grey–white matter tissue contrast. *Hum Brain Mapp*. 2018;39:4043-4054.
84. McCarron M, McCallion P, Reilly E, Dunne P, Carroll R, Mulryan N. A prospective 20-year longitudinal follow-up of dementia in persons with Down syndrome. *J Intellect Disabil Res*. 2017;61:843-852.

Downloaded from https://academic.oup.com/brain/advance-article/doi/10.1093/brain/awaf133/8115454 by guest on 16 May 2025

Study 2: Characterization of White Matter Hyperintensities in Down Syndrome

Alejandra O. Morcillo-Nieto[1,*]; Sara E. Zsadanyi[1,*]; Jose E. Arriola-Infante[1]; Maria Carmona-Iragui[1,2,3]; Victor Montal[1,2,4]; Jordi Pegueroles[1,2]; Mateus Rozalem Aranha[1,2]; Lídia Vaqué-Alcázar[1,5]; Concepción Padilla[1,2,6]; Bessy Benejam[3]; Laura Videla[1,2,3]; Isabel Barroeta[1,2]; Susana Fernandez[3]; Miren Altuna[1,2,7]; Sandra Giménez[1,8]; Sofía González-Ortiz[9,10]; Núria Bargalló[10,11]; Laia Ribas[1,2]; Javier Arranz[1]; Soraya Torres[1,2]; Maria Florencia Iulita[1,2]; Olivia Belbin[1,2]; Valle Camacho[9]; Daniel Alcolea[1,2]; Alberto Lleó[1,2]; Juan Fortea[1,2,3]; and Alexandre Bejanin[1,2]

*These authors contributed equally to this work.

[1]Sant Pau Memory Unit, Department of Neurology, Hospital de la Santa Creu i Sant Pau, Biomedical Research Institute Sant Pau, Universitat Autònoma de Barcelona, Barcelona, Spain. [2]Center of Biomedical Investigation Network for Neurodegenerative Diseases (CIBERNED), Madrid, Spain. [3]Barcelona Down Medical Center, Fundació Catalana de Síndrome de Down, Barcelona, Spain. [4]Barcelona Supercomputing Center, Barcelona, Spain. [5]Department of Medicine, Faculty of Medicine and Health Sciences, Institute of Neurosciences, University of Barcelona, Barcelona, Spain. Institut d'Investigacions Biomèdiques August Pi i Sunyer (IDIBAPS), Barcelona, Spain. [6]Estudis de Ciències de la Salut, Universitat Oberta de Catalunya, Barcelona, Spain. [7]Fundación CITA-Alzheimer Fundazia, Donostia, Spain. [8]Multidisciplinary Sleep Unit. Respiratory department. Hospital de la Santa Creu i Sant Pau, Institut d'Investigació Biomèdica Sant Pau (IIB SANT PAU), Barcelona, Spain. [9]Nuclear Medicine Department, Hospital de la Santa Creu i Sant Pau, Universitat Autònoma de Barcelona, Barcelona, Spain. [10]Neuroradiology Section, Radiology Department, Diagnostic Image Center, Hospital Clínic de Barcelona, Universitat de Barcelona, Barcelona, Spain. [11]Magnetic Resonance Image Core Facility, Institut d'Investigacions Biomèdiques August Pi i Sunyer (IDIBAPS), Barcelona, Spain.

Alzheimer's Dement (2024) 20(9):6527-6541 doi: 10.1002/alz.14146
IF (2024) =11.1, Rank= 6/202 in Clinical Neurology, D1

Check for updates

Received: 6 March 2024 | Revised: 20 June 2024 | Accepted: 2 July 2024

DOI: 10.1002/alz.14146

Alzheimer's & Dementia®
THE JOURNAL OF THE ALZHEIMER'S ASSOCIATION

RESEARCH ARTICLE

Characterization of white matter hyperintensities in Down syndrome

Alejandra O. Morcillo-Nieto[1] | Sara E. Zsadanyi[1] | Jose E. Arriola-Infante[1] | Maria Carmona-Iragui[1,2,3] | Victor Montal[1,2,4] | Jordi Pegueroles[1,2] | Mateus Rozalem Aranha[1,2] | Lídia Vaqué-Alcázar[1,5] | Concepción Padilla[1,2,6] | Bessy Benejam[3] | Laura Videla[1,2,3] | Isabel Barroeta[1,2] | Susana Fernandez[3] | Miren Altuna[1,2,7] | Sandra Giménez[1,8] | Sofía González-Ortiz[9] | Núria Bargalló[9,10] | Laia Ribas[1,2] | Javier Arranz[1] | Soraya Torres[1,2] | Maria Florencia Iulita[1,2] | Olivia Belbin[1,2] | Valle Camacho[11] | Daniel Alcolea[1,2] | Alberto Lleó[1,2] | Juan Fortea[1,2,3] | Alexandre Bejanin[1,2]

[1]Sant Pau Memory Unit, Department of Neurology, Hospital de la Santa Creu i Sant Pau, Biomedical Research Institute Sant Pau, Universitat Autònoma de Barcelona, Barcelona, Spain

[2]Center of Biomedical Investigation Network for Neurodegenerative Diseases (CIBERNED), Madrid, Spain

[3]Barcelona Down Medical Center, Fundació Catalana de Síndrome de Down, Barcelona, Spain

[4]Barcelona Supercomputing Center, Barcelona, Spain

[5]Department of Medicine, Faculty of Medicine and Health Sciences, Institute of Neurosciences, University of Barcelona, Barcelona, Spain. Institut d'Investigacions Biomèdiques August Pi i Sunyer (IDIBAPS), Barcelona, Spain

[6]Estudis de Ciències de la Salut, Universitat Oberta de Catalunya, Barcelona, Spain

[7]Fundación CITA-Alzheimer Fundazia, Donostia, Spain

[8]Multidisciplinary Sleep Unit, Respiratory Department, Hospital de la Santa Creu i Sant Pau, Institut d'Investigació Biomèdica Sant Pau (IIB SANT PAU), Barcelona, Spain

[9]Neuroradiology Section, Radiology Department, Diagnostic Image Center, Hospital Clínic de Barcelona, Universitat de Barcelona, Barcelona, Spain

[10]Magnetic Resonance Image Core Facility, Institut d'Investigacions Biomèdiques August Pi i Sunyer (IDIBAPS), Barcelona, Spain

[11]Nuclear Medicine Department, Hospital de la Santa Creu i Sant Pau, Universitat Autònoma de Barcelona, Barcelona, Spain

Correspondence
Alexandre Bejanin, Sant Pau Memory Unit – Department of Neurology, Institut de Recerca Sant Pau, Sant Quintí, 77-79 - 08041 Barcelona, España.
Email: abejanin@santpau.cat

Maria Florencia Iulita affiliation's during article conception and development.

Abstract

INTRODUCTION: In Down syndrome (DS), white matter hyperintensities (WMHs) are highly prevalent, yet their topography and association with sociodemographic data and Alzheimer's disease (AD) biomarkers remain largely unexplored.

METHODS: In 261 DS adults and 131 euploid controls, fluid-attenuated inversion recovery magnetic resonance imaging scans were segmented and WMHs were extracted in concentric white matter layers and lobar regions. We tested

Alejandra O. Morcillo-Nieto and Sara E. Zsadanyi contributed equally to this work and share first authorship.

This is an open access article under the terms of the Creative Commons Attribution-NonCommercial License, which permits use, distribution and reproduction in any medium, provided the original work is properly cited and is not used for commercial purposes.
© 2024 The Author(s). *Alzheimer's & Dementia* published by Wiley Periodicals LLC on behalf of Alzheimer's Association.

Funding information
Instituto de Salud Carlos III and co-funded by the European Union, Grant/Award Numbers: PI18/00335, PI18/00435, PI14/1561, PI20/01330, PI20/01473, PI22/00307; National Institutes of Health (NIH), Grant/Award Numbers: 1R01AG056850-01A1, 3RF1AG056850-01S1, AG056850, R21AG056974, R01AG061566; Horizon 2020, "MES-CoBraD", Grant/Award Numbers: H2020-SC1-BHC-2018-2020, GA 965422; Instituto de Salud Carlos III and co-funded by the European Union through the Predoctoral grant, Grant/Award Number: FI18/00275; Juan de la Cierva fellowship, Grant/Award Number: JDC2022-048492-I; Alzheimer's Association and Global Brain Health Institute, Grant/Award Number: GBHI_ALZ-18-543740; Jérôme Lejeune Foundation; Societat Catalana de Neurologia (Premi Beca Fundació SCN 2020); Alzheimer's Association Research Fellowship to Promote Diversity, Grant/Award Number: AARFD-21-852492; Margarita Salas junior postdoctoral fellowship, Grant/Award Number: UNI/551/2021; Instituto de Salud Carlos III and co-funded by the European Union through the Sara Borrell Postdoctoral Fellowship, Grant/Award Number: CD20/00133; Instituto de Salud Carlos III and co-funded by the European Union through the Río Hortega Fellowship, Grant/Award Numbers: CM22/00219, CM21/00243; Instituto de Salud Carlos III and co-funded by the European Union through the Miguel Servet Fellowship, Grant/Award Number: CP20/00038; Alzheimer's Association, Grant/Award Number: AARG-22-923680; Fundación Tatiana Pérez de Guzmán el Bueno, Grant/Award Number: IIBSP-DOW-2020-151

associations with AD clinical stages, sociodemographic data, cerebrospinal fluid (CSF) AD biomarkers, and gray matter (GM) volume.

RESULTS: In DS, total WMHs arose at age 43 and showed stronger associations with age than in controls. WMH volume increased along the AD continuum, particularly in periventricular regions, and frontal, parietal, and occipital lobes. Associations were found with CSF biomarkers and temporo-parietal GM volumes.

DISCUSSION: WMHs increase 10 years before AD symptom onset in DS and are closely linked with AD biomarkers and neurodegeneration. This suggests a direct connection to AD pathophysiology, independent of vascular risks.

KEYWORDS
Alzheimer's disease, Down syndrome, magnetic resonance imaging, neuroimaging, small vessel disease, white matter hyperintensities

Highlights

- White matter hyperintensities (WMHs) increased 10 years before Alzheimer's disease symptom onset in Down syndrome (DS).
- WMHs were strongly associated in DS with the neurofilament light chain biomarker.
- WMHs were more associated in DS with gray matter volume in parieto-temporal areas.

1 | BACKGROUND

Down syndrome (DS) is a genetic condition caused by an extra copy of chromosome 21 that has been associated with an ultra-high risk of developing Alzheimer's disease (AD), with virtually all individuals with DS showing full-blown AD neuropathology by the age of 40.[1,2] A key factor driving this increased risk is the triplication of the amyloid precursor protein (*APP*) gene, which is necessary and sufficient to cause AD pathology.[3] As a result of the overexpression of *APP*, amyloid beta (Aβ) plaques, a hallmark feature of AD, accumulate early and rapidly in the brain and eventually lead to cognitive impairment and dementia.[4] Thus, DS is currently considered a genetically determined form of AD.[2]

It is increasingly recognized that studying AD in individuals with DS can provide valuable insights into its pathogenesis. Alongside the predictable course of AD,[5] adults with DS present a distinct profile of vascular risk factors from aging in the general population,[6] as they are relatively protected from some conventional age-related vascular risk factors, such as hypertension.[7] Thus, this population provides a unique opportunity to further understand the emergence of cerebrovascular diseases, specifically small vessel disease (SVD), in the context of AD without the confounds of age-related vascular risk factors.

One of the main imaging markers of SVD is white matter hyperintensities (WMHs) of presumed vascular origin.[8] WMHs are areas of increased signal on T2-weighted or fluid-attenuated inversion recovery (FLAIR) magnetic resonance imaging (MRI).[9,10] They can reflect distinct pathological processes related to SVD, including increased interstitial fluid, demyelination, gliosis, loss of fibers and oligodendrocyte precursor cells, and failure of the glymphatic system.[8,11] These lesions are frequently found in healthy older adults and their prevalence and severity increase with age.[12] The occurrence of WMHs is also increased in individuals with sporadic[10,13] and other genetic forms of AD.[14,15] In adults with DS, the prevalence and severity of WMHs are increased in both asymptomatic and symptomatic DS with respect to euploid cognitively unimpaired controls[16] and WMH volume increases along the AD continuum.[17] Altogether, this suggests that these lesions may be related to AD development. However, little is known about the spatial distribution of WMHs in DS, which could provide insight into their etiology. Moreover, to our knowledge, no study has yet

15525279, 0, Downloaded from https://alz-journals.onlinelibrary.wiley.com/doi/10.1002/alz.14146 by Bejamin Alexandre - Readcube (Labtiva Inc.) , Wiley Online Library on [01/08/2024]. See the Terms and Conditions (https://onlinelibrary.wiley.com/terms-and-conditions) on Wiley Online Library for rules of use; OA articles are governed by the applicable Creative Commons License

assessed the relationships between WMHs and fluid and neuroimaging biomarkers of AD in DS.

In the present study, we aimed to better characterize WMHs and their relationship to sociodemographic, clinical, genetic, and AD biomarkers in a large population-based cohort of adults with DS. We particularly focused on regional WMH burden along the AD continuum and its associations with AD biomarkers. We hypothesize that the early accumulation of AD pathologies in DS will lead to WMHs years before symptoms onset, which will eventually increase as the disease progresses.

RESEARCH IN CONTEXT

1. **Systematic review**: White matter hyperintensities (WMHs) are recognized as vascular markers that contribute to cognitive decline. Previous studies have shown that WMHs are prevalent in Down syndrome (DS), a genetically determined form of Alzheimer's disease (AD) not complicated by some traditional age-related vascular risk factors. However, the evolution and topography of WMHs across age and disease severity, as well as their relationship to AD pathophysiology, have not been thoroughly studied in DS.
2. **Interpretation**: WMHs increased with age and AD clinical stage, and were correlated with cerebrospinal fluid AD biomarkers and gray matter volume in AD vulnerable areas. Our findings suggest that WMHs might be intrinsically related to AD pathophysiological processes in DS.
3. **Future directions**: *Post mortem* studies could shed light on the pathological substrates of WMHs in DS and other genetically determined forms of AD.

2 | METHODS

2.1 | Study design and participants

This cross-sectional study was conducted at a single center, where adults with DS aged ≥ 18 were recruited from the population-based Down-Alzheimer Barcelona Neuroimaging Initiative (DABNI) cohort.[2] A sample of euploid cognitively unimpaired control (HC) individuals was also included from the Sant Pau Initiative on Neurodegeneration (SPIN) cohort.[18] The study was approved by the Sant Pau Ethics Committee following the standards for medical research in humans recommended by the Declaration of Helsinki. All participants or their legally authorized representatives gave written informed consent before enrollment.

The participants with DS were screened for apolipoprotein E (*APOE*) haplotype and underwent a comprehensive neurological and neuropsychological evaluation, including, among other tests, the Cambridge Cognitive Examination for Older Adults with Down Syndrome (CAMCOG-DS) Spanish version for assessing global cognition.[19,20] The CAMCOG-DS is a cognitive battery that evaluates orientation, language, memory, attention, praxis, abstract thinking, and perception.

As in previous studies,[2,21] participants were clinically classified during a consensus meeting between neurologists and neuropsychologists, masked from biomarker data, into the following groups: asymptomatic (aDS) when there was no clinical or neuropsychological suspicion of AD-related cognitive decline, prodromal AD (pDS) when there was evidence of cognitive decline due to AD, but no significant impact on baseline activities of daily living, and AD dementia (dDS) when the cognitive decline impaired daily activities. This functional status, differentiating pDS and dDS, was assessed using anamnesis, Dementia Questionnaire for Persons with Mental Retardation, and the Cambridge Examination for Mental Disorders of Older People with Down Syndrome and Others with Intellectual Disabilities. Additionally, the Diagnostic and Statistical Manual of Mental Disorder, Fifth Edition, was used to stratify the level of intellectual disability (ID) into mild, moderate, or severe/profound based on the individuals' best-ever level of functioning.[22]

The HC group are volunteers, usually spouses or children of patients from the Sant Pau Memory Unit, that are informed about our studies at the outpatient clinics. They exhibited no cognitive complaints, scoring 0 on the Clinical Dementia Rating scale, and their neuropsychological evaluation was within the normal range for their respective normative groups regarding age and education. None of the participants in the HC group reported any neurological or psychiatric disorders, or other major medical illnesses.[18] We selected only the HC within the same age range as the DS group, from 18 to 63 years.

2.2 | Neuroimaging data

2.2.1 | MRI acquisition

T1-weighted and FLAIR images were acquired on a 3T Philips-Achieva scanner at Hospital del Mar (Barcelona, Spain) or a 3T Siemens Prisma scanner at Hospital Clinic (Barcelona, Spain). The detailed acquisition parameters of the imaging protocols are provided in Table S1 in supporting information.

The quality of each T1-weighted and FLAIR image was visually assessed. MRI scans of unsatisfactory quality in terms of low transverse resolution or low structural visibility due to movement or other sources of noise were excluded ($n = 21$ scans, 4.64%).

2.2.2 | Gray matter volume

The Computational Anatomy Toolbox (CAT12)[23] for the Statistical Parametric Mapping 12 (SPM12; Welcome Center for Human Neuroimaging) toolbox was used to preprocess the structural T1-weighted image and extract gray matter (GM) and total intracranial volumes.

15525279, 0, Downloaded from https://alz-journals.onlinelibrary.wiley.com/doi/10.1002/alz.14146 by Bejamin Alexandre - Readcube (Labtiva Inc.) , Wiley Online Library on [01/08/2024]. See the Terms and Conditions (https://onlinelibrary.wiley.com/terms-and-conditions) on Wiley Online Library for rules of use; OA articles are governed by the applicable Creative Commons License

2.2.3 | WMH segmentation

For the segmentation of WMHs, raw FLAIR images were first coregistered onto their corresponding T1-weighted scan using Advanced Normalization Tools (ANTs)[24] (Figure S1A in supporting information). Then, WMHs were segmented in the MRI native space using the lesion prediction algorithm (LPA)[25] implemented in the Lesion Segmentation Toolbox for SPM12. Specifically, the LPA method computed a WMH probability map for each participant based on a logistic regression algorithm to classify each voxel as either a lesion or non-lesion. The probability maps were then binarized by applying a threshold of 0.3 (Figure S1B).

2.2.4 | White matter parcellation

White matter (WM) was parcellated for each subject using an in-house pipeline inspired by the bull's-eye classification system previously developed by Sudre et al.[26] Specifically, two distinct sets of parcellations were created: concentric layers and lobar regions (for details, see supporting information). For the concentric layers, we followed the approach proposed by Jiménez-Balado et al.[27] and obtained a normalized distance map reflecting the distance of each WM voxel to the lateral and third ventricles (Figure S1C). For the lobar regions, we used the anatomical Hammers atlas to label the WM according to the lobes (frontal, parietal, temporal, occipital, and basal ganglia; Figure S1D). The normalized distance map was applied to each lobar region and subsequently divided into four concentric layers of similar volume. These layers spanned from the periventricular regions to juxtacortical areas. Regional WMH volumes were then extracted and summarized as an infographic in a bull's-eye plot (e.g., see Figure S1). Because different MRI acquisition protocols were used to acquire the data, we harmonized total and regional WMH volumes using the ComBat harmonization method[28] as implemented in the R library neuroCombat.

2.3 | Fluid biomarkers

A subset of participants underwent, within 1 year of the MRI acquisition, a lumbar puncture to acquire cerebrospinal fluid (CSF) sampling, as previously described.[21,29] Concentration levels of Aβ_{40} (n = 251), Aβ_{42} (n = 251), and tau phosphorylated at threonine 181 (pTau181; n = 251) were quantified using a commercially available immunoassay in a fully automated platform (Lumipulse; Fujirebio-Europe), following a previously published protocol.[18] CSF glial fibrillary acidic protein (GFAP; n = 183) concentrations were measured using the SR-X single molecule array. CSF neurofilament light chain (NfL; n = 267) and YKL-40 (also known as chitinase 3-like 1; n = 236) levels were measured with enzyme-linked immunosorbent assay (ELISA; NF-Light Assay; UmanDiagnostics) according to the manufacturer's recommendations. CSF Aβ_{42}/Aβ_{40} ratio and p-tau181 were used to stratify individuals with DS according to the presence of amyloid (A+) and tau (T+) pathologies using previously established cutoff values (i.e., CSF Aβ_{42}/Aβ_{40} < 0.062; CSF p-tau181 > 63 pg/mL[30]).

2.4 | Statistical analyses

All statistical analyses were performed with R software, version 4.3.1. Differences in baseline sociodemographic characteristics between DS and HC participants were assessed using the compareGroups library.[31] This package tests the normality of continuous variables and subsequently performs parametric or non-parametric statistical tests accordingly. Chi-squared tests were used for categorical variables, such as sex and *APOE* ε4 status, while Mann–Whitney tests were applied for continuous variables, including age, and CSF biomarkers, because they did not follow normality. To reduce skewness, total and regional volumes of WMHs, as well as concentrations of CSF biomarkers, were log-transformed.

To examine the association between WMH volume and age, we performed locally estimated scatterplot smoothing (LOESS) curves with a tricubic weight function and a span parameter of 0.75, providing an informative representation of the data. To assess the effect of factors such as sex, *APOE* ε4 status, ID, and AD clinical status on the distribution of WMH volume, we performed either a Mann–Whitney or Kruskal–Wallis test followed by the Dunn test as post hoc analysis. To investigate the relationship between total and regional WMH volume and CSF biomarkers, we performed Spearman correlation tests.

We used univariate linear regression models to assess the predictive capacity of individual CSF biomarkers on total WMH volume in the whole DS cohort, but also in aDS and symptomatic DS (sDS; comprising pDS and dDS) separately. Subsequently, we conducted a multivariate analysis incorporating all the CSF biomarkers to assess their relative contribution to the prediction of WMH volume. Additionally, we repeated both univariate and multivariate models including age as a predictor to evaluate its effect in relation to the CSF biomarkers. The standardized regression coefficients were used to compare the strength of the association between the predictors and total WMH volume. The threshold for significance was set at $p = 0.05$ and Bonferroni corrections were applied in regional volume analyses to account for multiple comparisons.

Finally, we used voxelwise linear models to compare the association of GM volume and WMHs in the DS cohort. Analyses were performed in a mask that excluded non-GM voxels, and the statistical models were corrected for total intracranial volume and the MRI acquisition protocol. Voxelwise results are presented at a corrected threshold $p < 0.05$ (family-wise error [pFWE], cluster size k > 100 mm^3).

3 | RESULTS

3.1 | Population

The study included 261 adults with DS from the DABNI cohort and 131 HC from the SPIN study (see Table 1 for demographic data). Individuals

15525279, 0, Downloaded from https://alz-journals.onlinelibrary.wiley.com/doi/10.1002/alz.14146 by Bejamin Alexandre - Readcube (Labtiva Inc.) , Wiley Online Library on [01/08/2024]. See the Terms and Conditions (https://onlinelibrary.wiley.com/terms-and-conditions) on Wiley Online Library for rules of use; OA articles are governed by the applicable Creative Commons License

TABLE 1 Study participants.

	HC *N* = 131	DS *N* = 261	*p*-value
Age, y, median [IQR]	53.65 [48.70;57.81]	46.96 [37.77;51.81]	<0.001
Sex, no. (%)			<0.001
Female	93 (70.99%)	108 (41.38%)	
APOE ε4 status, no. (%)			0.15
ε4+	36 (27.69%)	51 (20.56%)	
Intellectual disability, no. (%)			
Mild		76 (29.46%)	
Moderate		148 (57.36%)	
Severe/profound		34 (13.18%)	
AD diagnostic group, no. (%)			
aDS		158 (60.54%)	
pDS		41 (15.71%)	
dDS		62 (23.75%)	
Vascular risk factors, no (%)			
Hypertension (*N* = 323)	14 (21.88%)	4 (1.54%)	<0.001
Dyslipidemia (*N* = 323)	17 (26.56%)	47 (18.15%)	0.18
Diabetes mellitus (*N* = 322)	2 (3.12%)	12 (4.65%)	0.74
CAMCOG-DS, median [IQR]		69.00 [51.00;82.00]	
CSF biomarkers, pg/mL, median [IQR]			
$A\beta_{42}/A\beta_{40}$ (*N* = 251)	0.11 [0.10;0.11]	0.06 [0.04;0.08]	<0.001
pTau181 (*N* = 251)	32.30 [24.90;41.40]	55.05 [24.52;133.55]	<0.001
NfL (*N* = 267)	349.80 [298.92;418.61]	542.30 [304.32;871.20]	<0.001
GFAP (*N* = 183)	3.35 [3.14;3.50]	3.61 [3.40;3.78]	<0.001
YKL-40 (*N* = 236)	2.20 [2.11;2.29]	2.26 [2.03;2.37]	0.50

Notes: Data are n (%) or median (IQR).

Abbreviations: $A\beta_{42}/A\beta_{40}$, concentration ratio between amyloid beta peptide 1-42 and amyloid beta peptide 1-40 (pg/mL); AD, Alzheimer's disease; aDS, asymptomatic Down syndrome; *APOE*, apolipoprotein E; CAMCOG-DS, Cambridge Cognitive Examination for Older Adults with Down Syndrome; CSF, cerebrospinal fluid; dDS, Down syndrome with Alzheimer's disease dementia; DS, Down syndrome; GFAP, glial fibrillary acidic protein concentration (pg/mL); HC, euploid cognitively unimpaired controls; IQR, interquartile range; NfL, neurofilament light chain concentration (pg/mL); pDS, prodromal Down syndrome; pTau181, tau phosphorylated at threonine 181 concentration (pg/mL); YKL-40, chitinase 3-like 1.

in the DS group spanned the whole AD continuum; 158 were aDS, 41 pDS, and 62 dDS. Regarding the level of ID, 76 DS subjects had mild ID, 149 moderate ID, and 34 severe/profound ID. The HC group was significantly older than the DS group (W = 24666, $p < 0.05$). There was also a significant difference in the sex distribution, with fewer male participants in the HC group (29.01%) than in the DS group (58.62%, $p < 0.001$). No significant between-group differences were found for *APOE* ε4 status. Only 1.5% of individuals with DS presented hypertension, a significantly lower proportion compared to the HC group (21.9%, $p < 0.001$). Additionally, 18% had dyslipidemia and 4.7% had diabetes mellitus, versus 27% ($p = 0.18$) and 3.12% ($p = 0.74$), respectively. As expected, individuals with DS demonstrated lower values in CSF for the $A\beta_{42}/A\beta_{40}$ ratio and higher concentrations of pTau181, NfL, and GFAP than HC (all $p < 0.001$). CSF YKL-40 levels were not significantly different across groups ($p = 0.50$).

3.2 | Associations between WMH volume and sociodemographic, clinical, and genetic data

Total WMH volume was positively associated with age in both HC (rho = 0.36, $p < 0.001$) and adults with DS (rho = 0.67, $p < 0.001$). Looking at the LOESS curves (Figure 1A), we found an earlier increase in total WMH volume in DS with age. Specifically, the regression lines between DS and HC started diverging at age 40, and the confidence interval (CI) ceased to overlap at the age of 43.8. Regional associations revealed that, in HC, a significant relationship with age was mainly observed in the first layer (Figure 1B and Table S2 in supporting information for more details). In contrast, regional associations with age were more widespread and stronger in DS, including all lobes. The first and second layers (i.e., the region closest to the ventricles) showed the highest correlation strength and earliest changes

15525279, 0, Downloaded from https://alz-journals.onlinelibrary.wiley.com/doi/10.1002/alz.14146 by Bejamin Alexandre - Readcube (Labtiva Inc.) , Wiley Online Library on [01/08/2024]. See the Terms and Conditions (https://onlinelibrary.wiley.com/terms-and-conditions) on Wiley Online Library for rules of use; OA articles are governed by the applicable Creative Commons License

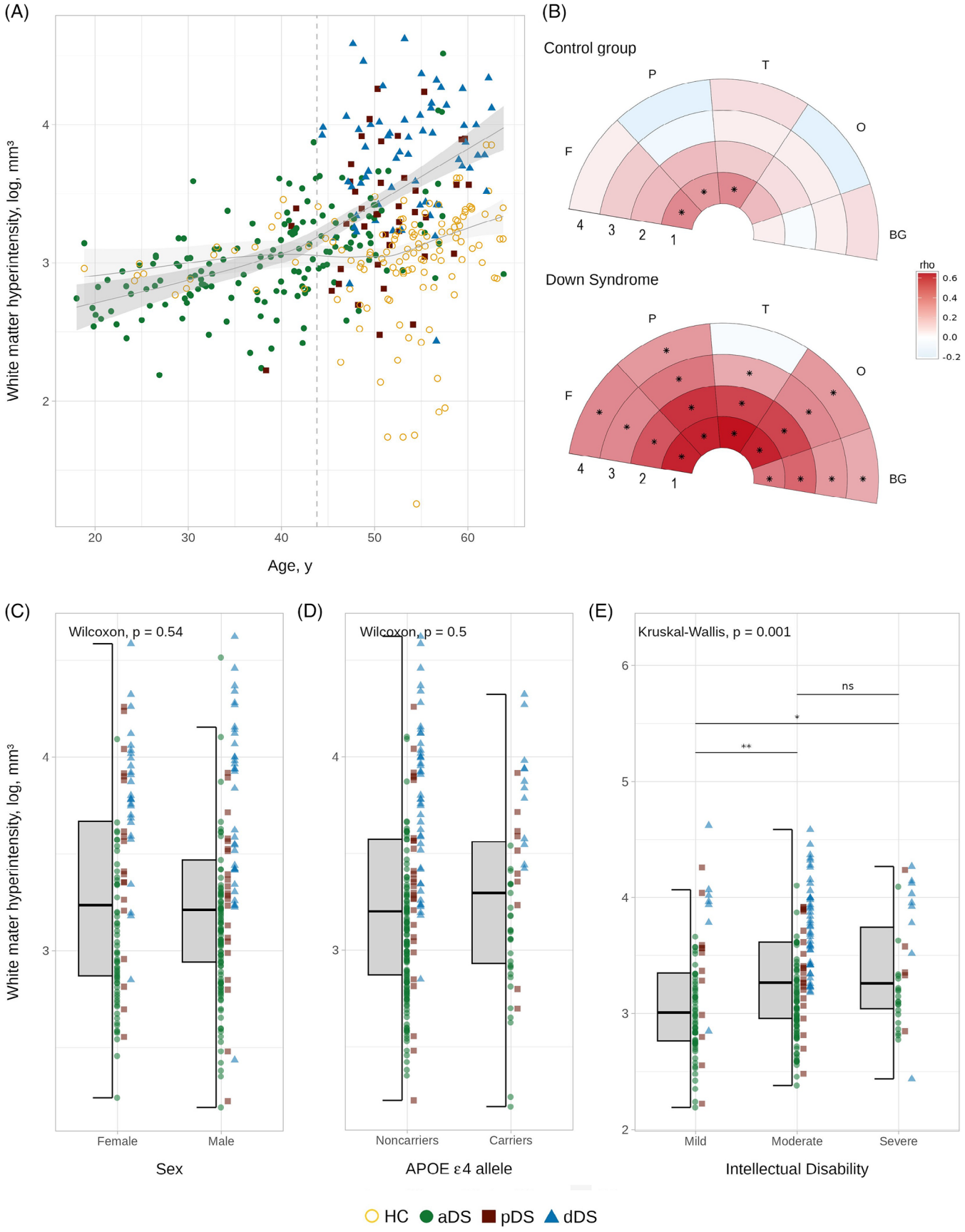

15525279, 0, Downloaded from https://alz-journals.onlinelibrary.wiley.com/doi/10.1002/alz.14146 by Bejamin Alexandre - Readcube (Labtiva Inc.) , Wiley Online Library on [01/08/2024]. See the Terms and Conditions (https://onlinelibrary.wiley.com/terms-and-conditions) on Wiley Online Library for rules of use; OA articles are governed by the applicable Creative Commons License

(Figures 1B, S2 in supporting information, and Table S2 for more details).

In DS, sex and *APOE* ε4 status did not significantly influence total WMH volume (Figure 1C,D) or the association between total WMH volume and age (Figure S3 in supporting information). However, we found a significant difference according to the degree of ID, with the moderate and severe ID levels showing greater WMH volume than the mild level (Figure 1E). Given that this result was unexpected, we assessed whether it may be explained by differences in clinical status across the ID groups. Results showed a higher proportion of moderate ID in dDS (77.97%) than aDS (50.64%; X^2 [4, N = 259] = 14.462, $p < 0.05$). Moreover, the effect of ID on WMH volume was no longer significant when groups were stratified by AD clinical diagnosis ($p > 0.05$; Figure S4 in supporting information) and associations with age appeared similar across ID groups (Figure S3).

3.3 | Spatial distribution of WMHs in DS

To assess the spatial distribution of WMHs in DS, we computed a frequency map of WMHs for all adults with DS. Results showed that WMHs had a symmetrical distribution, and were most frequently located in periventricular and deep regions (Figure 2). Specifically, WMHs were predominantly found in the corona radiata (mainly the posterior part), the posterior thalamic radiation, and the corpus callosum, especially in the splenium.

3.4 | Effect of AD clinical status on WMH volume

Total WMH volume progressively increased with AD clinical status in DS: dDS and pDS groups demonstrated significantly greater WMH volumes than aDS and HC, and dDS greater volumes compared to pDS. No significant differences were observed between HC and aDS (Figure 3A). Regarding regional WMH volumes, aDS showed significantly greater volumes in the temporal lobe with respect to the HC, while HC showed greater WMH in the occipital lobe and basal ganglia (Figure 3C). pDS presented significantly more WMH volume than aDS in the first and second WM layers, and in all lobes (Figure 3B,C). In the other regions (i.e., layers 3–4, and basal ganglia), there was a visible trend toward higher volumes in pDS compared to aDS, although statistical significance was not reached (Figure 3B-D). dDS consistently had greater WMH volumes compared to pDS in all regions of interest, except in the fourth WM layer (Figure 3B-D). Analyses considering both the concentric layers and lobar regions showed similar results, where the first WM layer and the occipital lobes showed the greatest WMH load in all the diagnostic groups. The dDS groups demonstrated both higher and more widespread WMH load compared to other disease stages (Figure 3E).

3.5 | Associations between WMH volume and CSF biomarkers

In DS, total WMH volume was negatively related to CSF $A\beta_{42}/A\beta_{40}$ ratio (rho = −0.58, $p < 0.001$) and positively associated with CSF pTau181 (rho = 0.63, $p < 0.001$), CSF NfL (rho = 0.72, $p < 0.001$), CSF GFAP (rho = 0.61, $p < 0.001$), and CSF YKL-40 (rho = 0.63, $p < 0.001$) concentrations (Figure 4A). Additionally, A+ and T+ individuals with DS presented greater WMH volume compared to negative participants ($p < 0.001$; Figure 4A). When assessed regionally, the strongest associations between CSF biomarkers of AD and WMHs were found in the frontal, parietal, and occipital lobes and in the first and second layers (Figure 4B). The univariate models revealed that all five CSF biomarkers were significant predictor variables in the whole DS cohort ($A\beta_{42}/A\beta_{40}$: $p < 0.001$, estimate: −0.59, 95% CI: [−0.70, −0.47]; pTau181: $p < 0.001$, estimate: 0.60 [0.48, 0.71]; NfL: $p < 0.001$, estimate: 0.68 [0.57, 0.79]; GFAP: $p < 0.001$, estimate: 0.57 [0.42, 0.69]; YKL-40: $p < 0.001$, estimate: 0.58 [0.47, 0.70]). Considering the groups separately, we found significant relationships between the five biomarkers and WMHs in aDS ($A\beta_{42}/A\beta_{40}$: $p < 0.001$, estimate: −0.40, [−0.60, −0.21]; pTau181: $p < 0.001$, estimate: 0.37 [0.18, 0.56]; NfL: $p < 0.001$, estimate: 0.44, [0.27, 0.62]; GFAP: $p < 0.001$, estimate: 0.32 [0.12, 0.52]; YKL-40: $p < 0.001$, estimate: 0.46 [0.29, 0.63]). In sDS, only the association with NfL concentrations reached significance ($A\beta_{42}/A\beta_{40}$: $p = 0.81$, estimate: 0.03 [−0.21, 0.27]; pTau181: $p = 0.06$, estimate: 0.21 [−0.01, 0.44]; NfL: $p < 0.001$, estimate: 0.44 [0.22, 0.66]; GFAP: $p = 0.08$, estimate: 0.21 [−0.03, 0.45]; YKL-40: $p = 0.20$, estimate: 0.16 [−0.09, 0.40]). When performing a multivariate analysis incorporating all five CSF AD biomarkers, only NfL significantly predicted total WMH volume in the whole DS cohort ($p < 0.001$, estimate: 0.37 [0.13, 0.61]) and in sDS ($p < 0.001$, estimate: 0.54 [0.18, 0.90]) group (Figure 4C). When age was included as a covariate, several results lost significance, especially in the aDS group, but the associations with NfL remained sig-

FIGURE 1 Associations between white matter hyperintensity volume and demographic, clinical, and genetic factors. (A) Association between total WMH volume and age. The points represent individual participants, and the color indicates their clinical diagnosis. Shaded areas represent 95% CI: dark gray represents the age-related change in DS and light gray in the HC group for visual reference. The dashed line indicates when the CI stops overlapping between DS and HC groups (43.8 years). (B) Spearman correlation coefficients between age and regional WMH volumes. The color scale represents the strength (rho) of Spearman correlation for significant results ($p < 0.05$). The star (*) indicates results surviving to the Bonferroni correction ($\alpha = 0.05$, $p < 0.0025$). (C), (D) and (E) Boxplots showing the effect of sex, *APOE* haplotype, and intellectual disability, respectively, on the distribution of the total WMH volume in DS. Abbreviations: 1, first layer; 2, second layer; 3, third layer; 4, fourth layer; aDS, asymptomatic Down syndrome; *APOE*, apolipoprotein E; BG, basal ganglia; CI, confidence interval; DS, Down syndrome; F, frontal; HC, euploid cognitively unimpaired controls; dDS, Down syndrome with Alzheimer's disease dementia; O, occipital; P, parietal; pDS, prodromal Down syndrome; rho, strength of the correlation; T, temporal; WMH, white matter hyperintensity.

15525279, 0, Downloaded from https://alz-journals.onlinelibrary.wiley.com/doi/10.1002/alz.14146 by Bejamin Alexandre - Readcube (Labtiva Inc.) , Wiley Online Library on [01/08/2024]. See the Terms and Conditions (https://onlinelibrary.wiley.com/terms-and-conditions) on Wiley Online Library for rules of use; OA articles are governed by the applicable Creative Commons License

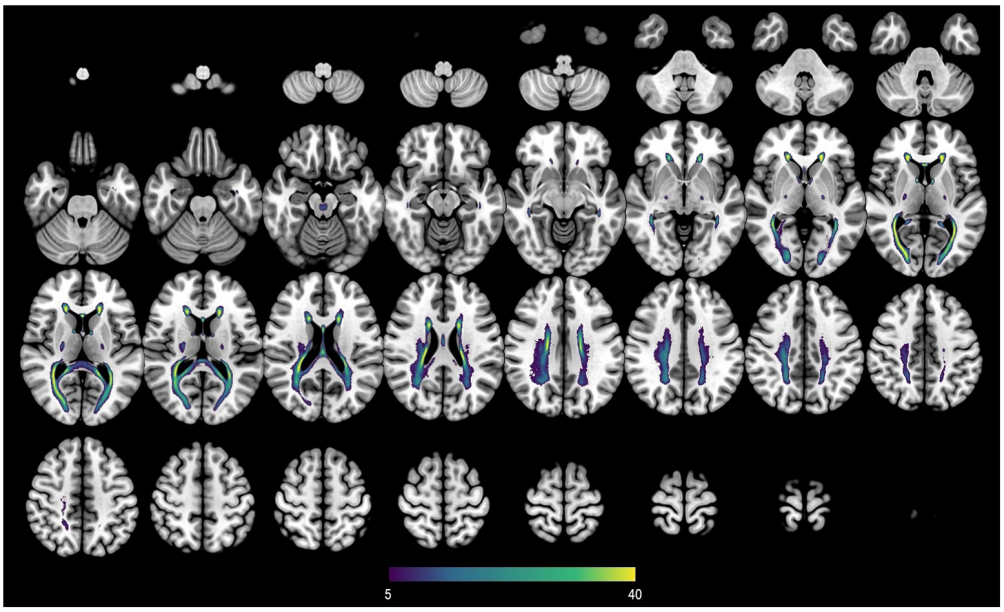

FIGURE 2 Lesion prevalence map of white matter hyperintensities in Down syndrome. Lesion frequency map of white matter hyperintensities is shown in the Montreal Neurological Institute 152 T1 template. The color of each voxel indicates the percentage of subjects that had white matter hyperintensities in this voxel, ranging from at least 5% (purple) to 40% or more (yellow).

nificant or showed a trend toward significance in the whole DS and sDS cohorts (Figure 5S in supporting information).

3.6 | Associations between WMH volume and GM volume

Finally, we also investigated voxelwise associations between total WMH volume and GM volumes within the DS population. These analyses revealed significant associations across the entire cortex for the whole cohort (Figure 5A). Specifically, the pattern predominated in the medial and lateral temporo-parietal regions, medial prefrontal and orbitofrontal cortex, anterior insula, hippocampi, and thalamus. The stratification of DS by clinical status revealed a very similar pattern in both aDS and sDS, although slightly less widespread and significant than in the whole population (Figure 5B,C).

4 | DISCUSSION

Our results highlighted an increase in the presence and severity of WMHs with age in DS, as well as with the incidence of both AD symptoms and AD pathology. We further demonstrated that lesions are mostly located in periventricular regions, especially in the frontal, parietal, and occipital lobes. WMHs expand into more cortical layers throughout the AD continuum in DS, suggesting a distinct underlaying pathophysiology compared to the general population. Together, these findings underscore that WMHs represent a core neuroimaging feature in DS, and provide novel insight into the interplay between these lesions and AD processes.

Consistent with previous studies,[17] we observed that WMH volume gradually increased with age in both DS and euploid populations. This age-related increase is stronger in DS individuals. This finding expands previous evidence from our group obtained in a smaller sample of DS and using the Fazekas visual scale.[16] We further demonstrated that WMHs emerge at a younger age in DS than HC, with CI no longer overlapping at the age of 43, around 10 years before symptom onset.[5] Interestingly, a recent study on *PSEN1* mutation carriers also reported a sharp increase in WMHs at 43 years,[15] and WMHs were found to increase approximately 6.6 years before estimated symptom onset in mutation carriers of AD-causing genes.[14] The presence of WMHs at an early age across distinct genetically determined AD forms suggests that AD-related mechanisms contribute, at least partially, to these lesions. Indeed, in population-based studies, WMHs typically increased at a later age,[10,32] starting from 55 years.[33]

We mapped WMH topography and found different associations in both populations. Associations with age predominated in the frontal lobe in HC, as previously described in elderly populations.[34] By contrast, associations in DS involved all brain lobes, particularly the fronto–parieto–occipital regions. This aligns with previous evidence showing a widespread age-related pattern of WMHs in DS, driven by frontal, parietal, and occipital lobes,[17] as well as the typical parieto–occipital AD pattern.[12] Further, correlation coefficients were strongest in the periventricular region, showing earlier age-related changes than total WMH volume, and progressively decreased in deep and juxtacortical areas. These results add to a body of work identifying different WMH topography in AD compared to age-related WMHs.[12]

Other sociodemographic and genetic factors may also contribute to WMHs. In line with previous studies,[16,17] we did not evidence an effect of sex or *APOE* haplotype on total WMH volume in DS. The specific

15525279, 0, Downloaded from https://alz-journals.onlinelibrary.wiley.com/doi/10.1002/alz.14146 by Bejamin Alexandre - Readcube (Labtiva Inc.) , Wiley Online Library on [01/08/2024]. See the Terms and Conditions (https://onlinelibrary.wiley.com/terms-and-conditions) on Wiley Online Library for rules of use; OA articles are governed by the applicable Creative Commons License

Alzheimer's & Dementia®
THE JOURNAL OF THE ALZHEIMER'S ASSOCIATION

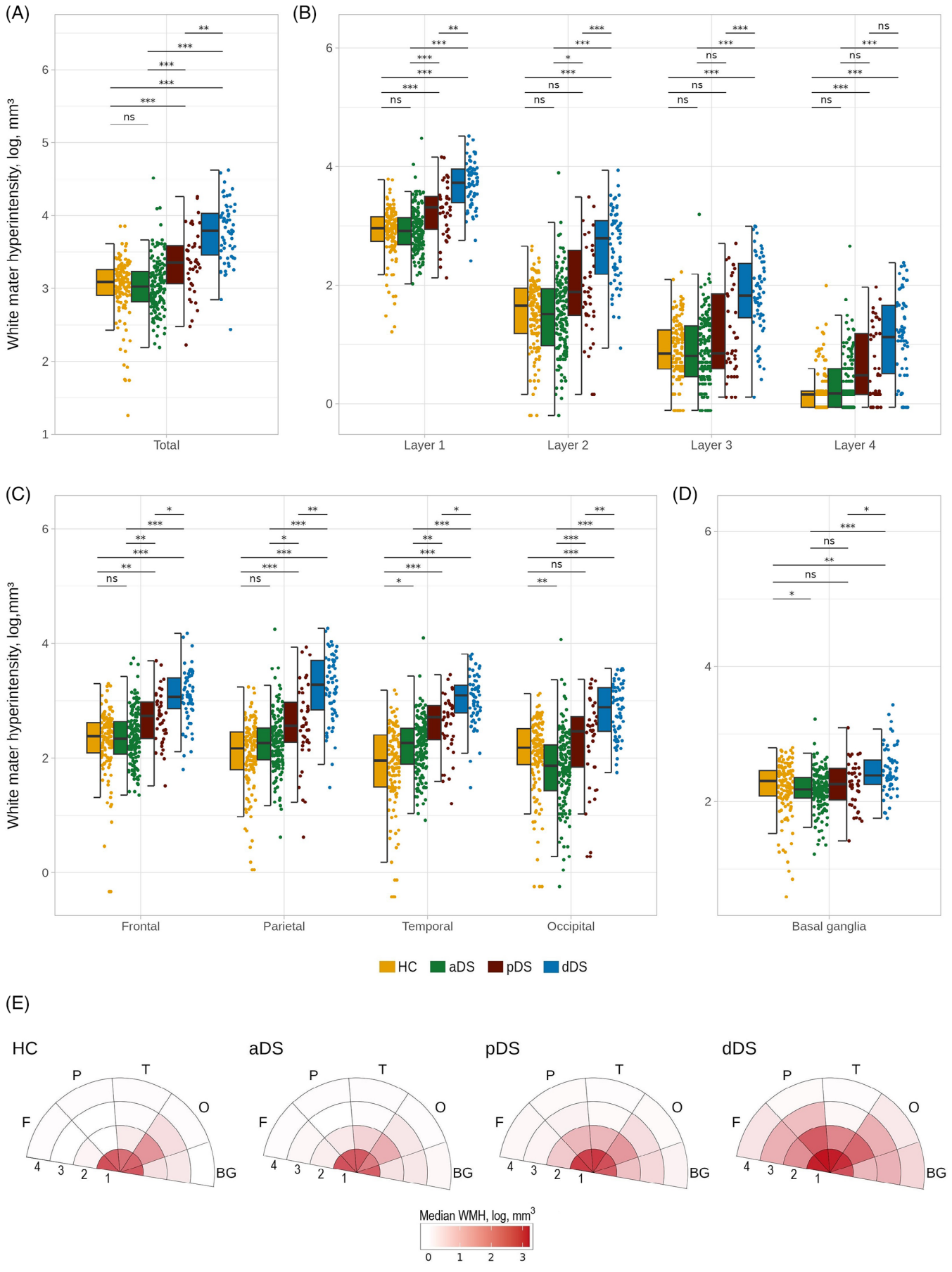

15525279, 0, Downloaded from https://alz-journals.onlinelibrary.wiley.com/doi/10.1002/alz.14146 by Bejamin Alexandre - Readcube (Labtiva Inc.) , Wiley Online Library on [01/08/2024]. See the Terms and Conditions (https://onlinelibrary.wiley.com/terms-and-conditions) on Wiley Online Library for rules of use; OA articles are governed by the applicable Creative Commons License

sex effect on AD in DS is still debated, with a recent study showing no impact on AD biomarkers.[35] Concerning the *APOE ε4* allele, it was found to influence AD processes in DS,[36] but this effect might be too subtle to be identified in WMHs. The link between *APOE ε4* and WMHs is also inconsistent in the general population and sporadic AD, with some studies suggesting a gene–dose effect on WMHs[37,38] and others reporting opposite or no effect.[39–42]

Surprisingly, greater ID was associated with higher WMH volumes. However, sensitivity analyses suggested that this effect might result from the different proportion of symptomatic cases across the different ID groups, that is, a higher proportion of moderate level in dDS. Two recent studies examining the effect of ID on AD trajectory in DS revealed no differences in AD biomarkers, cognitive impairments,[43] or decline.[44] Together these results suggest that ID has a limited impact on AD and vascular changes in DS. However, further research is warranted to confirm this result and assess if differences in lifestyle factors across ID can lead to differences in WMHs.

WMH volumes increased linearly with AD stage (aDS < pDS < dDS), consistent with previous studies in DS,[16,17] and investigations in early-[45] and late-onset sporadic AD[10,46] and autosomal dominant AD (ADAD),[14,47] all of which showed a gradual increase in WMH burden with disease severity. Topographically, WMHs increased locally and expanded to new layers as the disease progressed. Mainly circumscribed to the periventricular region at the asymptomatic stage, the lesions extended into deep and juxtacortical areas, including the frontal, parietal, and occipital lobes at the prodromal stage, and further increased in the same regions at the dementia stage. Similar topographical progression has been previously described in sporadic AD,[48] where periventricular WMHs were common at the mild cognitive impairment (MCI) stage, and in the AD group expanded outward, particularly to affect the corpus callosum. The frequency map further showed that posterior corona radiata, posterior thalamic radiation, and splenium of the corpus callosum were the most affected areas in DS. These structures were previously found vulnerable to AD processes,[49] and associated with Aβ pathology.[50]

Compared to HC, the aDS group presented increased WMH volume only in the temporal lobe. Previous studies in preclinical AD revealed larger WMH total volume in Aβ-positive compared to Aβ-negative individuals.[51] In ADAD, asymptomatic carriers present with increased WMHs in parieto-occipital regions.[14] Taken together, these results suggest that WMHs emerge at an early preclinical stage of AD. The different topographic patterns may reflect specificities of each presentation or differences in the preclinical or control groups. For instance, our aDS cohort included adults ranging from 19 to 63 years, with 32.9% at > 20 years from the estimated age of symptom onset (i.e., 53.8 years[5]).

Relationships between WMHs and CSF AD biomarkers revealed robust associations in DS with both Aβ and pTau181 concentrations. In the literature, the link between WMHs and AD pathology is inconsistent. Several studies in the euploid population reported no association between WMHs and Aβ-[52] and tau positron emission tomography (PET)[53] load. In DS, WMHs were also not significantly associated with Aβ PET.[17] However, some evidence supported a relationship with Aβ PET in non-demented individuals[12,53] and tau PET in preclinical ADAD.[45] Moreover, Aβ in CSF, but not tau, was found related to WMHs in ADAD,[14,54,55] MCI, and sporadic AD.[14,54–57] These discrepant results might be explained by the modality to measure AD pathology, or the composition of the cohort studied. Indeed, when we stratified our analyses by disease stage, we found significant associations at the asymptomatic but not symptomatic stages, aligning with findings in the AD continuum.[57]

Associations between WMHs and neurodegenerative markers were also strong. Consistent with previous observations in cognitively normal,[54] MCI,[54,58,59] sporadic AD,[59,60] and ADAD,[61] we found that NfL levels in CSF were associated with WMHs. Indeed, NfL showed i) the strongest association with total WMH volume, ii) was significantly related to WMH volume at different disease stages, and iii) was the only CSF biomarker to remain significantly associated with WMHs in the multivariate analyses. This strong link between WMHs and NfL is not surprising because WM mainly consists of myelinated axons and NfL, an axonal cytoskeleton protein particularly expressed in long myelinated axons, is released upon axonal damage.[62]

To further understand WMHs and neurodegeneration, we explored the association with GM volume. There were significant associations that encompassed the entire cortex, but were more pronounced in lateral and medial temporo-parietal regions. This pattern overlaps with the typical AD regions showing tau accumulation[63] and atrophy.[64] Similar associations between WMH burden and lower GM volume[9] and cortical thickness[65] were previously reported in sporadic AD.

The link between WMHs and both AD pathology and neurodegeneration can be explained by different non-exclusive hypotheses.[12,66] First, it is possible that WMHs, in the AD context, are caused by Wallerian degeneration secondary to neurofibrillary tangles.[67–69] Indeed, disruption of microtubules containing tau could lead to axonal degeneration, resulting in WM damage observed as WMHs on MRI.[70] Second, WMHs might be induced by subtle hypoperfusion or other cerebrovascular diseases, which in turn contribute to tau pathology[71] and/or the disruption of WM tracts affecting the cortical regions.[11] For instance, cerebral amyloid angiopathy is frequently found in AD[72] and DS,[16] and likely causes some posterior WM damage.[53,73] Another hypothesis is that neuroinflammation, which is a key pathogenic factor of both AD and vascular pathologies, might also participate in the gen-

FIGURE 3 Between-group differences for total and regional white matter hyperintensity volumes. (A), (B), (C) and (D) The boxplots illustrate WMH volumes across the brain regions. Significant results at $p < 0.05$ using the Bonferroni correction. (E) Median of WMH volume per region represented in bull's-eye plot. Colors represent the burden of WMH volume in log mm^3, darker colors indicate higher WMH load. Abbreviations: ns, no significance; *$p < 0.05$; **$p < 0.01$; ***$p < 0.001$; 1, first layer; 2, second layer; 3, third layer; 4, fourth layer; aDS, asymptomatic Down syndrome; BG, basal ganglia; dDS, Down syndrome with Alzheimer's disease dementia; DS, Down syndrome; F, frontal; HC, euploid cognitively unimpaired controls; O, occipital; P, parietal; pDS, prodromal Down syndrome; T, temporal; WMH, white matter hyperintensity.

15525279, 0, Downloaded from https://alz-journals.onlinelibrary.wiley.com/doi/10.1002/alz.14146 by Bejamin Alexandre - Readcube (Labtiva Inc.) , Wiley Online Library on [01/08/2024]. See the Terms and Conditions (https://onlinelibrary.wiley.com/terms-and-conditions) on Wiley Online Library for rules of use; OA articles are governed by the applicable Creative Commons License

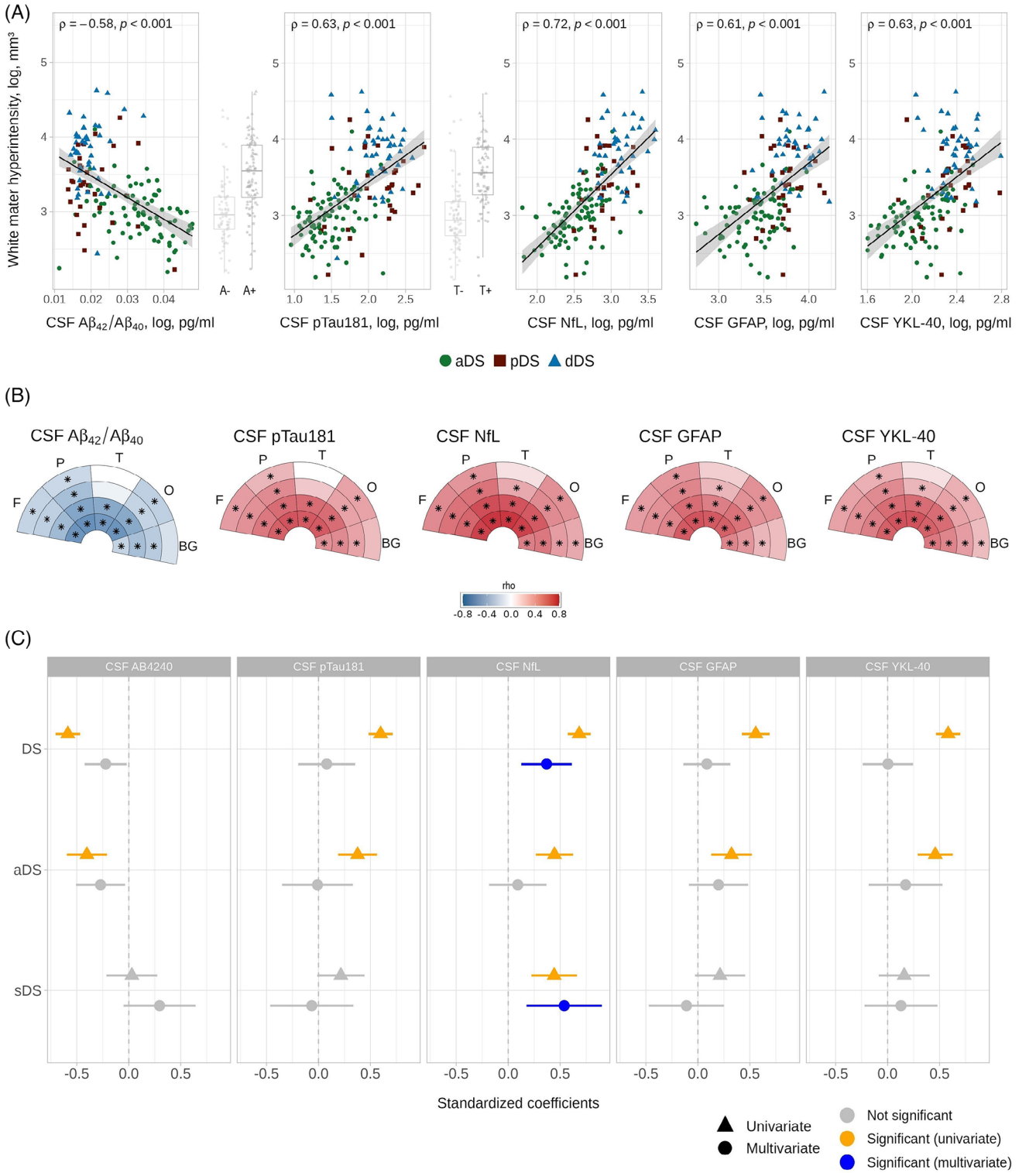

FIGURE 4 Associations between white matter hyperintensities and cerebrospinal fluid biomarkers in DS. (A) Correlation between total WMH volume and each corresponding CSF biomarker. Boxplots illustrate WMH volumes across the amyloid and tau status. The points represent individual participants, and the color indicates the clinical diagnosis. Shaded areas represent 95% CI. (B) Spearman correlation coefficients between each corresponding CSF biomarker and regional WMH volume in DS. The color scale represents the strength (rho) of Spearman correlation for significant results ($p < 0.05$). The star (*) indicates results surviving the Bonferroni correction ($\alpha = 0.05, p < 0.0025$). (C) Standardized coefficient of univariate and multivariate linear regression models for the WMH volume. The triangles and circles represent the univariate and multivariate models, respectively. The lines represent the 95% CI. Gray color indicates non-significant values, while orange color indicates significant values ($p < 0.01$) and blue color after applying Bonferroni correction ($\alpha = 0.05, p < 0.01$). Abbreviations: 1, first layer; 2, second layer; 3, third layer; 4, fourth layer; A^-, amyloid negative; A^+, amyloid positive; $A\beta_{42}/A\beta_{40}$, concentration ratio between amyloid beta peptide 1-42 and amyloid beta peptide 1-40 (pg/mL); aDS, asymptomatic Down syndrome; BG, basal ganglia; CI, confidence interval; CSF, cerebrospinal fluid;

15525279, 0, Downloaded from https://alz-journals.onlinelibrary.wiley.com/doi/10.1002/alz.14146 by Bejamin Alexandre - Readcube (Labtiva Inc.) , Wiley Online Library on [01/08/2024]. See the Terms and Conditions (https://onlinelibrary.wiley.com/terms-and-conditions) on Wiley Online Library for rules of use; OA articles are governed by the applicable Creative Commons License

dDS, Down syndrome with Alzheimer's disease dementia; DS, Down syndrome; F, frontal; GFAP, glial fibrillary acidic protein concentration (pg/mL); NfL, neurofilament light chain concentration (pg/mL); O, occipital; P, parietal; pDS, prodromal Down syndrome; pTau181, tau phosphorylated at threonine 181 concentration (pg/mL); sDS, symptomatic Down syndrome; T, temporal; T^-, tau negative; T^+, tau positive; WMH, white matter hyperintensity.

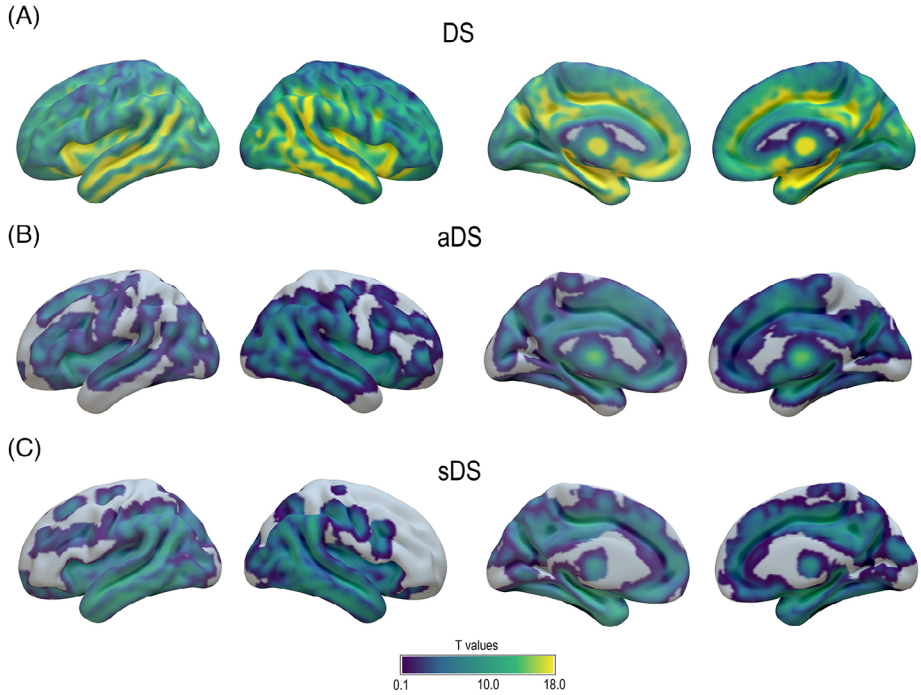

FIGURE 5 Voxelwise associations between white matter hyperintensities and gray matter volume. Results of voxelwise regression model showing gray matter volume negatively associated with WMH in (A) whole DS cohort and (B) aDS and (C) sDS subgroups. The significance of the results (T values) is shown using a threshold pFWE < 0.05. Abbreviations: aDS, asymptomatic Down syndrome; DS, Down syndrome; sDS, symptomatic Down syndrome; FWE, family-wise error.

esis of part of WMHs,[74,75] as suggested by the association with GFAP and YKL-40. Finally, we cannot exclude that the associations between these different biomarkers are partially driven by disease progression.

The current study has some limitations. First, the WMH segmentation algorithm and templates to parcellate the WM were not specifically designed for the DS population. Although a thorough visual quality control demonstrated that the segmentation and WM parcellation were correctly performed, with no visible impact of DS brain anatomy, we cannot discard a reduced sensitivity to detect some lesions. Second, the cross-sectional design of this study does not allow for the assessment of causality, such as the relationships among WMHs, AD pathology, and neurodegeneration. Future longitudinal studies will undoubtedly provide new insight into the etiology of WMHs in DS.

In summary, this study offers a comprehensive understanding of the development and distribution of WMHs in DS. Our findings revealed that WMHs are associated with AD clinical stages, manifesting even at the asymptomatic phase. The parcellation of the WM revealed the predominance of WMHs in periventricular regions of frontal, parietal, and occipital lobes, and their expansion into cortical layers with AD progression. These results demonstrate that WMHs are a core imaging feature in DS and shed light on their relationship with AD pathological processes.

AUTHOR CONTRIBUTIONS

Alejandra O. Morcillo-Nieto and Sara E. Zsadanyi contributed equally to this work and share first authorship. Alejandra O. Morcillo-Nieto, Sara E. Zsadanyi, and Alexandre Bejanin conceived and designed the study. Jose E. Arriola-Infante, Maria Carmona-Iragui, Victor Montal, Jordi Pegueroles, Mateus Rozalem Aranha, Lídia Vaqué-Alcázar, Concepción Padilla, Bessy Benejam, Laura Videla, Isabel Barroeta, Laura Videla, Miren Altuna, Sandra Giménez, Sofía González-Ortiz, Núria Bargalló, Laia Ribas, Javier Arranz, Soraya Torres, Maria Florencia Iulita, Olivia Belbin, Valle Camacho, Daniel Alcolea, Alberto Lleó, and Juan Fortea acquired and interpreted the data. Alejandra O. Morcillo-Nieto performed the statistical analysis. Alejandra O. Morcillo-Nieto, Sara E. Zsadanyi, and Alexandre Bejanin drafted the manuscript, which all authors critically reviewed for important intellectual content.

ACKNOWLEDGMENTS

The authors would like to thank all study participants, their families, and caregivers from the DABNI and SPIN cohort for their support of, and dedication to, this research. We also would acknowledge the Fundació Catalana Síndrome de Down (https://fcsd.org/) for global support. This study was funded by the Fondo de Investigaciones Sanitario, Instituto de Salud Carlos III and co-funded

15525279, 0, Downloaded from https://alz-journals.onlinelibrary.wiley.com/doi/10.1002/alz.14146 by Bejanin Alexandre - Readcube (Labtiva Inc.) , Wiley Online Library on [01/08/2024]. See the Terms and Conditions (https://onlinelibrary.wiley.com/terms-and-conditions) on Wiley Online Library for rules of use; OA articles are governed by the applicable Creative Commons License

by the European Union (PI18/00335 to MCI, PI18/00435 to DA, PI14/1561, PI20/01330 to AL, PI20/01473 to JF, PI22/00307 to AB), the CIBERNED Program 1, the National Institutes of Health (NIH; 1R01AG056850-01A1; 3RF1AG056850-01S1; AG056850, R21AG056974, and R01AG061566 to JF), the Departament de Salut de la Generalitat de Catalunya, Fundación Tatiana Pérez de Guzmán el Bueno (IIBSP-DOW-2020-151 to JF), the European Union's Horizon 2020, "MES-CoBraD" (H2020-SC1-BHC-2018-2020 / GA 965422 to JF), Brightfocus, and Life Molecular Imaging (LMI) to JF. JEAI was supported by Instituto de Salud Carlos III through the Río Hortega Fellowship "CM22/00219" and co-funded by the European Union. VM acknowledges support from the Instituto de Salud Carlos III through the Predoctoral grant "FI18/00275" and co-funded by the European Union, and Juan de la Cierva fellowship (JDC2022-048492-I) from the Ministry of Science of the Spanish Government. MCI acknowledges support from the Alzheimer's Association and Global Brain Health Institute (GBHI_ALZ-18-543740), the Jérôme Lejeune Foundation (#1913 Cycle 2019B), the Societat Catalana de Neurologia (Premi Beca Fundació SCN 2020). MRA acknowledges support from Alzheimer's Association Research Fellowship to Promote Diversity (AARFD-21-852492). MRA has provided paid consultancy for Veranex. MRA is a partner and director of production at Masima—Soluções em Imagens Médicas LTDA. LVA was supported by Margarita Salas junior postdoctoral fellowship (UNI/551/2021, NextGenerationUE). CP was supported by Instituto de Salud Carlos III through the Sara Borrell Postdoctoral Fellowship "CD20/00133" and co-funded by the European Union. JA was supported by Instituto de Salud Carlos III through the Río Hortega Fellowship "CM21/00243" and co-funded by the European Union. AB acknowledges support from Instituto de Salud Carlos III through the Miguel Servet grant "CP20/00038" and co-funded by the European Union, and the Alzheimer's Association "AARG-22-923680." The sponsors had no role in the design and conduct of the study; collection, management, analysis, and interpretation of the data; preparation, review, or approval of the manuscript; or decision to submit for publication.

CONFLICT OF INTEREST STATEMENT

MRA has provided paid consultancy for Veranex, and is a partner and director of production at Masima—Soluções em Imagens Médicas LTDA. MFI is now a paid employee of Altoida Inc. and may hold stock options in the company. The work in this manuscript only relates to the reported affiliation. DA reported receiving personal fees for advisory board services and/or speaker honoraria from Fujirebio-Europe, Roche, Nutricia, Krka Farmacéutica, Lilly, Zambon S.A.U., Grifols, and Esteve, outside the submitted work. AL has served as a consultant or on advisory boards for Fujirebio-Europe, Roche, Biogen, Grifols, Novartis, Eisai, Lilly, and Nutricia, outside the submitted work. JF reported serving on the advisory boards, adjudication committees, or speaker honoraria from Roche, NovoNordisk, Esteve, Biogen, Laboratorios Carnot, Adamed, LMI, Novartis, Lundbeck, Roche, AC Immune, Alzheon, Zambon, Lilly, Spanish Neurological Society, T21 Research Society, Lumind foundation, Jérôme-Lejeune Foundation, Alzheimer's Association, National Institutes of Health USA, and Instituto de Salud Carlos III. DA, AL, and JF report holding a patent for markers of synaptopathy in neurodegenerative disease (licensed to ADx, EPI8382175.0). No other competing interests were reported. Author disclosures are available in the supporting information.

DATA AVAILABILITY STATEMENT

The authors may share de-identified data that underlie the results reported in this article. Data will be available upon receipt of a request detailing the study hypothesis and statistical analysis plan. All requests should be sent to the corresponding authors. The steering committee of this study will discuss all requests and decide, based on the novelty and scientific rigor of the proposal, whether data sharing is appropriate. All applicants will be asked to sign a data access agreement.

CONSENT STATEMENT

All participants and/or their legally authorized representatives gave written informed consent.

ORCID

Alexandre Bejanin https://orcid.org/0000-0002-9958-0951

REFERENCES

1. Lott IT, Head E. Dementia in Down syndrome: unique insights for Alzheimer disease research. *Nat Rev Neurol*. 2019;15:135-147. 2019 153. doi:10.1038/s41582-018-0132-6
2. Fortea J, Vilaplana E, Carmona-Iragui M, et al. Clinical and biomarker changes of Alzheimer's disease in adults with Down syndrome: a cross-sectional study. *Lancet*. 2020;395:1988-1997. doi:10.1016/S0140-6736(20)30689-9
3. Fortea J, Zaman SH, Hartley S, Rafii MS, Head E, Carmona-Iragui M. Alzheimer's disease associated with Down syndrome: a genetic form of dementia. *Lancet Neurol*. 2021;20:930-942. doi:10.1016/S1474-4422(21)00245-3
4. McCarron M, McCallion P, Reilly E, Dunne P, Carroll R, Mulryan N. A prospective 20-year longitudinal follow-up of dementia in persons with Down syndrome. *J Intellect Disabil Res*. 2017;61:843-852. doi:10.1111/JIR.12390
5. Iulita MF, Garzón Chavez D, Klitgaard Christensen M, et al. Association of Alzheimer disease with life expectancy in people with Down syndrome. *JAMA Netw Open*. 2022;5:e2212910-e2212910. doi:10.1001/JAMANETWORKOPEN.2022.12910
6. Carmona-Iragui M, Videla L, Lleó A, Fortea J. Down syndrome, Alzheimer disease, and cerebral amyloid angiopathy: the complex triangle of brain amyloidosis. *Dev Neurobiol*. 2019;79:716-737. doi:10.1002/DNEU.22709
7. Draheim CC, Geijer JR, Dengel DR. Comparison of intima-media thickness of the carotid artery and cardiovascular disease risk factors in adults with versus without the Down syndrome. *Am J Cardiol*. 2010;106:1512-1516. doi:10.1016/J.AMJCARD.2010.06.079
8. Wardlaw JM, Smith C, Dichgans M. Small vessel disease: mechanisms and clinical implications. *Lancet Neurol*. 2019;18:684-696. doi:10.1016/S1474-4422(19)30079-1
9. Gaubert M, Lange C, Garnier-Crussard A, et al. Topographic patterns of white matter hyperintensities are associated with multimodal neuroimaging biomarkers of Alzheimer's disease. *Alzheimer's Res Ther*. 2021;13:1-11. 2021 131. doi:10.1186/S13195-020-00759-3
10. Prins ND, Scheltens P. White matter hyperintensities, cognitive impairment and dementia: an update. *Nat Rev Neurol*. 2015;11:157-165. 2015 113. doi:10.1038/nrneurol.2015.10
11. ter Telgte A, van Leijsen EMC, Wiegertjes K, Klijn CJM, Tuladhar AM, de Leeuw F-E. Cerebral small vessel disease: from a focal to

15525279, 0, Downloaded from https://alz-journals.onlinelibrary.wiley.com/doi/10.1002/alz.14146 by Bejanin Alexandre - Readcube (Labtiva Inc.) , Wiley Online Library on [01/08/2024]. See the Terms and Conditions (https://onlinelibrary.wiley.com/terms-and-conditions) on Wiley Online Library for rules of use; OA articles are governed by the applicable Creative Commons License

a global perspective. *Nat Rev Neurol*. 2018;14:387-398. 2018 147. doi:10.1038/s41582-018-0014-y
12. Garnier-Crussard A, Cotton F, Krolak-Salmon P, Chételat G. White matter hyperintensities in Alzheimer's disease: beyond vascular contribution. *Alzheimer's Dement*. 2023;19:3738-3748. doi:10.1002/ALZ.13057
13. Garnier-Crussard A, Bougacha S, Wirth M, et al. White matter hyperintensity topography in Alzheimer's disease and links to cognition. *Alzheimer's Dement*. 2022;18:422-433. doi:10.1002/ALZ.12410
14. Lee S, Viqar F, Zimmerman ME, et al. White matter hyperintensities are a core feature of Alzheimer's disease: evidence from the dominantly inherited Alzheimer network. *Ann Neurol*. 2016;79:929-939. doi:10.1002/ANA.24647
15. Schoemaker D, Zanon Zotin MC, Chen K, et al. White matter hyperintensities are a prominent feature of autosomal dominant Alzheimer's disease that emerge prior to dementia. *Alzheimer's Res Ther*. 2022;14:1-11. doi:10.1186/S13195-022-01030-7/FIGURES/3
16. Carmona-Iragui M, Balasa M, Benejam B, et al. Cerebral amyloid angiopathy in Down syndrome and sporadic and autosomal-dominant Alzheimer's disease. *Alzheimer's Dement*. 2017;13:1251-1260. doi:10.1016/J.JALZ.2017.03.007
17. Lao PJ, Gutierrez J, Keator D, et al. Alzheimer-related cerebrovascular disease in Down syndrome. *Ann Neurol*. 2020;88:1165-1177. doi:10.1002/ANA.25905
18. Alcolea D, Clarimón J, Carmona-Iragui M, et al. The Sant Pau Initiative on Neurodegeneration (SPIN) cohort: a data set for biomarker discovery and validation in neurodegenerative disorders. *Alzheimer's Dement Transl Res Clin Interv*. 2019;5:597-609. doi:10.1016/J.TRCI.2019.09.005
19. Hon J, Huppert FA, Holland AJ, Watson P. Neuropsychological assessment of older adults with Down's Syndrome: an epidemiological study using the Cambridge Cognitive Examination (CAMCOG). *Br J Clin Psychol*. 1999;38:155-165. doi:10.1348/014466599162719
20. Esteba-Castillo S, Dalmau-Bueno A, Ribas-Vidal N, Vilá-Alsina M, García Alba J, Novell R. Adaptation and validation of CAMDEX-DS (Cambridge Examination for Mental Disorders of Older People with Down's Syndrome and others with intellectual disabilities) in Spanish population with intellectual disabilities [in Spanish]. *Rev Neurol*. 2013;57:337-346. ISSN 0210-0010, Vol 57, Nº 8, 2013, Págs 337-346.
21. Fortea J, Carmona-Iragui M, Benejam B, et al. Plasma and CSF biomarkers for the diagnosis of Alzheimer's disease in adults with Down syndrome: a cross-sectional study. *Lancet Neurol*. 2018;17:860-869. doi:10.1016/S1474-4422(18)30285-0
22. Regier DA, Kuhl EA, Kupfer DJ. The DSM-5: classification and criteria changes. *World Psychiatry*. 2013;12:92-98. doi:10.1002/WPS.20050
23. Gaser C, Dahnke R, Thompson PM, Kurth F, Luders E, Initiative ADN. CAT – a computational anatomy toolbox for the analysis of structural MRI data. *Biorxiv*. 2022:11.495736. doi:10.1101/2022.06.11.495736. 2022.06.. bioRxiv.
24. Avants BB, Tustison NJ, Song G, Cook PA, Klein A, Gee JC. A reproducible evaluation of ANTs similarity metric performance in brain image registration. *Neuroimage*. 2011;54:2033-2044. doi:10.1016/J.NEUROIMAGE.2010.09.025
25. Schmidt P, Bayesian inference for structured additive regression models for large-scale problems with applications to medical imaging 2017. (accessed April 16, 2022) https://edoc.ub.uni-muenchen.de/20373/
26. Sudre CH, Gomez Anson B, Davagnanam I, et al. Bullseye's representation of cerebral white matter hyperintensities. *J Neuroradiol*. 2018;45:114-122. doi:10.1016/J.NEURAD.2017.10.001
27. Jiménez-Balado J, Corlier F, Habeck C, Stern Y, Eich T. Effects of white matter hyperintensities distribution and clustering on late-life cognitive impairment. *Sci Rep*. 2022;12:1-13. 2022 121. doi:10.1038/s41598-022-06019-8
28. Orlhac F, Eertink JJ, Cottereau AS, et al. A guide to ComBat harmonization of imaging biomarkers in multicenter studies. *J Nucl Med*. 2022;63(2):172-179. doi:10.2967/JNUMED.121.262464
29. Carmona-Iragui M, Santos T, Videla S, et al. Feasibility of lumbar puncture in the study of cerebrospinal fluid biomarkers for Alzheimer's disease in subjects with Down syndrome. *J Alzheimer's Dis*. 2017;55:1489-1496. doi:10.3233/JAD-160827
30. Alcolea D, Pegueroles J, Muñoz L, et al. Agreement of amyloid PET and CSF biomarkers for Alzheimer's disease on Lumipulse. *Ann Clin Transl Neurol*. 2019;6:1815-1824. doi:10.1002/ACN3.50873
31. Subirana I, Sanz H, Vila J. Building Bivariate Tables: the compareGroups Package for R. *J Stat Softw*. 2014;57:1-16. doi:10.18637/JSS.V057.I12
32. Garnier-Crussard A, Bougacha S, Wirth M, et al. White matter hyperintensities across the adult lifespan: relation to age, Aβ load, and cognition. *Alzheimer's Res Ther*. 2020;12:1-11. 2020 121. doi:10.1186/S13195-020-00669-4
33. Hopkins RO, Beck CJ, Burnett DL, Weaver LK, Victoroff J, Bigler ED. Prevalence of white matter hyperintensities in a young healthy population. *J Neuroimaging*. 2006;16:243-251. doi:10.1111/J.1552-6569.2006.00047.X
34. Holland CM, Smith EE, Csapo I, et al. Spatial distribution of white-matter hyperintensities in Alzheimer disease, cerebral amyloid angiopathy, and healthy aging. *Stroke*. 2008;39:1127. doi:10.1161/STROKEAHA.107.497438
35. Iulita MF, Bejanin A, Vilaplana E, et al. Association of biological sex with clinical outcomes and biomarkers of Alzheimer's disease in adults with Down syndrome. *Brain Commun*. 2023;5:14. doi:10.1093/BRAINCOMMS/FCAD074
36. Bejanin A, Iulita MF, Vilaplana E, et al. Association of apolipoprotein E ε4 allele with clinical and multimodal biomarker changes of Alzheimer disease in adults with Down syndrome. *JAMA Neurol*. 2021;78:937-947. doi:10.1001/JAMANEUROL.2021.1893
37. Operto G, Cacciaglia R, Grau-Rivera O, et al. White matter microstructure is altered in cognitively normal middle-aged APOE-ε4 homozygotes. *Alzheimers Res Ther*. 2018;10(1):48. doi:10.1186/S13195-018-0375-X
38. Rojas S, Brugulat-Serrat A, Bargalló N, et al. Higher prevalence of cerebral white matter hyperintensities inhomozygous APOE-ε4 allele carriers aged 45-75: results from theALFA study. *J Cereb Blood Flow Metab*. 2018;38:250. doi:10.1177/0271678x17707397
39. Habes M, Erus G, Toledo JB, et al. White matter hyperintensities and imaging patterns of brain ageing in the general population. *Brain*. 2016;139:1164. doi:10.1093/BRAIN/AWW008
40. Kumar D, Yatawara C, Wang B, et al. APOE4 and confluent white matter hyperintensities have a synergistic effect on episodic memory impairment in prodromal dementia. *J Alzheimer's Dis*. 2022;87:1103-1114. doi:10.3233/JAD-215556
41. Slattery CF, Zhang J, Paterson RW, et al. ApoE influences regional white-matter axonal density loss in Alzheimer's disease. *Neurobiol Aging*. 2017;57:8. doi:10.1016/J.NEUROBIOLAGING.2017.04.021
42. Morgen K, Schneider M, Frölich L, et al. Apolipoprotein E-dependent load of white matter hyperintensities in Alzheimer's disease: a voxel-based lesion mapping study. *Alzheimers Res Ther*. 2015;7(1):27. doi:10.1186/S13195-015-0111-8
43. Hartley SL, Fleming V, Schworer EK, et al. Timing of Alzheimer's disease by intellectual disability level in Down syndrome. *J Alzheimers Dis*. 2023;95:213-225. doi:10.3233/JAD-230200
44. Videla L, Benejam B, Pegueroles J, et al. Longitudinal clinical and cognitive changes along the Alzheimer disease continuum in Down syndrome. *JAMA Netw Open*. 2022;5:e2225573-e2225573. doi:10.1001/JAMANETWORKOPEN.2022.25573
45. Eloyan A, Thangarajah M, An N, et al. White matter hyperintensities are higher among early-onset Alzheimer's disease participants than their cognitively normal and early-onset nonAD peers: longitudinal

15525279, 0, Downloaded from https://alz-journals.onlinelibrary.wiley.com/doi/10.1002/alz.14146 by Bejanin Alexandre - Readcube (Labtiva Inc.) , Wiley Online Library on [01/08/2024]. See the Terms and Conditions (https://onlinelibrary.wiley.com/terms-and-conditions) on Wiley Online Library for rules of use; OA articles are governed by the applicable Creative Commons License

Early-onset Alzheimer's Disease Study (LEADS). *Alzheimer's Dement*. 2023;19(9):S89-S97. doi:10.1002/alz.13402. Suppl.
46. Brickman AM, Zahodne LB, Guzman VA, et al. Reconsidering harbingers of dementia: progression of parietal lobe white matter hyperintensities predicts Alzheimer's disease incidence. *Neurobiol Aging*. 2015;36:27-32. doi:10.1016/J.NEUROBIOLAGING.2014.07.019
47. Walsh P, Sudre CH, Manning EN, et al. White matter hyperintensity increases are a feature of familial AD and are associated with increased brain atrophy. *Alzheimer's Dement*. 2020;16:e038925. doi:10.1002/ALZ.038925
48. Yoshita M, Fletcher E, Harvey D, et al. Extent and distribution of white matter hyperintensities in normal aging, MCI, and AD. *Neurology*. 2006;67:2192. doi:10.1212/01.WNL.0000249119.95747.1F
49. Mayo CD, Garcia-Barrera MA, Mazerolle EL, Ritchie LJ, Fisk JD, Gawryluk JR. Relationship between DTI metrics and cognitive function in Alzheimer's disease. *Front Aging Neurosci*. 2019;10:436. doi:10.3389/FNAGI.2018.00436
50. Weaver NA, Doeven T, Barkhof F, et al. Cerebral amyloid burden is associated with white matter hyperintensity location in specific posterior white matter regions. *Neurobiol Aging*. 2019;84:225-234. doi:10.1016/J.NEUROBIOLAGING.2019.08.001
51. Caballero MÁA, Song Z, Rubinski A, et al. Age-dependent amyloid deposition is associated with white matter alterations in cognitively normal adults during the adult life span. *Alzheimer's Dement*. 2020;16:651-661. doi:10.1002/ALZ.12062
52. Roseborough A, Ramirez J, Black SE, Edwards JD. Associations between amyloid β and white matter hyperintensities: a systematic review. *Alzheimer's Dement*. 2017;13:1154-1167. doi:10.1016/J.JALZ.2017.01.026
53. Graff-Radford J, Arenaza-Urquijo EM, Knopman DS, et al. White matter hyperintensities: relationship to amyloid and tau burden. *Brain*. 2019;142:2483-2491. doi:10.1093/BRAIN/AWZ162
54. Osborn KE, Liu D, Samuels LR, et al. Cerebrospinal fluid β-amyloid42 and neurofilament light relate to white matter hyperintensities. *Neurobiol Aging*. 2018;68:18-25. doi:10.1016/J.NEUROBIOLAGING.2018.03.028
55. Van Waalwijk Van Doorn LJC, Ghafoorian M, Van Leijsen EMC, et al. White matter hyperintensities are no major confounder for Alzheimer's disease cerebrospinal fluid biomarkers. *J Alzheimers Dis*. 2021;79:163-175. doi:10.3233/JAD-200496
56. Pålhaugen L, Sudre CH, Tecelao S, et al. Brain amyloid and vascular risk are related to distinct white matter hyperintensity patterns. *J Cereb Blood Flow Metab*. 2021;41:1162. doi:10.1177/0271678x20957604
57. Walsh P, Sudre CH, Fiford CM, et al. CSF amyloid is a consistent predictor of white matter hyperintensities across the disease course from aging to Alzheimer's disease. *Neurobiol Aging*. 2020;91:5-14. doi:10.1016/J.NEUROBIOLAGING.2020.03.008
58. Walsh P, Sudre CH, Fiford CM, et al. The age-dependent associations of white matter hyperintensities and neurofilament light in early- and late-stage Alzheimer's disease. *Neurobiol Aging*. 2021;97:10-17. doi:10.1016/J.NEUROBIOLAGING.2020.09.008
59. Zetterberg H, Skillbäck T, Mattsson N, et al. Association of cerebrospinal fluid neurofilament light concentration with Alzheimer disease progression. *JAMA Neurol*. 2016;73:60. doi:10.1001/JAMANEUROL.2015.3037
60. Meeker KL, Butt OH, Gordon BA, et al. Cerebrospinal fluid neurofilament light chain is a marker of aging and white matter damage. *Neurobiol Dis*. 2022;166:105662. doi:10.1016/J.NBD.2022.105662
61. Schultz SA, Strain JF, Adedokun A, et al. Serum neurofilament light chain levels are associated with white matter integrity in autosomal dominant Alzheimer's disease. *Neurobiol Dis*. 2020;142:104960. doi:10.1016/J.NBD.2020.104960
62. Gaetani L, Blennow K, Calabresi P, Di Filippo M, Parnetti L, Zetterberg H. Neurofilament light chain as a biomarker in neurological disorders. *J Neurol Neurosurg Psychiatry*. 2019;90:870-881. doi:10.1136/JNNP-2018-320106
63. La Joie R, Visani AV, Baker SL, et al. Prospective longitudinal atrophy in Alzheimer's disease correlates with the intensity and topography of baseline tau-PET. *Sci Transl Med*. 2020;12(254):eaau5732. doi:10.1126/SCITRANSLMED.AAU5732
64. Dickerson BC, Bakkour A, Salat DH, et al. The cortical signature of Alzheimer's disease: regionally specific cortical thinning relates to symptom severity in very mild to mild AD dementia and is detectable in asymptomatic amyloid-positive individuals. *Cereb Cortex (New York, NY)*. 2009;19:497. doi:10.1093/CERCOR/BHN113
65. Lao PJ, Brickman AM. Multimodal neuroimaging study of cerebrovascular disease, amyloid deposition, and neurodegeneration in Alzheimer's disease progression. *Alzheimer's Dement Diagnosis, Assess Dis Monit*. 2018;10:638-646. doi:10.1016/J.DADM.2018.08.007
66. Brickman AM, Rizvi B. White matter hyperintensities and Alzheimer's disease: an alternative view of an alternative hypothesis. *Alzheimer's Dement*. 2023;19:4260-4261. doi:10.1002/ALZ.13371
67. Bozzali M, Falini A, Franceschi M, et al. White matter damage in Alzheimer's disease assessed in vivo using diffusion tensor magnetic resonance imaging. *J Neurol Neurosurg Psychiatry*. 2002;72:742. doi:10.1136/JNNP.72.6.742
68. McAleese KE, Walker L, Graham S, et al. Parietal white matter lesions in Alzheimer's disease are associated with cortical neurodegenerative pathology, but not with small vessel disease. *Acta Neuropathol*. 2017;134:459-473. doi:10.1007/S00401-017-1738-2/FIGURES/5
69. McAleese KE, Firbank M, Dey M, et al. Cortical tau load is associated with white matter hyperintensities 2015. doi:10.1186/s40478-015-0240-0
70. Salvadores N, Gerónimo-Olvera C, Court FA. Axonal degeneration in AD: the contribution of Aβ and Tau. *Front Aging Neurosci*. 2020;12:581767. doi:10.3389/FNAGI.2020.581767/BIBTEX
71. Laing KK, Simoes S, Baena-Caldas GP, et al. Cerebrovascular disease promotes tau pathology in Alzheimer's disease. *Brain Commun*. 2020;2(2):fcaa132. doi:10.1093/BRAINCOMMS/FCAA132
72. Iadecola C. The pathobiology of vascular dementia. *Neuron*. 2013;80:844-866. doi:10.1016/J.NEURON.2013.10.008
73. Thanprasertsuk S, Martinez-Ramirez S, Pontes-Neto OM, et al. Posterior white matter disease distribution as a predictor of amyloid angiopathy. *Neurology*. 2014;83:794-800. doi:10.1212/WNL.0000000000000732
74. Garnier-Crussard A, Cotton F, Krolak-Salmon P, Chételat G. White matter hyperintensities in Alzheimer's disease: beyond vascular contribution. *Alzheimer's Dement*. 2023;19(8):3738-3748. doi:10.1002/ALZ.13057
75. Low A, Mak E, Rowe JB, Markus HS, O'Brien JT. Inflammation and cerebral small vessel disease: a systematic review. *Ageing Res Rev*. 2019;53:100916. doi:10.1016/J.ARR.2019.100916

SUPPORTING INFORMATION

Additional supporting information can be found online in the Supporting Information section at the end of this article.

How to cite this article: Morcillo-Nieto AO, Zsadanyi SE, Arriola-Infante JE, et al. Characterization of white matter hyperintensities in Down syndrome. *Alzheimer's Dement*. 2024;1-15. https://doi.org/10.1002/alz.14146

15525279, 0, Downloaded from https://alz-journals.onlinelibrary.wiley.com/doi/10.1002/alz.14146 by Bejamin Alexandre - Readcube (Labtiva Inc.) , Wiley Online Library on [01/08/2024]. See the Terms and Conditions (https://onlinelibrary.wiley.com/terms-and-conditions) on Wiley Online Library for rules of use; OA articles are governed by the applicable Creative Commons License

Study 3: Temporal dynamics of white matter hyperintensities related to Alzheimer's disease in adults with Down syndrome

Alejandra O Morcillo-Nieto[1,2,3,*]; Mateus Rozalem-Aranha[1,4,*]; Lucia Maure-Blesa[1,2,5]; Íñigo Rodríguez-Baz[1,2]; José Enrique Arriola-Infante[6]; Maria Franquesa-Mullerat[1,3]; Sara E Zsadanyi[1,2,3]; Lídia Vaqué-Alcázar[1,7,8]; José Allende Parra[1,3]; Zili Zhao[1,3]; Javier Arranz[1,5]; Laura Videla[1,2,9]; Isabel Barroeta[1,2]; Laura Del Hoyo Soriano[1,2]; Bessy Benejam[1,9]; Susana Fernández[9]; Aida Sanjuan Hernandez[1]; Lucia Pertierra[1,2,10]; Sandra Giménez[1,2,11]; Daniel Alcolea[1,2]; Olivia Belbin[1,2]; Alberto Lleó[1,2]; María Carmona-Iragui[1,2,9]; Juan Fortea[1,2,9]; Alexandre Bejanin[1,2]

*These authors contributed equally to this work.

[1]Sant Pau Memory Unit, IR SANT PAU, Hospital de la Santa Creu i Sant Pau, Barcelona, Spain. [2]Center of Biomedical Investigation Network for Neurodegenerative Diseases (CIBERNED), Madrid, Spain. [3]Institut de Neurociències, Universitat Autònoma de Barcelona, Barcelona, Spain. [4]Neuroradiology Section, Department of Radiology, Hospital de la Santa Creu i Sant Pau, Facultad de Medicina, Universitat Autònoma de Barcelona, Barcelona, Spain. [5]Department of Medicine, Universitat Autònoma de Barcelona, Barcelona, Spain. [6]Department of Neurology, Torrecárdenas University Hospital, Almería, Spain. [7]Department of Medicine, Faculty of Medicine and Health Sciences, Institute of Neurosciences, University of Barcelona, Barcelona, Spain. [8]Institut d'Investigacions Biomèdiques August Pi i Sunyer (IDIBAPS), Barcelona, Spain. [9]Barcelona Down Medical Center, Fundació Catalana Síndrome de Down, Barcelona, Spain. [10]Cognitive Neurology, Neuropsychology and Neuropsychiatry Unit, Neurology Department, Fleni, Ciudad Autónoma de Buenos Aires, Argentina.[11]Multidisciplinary Sleep unit. IR SANT PAU, Hospital de la Santa Creu i Sant Pau, Barcelona, Spain

Alzheimer's Dement (2026) 22(2):e71157. doi: 10.1002/alz.71157
IF (2024) =11.1, Rank= 6/202 in Clinical Neurology, D1

Check for updates

Received: 22 October 2025 | Revised: 9 December 2025 | Accepted: 30 December 2025

DOI: 10.1002/alz.71157

Alzheimer's & Dementia®
THE JOURNAL OF THE ALZHEIMER'S ASSOCIATION

RESEARCH ARTICLE

Temporal dynamics of white matter hyperintensities related to Alzheimer's disease in adults with Down syndrome

Alejandra O. Morcillo-Nieto[1,2,3] | **Mateus Rozalem-Aranha**[1,4] | **Lucia Maure-Blesa**[1,2,5] | **Íñigo Rodríguez-Baz**[1,2] | **José Enrique Arriola-Infante**[6] | **Maria Franquesa-Mullerat**[1,3] | **Sara E. Zsadanyi**[1,2,3] | **Lídia Vaqué-Alcázar**[1,7,8] | **José Allende Parra**[1,3] | **Zili Zhao**[1,3] | **Javier Arranz**[1,5] | **Laura Videla**[1,2,9] | **Isabel Barroeta**[1,2] | **Laura Del Hoyo Soriano**[1,2] | **Bessy Benejam**[1,9] | **Susana Fernández**[9] | **Aida Sanjuan Hernandez**[1] | **Lucia Pertierra**[10,1,2] | **Sandra Giménez**[1,2,11] | **Daniel Alcolea**[1,2] | **Olivia Belbin**[1,2] | **Alberto Lleó**[1,2] | **María Carmona-Iragui**[1,2,9] | **Juan Fortea**[1,2,9] | **Alexandre Bejanin**[1,2]

[1]Sant Pau Memory Unit, IR SANT PAU, Hospital de la Santa Creu i Sant Pau, Barcelona, Spain

[2]Center of Biomedical Investigation Network for Neurodegenerative Diseases (CIBERNED), Madrid, Spain

[3]Institut de Neurociències, Universitat Autònoma de Barcelona, Barcelona, Spain

[4]Neuroradiology Section, Department of Radiology, Hospital de la Santa Creu i Sant Pau, Facultad de Medicina, Universitat Autònoma de Barcelona, Barcelona, Spain

[5]Department of Medicine, Universitat Autònoma de Barcelona, Barcelona, Spain

[6]Department of Neurology, Torrecárdenas University Hospital, Almería, Spain

[7]Department of Medicine, Faculty of Medicine and Health Sciences, Institute of Neurosciences, University of Barcelona, Barcelona, Spain

[8]Institut d'Investigacions Biomèdiques August Pi i Sunyer (IDIBAPS), Barcelona, Spain

[9]Barcelona Down Medical Center, Fundació Catalana Síndrome de Down, Barcelona, Spain

[10]Cognitive Neurology, Neuropsychology and Neuropsychiatry Unit, Neurology Department, Fleni, Buenos Aires, Argentina

[11]Multidisciplinary Sleep unit. IR SANT PAU, Hospital de la Santa Creu i Sant Pau, Barcelona, Spain

Correspondence
Alexandre Bejanin, Sant Pau Memory Unit, IR SANT PAU, Hospital de la Santa Creu i Sant Pau, Sant Quintí, 77-79 - 08041 Barcelona, Spain.
Email: abejanin@santpau.cat

Abstract

INTRODUCTION: White matter hyperintensities (WMH) are common in Down syndrome (DS), yet their longitudinal evolution and associations with Alzheimer's disease (AD) remain unclear.

METHODS: Longitudinal MRI study, including 80 DS adults and 53 euploid controls. WMH were segmented on serial FLAIR using a longitudinal pipeline. We assessed

Alejandra O. Morcillo-Nieto and Mateus Rozalem-Aranha contributed equally to this work and share first authorship.

Funding information: Department of Research and Universities from the Generalitat de Catalunya, Grant/Award Number: 2021SGR00979; Instituto de Salud Carlos III (ISCIII) and co-funded by the European Union. ERDF, Grant/Award Numbers: INT21/00073, PI20/01473, PI23/01786, PI18/00435, PI22/00611, INT19/00016, INT23/00048, CP20/00038, CP24/00112, PI22/00758, ICI23/00032, PI20/00836, CM22/00052, CM22/00243, CM23/00291; Centro de Investigación Biomédica en Red sobre Enfermedades Neurodegenerativas; National Institutes of Health, Grant/Award Numbers: 1R01AG056850-01A1, R21AG056974, R01AG061566, 1R01AG081394-01, 1R61AG066543-01; Department de Salut de la Generalitat de Catalunya, Grant/Award Number: SLT006/17/00119; Fundación Tatiana Pérez de Guzmán el Bueno, Grant/Award Number: IIBSP-DOW-2020-151; Horizon 2020 - Research and Innovation Framework Programme, Grant/Award Number: H2020-SC1-BHC-2018-2020; Department of Health Generalitat de Catalunya PERIS program, Grant/Award Numbers: SLT006/17/125, CP24/00112; Alzheimer's Association, Grant/Award Numbers: AARG-22-973966, AARFD-21-852492, AARG-22-923680; Ajuntament de Barcelona, Grant/Award Number: 23S06157-001; Global Brain Health Institute, Grant/Award Number: GBHI_ALZ-23-971107; Jérôme Lejeune Foundation, Grant/Award Numbers: #1801 Cycle 2020, #2425 cycle 2024B, 2326-GRT-2024A

This is an open access article under the terms of the Creative Commons Attribution-NonCommercial-NoDerivs License, which permits use and distribution in any medium, provided the original work is properly cited, the use is non-commercial and no modifications or adaptations are made.
© 2026 The Author(s). *Alzheimer's & Dementia* published by Wiley Periodicals LLC on behalf of Alzheimer's Association.

the effects of demographic, genetic factors, AD clinical stage, AD-related fluid, and cerebrovascular biomarkers on annual WMH volume changes.

RESULTS: In DS, annual WMH changes were relatively stable until age 40, and then exhibited fluctuations, with a significant decrease at the group level. Declines were larger in symptomatic cases, particularly in periventricular and fronto-parieto-occipital regions. Higher baseline WMH and microbleeds presence related to greater WMH reduction. Visual ratings and adjustment for white matter volume supported the robustness of the results.

DISCUSSION: WMH trajectories were heterogeneous in DS and declined over time with AD symptoms. This unexpected reduction may reflect different underlying pathological processes, including neurodegeneration or neuroinflammation.

KEYWORDS
Alzheimer's disease, cerebral amyloid angiopathy, Down syndrome, longitudinal analysis, magnetic resonance imaging, neuroimaging, white matter hyperintensities

Highlights

- The evolution of white matter hyperintensities (WMH) in Down syndrome (DS) is variable over time and with age.
- After age 40, more cases experienced significant WMH variations, primarily decreases.
- In DS, annual WMH change decreases with Alzheimer's symptoms.
- Higher baseline WMH and microbleeds are related to greater annual WMH reduction.
- WMH reduction likely reflects distinct processes, for example, degeneration or inflammation.

1 | BACKGROUND

Down syndrome (DS), caused by a full or partial trisomy of chromosome 21, is the most common genetic form of intellectual disability (ID), affecting approximately 6 million people worldwide.[1] Advances in healthcare have significantly increased the life expectancy of individuals with DS to around 60 years,[2] which has led to an increased prevalence of age-related conditions, notably Alzheimer's disease (AD). Indeed, AD is the leading cause of death in adults with DS.[3] This heightened risk is mainly due to the triplication of the amyloid precursor protein (*APP*) gene on chromosome 21, which is both necessary and sufficient to cause early-onset AD neuropathology in DS.[4] Amyloid-β (Aβ) accumulation begins during adolescence, and by the age of 40, nearly all individuals with DS exhibit the neuropathological features characteristic of AD.[5,6] In addition, Aβ can aggregate within the walls of leptomeningeal and cortical blood vessels, leading to the development of cerebral amyloid angiopathy (CAA).[7]

Interestingly, despite the low prevalence of hypertension and arteriolosclerosis in DS,[8,9] neuroimaging studies reveal changes classically associated with small vessel disease (SVD) in adults with DS.[10,11] Hence, white matter hyperintensities (WMH), a key neuroimaging hallmark of SVD, increase more markedly with age and begin at an earlier age in individuals with DS than in the euploid population.[10,12,13] Two large studies in DS have reported that WMH start to increase around age 40 and are strongly associated with the clinical progression of AD and AD pathology in DS.[11,12] A recent longitudinal study from the Alzheimer's Biomarker Consortium-Down Syndrome (ABC-DS) showed that WMH trajectories are heterogeneous, with declines over time in cognitively stable adults with DS and increases, at the group level, with advancing AD stages, even though a subset of symptomatic participants exhibited decreases. These findings suggest that WMH fluctuates over time in DS and may reflect pathophysiological processes related to the overproduction of the Aβ and AD.

With the introduction of anti-amyloid monoclonal antibodies into clinical practice as well as the development of new therapeutic agents, it is essential to delineate the natural progression of cerebrovascular lesions, particularly WMH, in populations likely to benefit from, such as individuals genetically predisposed to AD, including those with DS.[14]

15525279, 2026, 2, Downloaded from https://alz-journals.onlinelibrary.wiley.com/doi/10.1002/alz.71157 by Alejandra O. Morcillo-Nieto - Spanish Cochrane National Provision (Ministerio de Sanidad) , Wiley Online Library on [05/02/2026]. See the Terms and Conditions (https://onlinelibrary.wiley.com/terms-and-conditions) on Wiley Online Library for rules of use; OA articles are governed by the applicable Creative Commons License

WMH can resemble certain secondary effects of these drugs, such as amyloid-related imaging abnormalities (ARIA), complicating the interpretation of treatment-related imaging changes. Furthermore, WMH may be considered as primary or secondary outcomes in clinical trials targeting vascular integrity or neuroinflammatory pathways, underscoring the need for a thorough understanding of their natural history and pathophysiology to accurately assess therapeutic efficacy.

The aim of this study is to investigate the longitudinal changes of WMH in DS and their associations with demographic, clinical, and AD biomarker data, as well as other vascular markers. Based on previous evidence, we hypothesize that WMH accumulation accelerates during the symptomatic stages and is associated with neurodegeneration.

RESEARCH IN CONTEXT

1. **Systematic review**: White matter hyperintensities (WMH) are common in adults with Down syndrome (DS), a genetically determined form of Alzheimer's disease (AD). The prevalence and severity of WMH in DS increase markedly with age, particularly after ~40 years, coinciding with near-universal AD neuropathology in DS. WMH also relates to AD clinical progression and pathology, suggesting an interplay between small vessel disease (SVD) and AD. However, the longitudinal evolution of WMH in DS and their association with AD pathology remain unexplored.
2. **Interpretation**: Annual WMH changes fluctuated over time in DS. During the 20s-30s, most individuals exhibited minimal WMH changes; however, after age 40, many showed notable variations, mainly decreases. Greater reductions of annual WMH changes were observed in individuals with AD symptoms, higher baseline WMH burden, and the presence of microbleeds. Declines in WMH, not fully explained by white matter atrophy, suggest additional pathophysiological mechanisms.
3. **Future directions**: Future research combining long-term and multimodal neuroimaging with *post mortem* validation could provide a better characterization of the WMH etiology.

2 | METHODS

2.1 | Study design and participants

This single-center, longitudinal cohort study recruited adults with DS from the population-based Down-Alzheimer Barcelona Neuroimaging Initiative (DABNI) cohort[15] and euploid, cognitively unimpaired control individuals (HC) from the Sant Pau Initiative on Neurodegeneration (SPIN) cohort.[16] Participants of both sexes were aged 18 or older, with at least two magnetic resonance imaging (MRI) scans and comprehensive neurological and neuropsychological assessments. The study was approved by the Sant Pau Ethics Committee following the standards for medical research in humans recommended by the Declaration of Helsinki. All participants or their legally authorized representatives gave written informed consent before enrolment.

2.2 | Clinical assessment

Adults with DS underwent a specific neuropsychological assessment, including the Cambridge Cognitive Examination for Older Adults with Down Syndrome (CAMCOG-DS) Spanish version[17] to assess the global cognition by evaluating orientation, language, memory, attention, praxis, abstract thinking, and perception. Additionally, ID was categorized as mild, moderate, or severe/profound based on the Diagnostic and Statistical Manual of Mental Disorders, Fifth Edition,[18] and caregivers' report of the individual's best-ever level of functioning and the score of the Kaufman Brief Intelligence Test Spanish version.[19]

Participants were clinically classified in a consensus meeting between neurologists and neuropsychologists, after independent visits and blinded to biomarker data, into the following four groups: (1) asymptomatic (aDS, i.e., no clinical or neuropsychological suspicion of AD-related cognitive decline), (2) prodromal AD (pDS, i.e., evidence of cognitive decline due to AD, but no significant impact on baseline activities of daily living), (3) AD dementia (dDS, i.e., when the cognitive decline impaired the daily activities) and (4) uncertain (uDS, i.e., when there were medical, pharmacological, or psychiatric condition interfering with cognition or daily activities, but no suspicion of neurodegenerative origin). To maximize statistical power, we combined in this study pDS and dDS into a single symptomatic group (sDS). Clinical evaluations were performed at baseline and follow-up visits. Based on changes in clinical diagnosis along the AD continuum, participants were further categorized as progressors (aDS progressing to sDS at follow-up), or stable (no change or uDS at any visit).

The HC group consisted of cognitively unimpaired euploid individuals who had no cognitive complaints, scored 0 on the Clinical Dementia Rating scale and/or 1 in the Global Deterioration Scale–Functional Assessment Staging, and performed within the normal range on neuropsychological evaluations regarding their age and education. None reported any neurological or psychiatric disorders or other major medical illnesses.[16]

2.3 | Neuroimaging data

2.3.1 | Image acquisition

All participants underwent at least two MRI sessions at Hospital del Mar (3T Philips-Achieva) or Hospital Clinic (3T Siemens Prisma), separated by a minimum interval of 6 months. MRI protocols include high-resolution three-dimensional T1-weighted (T1w), fluid-attenuated inversion recovery (FLAIR), and susceptibility weighted images (SWI). Only participants scanned with the same MRI protocol

15525279, 2026, 2, Downloaded from https://alz-journals.onlinelibrary.wiley.com/doi/10.1002/alz.71157 by Alejandra O. Morcillo-Nieto - Spanish Cochrane National Provision (Ministerio de Sanidad) , Wiley Online Library on [05/02/2026]. See the Terms and Conditions (https://onlinelibrary.wiley.com/terms-and-conditions) on Wiley Online Library for rules of use; OA articles are governed by the applicable Creative Commons License

at baseline and follow-up were included. Detailed acquisition parameters of the imaging protocols are provided in Table S1 (see Supporting Information).

2.3.2 | WMH quantification

T1 preprocessing

Structural T1w images were preprocessed with the Computational Anatomy Toolbox 12 version 8 (CAT12v8)[20] toolbox of Statistical Parametric Mapping 12 (SPM12, Welcome Centre for Human Neuroimaging, University College London, Queen Square Institute of Neurology). For each participant and time point, CAT12 was used to segment total gray matter (GM), white matter (WM), and cerebrospinal fluid (CSF) maps. Hammer's atlas was also coregistered into the native T1w space at each visit.

WMH longitudinal segmentation

To accurately segment WMH across multiple time points, we employed the longitudinal pipeline implemented in the Lesion Segmentation Toolbox version 3.0.0 (LST)[21] for SPM12. This pipeline is specifically designed to compare lesion probability maps previously generated by the Lesion Prediction Algorithm (LPA)[22] across multiple time points.

As a preprocessing step, FLAIR scans were coregistered into their corresponding T1w images using Advanced Normalization Tools (ANTs).[23] We then applied the LPA method to each time point to generate lesion probability maps of WMH based on a logistic regression classifier that labels each voxel as a lesion or non-lesion. The resulting probability maps were binarized using a threshold of 0.3, following our previous work.[12]

Next, the WMH longitudinal pipeline of LST performed rigid between-time-point coregistration of each participant's FLAIR images. The resulting space transforms were subsequently applied to the lesion probability maps, ensuring that for each participant, all FLAIR images and corresponding lesion maps were aligned in a common space.

Finally, relative changes in intensity among FLAIR scans were computed for all voxels that were labeled as a lesion in at least one time point. Through an iterative procedure, the pipeline distinguishes true lesion change from natural variability in FLAIR signal across time points. This yielded refined and binarized lesion maps for each time point that were jointly informed by the full longitudinal series.

WM parcellation

We divided the WM into two distinct parcellation sets: concentric layers and lobar regions, following our previous methodology.[12] Briefly, for the lobar regions, we used the anatomical Hammers atlas, delineating the frontal, parietal, temporal, occipital, and basal ganglia regions. To define the concentric layers, we computed distance maps from the ventricles to the GM junction (using the GM and CSF maps derived from CAT12v8), thereby segmenting the WM into four layers: Layer 1 is proximal to the ventricles, while Layer 4 encompasses the juxtacortical areas. The resulting parcellations were applied to each time point's FLAIR scan.

Extraction of WMH volumes

Total WMH volumes were obtained as the intersection between longitudinal LPA-derived lesion maps and the WM masks from CAT12v8. Regional WMH volumes were computed from the overlap between the WMH maps and the WM parcellation using an in-house MATLAB script. To account for differences in MRI acquisition protocols, both total and regional WMH volumes were harmonized using the ComBat harmonization method[24] implemented in the R library *neuroCombat*.

Annualized change calculations

Annualized changes in total and regional Combat-harmonized WMH volumes were computed as the difference between the last follow-up and the baseline values, divided by the corresponding time interval between visits, expressed in years. Positive values indicate increases in WMH volume between the two time points, while negative values indicate decreases in WMH volume.

To determine significant changes in WMH volume, we applied a thresholding approach based on a previous study[25]: annual changes greater than 75 mm^3/year were considered indicative of progression (i.e., increased WMH volume at follow-up), while changes inferior to −75 mm^3/year were considered indicative of regression (i.e., decreased WMH volume at follow-up). Changes within the range of −75 mm^3/year to 75 mm^3/year were considered stable, indicating minimal change in WMH volume.

Visual read

To validate the results of the automatic WMH segmentation, an expert neuroradiologist (M.R.A.) performed a visual assessment of paired time points for each subject. Specifically, the rater was blinded to both the subject and the visit order and had to determine whether one scan showed more WMH than the other on a 5-point Likert scale: −2 (marked decrease), −1 (slight decrease), 0 (no change), +1 (slight increase), +2 (marked increase).

2.3.3 | Microbleed segmentation

SWI scans were N4 bias field corrected using ANTs and coregistered to their corresponding T1w image. Microbleed segmentation was manually performed using ITK-SNAP (v.3.8.0),[26] as previously described.[27]

2.4 | Blood and cerebrospinal fluid biomarkers

A subset of participants underwent lumbar puncture and/or blood extraction within 1 year of MRI baseline acquisition.[28,29] Most participants were screened for apolipoprotein E (*APOE*) haplotype via Sanger sequencing. We quantified Aβ peptide 1-40 (Aβ_{40}), Aβ peptide 1-42 (Aβ_{42}), and tau phosphorylated at threonine 181 (pTau181) in CSF using a commercially available immunoassay in a fully automated platform (Lumipulse; Fujirebio-Europe), following a previously published protocol.[16] Additionally, CSF and plasma glial fibrillary acidic protein

15525279, 2026, 2, Downloaded from https://alz-journals.onlinelibrary.wiley.com/doi/10.1002/alz.71157 by Alejandra O. Morcillo-Nieto - Spanish Cochrane National Provision (Ministerio de Sanidad) , Wiley Online Library on [05/02/2026]. See the Terms and Conditions (https://onlinelibrary.wiley.com/terms-and-conditions) on Wiley Online Library for rules of use; OA articles are governed by the applicable Creative Commons License

(GFAP) concentrations were measured using the SR-X single-molecule array (Quanterix). CSF neurofilament light chain (NfL) and YKL-40 (also known as chitinase 3-like 1) levels were measured with commercially available enzyme-linked immunosorbent assays (NF-Light Assay, UmanDiagnostics, and MicroVue EIA, Quidel, respectively) according to the manufacturer's recommendations.

2.5 | Statistical analyses

Statistical analyses were conducted using R software (version 4.5.0), and the statistical significance threshold was set at p = 0.05. Baseline demographic differences between DS and HC participants were assessed using the *compareGroups* library.[30] Chi-squared tests were used for categorical variables (e.g., sex, APOEε4 status, and vascular risk factors), and Mann–Whitney tests were applied for continuous variables (e.g., age and CSF biomarkers), due to non-normal distribution.

To examine the association between annual changes of WMH volume and age, we performed locally estimated scatterplot smoothing (LOESS) curves with a tricubic weight function and a span parameter of 0.75, providing an informative representation of the data. The effect of factors sex, APOEε4 status, ID, and AD clinical status on the annual WMH volume changes was assessed using the Mann–Whitney or Kruskal–Wallis tests. For group differences across AD clinical status, Dunn's post-hoc test was applied with Holm correction for multiple pairwise comparisons, and effect sizes were reported using Rosenthal's r.

Linear robust regression analyses, using the *robustbase* R library, were used to investigate relationships between annual WMH volume changes and baseline CSF biomarkers of AD, as well as baseline WMH volume. Both baseline WMH volume and fluid biomarker concentrations were log-transformed to reduce skewness. The impact of microbleed presence on annual WMH changes was evaluated using the Mann-Whitney test.

3 | RESULTS

3.1 | Population

In total, we evaluated 449 MRI scans; after a visual quality assessment, 34 of them (7.57%) were excluded due to low transverse resolution or low structural visibility. Then, 91 follow-up scans (22.64%) were also excluded because of the different acquisition protocols. Lastly, seven scans (2.25%) were excluded due to suboptimal longitudinal coregistration across time points.

Our final sample included 80 adults with DS (n = 178 scans) from the DABNI cohort and 53 HC (n = 124 scans) from the SPIN study. Demographic data at baseline are presented in Table 1. The DS group comprises individuals across the AD continuum, with 65 aDS, 13 sDS (61.55% pDS and 38.45% dDS), and 2 uDS at baseline (see Table S2 for demographic data stratified by clinical diagnosis). Regarding ID level, 26 DS participants had mild ID, 46 moderate ID, and 8 severe/profound ID. The HC group was significantly older than the DS group (median age [interquartile range {IQR}] = 56.91 [12.69] vs. 41.60 [13.9] years, respectively; $W = 3826$, $p < 0.001$). There was a trend toward a difference in sex distribution, with more female participants in the HC group (66.04%) compared to the DS group (47.50%, $p = 0.054$). No significant differences were found for *APOE*ε4 status between groups. Individuals with DS had a lower prevalence of hypertension and dyslipidemia than HC (1.25% vs. 31.8%, $p < 0.001$; 11.4% vs. 40.9%, $p = 0.003$), with no difference in diabetes mellitus (2.5% vs. 4.55%, $p = 0.521$). Individuals with DS demonstrated lower values in CSF for the Aβ42/Aβ40 ratio and higher concentrations of YKL-40 than HC ($p < 0.001$; $p = 0.003$, respectively). No significant differences were found in CSF pTau181, CSF GFAP, and plasma GFAP between groups ($p > 0.05$).

All participants underwent at least two MRI visits; a subset had a third (17 DS and 15 HC) and a fourth visit (1 DS and 3 HC). The minimum follow-up duration (baseline to last MRI visit) was 0.56 years for DS and 1.84 years for HC, whereas the maximum follow-up duration was 9.06 years for DS and 7.03 years for HC. The between-visit time delay, taking into account all the available intervals, was slightly shorter in HC (2.27 years) than in DS (2.67 years; W = 4464, p = 0.002), while the overall duration of the follow-up, based on the baseline and last MRI visit, was similar between both groups (HC: 2.69 years; DS: 2.87 years; $W = 2346.5$, $p = 0.299$). During follow-up, 10 aDS participants (16.92%) progressed to sDS. At baseline, there were no significant differences in total WMH volume between the HC and the overall DS groups (HC: median WMH = 2340.79 mm^3, DS: 2701.44 mm^3; W = 1875.5, $p = 0.261$). However, when stratifying the DS group into aDS and sDS, we observed significantly higher WMH volumes in sDS compared with both HC and aDS (sDS: 6716 mm^3, aDS: 2198.2 mm^3, $H(2,131) = 16.397$, $p < 0.001$). Annual changes were more pronounced in DS than in HC (-1.15 mm^3/year vs. -10.51 mm^3/year, $W = 2591$, $p = 0.03$).

3.2 | Effect of demographic, clinical, and genetic variables on longitudinal WMH

In both DS and HC, WMH exhibited variable changes with age, including both increases and decreases in volume over time (Figure 1A). A higher proportion of individuals with DS presented with decreased WMH compared to HC (26% vs. 9%) and a lower proportion with increased WMH [8% in DS vs. 25% in HC; $\chi^2(1,133) = 11.08$, $p = 0.004$; Table S3).

The annual change in WMH was negatively associated with age in the DS group (rho = −0.31, $p = 0.006$), while this association was not statistically significant in the HC group (rho = 0.07, $p = 0.632$). The LOESS curve revealed stable annual changes in WMH among individuals with DS until age 40, after which greater variability was observed, and the changes decreased at the group level (Figure 1B).

In individuals with DS, there was no effect of sex ($W = 688$, $p = 0.293$), *APOE*ε4 status ($W = 438$, $p = 0.475$), or ID [$H(2,78) = 2.57$, $p = 0.276$; Figure 1C–E] on the annual change in WMH volume.

15525279, 2026, 2, Downloaded from https://alz-journals.onlinelibrary.wiley.com/doi/10.1002/alz.71157 by Alejandra O. Morcillo-Nieto - Spanish Cochrane National Provision (Ministerio de Sanidad) , Wiley Online Library on [05/02/2026]. See the Terms and Conditions (https://onlinelibrary.wiley.com/terms-and-conditions) on Wiley Online Library for rules of use; OA articles are governed by the applicable Creative Commons License

TABLE 1 Study participants.

Parameter	HC *N* = 53	DS *N* = 80	*p*-value
Age at baseline, y	56.91 [51.42;64.11]	41.60 [33.18;47.08]	<0.001
Female	35 (66.04%)	38 (47.50%)	0.054
APOEε4 carriers	18 (34.62%)	17 (26.98%)	0.495
Intellectual disability			
Mild		26 (32.50%)	
Moderate		46 (57.50%)	
Severe/profound		8 (10.00%)	
AD clinical diagnosis			
aDS		65 (80.00%)	
sDS		13 (16.25%)	
uDS		2 (3.75%)	
Vascular risk factors			
Hypertension	7/22 (31.82%)	1/80 (1.25%)	<0.001
Dyslipidemia	9/22 (40.91%)	9/80 (11.39%)	0.003
Diabetes mellitus	1/21 (4.55%)	2/79 (2.50%)	0.521
CAMCOG-DS		74.00 [61.50;84.00]	
MRI data			
No. of visits 2/3/4	53 (100.00%) / 15 (28.30%) / 3 (5.66%)	80 (100.00%) / 17 (21.25%) / 1 (1.25%)	
Between-visit time delay, y	2.27 [2.10; 2.60]	2.67 [2.21; 3.54]	0.002
Duration of the follow-up, y	2.69 [2.20; 4.18]	2.87 [2.26; 4.57]	0.299
WMH measures			
WMH at baseline, mm^3	2340.79 [1274.43;4387.10]	2701.44 [1371.75;5157.92]	0.261
Annual WMH change, mm^3/year	−1.15 [−33.36;68.65]	−10.15 [−90.12;10.69]	0.030
Fluid biomarkers, pg/mL			
CSF Aβ42/Aβ40 (*N* = 33/45)	0.10 [0.10;0.11]	0.08 [0.05;0.09]	<0.001
CSF pTau181 (*N* = 33/45)	35.80 [26.70;44.00]	36.60 [20.30;69.60]	0.936
CSF NfL(*N* = 48/51)	382.25 [317.20;551.89]	366.00 [227.10;639.00]	0.190
CSF GFAP (*N* = 27/50)	3179.94 [1962.01;5246.57]	2869.42 [1669.07;4113.58]	0.411
Plasma GFAP (*N* = 29/35)	91.47 [72.87;123.45]	92.80 [66.72;156.76]	0.604
CSF YKL40 (*N* = 53/51)	178.58 [151.84;225.20]	141.41 [79.39;199.86]	0.003

Note: Data are *n*(%) or median [IQR]. *p*-Values indicate the statistical significance of differences between DS and HC participants.
Abbreviations: AD, Alzheimer's disease; aDS, asymptomatic Down syndrome; APOE, apolipoprotein E;Aβ42/Aβ40, concentration ratio between amyloid beta peptide 1-42 and amyloid beta peptide 1-40 (pg/mL); CAMCOG-DS, Cambridge Cognitive Examination for Older Adults with Down Syndrome; CSF, cerebrospinal fluid; DS, Down syndrome; GFAP, glial fibrillary acidic protein concentration (pg/mL); HC, euploid cognitively unimpaired controls; IQR, interquartile range; MRI, magnetic resonance imaging; NfL, neurofilament light chain concentration (pg/mL); pTau181, tau phosphorylated at threonine 181 concentration (pg/mL); sDS, symptomatic Down syndrome; WMH, white matter hyperintensities; YKL-40, chitinase 3-like 1.

3.3 | Effect of AD clinical status on the evolution of WMH

The annual changes in total WMH decrease with the progression of AD clinical status in DS [H(2,131) = 11.786, $p = 0.003$; Figure 2A]. Specifically, sDS exhibited significantly larger decreases in WMH volume compared to aDS ($z = 2.71$, $p = 0.014$; aDS: median ΔWMH = −5.39 mm^3/y, sDS = −130.83 mm^3/y) and HC ($z = 3.43$, $p = 0.002$; HC: ΔWMH = −1.15 mm^3/y). No significant differences were observed between HC and aDS ($z = 1.28$, $p = 0.201$). When examining regional changes, the sDS group showed smaller WMH changes in layer 1 and in the parietal and occipital lobes compared to both aDS and HC, and in layer 2 and the frontal lobe compared to the HC group only (Figure 2B–D; Table S4). Although the sample size was limited, we performed an exploratory analysis to examine annual changes in total WMH by subdividing the sDS group into pDS and dDS subgroups, and by distinguishing within the aDS group those individuals who progressed to sDS at follow-up (progressors). This analysis revealed greater WMH decreases in the pDS subgroup, which showed significantly larger reductions compared to both HC ($z = -4.47$, $p < 0.001$;

15525279, 2026, 2, Downloaded from https://alz-journals.onlinelibrary.wiley.com/doi/10.1002/alz.71157 by Alejandra O. Morcillo-Nieto - Spanish Cochrane National Provision (Ministerio de Sanidad) , Wiley Online Library on [05/02/2026]. See the Terms and Conditions (https://onlinelibrary.wiley.com/terms-and-conditions) on Wiley Online Library for rules of use; OA articles are governed by the applicable Creative Commons License

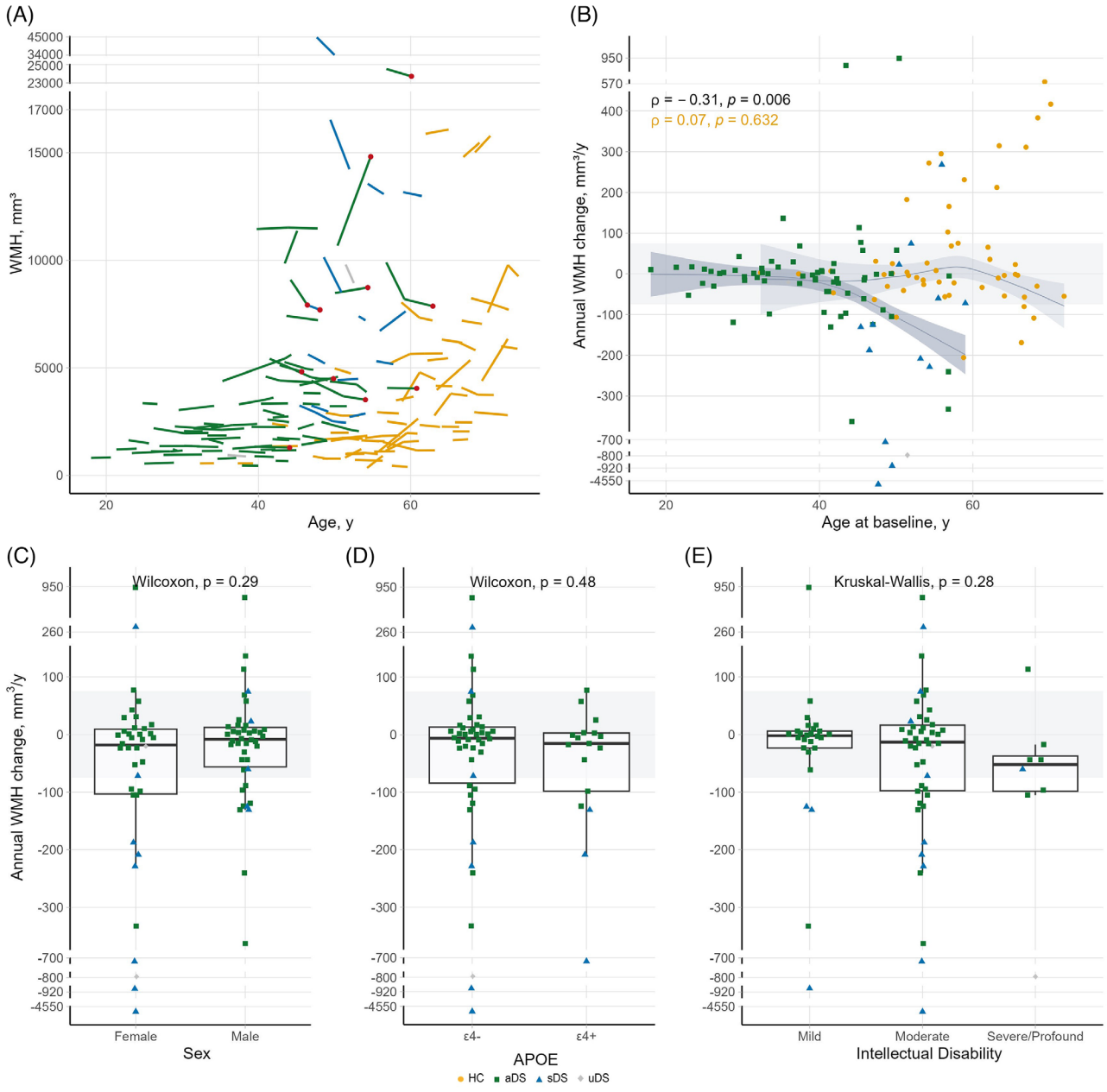

FIGURE 1 Effect of demographic, clinical, and genetic variables on longitudinal WMH. (A) Association between total WMH volume and (B) annual WMH volume with age. The lines/points represent individual participants, with colors indicating their clinical diagnosis. Red points denote participants who exhibited a clinical change between visits along the AD continuum. Shaded areas represent 95% CI: dark gray represents the age-related change in DS, and light gray in the HC group for visual reference. Boxplots showing the effect of (C) sex, (D) *APOE* genotype, and (E) intellectual disability on annual WMH volume changes in DS. The light gray background (−75 mm^3/year to +75 mm^3/year) serves as a visual reference for stable WMH change. AD, Alzheimer's disease; aDS, DS asymptomatic; APOE, apolipoprotein E; DS, Down syndrome; HC, euploid cognitively unimpaired controls; sDS, symptomatic DS; uDS, uncertain DS; and WMH, white matter hyperintensities.

pDS: ΔWMH = −197.98 mm^3/y) and aDS ($z = -4.10$, $p < 0.001$; aDS: ΔWMH = 0.33 mm^3/y). The progressors (median ΔWMH = −57.95 mm^3/y) showed intermediate changes between aDS and pDS, although these differences did not reach statistical significance. In contrast, the dDS subgroup exhibited a significant increase in WMH relative to pDS ($z = 2.91$, $p = 0.03$; median ΔWMH = 22.80 mm^3/y; Figure S1).

3.4 | Association between longitudinal WMH, AD, and SVD markers

In individuals with DS, annual changes in WMH were not significantly associated with any of the fluid biomarkers (all $p > 0.05$; Figure 3A–F). However, a trend toward mild negative associations was observed with NfL ($R^2 = 0.04$, $p = 0.09$) and plasma GFAP ($R^2 = 0.09$, $p = 0.06$).

15525279, 2026, 2, Downloaded from https://alz-journals.onlinelibrary.wiley.com/doi/10.1002/alz.71157 by Alejandra O. Morcillo-Nieto - Spanish Cochrane National Provision (Ministerio de Sanidad) , Wiley Online Library on [05/02/2026]. See the Terms and Conditions (https://onlinelibrary.wiley.com/terms-and-conditions) on Wiley Online Library for rules of use; OA articles are governed by the applicable Creative Commons License

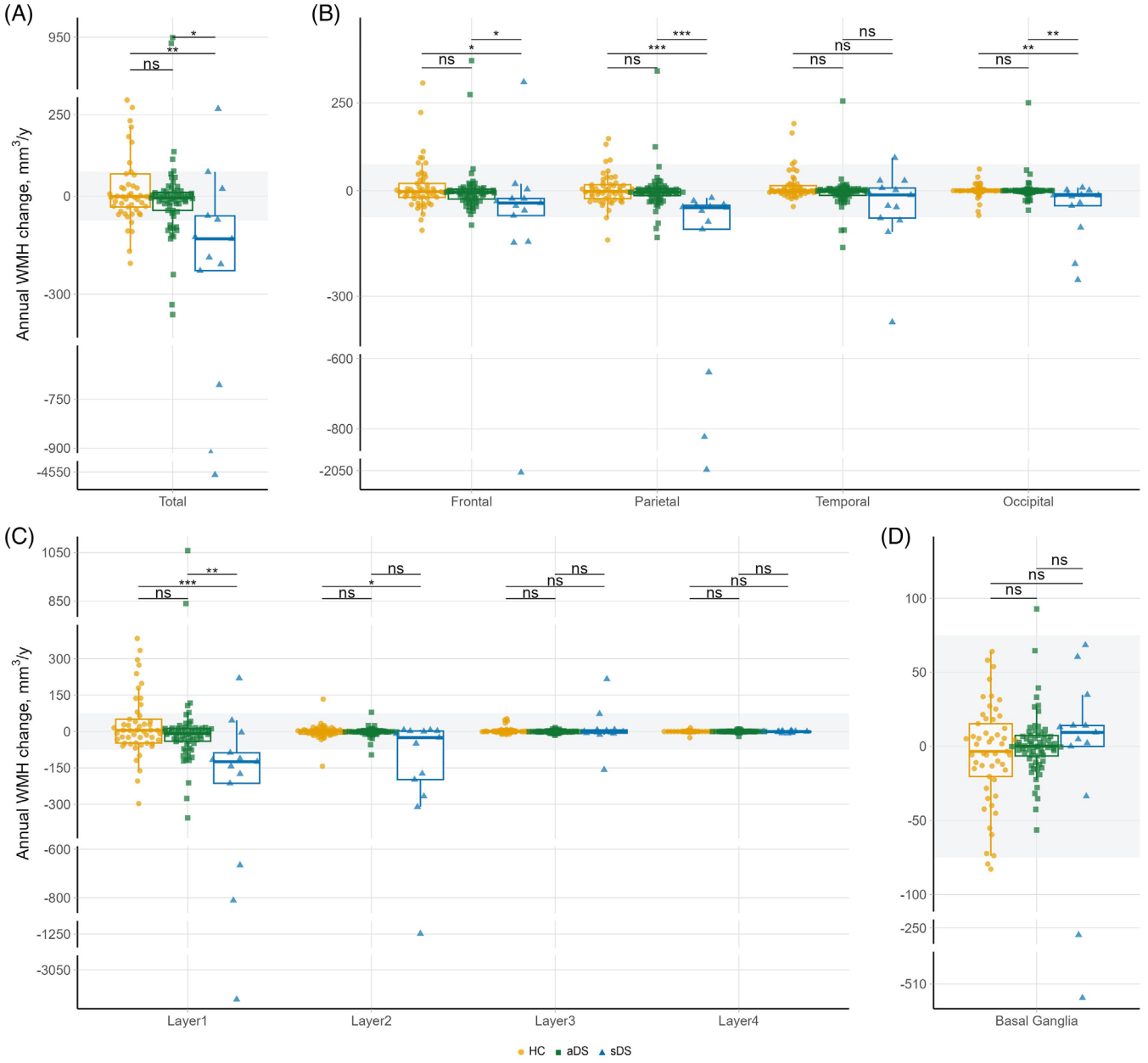

FIGURE 2 Between-group differences for total and regional annual WMH volume changes. (A–D) Boxplots illustrate WMH volumes across the brain regions. Significant results at $p < 0.05$ using the Holm correction. The light gray background (−75 mm^3/year to +75 mm^3/year) serves as a visual reference for stable WMH change. ns, no significance; $^*p < 0.05$; $^{**}p < 0.01$; $^{***}p < 0.001$. aDS: DS asymptomatic; DS: Down syndrome; HC: euploid cognitively unimpaired controls; sDS: symptomatic DS; and WMH: white matter hyperintensities.

Concerning SVD neuroimaging markers, a significant negative association was found between annual changes in WMH and baseline WMH volume in DS ($R^2 = 0.18$, $p < 0.001$; Figure 3G). Additionally, the presence of at least one cerebral microbleed was associated with lower annual changes in WMH ($W = 412$, $p = 0.024$; Figure 3H).

3.5 | Sensitivity analyses

Contrary to our expectations, our results demonstrated considerable variability in the evolution of WMH, with a significant proportion of adults with DS showing decreases in WMH volume over time. As these findings were unexpected, we conducted sensitivity analyses to rule out (i) issues related to automatic quantification, and (ii) the confounding effect of WM atrophy. First, we performed a blinded visual assessment, which showed that WMH remained stable in 65% of individuals with DS and 60% of HC. The visual read further showed that 23% of DS and 23% of HC demonstrated a decrease in WMH at follow-up, whereas 12% of DS and 17% of HC exhibited an increase in WMH volume (Table S5). Specifically, among the aDS group, 72.3% were stable, 18.5% were regressors, and 9.2% were progressors. In the sDS group, 31% were stable, 38% were regressors, and 31% were progres-

15525279, 2026, 2, Downloaded from https://alz-journals.onlinelibrary.wiley.com/doi/10.1002/alz.71157 by Alejandra O. Morcillo-Nieto - Spanish Cochrane National Provision (Ministerio de Sanidad) , Wiley Online Library on [05/02/2026]. See the Terms and Conditions (https://onlinelibrary.wiley.com/terms-and-conditions) on Wiley Online Library for rules of use; OA articles are governed by the applicable Creative Commons License

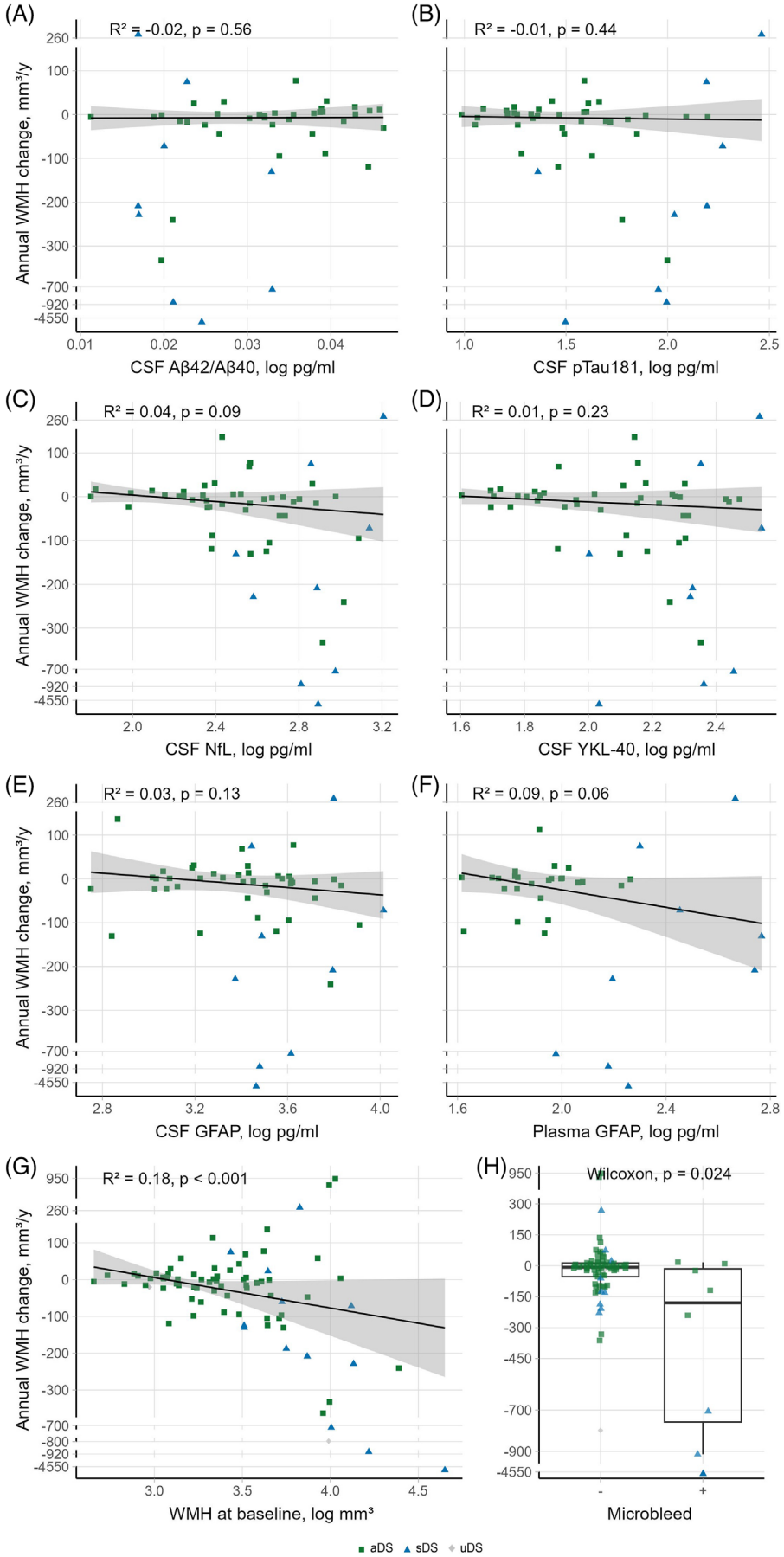

15352379, 2026, 2, Downloaded from https://alz-journals.onlinelibrary.wiley.com/doi/10.1002/alz.71157 by Alejandra O. Morcillo-Nieto - Spanish Cochrane National Provision (Ministerio de Sanidad) , Wiley Online Library on [05/02/2026]. See the Terms and Conditions (https://onlinelibrary.wiley.com/terms-and-conditions) on Wiley Online Library for rules of use; OA articles are governed by the applicable Creative Commons License

sors (Table S5). Second, to ensure that our findings were not merely reflecting progressive WM atrophy, we repeated the primary analyses using WMH volumes adjusted for total WM at the corresponding MRI visit (i.e., WMH/total WM per visit). This adjustment reduced the overall variability and the trajectory of WMH over time (Figure S2). Hence, the association between age and annual change was no longer statistically significant in the DS group (rho = , $p = 0.939$). However, several DS cases continued to present increased/decreased WMH, and we still observed larger reductions in total WMH volume in the sDS group than in HC, particularly in layer 1 and the parietal and occipital lobes (Figure S3). Results for other demographic variables were consistent, showing no significant effects of sex, *APOEε4* status, or ID.

4 | DISCUSSION

In the present study, we investigated the evolution of WMH over time in DS. Unlike our hypotheses, we did not observe increases in WMH with age; instead, we found a decrease that was independent of other demographic variables. This reduction in WMH was more pronounced at the symptomatic stage, and was primarily observed in the frontal, parietal, and occipital lobes and the periventricular region (i.e., Layer 1 and Layer 2). Unexpectedly, annual changes in WMH showed no association with any fluid biomarker and were inversely related to baseline WMH volume. Participants with DS who had at least one microbleed exhibited a greater WMH reduction. Visual assessment and adjustment for WM volume confirmed the heterogeneity in WMH trajectories over time in DS and the reduction at symptomatic stages. Together, these results highlight the inconsistent trajectory over time of WMH in DS and provide novel insight into the underlying etiologies of these lesions.

Although cross-sectional evidence has demonstrated an age-related increase in WMH in DS,[10–12] we found a significant negative association between annual changes in WMH and age in DS. Between the ages of 20 and 40, most individuals with DS exhibited minimal changes in WMH. After age 40, an increasing number of cases experienced significant fluctuations in WMH; primarily decreases, although some increases were also observed. This aligns with a recent study that reported similar fluctuations, both increases and decreases, at older ages in DS, although the association did not reach statistical significance.[31] In contrast, in the HC group, the age-related trajectory showed that WMH burden remained relatively stable until approximately age 55. Beyond this age, most participants continued to show stability, with a few cases demonstrating a substantial increase in WMH volume and a few exhibiting notable decreases. Advancing age has been widely associated with larger WMH volume changes, whereas younger age showed smaller changes over time.[32–35] While WMH generally increase with age in euploid individuals, several studies have also reported WMH shrinkage over time.[32,36] Population-based studies have found that approximately 11%–34% of the participants show regression,[37–39] consistent with our results, 9.4% for HC and 26% for DS. We observed no effect of sex, *APOEε4* status, or ID on annual WMH changes in DS. This lack of effect is consistent with prior cross-sectional[11,12] and longitudinal WMH findings,[31] as well as evidence from other vascular lesions,[11,27,40] suggesting that sex, *APOEε4*, and ID have limited impact on SVD features in DS.

We observed significantly greater annual reductions in WMH volumes in DS participants compared to HC, especially in DS individuals at the symptomatic stage of AD (i.e., sDS subgroup). Regional analyses revealed these differences were most prominent in frontal, parietal, and occipital lobes and in periventricular WM regions. A previous longitudinal study in DS reported a monotonic increase in WMH change across diagnostic groups, with negative changes in the asymptomatic and prodromal AD stages and positive rates in more advanced stages.[31] The discrepancy with our results might be explained by the fact that we merged the prodromal and dementia stages; indeed, subgroup analyses indicated a positive rate in dementia cases. It is also possible that differences in lesion-segmentation methods (longitudinal LPA in the present study vs. an in-house Gaussian mixture model-based script in Lao et al., 2025) may influence the results. Here, we used a preprocessing pipeline tailored to longitudinal data and additionally performed a blinded visual read. In sporadic AD cohorts, WMH volumes generally increase over time in both mild cognitive impairment (MCI) and dementia, and rates do not significantly differ among groups.[41–43] Moreover, MCI individuals with amyloid pathology accumulate WMH faster than those who are Aβ negative.[44] Interestingly, one study reported both greater reductions and increases in WMH in AD patients with a high SVD burden compared to cognitively normal controls and AD with low SVD,[45] highlighting potential vascular contribution to the WMH trajectories.

Associations between annual changes in WMH and fluid biomarkers did not reveal robust relationships. This lack of association may reflect heterogeneity across the adult DS lifespan, where non-linear and stage-specific biomarker trajectories can mask significant effects. In addition, fluid biomarker data were available only at baseline, preventing change-change analysis. Interestingly, a greater baseline WMH burden and the presence of cerebral microbleeds, a well-established neuroradiological feature of CAA, were both associated with a decrease in WMH volume over time. A similar negative relationship between baseline WMH burden and WMH changes was

FIGURE 3 Association between longitudinal WMH, AD, and SVD markers. Linear robust regression analyses of annual WMH volume changes against (A–F) fluid biomarkers, and (G) baseline WMH volume. The points represent individual participants, with colors indicating their clinical diagnosis. Shaded areas represent 95% CI. (H) Boxplot showing the effect of microbleeds presence. AD, Alzheimer's disease; aDS, DS asymptomatic; Aβ42/Aβ 40, concentration ratio between amyloid β peptide 1–42 and amyloid β peptide 1–40 (pg/mL); CI, confidence interval; CSF, cerebrospinal fluid; DS, Down syndrome; GFAP, glial fibrillary acidic protein concentration (pg/mL); NfL, neurofilament light chain concentration (pg/mL); pTau181, tau phosphorylated at threonine 181 concentration (pg/mL); sDS, symptomatic DS; SVD, small vessel disease; uDS, uncertain DS; WMH, white matter hyperintensities; and YKL-40, chitinase 3-like 1 (pg/mL).

15525279, 2026, 2, Downloaded from https://alz-journals.onlinelibrary.wiley.com/doi/10.1002/alz.71157 by Alejandra O. Morcillo-Nieto - Spanish Cochrane National Provision (Ministerio de Sanidad) , Wiley Online Library on [05/02/2026]. See the Terms and Conditions (https://onlinelibrary.wiley.com/terms-and-conditions) on Wiley Online Library for rules of use; OA articles are governed by the applicable Creative Commons License

reported by Lao and colleagues.[31] These results indicate that the WMH decrease likely reflects dynamics of pathological processes that are more likely in individuals with pre-existing SVD pathology.

The etiology and pathogenesis of WMH are multifactorial and remain incompletely understood. WMH may, in some instances, reflect irreversible WM damage due to demyelination and axonal loss.[46] In DS, we previously reported cross-sectional associations between WMH and both NfL and GM volume loss,[12] underscoring a contribution of neurodegeneration to WMH in DS. Here, sensitivity analyses accounting for WM atrophy explained some of the observed WMH reductions, indicating that neurodegeneration partly explains the apparent WMH shrinkage. However, some reductions persisted after adjusting for atrophy, suggesting the involvement of additional mechanisms such as neuroinflammation. There is growing evidence linking inflammation to WMH in DS.[12,47,48] In DS, neuroinflammation may arise from at least three non-exclusive sources: (i) trisomy 21–related immune dysregulation that promotes chronic neuroinflammation[49]; (ii) AD pathology, as deposition and accumulation of pathological aggregates can exacerbate the inflammatory response[50]; and (iii) CAA, vascular Aβ deposition compromises small-vessel endothelium, can damage the brain-blood barrier, and can trigger neuroinflammation.[51] In some cases, brain-blood barrier disruption increases permeability, allowing extravasation of interstitial fluid with vasogenic edema; a mechanism consistent with CAA-related inflammation (CAA-ri).[52] Notably, CAA-ri has been confirmed in some cases in our DS cohort, including one previously described in a case report.[53] Regardless of cause, neuroinflammation may contribute to the emergence of WMH, but can also partially resolve, leading to subsequent WMH reduction.

As people with DS increasingly participate in clinical trials of anti-amyloid therapies that can cause cerebral edema and microhemorrhages, rigorously defining the natural history and dynamics of cerebrovascular lesions, such as WMH, becomes essential to guide care.[14] Our data reveal that WMH changes over time in DS are a nonlinear process. This finding underscores the importance of accounting for this intrinsic variability, not only to avoid confounding interpretations of drug effects but also to exercise caution when WMH are considered as primary or secondary endpoints in clinical trials. Furthermore, a thorough examination of potential pathologic, imaging, demographic, and clinical factors associated with WMH regression could unveil new important targets for intervention.

This study had some limitations. First, the relatively small and unbalanced sample size (n = 65 aDS, 13 sDS, and 2 uDS) reduced statistical power and limited the likelihood of detecting differences in WMH between clinical groups. The limited number of symptomatic participants reflects real-world constraints on recruiting and scanning adults with DS at advanced AD stages, including reduced MRI tolerability that limits participation and return visits. As a result, a survivor bias is possible as individuals with greater WMH burden are more likely to be symptomatic. Second, while we implemented a specific longitudinal WMH segmentation pipeline and a visual assessment by a neuroradiologist, variability in MRI acquisition parameters may have introduced technical confounding. To minimize intra-subject variability, we retained only those participants whose MRI visits were all acquired on the same scanner using the same protocol. In addition, we applied a harmonization step to further reduce inter-subject variability in acquisition parameters across scanners. Third, because most participants had only two MRI timepoints, we were unable to estimate nonlinear rates of change. Future studies using mixed-effects models, together with additional follow-up visits over a longer observation window, could capture individual-level WMH trajectories and potential nonlinearities over time. Finally, the threshold used to classify individuals as exhibiting WMH regression, stability, or progression was adapted from research conducted in non-DS populations. Such thresholds can influence participant categorization and, consequently, the interpretation of longitudinal WMH changes.[54] Future research in DS should aim to establish population-appropriate thresholds to improve the accuracy, reproducibility, and clinical relevance of WMH quantification in individuals with Down syndrome.

In summary, our findings highlight the variability in the longitudinal evolution of WMH in DS. In younger adults with DS, WMH volumes are low, and annual changes remain minimal, typically close to zero. As individuals age and reach approximately 40–45 years, they exhibit a higher WMH burden, as evidenced by prior cross-sectional observations, along with greater longitudinal variability, including both increases and decreases over time. Between-visit decreased WMH was observed more frequently than increased WMH and was related to older age, AD symptoms, and higher baseline WMH. This reduction was only partially explained by the WM atrophy and may suggest mechanisms such as inflammatory resolution. This challenges the assumption that WMH in DS are static accumulations of irreversible injury and underscores the need to better characterize these lesions.

AUTHOR CONTRIBUTIONS

Conceived and designed the study: Alejandra O. Morcillo-Nieto, Mateus Rozalem-Aranha, and Alexandre Bejanin. *Acquired and interpreted the data*: José Enrique Arriola-Infante, Maria Franquesa-Mullerat, Sara E. Zsadanyi, Lídia Vaqué-Alcázar, José Allende Parra, Zili Zhao, Javier Arranz, Isabel Barroeta, Lucia Maure-Blesa, Laura Videla, Íñigo Rodríguez-Baz, Laura Del Hoyo Soriano, Bessy Benejam, Susana Fernández, Aida Sanjuan Hernandez, Sandra Giménez, Lucia Pertierra, Daniel Alcolea, Olivia Belbin, Alberto Lleó, María Carmona-Iragui, and Juan Fortea. *Performed the statistical analysis*: Alejandra O. Morcillo-Nieto. *Drafted the manuscript, which all authors critically reviewed for important intellectual content*: Alejandra O. Morcillo-Nieto, Mateus Rozalem-Aranha, and Alexandre Bejanin.

ACKNOWLEDGMENTS

The authors thank all the participants, their families, and their carers from the DABNI and SPIN cohorts for their support of, and dedication to this research. We also acknowledge the Fundació Catalana Síndrome de Down (https://fcsd.org/) for their global support. We also acknowledge the Department of Medicine and the Institute of Neuroscience at the Universitat Autònoma de Barcelona. We acknowledge the Support for Research Groups funding from the Department of Research and Universities from the Generalitat de Catalunya (2021 SGR 00979). JF reports grants from the Fondo de Investigaciones Sanitario, Instituto de Salud Carlos III (ISCIII) (INT21/00073, PI20/01473

15525279, 2026, 2, Downloaded from https://alz-journals.onlinelibrary.wiley.com/doi/10.1002/alz.71157 by Alejandra O. Morcillo-Nieto - Spanish Cochrane National Provision (Ministerio de Sanidad) , Wiley Online Library on [05/02/2026]. See the Terms and Conditions (https://onlinelibrary.wiley.com/terms-and-conditions) on Wiley Online Library for rules of use; OA articles are governed by the applicable Creative Commons License

and PI23/01786 to JF) and the Centro de Investigación Biomédica en Red sobre Enfermedades Neurodegenerativas (CIBERNED) Program 1. This work was also supported by the National Institutes of Health grants (1R01AG056850-01A1, R21AG056974, R01AG061566, 1R01AG081394-01 and 1R61AG066543-01 to JF), the Department de Salut de la Generalitat de Catalunya (SLT006/17/00119 to JF), Fundación Tatiana Pérez de Guzmán el Bueno (IIBSP-DOW-2020-151). It was also supported by Horizon 2020 - Research and Innovation Framework Programme from the European Union (H2020-SC1-BHC-2018-2020 to JF). DA acknowledges support from Instituto de Salud Carlos III (ISCIII) (PI18/00435, PI22/00611, INT19/00016, INT23/00048) co-funded by the European Union (ERDF) , and by the Department of Health Generalitat de Catalunya PERIS program (SLT006/17/125). He also received support for Research Groups funding from the Department of Research and Universities from the Generalitat de Catalunya (2021 SGR 00979). AB acknowledges support from Instituto de Salud Carlos III (ISCIII) and co-funded by the European Union (ERDF) through the Miguel Servet grant (CP20/00038) and Fondo de Investigaciones Sanitario (PI22/00307), the Alzheimer's Association (AARG-22-923680), and the Ajuntament de Barcelona, in collaboration with Fundació La Caixa (23S06157-001). LDHS acknowledges support from Instituto de Salud Carlos III (ISCIII) and co-funded by the European Union (ERDF) through the Miguel Servet grant (CP24/00112), and the Jérôme Lejeune Foundation (2326 - GRT-2024A). MCI acknowledges support from Instituto de Salud Carlos III (ISCIII) (PI18/00335, PI22/00758, ICI23/00032), co-funded by the European Union (ERDF), Centro de Investigación Biomédica en Red sobre Enfermedades Neurodegenerativas (CIBERNED) Program 1, Alzheimer's Association (AARG-22-973966), the Global Brain Health Institute (GBHI_ALZ-18-543740), the Jérôme Lejeune Foundation (#1913 cycle 2019B; #2425 cycle 2024B). MRA was supported by the Alzheimer's Association Research Fellowship to Promote Diversity (AARF-D) Program (AARFD-21-852492) from 2022 until 2025. LVA is supported by Instituto de Salud Carlos III (ISCIII) and co-funded by the European Union (ERDF) through Sara Borrell postdoctoral fellowship (CD23/00235). SG acknowledges support from the Instituto de Salud Carlos III (ISCIII) (PI20/00836), and co-funded by the European Union (ERDF), the Global Brain Health Institute (GBHI_ALZ-23-971107), the Jérôme Lejeune Foundation (#1801 Cycle 2020). LMB was supported by Instituto de Salud Carlos III (ISCIII) and co-funded by the European Union (ERDF) through the Río Hortega Fellowhip (CM23/00291). IRB was supported by Instituto de Salud Carlos III (ISCIII) and co-funded by the European Union (ERDF) through the Río Hortega Fellowship (CM22/00052). JA was supported by Instituto de Salud Carlos III (ISCIII) and co-funded by the European Union (ERDF) through the Río Hortega Fellowship (CM22/00243).

CONFLICT OF INTEREST STATEMENT

JF reported serving on the advisory boards, adjudication committees, or speaker honoraria from AC Immune, Adamed, Alzheon, Biogen, Eisai, Esteve, Fujirebio, Ionis, Laboratorios Carnot, Life Molecular Imaging, Lilly, Novo Nordisk, Perha, Roche, Zambón. DA participated in advisory boards from Fujirebio-Europe, Roche Diagnostics, Grifols S.A. and Lilly, and received speaker honoraria from Fujirebio-Europe, Roche Diagnostics, Nutricia, Krka Farmacéutica S.L., Zambon S.A.U., Neuraxpharm, Alter Medica, Lilly and Esteve Pharmaceuticals S.A. JF, DA and OB report holding a patent for markers of synaptopathy in neurodegenerative disease (licensed to ADx NeuroSciences N.V., WO2019175379). MRA is a co-founder and partner of Masima Soluções em Imagens Médicas LTDA (Porto Alegre, Brazil) and serves an independent consultant to Ionis Pharmaceuticals. MCI has received personal fees for service on the advisory boards, speaker honoraria or educational activities from IMSERSO, Esteve, Lilly, Neuraxpharm, Adium Pharma, and Roche. AL reported receiving personal fees for service on advisory boards, or speaker honoraria from Almirall, Beckman-Coulter, Biogen, Eisai, Esteve, Fujirebio-Europe, Grifols, KRKA, Lilly, Novartis, NovoNordisk, Nutricia, Otsuka Pharmaceutical, Roche, and Zambon. AL is co-author of a patent for markers of synaptopathy in neurodegenerative disease (licensed to ADx, EPI8382175.0) and on antibodies for amyloid precursor, methods and uses thereof European priority (N°EP25382226). SG has received personal fees for service on the advisory boards, speaker honoraria or educational activities from Esteve, Idorsia, Novo Nordisk and Bioproject. JA reported receiving personal fees for service on speaker honoraria or educational activities from Lilly, Esteve, Fujirebio-Europe and Roche diagnostics. AOMN, LMB, IRB, JEAI, MFM, SEZ, LVA, JAP, ZZ, LV, IB, LDHS, BB, SF, ASH, LP and AB have nothing to disclose. Author disclosures are available in the Supporting Information.

DATA AVAILABILITY STATEMENT

The authors may share de-identified data that underlie the results reported in this article. Data will be available upon receipt of a request detailing the study hypothesis and statistical analysis plan. All requests should be sent to the corresponding authors. The steering committee of this study will discuss all requests and decide, based on the novelty and scientific rigor of the proposal, whether data sharing is appropriate. All applicants will be asked to sign a data access agreement.

CONSENT STATEMENT

All participants and/or their legally authorized representatives gave written informed consent.

ORCID

Alejandra O. Morcillo-Nieto https://orcid.org/0000-0003-2202-3521
Lucia Maure-Blesa https://orcid.org/0000-0001-5643-7971
Íñigo Rodríguez-Baz https://orcid.org/0000-0003-3039-9115
José Enrique Arriola-Infante https://orcid.org/0000-0002-3298-4601
Maria Franquesa-Mullerat https://orcid.org/0009-0006-1484-7132
Sara E. Zsadanyi https://orcid.org/0000-0002-2033-5989
Lídia Vaqué-Alcázar https://orcid.org/0000-0002-6776-6559
Zili Zhao https://orcid.org/0009-0007-8373-8404
Javier Arranz https://orcid.org/0000-0003-0891-1215
Laura Videla https://orcid.org/0000-0002-9748-8465
Isabel Barroeta https://orcid.org/0000-0003-2764-7923

15525279, 2026, 2, Downloaded from https://alz-journals.onlinelibrary.wiley.com/doi/10.1002/alz.71157 by Alejandra O. Morcillo-Nieto - Spanish Cochrane National Provision (Ministerio de Sanidad) , Wiley Online Library on [05/02/2026]. See the Terms and Conditions (https://onlinelibrary.wiley.com/terms-and-conditions) on Wiley Online Library for rules of use; OA articles are governed by the applicable Creative Commons License

Laura Del Hoyo Soriano https://orcid.org/0000-0003-4372-1599
Bessy Benejam https://orcid.org/0000-0002-6789-8615
Susana Fernández https://orcid.org/0000-0002-9777-1156
Aida Sanjuan Hernandez https://orcid.org/0009-0009-4800-6894
Lucia Pertierra https://orcid.org/0009-0000-1155-8286
Sandra Giménez https://orcid.org/0000-0001-8031-2319
Daniel Alcolea https://orcid.org/0000-0002-3819-3245
Olivia Belbin https://orcid.org/0000-0002-6109-6371
Alberto Lleó https://orcid.org/0000-0002-2568-5478
María Carmona-Iragui https://orcid.org/0000-0001-6914-2339
Juan Fortea https://orcid.org/0000-0002-1340-638X
Alexandre Bejanin https://orcid.org/0000-0002-9958-0951

REFERENCES

1. Ballard C, Mobley W, Hardy J, Williams G, Corbett A. Dementia in Down's syndrome. *Lancet Neurol*. 2016;15:622-636. doi:10.1016/S1474-4422(16)00063-6
2. Bittles AH, Bower C, Hussain R, Glasson EJ. The four ages of Down syndrome. *Eur J Public Health*. 2007;17:221-225. doi:10.1093/EURPUB/CKL103
3. Iulita MF, Chavez DG, Christensen MK, et al. Association of Alzheimer disease with life expectancy in people with Down syndrome. *JAMA Netw Open*. 2022;5:e2212910-e2212910. doi:10.1001/JAMANETWORKOPEN.2022.12910
4. Fortea J, Zaman SH, Hartley S, Rafii MS, Head E, Carmona-Iragui M. Alzheimer's disease associated with Down syndrome: a genetic form of dementia. *Lancet Neurol*. 2021;20:930-942. doi:10.1016/S1474-4422(21)00245-3
5. Lott IT, Head E. Dementia in Down syndrome: unique insights for Alzheimer disease research. *Nat Rev Neurol*. 2019;15(3):135-147. doi:10.1038/s41582-018-0132-6
6. Fortea J, Vilaplana E, Carmona-Iragui M, et al. Clinical and biomarker changes of Alzheimer's disease in adults with Down syndrome: a cross-sectional study. *Lancet*. 2020;395:1988-1997. doi:10.1016/S0140-6736(20)30689-9
7. Greenberg SM, Bacskai BJ, Hernandez-Guillamon M, Pruzin J, Sperling R, van Veluw SJ. Cerebral amyloid angiopathy and Alzheimer disease — one peptide, two pathways. *Nat Rev Neurol*. 2020;16:30-42. doi:10.1038/S41582-019-0281-2
8. Carmona-Iragui M, Videla L, Lleó A, Fortea J. Down syndrome, Alzheimer disease, and cerebral amyloid angiopathy: the complex triangle of brain amyloidosis. *Dev Neurobiol*. 2019;79:716-737. doi:10.1002/DNEU.22709
9. Head E, Phelan MJ, Doran E, et al. Cerebrovascular pathology in Down syndrome and Alzheimer disease. *Acta Neuropathol Commun*. 2017;5:93. doi:10.1186/S40478-017-0499-4
10. Carmona-Iragui M, Balasa M, Benejam B, et al. Cerebral amyloid angiopathy in Down syndrome and sporadic and autosomal-dominant Alzheimer's disease. *Alzheimers Dement*. 2017;13:1251-1260. doi:10.1016/J.JALZ.2017.03.007
11. Lao PJ, Gutierrez J, Keator D, et al. Alzheimer-related cerebrovascular disease in Down syndrome. *Ann Neurol*. 2020;88:1165-1177. doi:10.1002/ANA.25905
12. Morcillo-Nieto AO, Zsadanyi SE, Arriola-Infante JE, et al. Characterization of white matter hyperintensities in Down syndrome. *Alzheimers Dement*. 2024;20(9):6527-6541. doi:10.1002/ALZ.14146
13. Lao P, Edwards N, Flores-Aguilar L, et al. Cerebrovascular disease emerges with age and Alzheimer's disease in adults with Down syndrome. *Sci Rep*. 2024;14:12334. doi:10.1038/S41598-024-61962-Y
14. Barroeta I, Videla L, Carmona-Iragui M, Fortea J, Rafii MS. Current advances and unmet needs in Alzheimer's disease trials for individuals with Down syndrome: navigating new therapeutic frontiers. *Alzheimers Dement*. 2025;21(6):e70258. doi:10.1002/ALZ.70258
15. Videla L, Benejam B, Barroeta I, et al. The Down Alzheimer Barcelona Neuroimaging Initiative (DABNI) and its contributions to understanding Alzheimer's disease in Down syndrome: a decade of discovery. *Alzheimers Dement*. 2025;21(6):e70259. doi:10.1002/ALZ.70259
16. Alcolea D, Clarimón J, Carmona-Iragui M, et al. The Sant Pau Initiative on Neurodegeneration (SPIN) cohort: a data set for biomarker discovery and validation in neurodegenerative disorders. *Alzheimer's Dement Transl Res Clin Interv*. 2019;5:597-609. doi:10.1016/J.TRCI.2019.09.005
17. Esteba-Castillo S, Dalmau-Bueno A, Ribas-Vidal N, Vilá-Alsina M, García Alba J, Novell R. Adaptation and validation of CAMDEX-DS (Cambridge Examination for Mental Disorders of Older People with Down's Syndrome and others with intellectual disabilities) in Spanish population with intellectual disabilities [in Spanish]. *Rev Neurol*. 2013;57(8):337-346. ISSN 0210-0010.
18. Regier DA, Kuhl EA, Kupfer DJ. The DSM-5: classification and criteria changes. *World Psychiatry*. 2013;12:92-98. doi:10.1002/WPS.20050
19. Kaufman AS, Calonge Romano I, Cordero Pando A, Kaufman NL. *Test breve de inteligencia de Kaufman (K.BIT)*. Pearson; 2011.
20. Gaser C, Dahnke R, Thompson PM, Kurth F, Luders E, Initiative ADN, CAT – A Computational Anatomy Toolbox for the Analysis of Structural MRI Data. BioRxiv 2022:2022.06.11.495736. doi:10.1101/2022.06.11.495736
21. Schmidt P, Pongratz V, Küster P, et al. Automated segmentation of changes in FLAIR-hyperintense white matter lesions in multiple sclerosis on serial magnetic resonance imaging. *NeuroImage Clin*. 2019;23:101849. doi:10.1016/J.NICL.2019.101849
22. Schmidt P, Bayesian inference for structured additive regression models for large-scale problems with applications to medical imaging 2017. (accessed April 16, 2022). https://edoc.ub.uni-muenchen.de/20373/
23. Avants BB, Tustison NJ, Song G, Cook PA, Klein A, Gee JC. A reproducible evaluation of ANTs similarity metric performance in brain image registration. *Neuroimage*. 2011;54:2033-2044. doi:10.1016/J.NEUROIMAGE.2010.09.025
24. Fortin JP, Parker D, Tunç B, et al. Harmonization of multi-site diffusion tensor imaging data. *Neuroimage*. 2017;161:149-170. doi:10.1016/J.NEUROIMAGE.2017.08.047
25. Al-Janabi OM, Bauer CE, Goldstein LB, et al. White matter hyperintensity regression: comparison of brain atrophy and cognitive profiles with progression and stable groups. *Brain Sci*. 2019;9(7):170. doi:10.3390/BRAINSCI9070170
26. Yushkevich PA, Piven J, Hazlett HC, et al. User-guided 3D active contour segmentation of anatomical structures: significantly improved efficiency and reliability. *Neuroimage*. 2006;31:1116-1128. doi:10.1016/J.NEUROIMAGE.2006.01.015
27. Zsadanyi SE, Morcillo-Nieto AO, Aranha MR, et al. Associations of microbleeds and their topography with imaging and CSF biomarkers of Alzheimer pathology in individuals with Down syndrome. *Neurology*. 2024;103:e209676. doi:10.1212/WNL.0000000000209676
28. Fortea J, Carmona-Iragui M, Benejam B, et al. Plasma and CSF biomarkers for the diagnosis of Alzheimer's disease in adults with Down syndrome: a cross-sectional study. *Lancet Neurol*. 2018;17:860-869. doi:10.1016/S1474-4422(18)30285-0
29. Carmona-Iragui M, Santos T, Videla S, et al. Feasibility of lumbar puncture in the study of cerebrospinal fluid biomarkers for Alzheimer's disease in subjects with Down syndrome. *J Alzheimer's Dis*. 2017;55:1489-1496. doi:10.3233/JAD-160827
30. Subirana I, Sanz H, Vila J. Building Bivariate Tables: the compareGroups package for R. *J Stat Softw*. 2014;57:1-16. doi:10.18637/JSS.V057.I12
31. Lao P, Edwards N, Flores-Aguilar L, et al. Longitudinal changes in white matter hyperintensity volume accelerate across the Alzheimer's

15525279, 2026, 2, Downloaded from https://alz-journals.onlinelibrary.wiley.com/doi/10.1002/alz.71157 by Alejandra O. Morcillo-Nieto - Spanish Cochrane National Provision (Ministerio de Sanidad) , Wiley Online Library on [05/02/2026]. See the Terms and Conditions (https://onlinelibrary.wiley.com/terms-and-conditions) on Wiley Online Library for rules of use; OA articles are governed by the applicable Creative Commons License

continuum in adults with Down syndrome. *Alzheimers Dement*. 2025;21(9):e70679. doi:10.1002/ALZ.70679
32. Jochems ACC, Arteaga C, Chappell F, et al. Longitudinal changes of white matter hyperintensities in sporadic small vessel disease: a systematic review and meta-analysis. *Neurology*. 2022;99:E2454-63. doi:10.1212/WNL.0000000000201205
33. Li Y, Kalpouzos G, Laukka EJ, et al. Progression of neuroimaging markers of cerebral small vessel disease in older adults: a 6-year follow-up study. *Neurobiol Aging*. 2022;112:204-211. doi:10.1016/j.neurobiolaging.2022.01.006
34. Luo J, Ma Y, Agboola FJ, et al. Longitudinal relationships of white matter hyperintensities and Alzheimer disease biomarkers across the adult life span. *Neurology*. 2023;101:E164-77. doi:10.1212/WNL.0000000000207378
35. Van Leijsen EMC, Van Uden IWM, Ghafoorian M, et al. Nonlinear temporal dynamics of cerebral small vessel disease. *Neurology*. 2017;89:1569-1577. doi:10.1212/WNL.0000000000004490
36. van Leijsen EMC, de Leeuw FE, Tuladhar AM. Disease progression and regression in sporadic small vessel disease-insights from neuroimaging. *Clin Sci*. 2017;131:1191-1206. doi:10.1042/CS20160384
37. van Leijsen EMC, Bergkamp MI, van Uden IWM, et al. Cognitive consequences of regression of cerebral small vessel disease. *Eur Stroke J*. 2019;4:85-89. doi:10.1177/2396987318820790
38. Callisaya ML, Beare R, Phan T, et al. Progression of white matter hyperintensities of presumed vascular origin increases the risk of falls in older people. *J Gerontol A Biol Sci Med Sci*. 2015;70:360-366. doi:10.1093/GERONA/GLU148
39. Sachdev P, Wen W, Chen X, Brodaty H. Progression of white matter hyperintensities in elderly individuals over 3 years. *Neurology*. 2007;68:214-222. doi:10.1212/01.WNL.0000251302.55202.73
40. Rozalem Aranha M, Montal V, van den Brink H, et al. Cortical microinfarcts in adults with Down syndrome assessed with 3T-MRI. *Alzheimers Dement*. 2024;20:3906-3917. doi:10.1002/ALZ.13797
41. Wang YL, Chen W, Cai WJ, et al. Associations of white matter hyperintensities with cognitive decline: a longitudinal study. *J Alzheimers Dis*. 2020;73:759-768. doi:10.3233/JAD-191005
42. Carmichael O, Schwarz C, Drucker D, et al. Longitudinal changes in white matter disease and cognition in the first year of the Alzheimer disease neuroimaging initiative. *Arch Neurol*. 2010;67:1370-1378. doi:10.1001/ARCHNEUROL.2010.284
43. Dadar M, Camicioli R, Duchesne S, Collins DL. The temporal relationships between white matter hyperintensities, neurodegeneration, amyloid beta, and cognition. *Alzheimers Dement*. 2020;12:e12091. doi:10.1002/DAD2.12091
44. Kamal F, Morrison C, Maranzano J, Zeighami Y, Dadar M. White matter hyperintensity trajectories in patients with progressive and stable mild cognitive impairment. *Neurology*. 2023;101:E815-24. doi:10.1212/WNL.0000000000207514
45. Ramirez J, McNeely AA, Berezuk C, Gao F, Black SE. Dynamic progression of white matter hyperintensities in Alzheimer's disease and normal aging: results from the Sunnybrook dementia study. *Front Aging Neurosci*. 2016;8:62. doi:10.3389/FNAGI.2016.00062
46. Debette S, Markus HS. The clinical importance of white matter hyperintensities on brain magnetic resonance imaging: systematic review and meta-analysis. *BMJ*. 2010;341:288. doi:10.1136/BMJ.C3666
47. Edwards NC, Lao PJ, Alshikho MJ, et al. Cerebrovascular disease drives Alzheimer plasma biomarker concentrations in adults with Down syndrome. *MedRxiv Prepr Serv Heal Sci*. 2023;6(5):fcae331. doi:10.1101/2023.11.28.23298693
48. Edwards NC, Lao PJ, Alshikho MJ, et al. Alzheimer's disease diagnostic progression is associated with cerebrovascular disease and neuroinflammation in adults with Down syndrome. *Alzheimers Dement*. 2025;21(10):e70726. doi:10.1002/ALZ.70726
49. Martini AC, Gross TJ, Head E, Mapstone M. Beyond amyloid: immune, cerebrovascular, and metabolic contributions to Alzheimer disease in people with Down syndrome. *Neuron*. 2022;110:2063-2079. doi:10.1016/j.neuron.2022.04.001
50. Flores-Aguilar L, Iulita MF, Kovecses O, et al. Evolution of neuroinflammation across the lifespan of individuals with Down syndrome. *Brain*. 2020;143:3653-3671. doi:10.1093/BRAIN/AWAA326
51. Grinberg LT, Korczyn AD, Heinsen H. Cerebral amyloid angiopathy impact on endothelium. *Exp Gerontol*. 2012;47:838-842. doi:10.1016/j.exger.2012.08.005
52. de Souza A, Tasker K. Inflammatory cerebral amyloid angiopathy: a broad clinical spectrum. *J Clin Neurol*. 2023;19:230-241. doi:10.3988/JCN.2022.0493
53. Aranha MR, Fortea J, Carmona-Iragui M. Cerebral amyloid angiopathy-related inflammation in Down syndrome-related Alzheimer disease. *Neurology*. 2022;98:1021-1022. doi:10.1212/WNL.0000000000200704
54. Jochems ACC, Muñoz Maniega S, Clancy U, et al. Definitions of white matter hyperintensity change: impact on estimates of progression and regression. *Stroke Vasc Neurol*. 2025;10:411-414. doi:10.1136/SVN-2024-003300

SUPPORTING INFORMATION

Additional supporting information can be found online in the Supporting Information section at the end of this article.

How to cite this article: Morcillo-Nieto AO, Rozalem-Aranha M, Maure-Blesa L, et al. Temporal dynamics of white matter hyperintensities related to Alzheimer's disease in adults with Down syndrome. *Alzheimer's Dement*. 2026;22:e71157. https://doi.org/10.1002/alz.71157

15525279, 2026, 2, Downloaded from https://alz-journals.onlinelibrary.wiley.com/doi/10.1002/alz.71157 by Alejandra O. Morcillo-Nieto - Spanish Cochrane National Provision (Ministerio de Sanidad) , Wiley Online Library on [05/02/2026]. See the Terms and Conditions (https://onlinelibrary.wiley.com/terms-and-conditions) on Wiley Online Library for rules of use; OA articles are governed by the applicable Creative Commons License

Study 4: Peak Width of Skeletonized Mean Diffusivity Reveals Early and Multifactorial White Matter Injury Across Sporadic and Down Syndrome-Associated Alzheimer's Disease

Alejandra O. Morcillo-Nieto[1,2,3]; Maria Franquesa-Mullerat[1,3]; Sara E. Zsadanyi[1,2,3]; José Enrique Arriola-Infante[4]; Lídia Vaqué-Alcázar[1,5,6]; Mateus Rozalem-Aranha[1,7]; José Allende Parra[1,3]; Zili Zhao[1,3]; Javier Arranz[1,8]; Íñigo Rodríguez-Baz[1,2]; Lucia Maure-Blesa[1,2,8]; Laura Videla[1,2,9]; Isabel Barroeta[1,2]; Laura Del Hoyo Soriano[1,2]; Bessy Benejam[1,9]; Susana Fernández[9]; Aida Sanjuan Hernandez[1]; Lucia Pertierra[1,3,10]; Sandra Giménez[1,2,11]; Miguel Santos-Santos[1,2]; Oriol Dols-Icardo[1,2]; Ignacio Illán-Gala[1,2]; Daniel Alcolea1,2; Olivia Belbin1,2; Alberto Lleó[1,2]; María Carmona-Iragui[1,2,9]; Juan Fortea[1,2,9]; and Alexandre Bejanin[1,2]

[1]Sant Pau Memory Unit, IR SANT PAU, Hospital de la Santa Creu i Sant Pau, Barcelona, Spain. [2]Center of Biomedical Investigation Network for Neurodegenerative Diseases (CIBERNED), Madrid, Spain. [3]Institut de Neurociències, Universitat Autònoma de Barcelona, Barcelona, Spain. [4]Department of Neurology, Torrecárdenas University Hospital, Almería, Spain. [5]Department of Medicine, Faculty of Medicine and Health Sciences, Institute of Neurosciences, University of Barcelona, Barcelona, Spain. [6]Institut d'Investigacions Biomèdiques August Pi i Sunyer (IDIBAPS), Barcelona, Spain. [7]Neuroradiology Section, Department of Radiology, Hospital de la Santa Creu i Sant Pau, Facultad de Medicina, Universitat Autònoma de Barcelona, Barcelona, Spain. [8]Department of Medicine, Universitat Autònoma de Barcelona, Barcelona, Spain. [9]Barcelona Down Medical Center, Fundació Catalana Síndrome de Down, Barcelona, Spain. [10]Cognitive Neurology, Neuropsychology and Neuropsychiatry Unit, Neurology Department, Fleni, Ciudad Autónoma de Buenos Aires, Argentina. [11]Multidisciplinary Sleep unit. IR SANT PAU, Hospital de la Santa Creu i Sant Pau, Barcelona, Spain

Alzheimer's Dement (2026) Accepted
IF (2024) =11.1, Rank= 6/202 in Clinical Neurology, D1

STRUCTURED ABSTRACT

Introduction; This study investigates the evolution with disease progression and pathological correlates of Peak width of skeletonized mean diffusivity (PSMD), a sensitive diffusion MRI marker of microvascular white matter (WM) injury, in sporadic Alzheimer's disease (sAD) and Down syndrome (DS)-associated AD.

Method; This cross-sectional study included 150 euploid controls, 118 subjects with sAD, and 228 DS adults (34.65% with symptomatic AD). PSMD was derived from 3T-MRI diffusion tensor imaging. Associations with sociodemographic, clinical stage, CSF, and small vessel disease markers were examined.

Results; PSMD correlated with age in all groups, showing a stronger association in DS, with alterations apparent 15 years before the population's dementia age of onset. In euploid and DS, higher PSMD correlated with AD severity, CSF-NfL, microbleeds, and WMH. PSMD abnormalities were more frequent than WMH, especially in DS.

Discussion; PSMD is a sensitive early biomarker of WM injury across sAD and DSAD, preceding symptom onset and capturing multifactorial disease processes.

Keywords: *Alzheimer's disease; Down syndrome; magnetic resonance imaging; diffusion weighted imaging; white matter integrity; small vessel disease*

1. BACKGROUND

Down syndrome (DS) is the most common genetic cause of intellectual disability (ID), caused by a full or partial trisomy of chromosome 21 [1]. DS also represents the largest genetic form of Alzheimer's disease (AD), mainly due to the triplication of the Amyloid Precursor Protein (APP) gene on chromosome 21 [2]. The overexpression of APP accelerates amyloid-β (Aβ) accumulation, starting during adolescence, and by the age of 40, virtually all individuals with DS exhibit the neuropathological hallmarks of AD [3,4]. In parallel, cerebral amyloid angiopathy (CAA), characterized by Aβ deposition in the walls of leptomeningeal and cortical blood vessels, is frequently observed in DS [5,6] and likely contributes to microvascular injury and white matter (WM) damage.

Although AD is traditionally considered a disease primarily affecting grey matter (GM), it is now established that WM degeneration also occurs early in the disease process [7,8]. Pioneer post-mortem studies described loss of myelin, axonal degeneration, and gliosis in the WM in AD patients [9]. These lesions were not fully explained by Wallerian degeneration from cortical atrophy [9], implicating additional mechanisms such as microvascular injury [10] and/or demyelination [11].

Diffusion weighted imaging (DWI), specifically diffusion tensor imaging (DTI), is a neuroimaging technique capable of detecting subtle WM changes not visible on conventional structural magnetic resonance imaging (MRI) [12]. By modeling the magnitude and directionality of water diffusion, DTI yields indices such as fractional anisotropy (FA) and mean diffusivity (MD) that are sensitive to myelin and axonal integrity [13]. DWI sensitively captures WM changes with consistently decreasing FA and increasing MD values in normal aging [14–17] and AD [7,8]. In DS, DTI studies demonstrated reduced FA and increased MD compared to the euploid population [18–21]. These alterations were more prominent with Aβ burden and AD progression [22–24], with early changes in late-myelinating and relative preservation of early-myelinating fiber pathways [23].

Beyond the traditional DTI metrics, the peak width of skeletonized mean diffusivity (PSMD) represents a dispersion-based measure that captures the heterogeneity of MD values sampled along the WM skeleton. A higher PSMD value indicates greater heterogeneity, increased water dispersion, and greater WM microstructural damage [25]. Originally studied in the context of CAA [26–30], PSMD has since been

proposed as a promising imaging biomarker of small vessel disease (SVD) [25,31,32]. In addition, increased PSMD has been reported in other conditions associated with WM damages, in which SVD is common, such as normal aging [33], and AD [29,34,35]. In AD, specifically, a recent study further suggested that PSMD may improve the prediction of conversion from cognitively stable status to mild cognitive impairment (MCI) or AD dementia. [34]. To our knowledge, there are no yet studies investigating its performance in DS, a population with ultrahigh risk of developing both AD and CAA.

The aim of this study is therefore to characterize PSMD across the AD continuum in both DS-associated AD (DSAD) and sporadic AD (sAD). The inclusion of the sAD group serves as a clinical benchmark, enabling us to determine whether early WM microstructural injury in DS shares common pathophysiological mechanisms with sporadic AD or is primarily driven by DS-specific genetic factors. We further examined the relationships between PSMD with sociodemographic variables, *APOE* and clinical stage, and biomarkers of AD and SVD. We hypothesize that (i) PSMD will be higher in AD groups (both sAD and DS) compared to euploid cognitively unimpaired (CU) controls; (ii) higher PSMD will be associated with greater AD pathology (as reflected by CSF biomarkers) and SVD burden; and (iii) in DS, PSMD alterations will precede the emergence of AD symptoms. Such deep characterization has the potential to provide novel insight into the utility of PSMD as a sensitive, clinically relevant metric to detect early WM changes in AD.

2. METHODS

2.1 Study design and participants

This single-center, cross-sectional cohort study enrolled adults with DS from the population-based Down-Alzheimer Barcelona Neuroimaging Initiative (DABNI) cohort [36], euploid, cognitively unimpaired controls (CU), and individuals with sAD from the Sant Pau Initiative on Neurodegeneration (SPIN) cohort [37]. Participants were eligible for the present study only if they underwent an MRI scan comprising both T1-weighted (T1w) and DWI imaging. The study was approved by the Sant Pau Ethics Committee following the standards for medical research in humans recommended by the Declaration of Helsinki. All participants or their legally authorized representatives gave written informed consent before enrolment.

2.2 Clinical assessment

Most participants were screened for apolipoprotein E (*APOE*) haplotype and underwent a comprehensive neurological and neuropsychological evaluation, including the assessment for the presence of traditional vascular risk factors (hypertension, dyslipidemia, and diabetes mellitus). Clinical diagnoses were based on the diagnostic workup closest to the MRI scan (within 1 year), without relying on prior longitudinal research visits. Instead, clinical decline was ascertained cross-sectionally through structured anamnesis, standardized clinical scales, and informant reports.

For the DABNI cohort, adults with DS underwent a specific neuropsychological assessment, including the Cambridge Cognitive Examination for Older Adults with Down Syndrome (CAMCOG-DS) Spanish version to evaluate the global cognition. Additionally, ID was categorized as mild, moderate, or severe/profound based on the Diagnostic and Statistical Manual of Mental Disorders, Fifth Edition, and caregivers' report of the individual's best-ever level of functioning and the score of the Kaufman Brief Intelligence Test Spanish version. To account for the effect of ID on cognitive performance, we excluded severe/profound cases to prevent floor effects and z-transformation on each test in mild and moderate ID groups separately. Participants were clinically classified in a consensus meeting between neurologists and neuropsychologists, after independent visits and blinded to biomarker data, into the following four groups: (1) asymptomatic (aDS, i.e., no clinical or neuropsychological suspicion of AD-related cognitive decline), (2) prodromal AD (pDS, i.e., evidence of cognitive decline due to AD, but no significant impact on baseline activities of daily living), (3) AD dementia (dDS, i.e., when the cognitive decline impaired the daily activities) and (4) uncertain (uDS, i.e., when there were medical, pharmacological, and/or psychiatric conditions interfering with cognition or daily activities, but no suspicion of neurodegenerative origin).

Participants in the SPIN cohort underwent a standardized neurological and neuropsychological assessment to

evaluate multiple cognitive domains, as well as neuropsychiatric symptoms, functional impact, and global cognitive impairment. For clinical diagnostic staging, we prioritized the Clinical Dementia Rating (CDR) global scale or Global Deterioration Scale – Functional Assessment Staging (GDS-FAST) over the Mini-Mental State Examination (MMSE). The clinical diagnosis of sAD, identifying individuals in the MCI and dementia stages of AD, was established following the National Institute on Aging-Alzheimer's Association (NIA-AA) criteria. In a subset of participants with available fluid biomarkers, AD diagnosis was further confirmed according to a previously validated cerebrospinal fluid (CSF) biomarker cutoff, defined as an Aβ peptide 1-42 (Aβ42), Aβ peptide 1-40 (Aβ40) ratio < 0.062 pg/mL, indicating the presence of amyloid pathology. CU individuals did not present neurological or psychiatric disorders or other major medical illnesses, were required to have a CDR global scale of 0 and/or a GDS-FAST score of 1, and to perform within the normal range on neuropsychological evaluations regarding their age and education [37].

2.3 Neuroimaging data

2.3.1 Image acquisition

MRI was acquired on 3T scanners at Hospital del Mar (Philips Achieva) and Hospital Clínic (Siemens Prisma). The protocols included high-resolution three-dimensional T1w, DWI, fluid-attenuated inversion recovery (FLAIR), and susceptibility-weighted imaging (SWI). Detailed acquisition parameters are provided in Table S1.

2.3.2 PSMD computation

All DWI scans underwent visual quality control, and those with unsatisfactory raw quality were excluded. DWI acquisition was either single-shell (n= 405) with b-value = 1000 s/mm^2 or multi-shell (n=91) with b-values=0,500,1000, and 2000 s/mm^2. To harmonize the data and follow the PSMD developers' guidance that b-values between 700 and 1200 s/mm^2 are required [25], we retained only the b-value = 1000 s/mm^2 volume, which was extracted using fslsplit and reassembled with fslmerge in FSL (v6.0.7.15).

Preprocessing was performed with an in-house Python pipeline using Diffusion Imaging in Python (DIPY). First, DWI images were denoised with Marchenko-Pastur principal component analysis (PCA) with dipy_denoise_mppca. Although a subset of participants (n = 276) had additional reverse phase-encoded b = 0 images enabling susceptibility distortion correction with FSL TOPUP, this step was not applied in order to maintain a uniform processing pipeline across the full cohort. Exploratory analyses indicated that applying TOPUP did not significantly affect the resulting PSMD values. Finally, for all participants, eddy-current and motion correction were then applied with FSL EDDY.

PSMD was automatically computed using the freely available script from Baykara and colleagues (2016) [25]. Briefly, eddy-corrected DWI scans were processed with the standard Tract-Based Spatial Statistics (TBSS) pipeline in FSL. First, FA volumes were registered to the FMRIB 1 mm FA template in standard space. Second, a WM skeleton was derived from the mean FA image and thresholded at FA ≥ 0.2 to exclude predominantly non-WM voxels. Third, MD maps were projected onto the FA skeleton and further masked using the WM skeleton mask, provided by Baykara and colleagues, with an FA threshold of > 0.3 to mitigate CSF partial volume effects. Finally, PSMD was calculated as the difference between the 95th and 5th percentile values of the MD histogram within the entire skeleton mask, representing a global WM diffusion metric. To account for differences in MRI acquisition protocols, PSMD was harmonized using the ComBat method, implemented in the R library neuroCombat.

2.3.3 White matter hyperintensities quantification

Total white matter hyperintensity (WMH) volume was quantified as previously described [38]. In brief, FLAIR images were coregistered to their corresponding T1w images using Advanced Normalization Tools (ANTs). Then, lesion probability maps were generated with the Lesion Prediction Algorithm implemented in the Lesion Segmentation Toolbox (LST v3.0.0) for SPM12. Probability maps were binarized at a threshold of 0.3 to extract a global metric of total WMH volumes, and ComBat harmonization was applied to adjust for differences in MRI acquisition protocols.

2.3.4 Microbleed segmentation

SWI images underwent N4 bias-field correction (ANTs) and were coregistered to their corresponding T1w image. Cerebral microbleeds were manually segmented in ITK-SNAP (v3.8.0), as previously described [39]. Most segmentations were obtained from a previous study in which two independent raters performed the segmentations; the remaining scans were segmented by only one of these raters (S.Z.). All raters were blinded to demographic, clinical, and fluid biomarker data. Participants were classified according to the presence of microbleed (microbleed negative [MB-] and microbleeds positive [MB+]).

2.4 Cerebrospinal fluid biomarkers

A subset of participants underwent lumbar puncture within 1 year of MRI acquisition. We quantified Aβ40, Aβ42, and tau phosphorylated at threonine 181 (pTau181) in CSF using a commercially available immunoassay in a fully automated platform (Lumipulse; Fujirebio-Europe), following a previously published protocol. CSF neurofilament light chain (NfL) and YKL-40 (also known as chitinase 3-like 1) levels were measured with commercially available enzyme-linked immunosorbent assays (NF-Light Assay, UmanDiagnostics and MicroVue EIA, Quidel, respectively) according to the manufacturer's recommendations. Additionally, CSF glial fibrillary acidic protein (GFAP) concentrations were measured using the SR-X single-molecule array (Quanterix).

2.5 Statistical analyses

Statistical analyses were conducted using R software (version 4.5.1), and the statistical significance threshold was set at $p=0.05$. Differences in baseline sociodemographic characteristics among DS, CU, and sAD were assessed using the compareGroups library. Chi-squared tests were used for categorical variables, such as sex and *APOE*ε4 status, while Kruskal-Wallis tests were applied for continuous variables, including age and CSF biomarkers, since they did not follow normality. To reduce skewness, PSMD, WMH, and concentrations of CSF biomarkers were log-transformed. Participants classified as uDS were included in all combined DS analyses but excluded from analyses stratified by AD clinical diagnosis.

To examine the age-related trajectories of PSMD, we performed locally estimated scatterplot smoothing (LOESS) curves using a tricubic weight function and a span parameter of 0.75, providing an informative representation of the data. We additionally used robust linear regression, separately in CU, sAD, and DS, to assess associations between PSMD and age, as well as global cognitive scores (CAMCOG-DS z-scores for the DS cohort and MMSE for the euploid population). To assess the effect of sex, *APOE*ε4 status, ID, and AD clinical status on the distribution of PSMD, we performed either Mann-Whitney or Kruskal-Wallis tests followed by the Dunn test for post-hoc analysis and Holm correction for multiple comparisons.

Associations between PSMD and CSF biomarkers were evaluated using robust linear models and adjusted for multiple comparisons using the False Discovery Rate (FDR). First, we used univariate robust linear regression models to assess the predictive capacity of individual fluid biomarkers on total PSMD in CU, sAD, and the whole DS cohort, and stratified in aDS and symptomatic DS (sDS; comprising pDS and dDS). The standardized regression coefficients were used to compare the strength of the association between the predictors and PSMD. Additionally, we implemented Elastic Net regression to assess the relative contribution of all CSF biomarkers to PSMD within each clinical subgroup. For these models, we analysed a subset of participants with the complete panel of CSF biomarkers available. Note that this subset did not differ significantly from the remaining participants in demographic or clinical characteristics. This approach combines the strengths of lasso and ridge regularization, enabling effective handling of multicollinearity, mitigation of overfitting, and data-driven feature selection. All predictors were standardized before model fitting. The Elastic Net mixing parameter α was fixed at 0.5, providing equal weighting to L1 (variable selection) and L2 (coefficient stabilization) penalties. The penalty parameter λ was selected using Leave-One-Out Cross-Validation (LOOCV), we retained λ_min, corresponding to the model with the minimum mean cross-validated error. To evaluate the stability of

variable selection, we performed 200 bootstrap resamples of each subgroup dataset. For each resample, an Elastic Net model was fit using the same α and λ-selection procedure. Biomarkers were considered robust predictors if they were selected (non-zero coefficient) in at least 70% of the bootstrap models.

The impact of microbleed presence on PSMD was evaluated using the Mann–Whitney test. The relationship between PSMD and WMH was tested with a robust linear regression. We additionally performed a conditional probability analysis to assess the concordance between PSMD alterations and WMH and to determine whether isolated positivity in one marker was more frequent than in the other. The theoretical background and details of this method have been previously described [40]. In brief, we dichotomized both PSMD and WMH using thresholds (mean + 1.5 SD) defined in the CU group. Values above the threshold were labeled abnormal (i.e., PSMD+, WMH+), and values equal to or below were labeled normal (i.e., PSMD−, WMH−). Finally, we used McNemar's test to assess, within each population (euploid and DS), the evidence against the null hypothesis that the probability that PSMD is pathological but not WMH (PSMD+WMH−) is equally likely than WMH is pathological but not PSMD (PSMD−WMH+).

Table 1. Study participants	CU	sAD	DS	
	N = 150	N = 118	N = 228	p-value
Age, y	56.35 [51.08;63.27]	72.80 [68.12;76.37]	44.72 [37.05;51.44]	<0.001[a]
Female	101 (67.33%)	69 (58.47%)	99 (43.42%)	<0.001[b]
*APOE*ε4 carriers	41 (30.60%)	68 (60.18%)	45 (21.23%)	<0.001[c]
AD clinical diagnosis				
CU/aDS	150 (100.00%)	0 (0.00%)	141 (61.84%)	
MCI/pDS	0 (0.00%)	84 (71.19%)	39 (17.11%)	
AD Dementia/dDS	0 (0.00%)	34 (28.81%)	40 (17.54%)	
uDS			8 (3.51%)	
Intellectual disability				
Mild			74 (32.89%)	
Moderate			115 (51.11%)	
Severe/Profound			36 (16.00%)	
Vascular risk factors				
Hypertension	16/78 (20.51%)	32/60 (53.33%)	5/211 (2.26%)	<0.001[d]
Dyslipidemia	25/78 (32.05%)	33/60 (55.00%)	41/218 (18.81%)	<0.001[d]
Diabetes mellitus	3/78 (3.85%)	5/58 (8.62%)	10/221 (4.52%)	0.374
CSF biomarkers, pg/mL				
Aβ42/Aβ40 (N=102/94/127)	0.10 [0.10;0.11]	0.04 [0.04;0.05]	0.06 [0.04;0.08]	<0.001[e]
pTau181 (N=102/94/127)	32.70 [26.95;42.38]	106.00 [78.90;155.00]	48.10 [22.30;100.70]	<0.001[f]
NfL (N=128/83/126)	369.05 [307.20;496.92]	997.39 [822.05;1343.45]	462.92 [263.85;754.11]	<0.001[f]
GFAP (N=45/50/110)	3019.55 [1510.64;5335.14]	10148.46 [5829.18;13852.84]	3744.11 [2190.58;5493.55]	<0.001[g]
YKL-40 (N=140/79/126)	176.97 [134.78;223.54]	301.85 [262.10;335.67]	153.29 [99.81;218.68]	<0.001[a]

Notes: Data are n (%) or median [IQR]. P-values indicate the statistical significance of differences among CU, AD, and DS participants using Chi-squared and Kruskal-Wallis tests, followed by Dunn's test for post-hoc analysis. a: DS<CU<sAD; b: DS != CU; DS!=sAD; c: sAD != CU; sAD!= DS; d: CU != sAD != DS; e: sAD < DS < CU; f: CU < DS < sAD; g: CU == DS < sAD. Notes: Data are n (%) or median [IQR]. P-values indicate the statistical significance of differences among CU, AD, and DS participants using Chi-squared and Kruskal-Wallis tests, followed by Dunn's test for post-hoc analysis. Abbreviations: Aβ42/Aβ40, concentration ratio between amyloid beta peptide 1-42 and amyloid beta peptide 1-40 (pg/mL); AD, Alzheimer's disease; aDS, asymptomatic Down syndrome; *APOE*, apolipoprotein E; CSF, cerebrospinal fluid; CU, euploid cognitively unimpaired controls; dDS, Down syndrome with Alzheimer's disease dementia; DS, Down syndrome; GFAP, glial fibrillary acidic protein concentration (pg/mL); IQR, interquartile range; MCI, mild cognitive impairment; NfL, neurofilament light chain concentration (pg/mL); pDS, prodromal Down syndrome; pTau181, tau phosphorylated at threonine 181 concentration (pg/mL); sAD, sporadic Alzheimer's disease; uDS, Down syndrome with an uncertain diagnosis of neurodegenerative disease; YKL-40, chitinase 3-like.

3. RESULTS

3.1 Population

The study included 228 adults with DS from the DABNI cohort, 150 CU, and 118 sAD patients from the SPIN cohort (Table 1). Participants spanned the whole AD clinical continuum. In the DS group, 141 were aDS, 39 pDS, 40 dDS, and 8 uDS, while in the sAD group, 84 had MCI and 34 had AD dementia (see Table S2 for demographic data stratified by clinical diagnosis). Within DS, ID levels were distributed as 74 mild ID, 115 moderate ID, and 36 severe/profound ID. Age differed significantly across groups: sAD (median [IQR] = 72.80 [8.25]) were older than CU (56.35 [12.19]) and DS (44.72 [14.39]; $H(2,496)=293.08$, $p<0.001$). There was also a significant difference in the sex distribution, with fewer females in DS (43.42%) compared with CU (67.36%) and sAD (58.47%; $p<0.001$). *APOE*ε4 carriers were more

frequent in sAD (60.18%) than in CU (30.60%) or DS (21.23%; p<0.001). The prevalence of hypertension and dyslipidemia was higher in the sAD cohort (53.33%; 55.00%, respectively) than in the CU (20.51%; 32.05%) and DS groups (2.26%; 18.81%; both conditions p<0.001), with no significant difference in diabetes mellitus (CU: 2.50%; sAD: 4.55%; DS: 4.52%; p=0.37). Asexpected, sAD demonstrated the lowest CSF Aβ42/Aβ40 ratio and the highest concentrations of CSF pTau181, GFAP, and YKL40, compared with both CU and DS groups (all p<0.001). Participants with DS exhibited lower CSF Aβ42/Aβ40 and higher CSF pTau181 and NfL levels compared with CU (all p<0.05). CSF GFAP did not differ between (p=0.13), and CSF YKL-40 concentrations were higher in CU than DS (p=0.03).

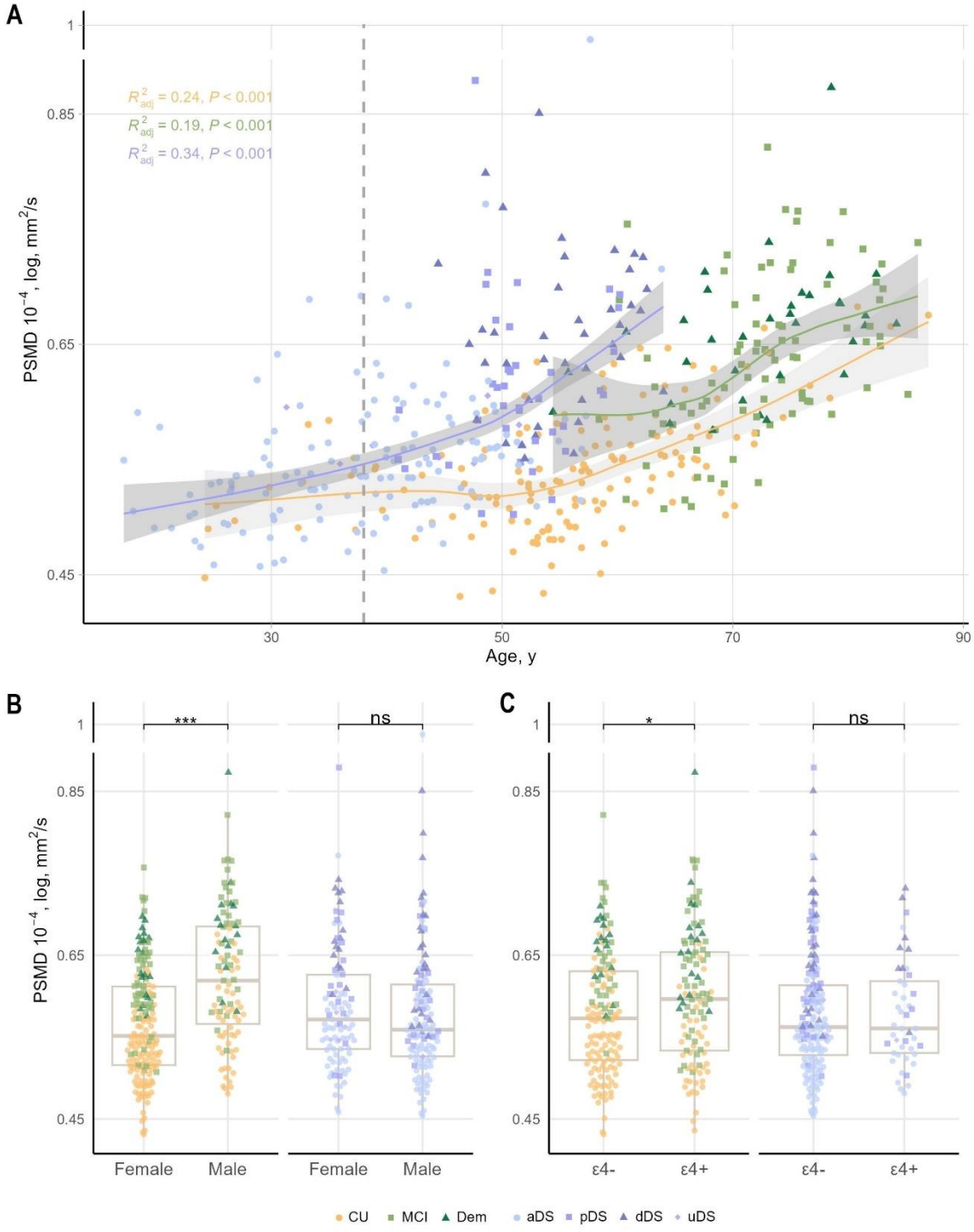

Figure 1. Effect of sociodemographic, and genetic data variables on PSMD. (A) Association between PSMD age. The points represent individual participants, and the color indicates their clinical diagnosis. Shaded areas represent 95% CI: dark gray represents the age-related changes in DS and sporadic AD, and light gray in the CU group for visual reference. The dashed line indicates when the CI stops overlapping between the DS and CU groups (38 years). Boxplots showing the effect of (B) sex, and (C) *APOE* genotype, on PSMD. Abbreviations: aDS, asymptomatic Down syndrome; CU, cognitively unimpaired; dDS, Down syndrome with Alzheimer's disease dementia; Dem, Alzheimer's disease dementia; MCI, mild cognitive impairment; PSMD, peak width of skeletonized mean diffusivity (mm^2/s, log); ns: no significance; *: p<0.05; **: p<0.01; ***: p<0.001.

3.2 Effect of sociodemographic, and genetic variables on PSMD

PSMD was associated with age in all groups: CU (R^2=0.24, p<0.001), sAD (R^2=0.19, p<0.001), and DS (R^2=0.34, p<0.001; Figure 1A). LOESS curves indicated that age-related PSMD elevations appeared earlier in DS than CU, with confidence intervals ceasing to overlap at age 38. When evaluating the DS population by clinical status, PSMD remained positively associated with age within both the asymptomatic (aDS; R^2=0.13, p<0.001) and symptomatic (sDS; R^2=0.12, p=0.001) groups (Figure S1A). In CU, higher PSMD values were observed around 50 years. At all ages, PSMD values were lower in CU than in sAD.

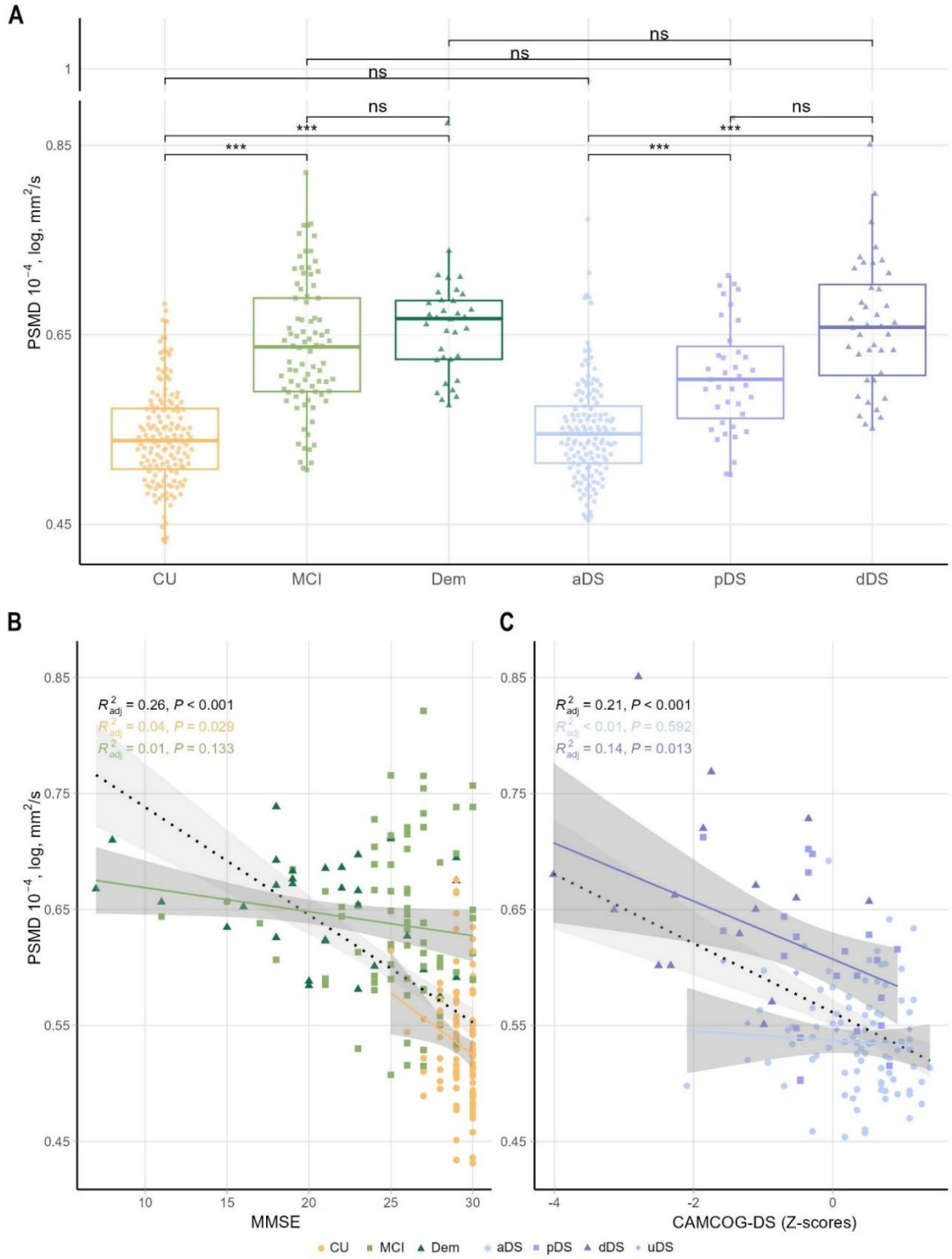

Figure 2. Effect of AD clinical status and cognitive scores on PSMD. (A) Boxplots showing the effect of clinical AD diagnosis on PSMD. (B) Associations between cognitive scores and PSMD. Abbreviations: aDS, asymptomatic Down syndrome; CAMCOG-DS, Cambridge Cognitive Examination for Older Adults with Down Syndrome; CU, cognitively unimpaired; dDS, Down syndrome with Alzheimer's disease dementia; Dem, Alzheimer's disease dementia; MCI, mild cognitive impairment; MMSE, Mini-Mental State Examination; PSMD, peak width of skeletonized mean diffusivity (mm²/s, log); ns: no significance; *: p<0.05; **: p<0.01; ***: p<0.001.

In the euploid population (CU and sAD), PSMD was higher in males than females (W=4870, p<0.001; Figure 1B) and in *APOE*ε4 carriers than non-carriers (W=6348, p=0.04; Figure 1C). When examining these effects within each diagnostic group separately, males still exhibited higher PSMD values than women (CU: W=1346, p<0.001; sAD: W= 9119, p<0.001; Figure S1B), while the effect of *APOE*ε4 status was not significant (CU: W=2051, p=0.49; sAD: W=1683, p=0.37; Figure S1C) In DS, there was no significant effect of sex (W=6918, p=0.21) or *APOE*ε4 status (W=3712, p=0.90; Figure 1B, C), independently of the diagnostic group (Figure 1SB, C).

Within DS, PSMD significantly differed by ID level, with moderate and severe/profound ID showing slightly higher values than mild ID (H(2,225)=9.43, p=0.009, Figure S2A). This result may be explained by differences in clinical status across the ID groups: aDS was more frequent in the mild ID subgroup (75%) than in the moderate (55%) and severe/profound (58%) subgroups. Age-PSMD trajectories were otherwise similar across ID levels (Figure S2B).

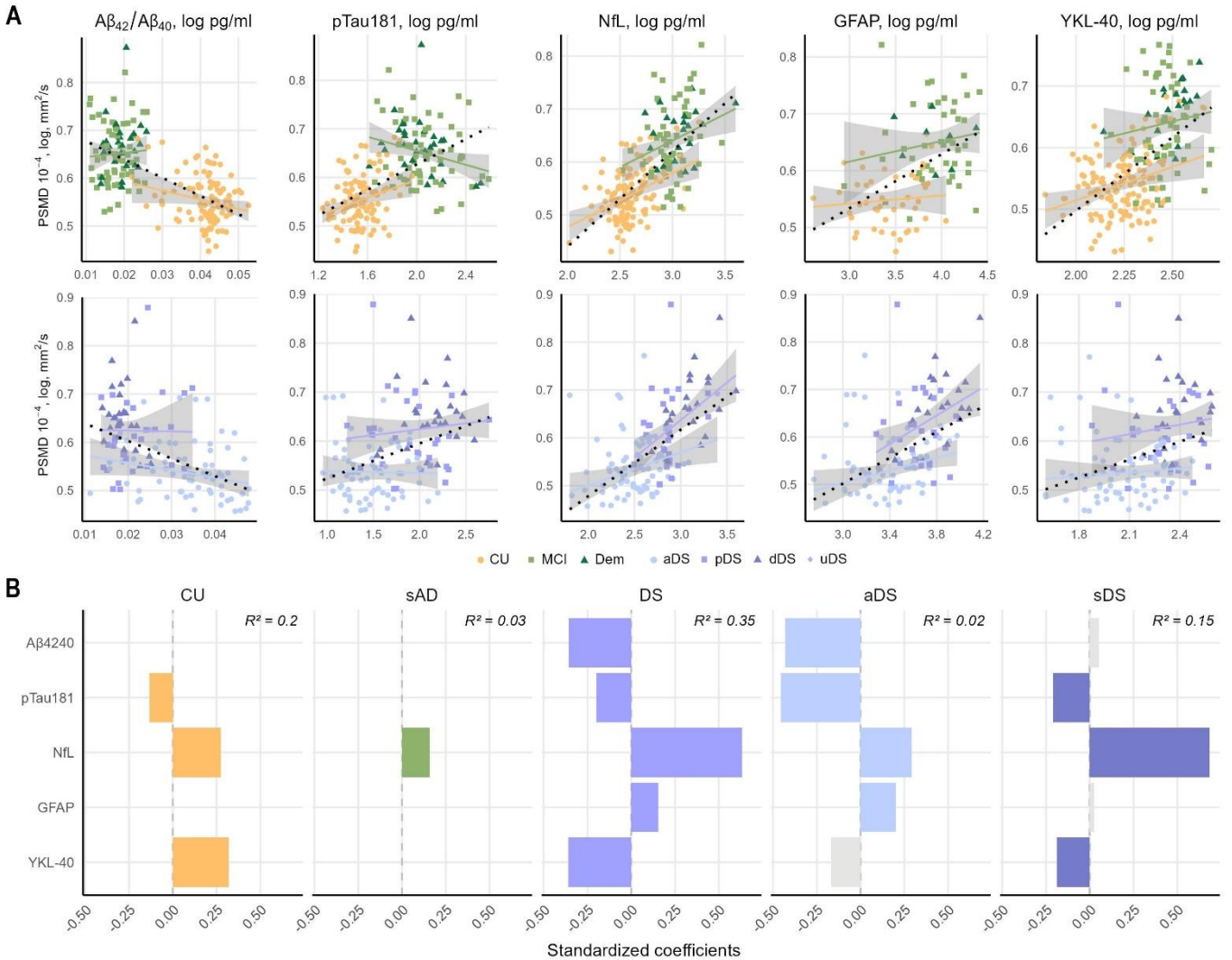

Figure 3. Association between PSMD and CSF AD biomarkers. (A) Robust linear regression of PSMD versus CSF biomarkers. The points represent individual participants, with colors indicating their clinical diagnosis. Shaded areas represent 95% CI. The dotted lines represent the entire population, either DS or euploid, while the solid lines represent the cognitively unimpaired (CU), asymptomatic (aDS), and symptomatic (sDS or sAD) groups. (B) Barplot showing the coefficients of the elastic net regression model for each predictor across clinical cohorts. Colors indicate the clinical group; predictors shown in gray did not meet the robustness threshold. Abbreviations: CSF: cerebrospinal fluid; Aβ42/Aβ40: concentration ratio between amyloid β peptide 1-42 and amyloid β peptide 1-40 (pg/mL); pTau181: tau phosphorylated at threonine 181 concentration (pg/mL); NfL: neurofilament light chain concentration (pg/mL); GFAP, glial fibrillary acidic protein concentration (pg/mL); YKL-40, chitinase 3-like 1 (pg/mL); sAD: sporadic Alzheimer's disease; DS: Down syndrome; aDS: DS asymptomatic; sDS: symptomatic DS; CU, euploid cognitively unimpaired controls; PSMD, peak width of skeletonized mean diffusivity (mm²/s, log); Dem, Alzheimer's disease dementia; MCI, mild cognitive impairment.

3.3 Effect of AD clinical status and cognitive scores on PSMD

Regarding the AD clinical status, PSMD values were progressively higher with advancing clinical severity across the AD continuum in both euploid and DS populations ($H(5,488)=200.15$, $p<0.001$; Figure 2A). Pairwise comparisons showed higher PSMD in symptomatic relative to CU and asymptomatic stages (CU vs MCI: $z=9.41$, $p<0.001$; CU vs AD dementia: $z=8.40$, $p<0.001$; aDS vs pDS: $z=4.77$, $p<0.001$; aDS vs dDS: $z=7.92$, $p<0.001$). Within symptomatic status, PSMD did not differ significantly between MCI and AD dementia in euploid participants ($z=1.54$, $p=0.12$) or between pDS and dDS in DS ($z=2.47$, $p=0.14$). Clinical stage-matched comparisons across populations showed no differences between CU and aDS ($z=0.89$, $p=0.37$), MCI and pDS ($z=-1.63$, $p=0.10$), or AD dementia and dDS ($z=-0.31$, $p=0.76$).

Furthermore, higher PSMD values were significantly associated with lower global cognitive scores in both the euploid ($R^2=0.26$, $p<0.001$) and DS populations ($R^2=0.21$, $p<0.001$). When stratifying by clinical diagnosis, these associations were attenuated or no longer significant (Figure 2B, C).

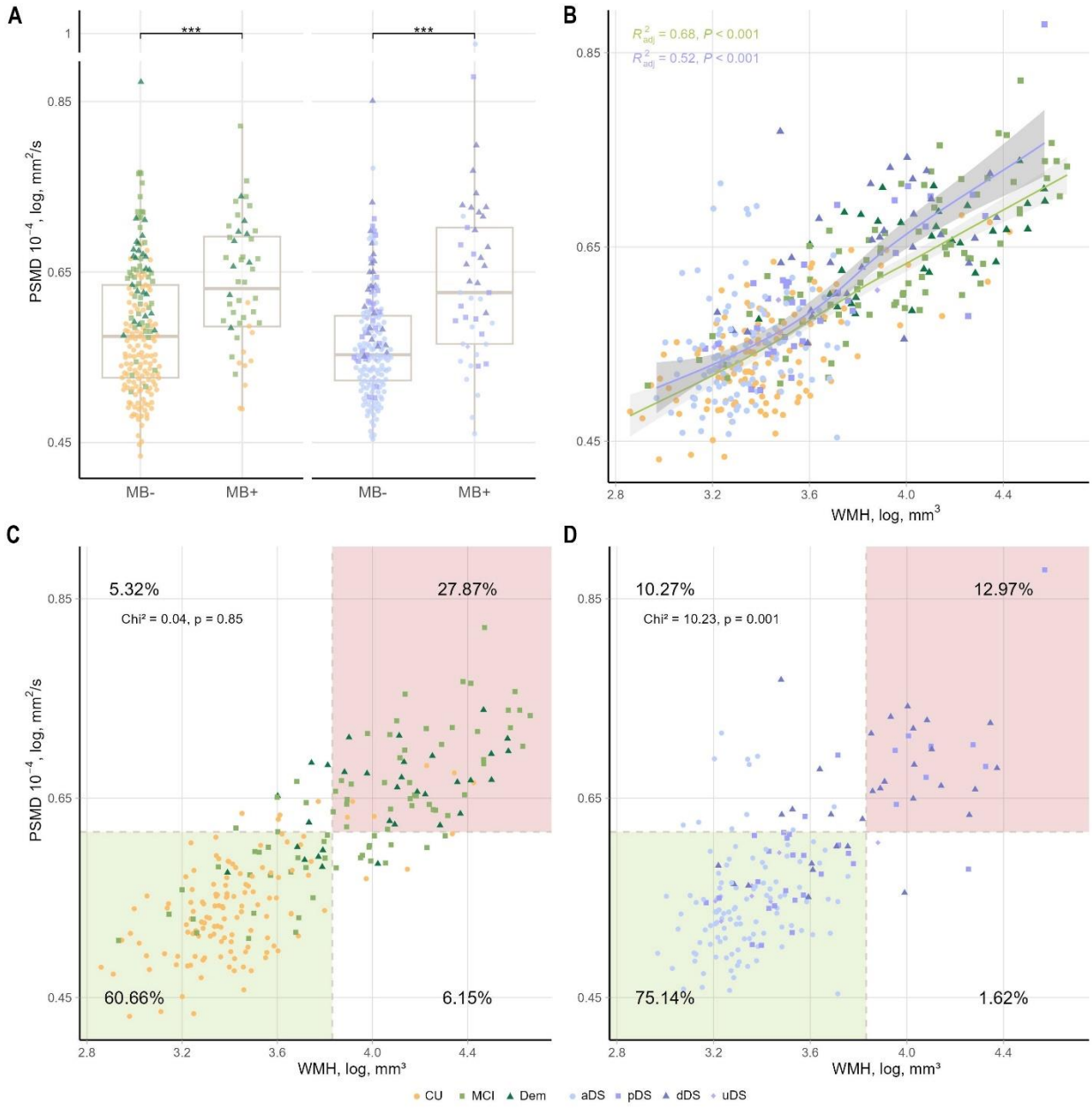

Figure 4. Associations between PSMD and SVD markers. (A) Boxplots showing the effect of microbleeds presence on PSMD, (B) robust linear regression analysis of PSMD and WMH, and conditional probability analysis in euploid (C) and Down syndrome (D) populations. The points represent individual participants, with colors indicating their clinical diagnosis. Abbreviations: aDS, asymptomatic Down syndrome; CU, euploid cognitively unimpaired controls; dDS, Down syndrome with Alzheimer's disease dementia; Dem, Alzheimer's disease dementia, MCI, mild cognitive impairment; PSMD, peak width of skeletonized mean diffusivity (mm^2/s, log); WMH, white matter hyperintensity (mm^3, log); MB, microbleed status.

3.4 Associations between PSMD and CSF biomarkers

In CU participants, PSMD was negatively associated with CSF Aβ42/Aβ40 ratio (β = −0.22, 95% CI [−0.43, −0.02], R^2 =0.04, p=0.05) and positively associated with CSF pTau181 (β= 0.26 [0.05, 0.46], R^2=0.05, p=0.02), CSF NfL (β = 0.39 [0.22, 0.56], R^2=0.14, p<0.001), and CSF YKL-40 (β = 0.30 [0.13, 0.47], R^2=0.08, p=0.001; Figure 2). In sAD, PSMD was associated with CSF pTau181 (β = −0.24 [−0.42, −0.05], R^2=0.05, p=0.03) CSF NfL (β = 0.26 [0.03, 0.48], R^2=0.05, p=0.04; Figure 3A; Table S3).

In individuals with DS, PSMD was associated with all fluid biomarkers (CSF Aβ42/Aβ40: β = −0.46 [−0.60, −0.32], R^2=0.24, p<0.001; CSF pTau181: β = 0.39 [0.23, 0.54], R^2=0.16, p<0.001; CSF NfL: β = 0.59 [0.46, 0.73], R^2=0.38, p<0.001; CSF YKL-40: β = 0.35 [0.20, 0.50], R^2=0.13, p<0.001; CSF GFAP: β = 0.46 [0.30, 0.62], R^2=0.22, p<0.001; Figure 3A; Table S3).

When stratifying DS by clinical stage, in aDS, PSMD was associated with CSF NFL (β = 0.31 [0.13, 0.49], R^2= 0.12, p=0.007), and CSF GFAP (β = 0.25 [0.08, 0.42], R^2=0.10, p=0.03). In sDS, CSF NfL (β = 0.46 [0.21, 0.70], R^2=0.21, p=0.001) and CSF GFAP (β = 0.32 [0.04, 0.60], R^2=0.09, p=0.02) remained significant (Figure 3A; Table S3).

Elastic net regression revealed distinct biomarker profiles associated with PSMD across clinical cohorts (Figure 3B; Table S4). In the CU cohort (n=40), CSF pTau181 (coefficient=−0.13), NfL (coefficient=0.27), and YKL-40 (coefficient=0.32) were selected as the main predictors (R2=0.20, MSE=0.80). In sAD (n=40), the model explained little variance, and only NfL was retained (coefficient=0.16, R2=0.03, MSE=0.97). Within the overall DS cohort (n=102), all biomarkers contributed significantly to PSMD prediction (Aβ42/Aβ40=−0.36, pTau181=−0.20, NfL=0.63, GFAP=0.16, YKL-40=−0.36; R^2=0.35, MSE=0.64). In aDS (n=57), Aβ42/Aβ40 (coefficient=−0.43), pTau181 (coefficient=−0.45), NfL (coefficient=0.29), GFAP (coefficient=0.20), and YKL-40 (coefficient=−0.17) were selected, although YKL-40 did not meet the robustness threshold (Table S4) and the model explained very little variance (R^2=0.02, MSE = 0.98). In sDS (n=44), pTau181 (coefficient=−0.21), NfL (coefficient=0.60), and YKL-40 (coefficient=−0.21) emerged as the most robust predictors (R^2=0.13, MSE=0.87).

3.5 Associations between PSMD and SVD markers

The presence of at least one microbleed was associated with higher PSMD in both euploid (W=2717, p<0.001) and DS (W=2059, p<0.001) groups (Figure 4A). PSMD also correlated strongly with WMH volume in euploid (R^2=0.68, p<0.001) and DS (R^2=0.52, p<0.001) populations, with the greatest association in DS (Figure 4B).

To assess the concordance between dichotomized PSMD and WMH status, we defined positivity thresholds using the euploid CU as the reference. The resulting thresholds (mean + 1.5 SD) were PSMD=0.61×10−4 mm^2/s and WMH=3.83 mm^3. In the euploid population, the proportion of PSMD+WMH− cases (5.32%) did not differ significantly from PSMD−WMH+ cases (6.15%; χ^2=0.04, p=0.85; Figure 4C). In contrast, within DS, PSMD+WMH− cases (10.27%) were much more frequent than PSMD−WMH+ cases (1.62%; χ^2=10.23, p=0.001; Figure 4D). We conducted sensitive analysis applying alternative thresholds (1.0 SD to 3.0 SD) to define biomarker positivity. Consistently, the proportions of PSMD+WMH− and PSMD−WMH+ remained similar in the euploid group across thresholds (Table S5), whereas in individuals with DS, PSMD+WMH− cases systematically outnumbered PSMD−WMH+ cases (Table S6).

4. DISCUSSION

WM injury is increasingly recognized as an early feature of AD, yet its characterization across distinct AD populations remains limited. In this study, we provide for the first time an integrated evaluation of PSMD, a clinically relevant WM metric, across DSAD and sAD, with the aim of determining which WM microstructural changes reflect pathophysiological mechanisms shared across both AD conditions and which are predominantly driven by the unique genetic background of DS. Our findings demonstrate that PSMD captures early WM injury in both populations, with changes detectable at the prodromal stage and, in DS, approximately 15 years before expected symptom onset. Critically, the strong associations between PSMD and both CSF NfL and SVD

neuroimaging markers across all cohorts indicate that WM damage in AD reflects a mixed pathophysiology, encompassing both AD-related neurodegeneration and microvascular disease. Furthermore, elevated PSMD in the absence of visible WMH was more frequent than the reverse pattern. This likely reflects a temporal precedence of microstructural changes over macrostructural lesions, highlighting the sensitivity of PSMD to underlying early-stage WM pathology. Together, these results refine our understanding of WM injury across the AD continuum and establish PSMD as a promising marker for tracking it.

PSMD was associated with age in all three groups. In CU, the age-related trajectory was relatively stable and rose after approximately 52 years, consistent with multi-cohort evidence [33]. In DS, PSMD was monotonically higher with age, and by age 38, confidence intervals no longer overlapped those of CU. This precedes by approximately 15 years the estimated age of onset of AD dementia in DS, estimated at 53.8 years in a large meta-analysis [41]. At this age, AD neuropathology is virtually universal [2], and SVD lesions are increasingly observed [5,38,39,42–44]. In sAD, PSMD was systematically higher than CU at all ages, indicating a clear AD pathology effect. However, the age-related PSMD trajectory paralleled that of CU, suggesting a similar age effect. Together, these results align with previous DTI studies reporting age-related WM changes in the general population [45–48], but also in AD [8] and DS [19,49].

Regarding sex, males showed higher PSMD values than females in the euploid population, but not in DS. While traditional DTI metrics reported lower WM integrity in females [33,50–55], PSMD tends to be higher in males [33], potentially capturing accelerated WM heterogeneity associated with earlier-onset vascular aging in men [56], driven by sex-specific vascular risk factor profiles [57]. In DS, the absence of sex differences in PSMD aligns with studies for AD biomarkers [58] and for vascular lesions [38,39,44].

*APOE*ε4 was associated with higher PSMD in the whole euploid population. However, this effect appeared to be driven by sample composition differences and *APOE*ε4 carriers proportion across CU and sAD cohorts, not reaching significance when stratifying by clinical status. Evidence for *APOE*ε4 effects on WM microstructure remains mixed [50,60–62], although a large-scale UK Biobank study has demonstrated that *APOE*ε4 carriers, particularly ε4 homozygotes, exhibit lower WM integrity and steeper age-related decline [63]. In DS, *APOE*ε4 did not significantly impact PSMD, consistent with previous investigations that, despite showing an influence of *APOE*ε4 on AD biomarkers [64], have not found a significant effect on SVD markers in DS [38,39,42,44].

Across the AD clinical continuum, PSMD was higher in symptomatic compared to asymptomatic stages in both euploid and DS populations, and was associated with lower global cognitive scores. In autosomal dominant AD, PSMD rises years before expected symptom onset, suggesting the sensitivity to capture preclinical WM changes [65]. However, once symptoms emerged, even though PSMD trended higher from prodromal to dementia stage, this difference was not significant in either sAD or DS. Prior work consistently showed that PSMD is higher in AD than in CU, with MCI typically intermediate, but differences between MCI and AD dementia stages do not reach significance [25,26,66,67]. In DS, DTI studies showed lower integrity compared with euploid controls [18,19,23], with more pronounced abnormalities in dDS [22]. Interestingly, within-clinical stage comparisons between euploid and DS (aDS vs. CU, pDS vs. MCI, dDS vs. AD dementia) did not reveal significant differences, aligning with a recent review showing the overlap of PSMD ranges across neurological conditions [32]. These results highlight that WM integrity is altered early in the AD clinical course, and that PSMD is sensitive to diffuse WM injury rather than disease stage.

Univariate models showed an unexpected negative association between PSMD and CSF pTau181 in the sAD, possibly reflecting the non-linear trajectory of CSF pTau181 across the AD continuum: as neurodegeneration advances, progressive loss of neuronal substrate can reduce pTau181 release into the CSF [68] even as WM damage accumulates. CSF NfL was the only fluid biomarker consistently related to PSMD across cohorts and AD stages, and one of the most robust biomarkers in elastic net regressions, although the

models explained minimal variance in sAD (R^2=0.03) and aDS (R^2=0.02). A previous study similarly reported a link between PSMD and plasma NfL in an MCI cohort [66]. In DS, DTI metrics have also been associated with plasma NfL [69]. Because WM mainly consists of myelinated axons and NfL is released upon axonal damage [70], this tight association was expected, and supports PSMD as a marker of WM injury [32].

Finally, we found robust associations between PSMD and SVD burden in both euploid and DS populations. Participants with microbleeds exhibited higher PSMD, and PSMD strongly correlated with WMH, aligning with prior DTI studies [71] and further supporting that, within the AD continuum, PSMD captures SVD-related microstructural injury alongside neurodegenerative change. The mechanisms underlying WM pathology in AD remain incompletely understood. Part of the injury may be secondary to cortical GM pathology via Wallerian degeneration [72], while additional damage likely arises through vascular disease [73] and impaired myelination [11]. Indeed, CAA is common in AD [74] and DS [5,6], and vascular Aβ accumulation can compromise microvascular integrity and perfusion, promoting the disruption of the WM tracts [75]. Additionally, individuals with DS show neurodevelopmental myelination deficits [76], which may influence WM integrity and potentially interact with AD-related demyelination processes, amplifying WM vulnerability in DS [23]. In further analysis, we found that in DS, but not in the euploid population, the proportion of individuals with abnormal PSMD and normal WMH exceeded the reverse. This asymmetry is consistent with a model in which diffuse microstructural WM damage precedes the emergence of focal macroscopic lesions (WMH) [77]. However, cross-sectional data cannot establish temporal ordering, and the asymmetry could alternatively reflect greater sensitivity of PSMD to early-stage WM pathology. Longitudinal studies are therefore needed to confirm whether PSMD positivity predicts subsequent WMH accrual.

This pattern was exclusively observed in DS. Notably, the DS population exhibits a markedly lower prevalence of traditional vascular risk factors, such as hypertension and dyslipidemia, and has an increased risk of severe CAA compared with controls and sAD, whereas age-related arteriolosclerosis is more common in the euploid population [5]. It is therefore possible that PSMD is more sensitive to CAA-related microstructural disruption than to other SVD forms [27,28]. Alternatively, the higher prevalence of vascular risk factors, alongside the broader comorbidity and copathology burden typical of the aging population likely introduces heterogeneous mechanisms of WM injury that obscure a clear temporal sequence between microstructural and macrostructural changes. Thus, DS may provide a more "pure" model in which early vascular-related WM alterations, potentially driven by CAA, can be detected more cleanly through PSMD.

The strengths of our study are twofold: i) the first application of PSMD in one of the largest multimodal cohorts of DS, and ii) integrated characterization that combines demographics, CSF AD-related, and SVD imaging markers in both sAD and DS along the AD continuum. This study also has some limitations. First, even though different diffusion MRI protocols were used, we applied ComBat harmonization to mitigate scanner effects. Sensitivity analyses, including restriction to a single protocol, confirmed that our findings are independent of acquisition-related biases (data not shown). Second, the unbalanced proportion of *APOE*ε4 carriers prevented us from stratifying by homozygotes to evaluate potential gene-dosage effects on WM integrity. Third, our sAD group did not include individuals in the preclinical stage of AD, which constrains the characterization of the full disease spectrum, since only symptomatic participants with established amyloid-β pathology were included. Finally, the cross-sectional design does not allow causal inferences regarding the relationships among AD pathology, SVD burden, and PSMD. Future longitudinal studies are therefore needed to clarify temporal ordering and quantify the respective contributions of AD and SVD pathology to WM integrity in both DS and sAD.

In summary, our results demonstrate that PSMD is a sensitive marker of WM injury in both sporadic and genetic forms of AD. In DS, PSMD alterations emerge approximately 15 years before expected symptom onset and are frequently observed in the absence of WMH, consistent with temporal precedence of microstructural changes, greater sensitivity of PSMD to underlying

pathology, or both. Its strong association with NfL and SVD burden underscores the multifactorial involvement in WM damage and the need for multimodal tools to disentangle the interplay between vascular and AD processes.

REFERENCES

[1] Ballard C, Mobley W, Hardy J, Williams G, Corbett A. Dementia in Down's syndrome. Lancet Neurol 2016;15:622–36. https://doi.org/10.1016/S1474-4422(16)00063-6.

[2] Fortea J, Zaman SH, Hartley S, Rafii MS, Head E, Carmona-Iragui M. Alzheimer's disease associated with Down syndrome: a genetic form of dementia. Lancet Neurol 2021;20:930–42. https://doi.org/10.1016/S1474-4422(21)00245-3.

[3] Lott IT, Head E. Dementia in Down syndrome: unique insights for Alzheimer disease research. Nat Rev Neurol 2019 153 2019;15:135–47. https://doi.org/10.1038/s41582-018-0132-6.

[4] Fortea J, Vilaplana E, Carmona-Iragui M, Benejam B, Videla L, Barroeta I, et al. Clinical and biomarker changes of Alzheimer's disease in adults with Down syndrome: a cross-sectional study. Lancet 2020;395:1988–97. https://doi.org/10.1016/S0140-6736(20)30689-9.

[5] Head E, Phelan MJ, Doran E, Kim RC, Poon WW, Schmitt FA, et al. Cerebrovascular pathology in Down syndrome and Alzheimer disease. Acta Neuropathol Commun 2017;5:93. https://doi.org/10.1186/S40478-017-0499-4,.

[6] Carmona-Iragui M, Balasa M, Benejam B, Alcolea D, Fernández S, Videla L, et al. Cerebral amyloid angiopathy in Down syndrome and sporadic and autosomal-dominant Alzheimer's disease. Alzheimer's Dement 2017;13:1251–60. https://doi.org/10.1016/J.JALZ.2017.03.007.

[7] Mayo CD, Garcia-Barrera MA, Mazerolle EL, Ritchie LJ, Fisk JD, Gawryluk JR. Relationship Between DTI Metrics and Cognitive Function in Alzheimer's Disease. Front Aging Neurosci 2019;10. https://doi.org/10.3389/FNAGI.2018.00436.

[8] Mayo CD, Mazerolle EL, Ritchie L, Fisk JD, Gawryluk JR. Longitudinal changes in microstructural white matter metrics in Alzheimer's disease. NeuroImage Clin 2017;13:330–8. https://doi.org/10.1016/j.nicl.2016.12.012.

[9] Brun A, Englund E. A white matter disorder in dementia of the Alzheimer type: a pathoanatomical study. Ann Neurol 1986;19:253–62. https://doi.org/10.1002/ANA.410190306.

[10] Weller RO, Boche D, Nicoll JAR. Microvasculature changes and cerebral amyloid angiopathy in Alzheimer's disease and their potential impact on therapy. Acta Neuropathol 2009;118:87–102. https://doi.org/10.1007/S00401-009-0498-Z.

[11] Nasrabady SE, Rizvi B, Goldman JE, Brickman AM. White matter changes in Alzheimer's disease: a focus on myelin and oligodendrocytes. Acta Neuropathol Commun 2018;6:22. https://doi.org/10.1186/S40478-018-0515-3.

[12] Alexander AL, Lee JE, Lazar M, Field AS. Diffusion Tensor Imaging of the Brain. Neurotherapeutics 2007;4:316–29. https://doi.org/10.1016/j.nurt.2007.05.011.

[13] Terence CC, Wen W, Slavin MJ, Sachdev PS. Diffusion tensor imaging in mild cognitive impairment and Alzheimer's disease: a review. Curr Opin Neurol 2008;21:83–92. https://doi.org/10.1097/WCO.0B013E3282F4594B.

[14] Bennett IJ, Madden DJ. Disconnected aging: Cerebral white matter integrity and age-related differences in cognition. Neuroscience 2014;276:187–205. https://doi.org/10.1016/j.neuroscience.2013.11.026.

[15] de Lange AMG, Bråthen ACS, Grydeland H, Sexton C, Johansen-Berg H, Andersson JLR, et al. White-matter integrity as a marker for cognitive plasticity in aging. Neurobiol Aging 2016;47:74–82. https://doi.org/10.1016/j.neurobiolaging.2016.07.007.

[16] Madden DJ, Bennett IJ, Song AW. Cerebral white matter integrity and cognitive aging: contributions from diffusion tensor imaging. Neuropsychol Rev 2009;19:415–35. https://doi.org/10.1007/S11065-009-9113-2.

[17] Madden DJ, Bennett IJ, Burzynska A, Potter GG, Chen N kuei, Song AW. Diffusion tensor imaging of cerebral white matter integrity in cognitive aging. Biochim Biophys Acta - Mol Basis Dis 2012;1822:386–400. https://doi.org/10.1016/j.bbadis.2011.08.003.

[18] Romano A, Moraschi M, Cornia R, Bozzao A, Rossi-Espagnet MC, Giove F, et al. White matter involvement in young non-demented Down's syndrome subjects: a tract-based spatial statistic analysis. Neuroradiology 2018;60:1335–41. https://doi.org/10.1007/S00234-018-2102-5.

[19] Fenoll R, Pujol J, Esteba-Castillo S, De Sola S, Ribas-Vidal N, García-Alba J, et al. Anomalous White Matter Structure and the Effect of Age in Down Syndrome Patients. J Alzheimers Dis 2017;57:61–70. https://doi.org/10.3233/JAD-161112.

[20] Lee NR, Nayak A, Irfanoglu MO, Sadeghi N, Stoodley CJ, Adeyemi E, et al. Hypoplasia of cerebellar afferent networks in Down syndrome revealed by DTI-driven tensor based morphometry. Sci Rep 2020;10. https://doi.org/10.1038/S41598-020-61799-1.

[21] Saini F, Dell'Acqua F, Strydom A. Structural Connectivity in Down Syndrome and Alzheimer's Disease. Front Neurosci 2022;16. https://doi.org/10.3389/FNINS.2022.908413.

[22] Powell D, Caban-Holt A, Jicha G, Robertson W, Davis R, Gold BT, et al. Frontal white matter integrity in adults with Down syndrome with and without dementia. Neurobiol Aging 2014;35:1562–9. https://doi.org/10.1016/j.neurobiolaging.2014.01.137.

[23] Rosas HD, Hsu E, Mercaldo ND, Lai F, Pulsifer M, Keator D, et al. Alzheimer-related altered white matter microstructural integrity in Down syndrome: A model for sporadic AD? Alzheimer's Dement (Amsterdam, Netherlands) 2020;12. https://doi.org/10.1002/DAD2.12040.

[24] Bazydlo AM, Zammit MD, Wu M, Lao PJ, Dean DC, Johnson SC, et al. White matter microstructure associations to amyloid burden in adults with Down syndrome. NeuroImage Clin 2022;33. https://doi.org/10.1016/j.nicl.2021.102908.

[25] Baykara E, Gesierich B, Adam R, Tuladhar AM, Biesbroek JM, Koek HL, et al. A Novel Imaging Marker for Small Vessel Disease Based on Skeletonization of White Matter Tracts and Diffusion Histograms. Ann Neurol 2016;80:581–92. https://doi.org/10.1002/ANA.24758.

[26] McCreary CR, Beaudin AE, Subotic A, Zwiers AM, Alvarez A, Charlton A, et al. Cross-sectional and longitudinal differences in peak skeletonized white matter mean diffusivity in cerebral amyloid angiopathy. NeuroImage Clin 2020;27. https://doi.org/10.1016/j.nicl.2020.102280.

[27] Zanon Zotin MC, Schoemaker D, Raposo N, Perosa V, Bretzner M, Sveikata L, et al. Peak width of skeletonized mean diffusivity in cerebral amyloid angiopathy: Spatial signature, cognitive, and neuroimaging associations. Front Neurosci 2022;16. https://doi.org/10.3389/FNINS.2022.1051038/PDF.

[28] Raposo N, Zanon Zotin MC, Schoemaker D, Xiong L, Fotiadis P, Charidimou A, et al. Peak Width of Skeletonized Mean Diffusivity as Neuroimaging Biomarker in Cerebral Amyloid Angiopathy. AJNR Am J Neuroradiol 2021;42:875–81. https://doi.org/10.3174/AJNR.A7042.

[29] Chen CH, Khnaijer MK, Beaudin AE, McCreary CR, Gee M, Saad F, et al. Subcortical volumes in cerebral amyloid angiopathy compared with Alzheimer's disease and controls. Front Neurosci 2023;17. https://doi.org/10.3389/FNINS.2023.1139196.

[30] Horn MJ, Gokcal E, Becker JA, Das AS, Schwab K, Zanon Zotin MC, et al. Peak width of skeletonized mean diffusivity and cognitive performance in cerebral amyloid angiopathy. Front Neurosci 2023;17. https://doi.org/10.3389/FNINS.2023.1141007.

[31] Luckey AM, Ghosh S, Wang CP, Beiser A, Bernal R, Li Z, et al. Biological validation of peak-width of skeletonized mean diffusivity as a VCID biomarker: The MarkVCID Consortium. Alzheimers Dement 2024;20:8814–24. https://doi.org/10.1002/ALZ.14345.

[32] Zotin MCZ, Yilmaz P, Sveikata L, Schoemaker D, van Veluw SJ, Etherton MR, et al. Peak Width of Skeletonized Mean Diffusivity: A Neuroimaging Marker for White Matter Injury. Radiology 2023;306. https://doi.org/10.1148/RADIOL.212780.

[33] Beaudet G, Tsuchida A, Petit L, Tzourio C, Caspers S, Schreiber J, et al. Age-Related Changes of Peak Width Skeletonized Mean Diffusivity (PSMD) Across the Adult Lifespan: A Multi-Cohort Study. Front Psychiatry 2020;11. https://doi.org/10.3389/FPSYT.2020.00342.

[34] Hu HY, Li HQ, Gong WK, Huang SY, Fu Y, Hu H, et al. Microstructural white matter injury contributes to cognitive decline: Besides amyloid and tau. J Prev Alzheimer's Dis 2025;12:100037. https://doi.org/10.1016/j.tjpad.2024.100037.

[35] Luo X, Hong H, Li K, Zeng Q, Wang S, Li Z, et al. Distinct cerebral small vessel disease impairment in early- and late-onset Alzheimer's disease. Ann Clin Transl Neurol 2023;10:1326–37. https://doi.org/10.1002/ACN3.51824.

[36] Videla L, Benejam B, Barroeta I, Fernandez S, Altuna M, Arranz J, et al. The Down Alzheimer Barcelona Neuroimaging Initiative (DABNI) and its contributions to understanding Alzheimer's disease in Down syndrome: A decade of discovery. Alzheimer's Dement 2025;21. https://doi.org/10.1002/ALZ.70259,.

[37] Alcolea D, Clarimón J, Carmona-Iragui M, Illán-Gala I, Morenas-Rodríguez E, Barroeta I, et al. The Sant Pau Initiative on Neurodegeneration (SPIN) cohort: A data set for biomarker discovery and validation in neurodegenerative disorders. Alzheimer's Dement Transl Res Clin Interv 2019;5:597–609. https://doi.org/10.1016/J.TRCI.2019.09.005.

[38] Morcillo-Nieto AO, Zsadanyi SE, Arriola-Infante JE, Carmona-Iragui M, Montal V, Pegueroles J, et al. Characterization of white matter hyperintensities in Down syndrome. Alzheimers Dement 2024. https://doi.org/10.1002/ALZ.14146.

[39] Zsadanyi SE, Morcillo-Nieto AO, Aranha MR, Aragón I, Arriola-Infante JE, Vaqué-Alcázar L, et al. Associations of Microbleeds and Their Topography With Imaging and CSF Biomarkers of Alzheimer Pathology in Individuals With Down Syndrome. Neurology 2024;103:e209676. https://doi.org/10.1212/WNL.0000000000209676.

[40] Josephs KA, Murray ME, Whitwell JL, Tosakulwong N, Weigand SD, Petrucelli L, et al. Updated TDP-43 in Alzheimer's disease staging scheme. Acta Neuropathol 2016;131:571. https://doi.org/10.1007/S00401-016-1537-1.

[41] Iulita MF, Garzón Chavez D, Klitgaard Christensen M, Valle Tamayo N, Plana-Ripoll O, Rasmussen SA, et al. Association of Alzheimer Disease With Life Expectancy in People With Down Syndrome. JAMA Netw Open 2022;5:e2212910–e2212910. https://doi.org/10.1001/JAMANETWORKOPEN.2022.12910.

[42] Lao PJ, Gutierrez J, Keator D, Rizvi B, Banerjee A, Igwe KC, et al. Alzheimer-Related Cerebrovascular Disease in Down Syndrome. Ann Neurol 2020;88:1165–77. https://doi.org/10.1002/ANA.25905.

[43] Lao P, Edwards N, Flores-Aguilar L, Alshikho M, Rizvi B, Tudorascu D, et al. Cerebrovascular disease emerges with age and Alzheimer's disease in adults with Down syndrome. Sci Rep 2024;14. https://doi.org/10.1038/S41598-024-61962-Y,.

[44] Aranha MR, Montal V, van den Brink H, Pegueroles J, Carmona-Iragui M, Videla L, et al. Cortical microinfarcts in adults with Down syndrome assessed with 3T-MRI. Alzheimers Dement 2024;20. https://doi.org/10.1002/ALZ.13797.

[45] Lawrence KE, Nabulsi L, Santhalingam V, Abaryan Z, Villalon-Reina JE, Nir TM, et al. Age and sex effects on advanced white matter microstructure measures in 15,628 older adults: A UK biobank study. Brain Imaging Behav 2021;15:2813–23. https://doi.org/10.1007/S11682-021-00548-Y.

[46] Boban J, Thurnher MM, Boban N, Law M, Jahanshad N, Nir TM, et al. Gradient Patterns of Age-Related Diffusivity Changes in Cerebral White Matter. Front Neurol 2022;13. https://doi.org/10.3389/FNEUR.2022.870909.

[47] Burzynska AZ, Preuschhof C, Bäckman L, Nyberg L, Li SC, Lindenberger U, et al. Age-related differences in white matter microstructure: Region-specific patterns of diffusivity. Neuroimage 2010;49:2104–12. https://doi.org/10.1016/j.neuroimage.2009.09.041.

[48] Nusbaum AO, Tang CY, Buchsbaum MS, Tsei Chung Wei, Atlas SW. Regional and Global Changes in Cerebral Diffusion with Normal Aging. AJNR Am J Neuroradiol 2001;22:136.

[49] Saini F, Ivain P, Idris M, Wells J, Bianchi L, Tamayo-Elizalde M, et al. White matter trajectories in Down syndrome and Alzheimer's disease: Insights from diffusion tensor-based morphometry. Alzheimers Dement 2025;21. https://doi.org/10.1002/ALZ.70382.

[50] Peterson A, Sathe A, Zaras D, Yang Y, Durant A, Deters KD, et al. Sex and APOE ϵ4 allele differences in longitudinal white matter microstructure in multiple cohorts of aging and Alzheimer's disease. Alzheimers Dement 2025;21. https://doi.org/10.1002/ALZ.14343.

[51] Cox SR, Ritchie SJ, Tucker-Drob EM, Liewald DC, Hagenaars SP, Davies G, et al. Ageing and brain white matter structure in 3,513 UK Biobank participants. Nat Commun 2016;7. https://doi.org/10.1038/NCOMMS13629.

[52] Isaac Tseng WY, Hsu YC, Chen C Le, Kang YJ, Kao TW, Chen PY, et al. Microstructural differences in white matter tracts across middle to late adulthood: a diffusion MRI study on 7167 UK Biobank participants. Neurobiol Aging 2021;98:160–72. https://doi.org/10.1016/j.neurobiolaging.2020.10.006.

[53] Bergamino M, Keeling EG, Baxter LC, Sisco NJ, Walsh RR, Stokes AM. Sex Differences in Alzheimer's Disease Revealed by Free-Water Diffusion Tensor Imaging and Voxel-Based Morphometry. J Alzheimers Dis 2022;85:395–414. https://doi.org/10.3233/JAD-210406.

[54] Chou KH, Cheng Y, Chen IY, Lin CP, Chu WC. Sex-linked white matter microstructure of the social and analytic brain. Neuroimage 2011;54:725–33. https://doi.org/10.1016/j.neuroimage.2010.07.010.

[55] Inano S, Takao H, Hayashi N, Abe O, Ohtomo K. Effects of age and gender on white matter integrity. AJNR Am J Neuroradiol 2011;32:2103–9. https://doi.org/10.3174/AJNR.A2785.

[56] Merz AA, Cheng S. Sex differences in cardiovascular ageing. Heart 2016;102:825–31. https://doi.org/10.1136/HEARTJNL-2015-308769.

[57] Merz CNB, Ramineni T, Leong D. Sex-specific risk factors for cardiovascular disease in women-making cardiovascular disease real. Curr Opin Cardiol 2018;33:500–5. https://doi.org/10.1097/HCO.0000000000000543.

[58] Del Hoyo Soriano L, Wagemann O, Bejanin A, Levin J, Fortea J. Sex-related differences in genetically determined Alzheimer's disease. Front Aging Neurosci 2025;17. https://doi.org/10.3389/FNAGI.2025.1522434,.

[59] Reinvang I, Espeseth T, Westlye LT. APOE-related biomarker profiles in non-pathological aging and early phases of Alzheimer's disease. Neurosci Biobehav Rev 2013;37:1322–35. https://doi.org/10.1016/j.neubiorev.2013.05.006.

[60] Goltermann J, Repple J, Redlich R, Dohm K, Flint C, Grotegerd D, et al. Apolipoprotein E homozygous ϵ4 allele status: Effects on cortical structure and white matter integrity in a young to mid-age sample. Eur Neuropsychopharmacol 2021;46:93–104. https://doi.org/10.1016/j.euroneuro.2021.02.006.

[61] Srisaikaew P, Chad JA, Mahakkanukrauh P, Anderson ND, Chen JJ. Effect of sex on the APOE4-aging interaction in the white matter microstructure of cognitively normal older adults using diffusion-tensor MRI with orthogonal-tensor decomposition (DT-DOME). Front Neurosci 2023;17:1049609. https://doi.org/10.3389/FNINS.2023.1049609/FULL.

[62] Adluru N, Destiche DJ, Lu SYF, Doran ST, Birdsill AC, Melah KE, et al. White matter microstructure in late middle-age: Effects of

apolipoprotein E4 and parental family history of Alzheimer's disease. NeuroImage Clin 2014;4:730–42. https://doi.org/10.1016/j.nicl.2014.04.008.
[63] Heise V, Offer A, Whiteley W, Mackay CE, Armitage JM, Parish S. A comprehensive analysis of APOE genotype effects on human brain structure in the UK Biobank. Transl Psychiatry 2024;14. https://doi.org/10.1038/S41398-024-02848-5.
[64] Bejanin A, Iulita MF, Vilaplana E, Carmona-Iragui M, Benejam B, Videla L, et al. Association of Apolipoprotein E ε4 Allele With Clinical and Multimodal Biomarker Changes of Alzheimer Disease in Adults With Down Syndrome. JAMA Neurol 2021;78:937–47. https://doi.org/10.1001/JAMANEUROL.2021.1893.
[65] Araque Caballero MA, Suárez-Calvet M, Duering M, Franzmeier N, Benzinger T, Fagan AM, et al. White matter diffusion alterations precede symptom onset in autosomal dominant Alzheimer's disease. Brain 2018;141:3065–80. https://doi.org/10.1093/brain/awy243.
[66] Cui RP, Hu HY, Han SL, Liang SY, Liu M, Gao PY, et al. Association of Peak Width of Skeletonized Mean Diffusivity With Neurofilament Light Chain in Non-Dementia Adults. J Neurochem 2025;169. https://doi.org/10.1111/JNC.70076.
[67] Hu Q, Zhou X, Xiao Z, Zhao Q, Ding D, Zhang J. White matter injury, plasma Alzheimer's disease, and neurodegenerative biomarkers on cognitive decline in community-dwelling older adults: A 10-year longitudinal study. Alzheimers Dement 2025;21. https://doi.org/10.1002/ALZ.14594.
[68] Lleó A, Alcolea D, Martínez-Lage P, Scheltens P, Parnetti L, Poirier J, et al. Longitudinal cerebrospinal fluid biomarker trajectories along the Alzheimer's disease continuum in the BIOMARKAPD study. Alzheimers Dement 2019;15:742–53. https://doi.org/10.1016/j.jalz.2019.01.015.
[69] Rosas HD, Mercaldo ND, Hasimoglu Y, Petersen M, Lewis LR, Lai F, et al. Association of plasma neurofilament light chain with microstructural white matter changes in Down syndrome. Alzheimer's Dement (Amsterdam, Netherlands) 2024;16. https://doi.org/10.1002/DAD2.70023.
[70] Gaetani L, Blennow K, Calabresi P, Di Filippo M, Parnetti L, Zetterberg H. Neurofilament light chain as a biomarker in neurological disorders. J Neurol Neurosurg Psychiatry 2019;90:870–81. https://doi.org/10.1136/JNNP-2018-320106.
[71] Maniega SM, Valdés Hernández MC, Clayden JD, Royle NA, Murray C, Morris Z, et al. White matter hyperintensities and normal-appearing white matter integrity in the aging brain. Neurobiol Aging 2015;36:909–18.
https://doi.org/10.1016/j.neurobiolaging.2014.07.048.
[72] Salvadores N, Gerónimo-Olvera C, Court FA. Axonal Degeneration in AD: The Contribution of Aβ and Tau. Front Aging Neurosci 2020;12:581767. https://doi.org/10.3389/FNAGI.2020.581767/BIBTEX.
[73] ter Telgte A, van Leijsen EMC, Wiegertjes K, Klijn CJM, Tuladhar AM, de Leeuw F-E. Cerebral small vessel disease: from a focal to a global perspective. Nat Rev Neurol 2018 147 2018;14:387–98. https://doi.org/10.1038/s41582-018-0014-y.
[74] Brenowitz WD, Nelson PT, Besser LM, Heller KB, Kukull WA. Cerebral amyloid angiopathy and its co-occurrence with Alzheimer's disease and other cerebrovascular neuropathologic changes. Neurobiol Aging 2015;36:2702–8. https://doi.org/10.1016/j.neurobiolaging.2015.06.028.
[75] Sachdev PS, Zhuang L, Braidy N, Wen W. Is Alzheimer's a disease of the white matter? Curr Opin Psychiatry 2013;26:244–51. https://doi.org/10.1097/YCO.0B013E32835ED6E8.

[76] Bartzokis G, Sultzer D, Lu PH, Nuechterlein KH, Mintz J, Cummings JL. Heterogeneous age-related breakdown of white matter structural integrity: Implications for cortical "disconnection" in aging and Alzheimer's disease. Neurobiol Aging 2004;25:843–51. https://doi.org/10.1016/j.neurobiolaging.2003.09.005.
[77] Van Leijsen EMC, Bergkamp MI, Van Uden IWM, Ghafoorian M, Van Der Holst HM, Norris DG, et al. Progression of White Matter Hyperintensities Preceded by Heterogeneous Decline of Microstructural Integrity. Stroke 2018;49:1386–93. https://doi.org/10.1161/STROKEAHA.118.020980.

5. DISCUSSION

5.1 OVERVIEW

The present thesis provides a comprehensive neuroimaging investigation by mapping both the MTL atrophy and the WM changes across the AD continuum to unravel the trajectories of neurodegeneration and SVD in individuals with DSAD.

First, Study 1 characterized the topographical and temporal sequence of atrophy in MTL subregions. We found a non-linear pattern of atrophy across EYO, including an initial phase of cortical thickening followed by progressive decline. Crucially, the ERC and posterior hippocampus were identified as the earliest regions of structural loss, exhibiting detectable changes up to 15 years prior to symptom onset. Furthermore, we validated the posterior hippocampal volume as a highly robust biomarker, comparable to the performance of core CSF AD biomarkers in detecting symptomatic AD in DS.

In parallel, Study 2 and Study 3 provided a deep examination of WMH. Cross-sectionally, we reported that WMH severity increases with advancing age, AD pathology, and clinical staging in DS. These lesions initially predominate in a periventricular topography and subsequently expand into more cortical layers as AD advances. Surprisingly, our longitudinal evaluation yielded an unexpected finding: rather than following a strict monotonic accumulation, 2.5-years changes in WMH are remarkably heterogeneous in DS. Specifically, in symptomatic stages, we observed a paradoxical shrinkage of WMH over time, which was strongly associated with baseline lesion volume and the presence of cerebral microbleeds. This dynamic volumetric fluctuation likely reflects distinct underlying processes in DSAD, such as resolving neuroinflammation or progressive tissue degeneration.

Finally, Study 4 presented the first integrated evaluation of the PSMD across both DSAD and sAD. We demonstrated that diffuse WM injury occurs up to 15 prior to symptom onset in DS. The strong correlations between PSMD, fluid biomarkers of neurodegeneration, and SVD imaging markers confirmed that early WM damage represents a mixed pathophysiology driven by both SVD- and AD-related processes.

Taken together, these four studies highlight the utility of MRI to capture structural and microstructural brain changes in DS before the clinical emergence of AD. The following sections will integrate these findings into a coherent discussion, addressing: (i) GM and WM changes as early, core features of DSAD; (ii) the apparent lack of effect of disease-modifying factors on WM markers in DSAD; (iii) the convergent mechanisms that drive both GM and WM injury; and (iv) a hypothetical biomarker model that situates our MRI findings within the broader established biomarker framework for DSAD. We conclude by outlining the key limitations of the present work and proposing future lines of investigation to advance the characterisation of neurodegeneration and SVD in DS.

5.2 GREY AND WHITE MATTER CHANGES AS AN EARLY CORE FEATURE IN DSAD

5.2.1 Medial temporal lobe atrophy

Global GM atrophy is a well-established MRI finding in the DS population, characterized by pronounced MTL involvement and a posterior-predominant pattern of cortical thinning.[17,111] Among MTL structures, the hippocampus has been the most extensively characterized, given its central role in memory[198] and its early vulnerability to tau pathology.[199] Hippocampal volume loss has been

reported 5 to 10 years prior to symptom onset[83] and this window has recently been extended to nearly 18 years before clinical manifestation.[200] In this thesis, we expand the characterization of MTL neurodegeneration beyond the hippocampus, assessing both its anterior and posterior subregions, by additionally examining atrophy in the ERC, PHC, and perirhinal cortex (Br35 and Br36). Our findings demonstrate that, in DS, the loss of MTL integrity begins before the emergence of clinical symptoms and progresses across all MTL regions with advancing clinical stages of AD. Specifically, individuals with AD dementia exhibited significantly lower volumes and cortical thickness across MTL subregions compared with both prodromal and asymptomatic adults with DS, whereas the prodromal group displayed an intermediate atrophy profile, with significant differences from aDS observed exclusively in the posterior hippocampus. Moreover, among all MTL subregions examined, the posterior hippocampus showed the strongest discriminative ability between asymptomatic and symptomatic stages, performing comparably to established CSF biomarkers (Aβ42/Aβ40 ratio, pTau181, and NfL). Importantly, the posterior hippocampus was retained in multivariate predictive models incorporating both individual MTL regions and core CSF biomarkers, underscoring its independent and complementary diagnostic value. Collectively, these findings support the hippocampus, and particularly its posterior region, as a highly sensitive structural marker of early AD-related neurodegeneration in DS.

5.2.2 White matter damage

In individuals with DS, WM damage is detectable by MRI years before symptoms onset and increase across the AD clinical continuum. By combining FLAIR-based WMH quantification with diffusion-based PSMD, this work provides a dual-resolution characterization of WM injury that spans from diffuse microstructural compromise to focal macroscopic lesion formation. Taken together, these

findings reframe WM damage not as a late consequence of neurodegeneration, nor as an incidental vascular comorbidity, but as a core pathological hallmark of DSAD that parallels the core AD pathologies and may both result from and interact with them.

Both WMH burden and PSMD demonstrated robust associations with age in adults with DS, following trajectories that markedly exceeded the age-related changes observed in euploid controls. WM injury expanded from the late 30s through the mid-40s, with PSMD abnormalities becoming identifiable approximately 15 years before symptom onset and WMH emerging somewhat later, around 10 years before symptom onset. These temporal dynamics are consistent with DS studies reporting increased WMH from the fourth decade onward[166] and with microstructural evidence of early diffusion abnormalities in DS adults.[118,122] Both MRI modalities further revealed a consistent, stepwise elevation across the clinical stages of DSAD, confirming that WM injury is not only an early event but also a progressive pathological process that escalates in parallel with the clinical trajectory of the disease.

The temporal delay between the two markers indicates that diffusion-based metrics and macroscopic lesion quantification may not capture identical aspects of WM pathology, and that PSMD is sensitive to an earlier phase of injury. Consistent with this interpretation, adults with DS exhibiting abnormal PSMD values together with low WMH burden were substantially more frequent than those showing the opposite pattern. This dissociation indicates that a greater proportion of adults with DS harbor diffuse WM microstructural compromise that has not yet manifested into the focal, macroscopically visible lesions detected on FLAIR. Such a sequence is in line with evidence from the general population, where diffusion abnormalities in the normal-appearing WM precede and predict the subsequent emergence of WMH,[201–203] representing a "penumbral" tissue at

high risk of converting into overt hyperintensities over time.[204,205] The asymmetry observed in DS thus strongly supports a pathogenic model in which diffuse microstructural WM damage precedes the emergence of macroscopic focal lesions, [206] and positions PSMD as a biomarker capable of capturing a pre-lesional, and potentially reversible, stage of WM injury. A complementary explanation for this temporal asymmetry relates to the intrinsic nature of each metric. PSMD is a global, whole-brain summary of WM microstructural integrity derived from the histogram of skeletonized MD. In contrast, WMH quantification inherently preserves spatial information, which is obscured when reduced to a single global volume, potentially diluting early, regionally restricted changes. The two markers should therefore be regarded as complementary: PSMD offers superior sensitivity to early, diffuse microstructural injury, whereas regional WMH mapping provides spatial signatures informative of the underlying pathophysiology.

Overall, situating these findings within the broader landscape of SVD in DS further reinforces the notion of WM injury as an early core feature. A recent chronological model of SVD lesion emergence in DS proposed a sequential pattern starting in the early 30s with ePVS, followed by WMH, cerebral MB, and ultimately infarcts.[166] The results from this thesis extend this framework by positioning diffusion-based microstructural injury as an even earlier event in the cascade, one that precedes the appearance of macroscopically visible SVD lesions and may constitute the earliest detectable signature of cerebrovascular compromise in DSAD.

5.3 DISEASE MODIFIERS OF WHITE MATTER INJURY IN DS

A consistent finding across the studies comprising this thesis is the limited influence of two traditional disease modifiers, sex and *APOE* ε4 genotype, on

WM injury in DS. Neither WMH burden nor PSMD was significantly affected by these factors. These results align with a growing body of evidence in DS reporting subtle effects of sex and *APOE* ε4 across AD-related biomarkers, and stand in sharp contrast to the well-established modifying roles of these factors in sAD.

5.3.1 The absence of a sex effect

In the general population, female sex is associated with a higher lifetime risk of AD and with distinct biomarker trajectories, including more rapid tau accumulation and hippocampal atrophy in symptomatic stages.[207,208] Women also show greater WMH accumulation in older age than men,[209,210] together with lower WM integrity and accelerated microstructural decline on classical DTI metrics.[211,212] Interestingly, PSMD follows the opposite pattern with lower values in women than in men,[213] a finding we also report in Study 4. This suggest PSMD may reflect partially distinct aspects of WM pathology compared with conventional DTI metrics.

Several mechanisms have been proposed to account for these disparities.[214] First, hormonal mechanisms, particularly the rapid decline in estrogen during menopause that may increase female vulnerability by impairing cerebral metabolism, promoting amyloid-β deposition, and exacerbating neuroinflammation.[215] Estrogen loss may also compromise endothelial function and blood-brain barrier integrity,[216] thereby promoting greater WM damage through perivascular leakage, neuroinflammation, and impaired clearance of interstitial solutes. Second, sex-specific differences in immune reactivity, including microglial activation and cytokine signaling, may modulate the trajectory of AD pathology and WM injury.[217] Third, men and women differ in the manifestation of cerebrovascular and cardiovascular pathologies,[207] with men

showing a higher prevalence of ischemic events such as myocardial infarction and stroke, while women more frequently developing hypertension and atrial fibrillation in later life,[214] exposures that differentially shape the topography and severity of WM injury. Finally, gender-related factors, encompassing differential lifetime exposure to education, occupational complexity, physical activity, smoking and alcohol use, traumatic brain injury, and chronic psychosocial stress, may interact with biological sex to further modulate both cerebrovascular burden and AD risk.[214]

In DS, neither WMH nor PSMD trajectories revealed significant sex-related differences. This parallels growing evidence that sex exerts a subtle or null effect on AD biomarker profiles and clinical trajectories in DS,[218] and extends to the wider spectrum of cerebral SVD showing no effect in DS, including cortical microinfarcts, MB, and ePVS.[161,163,166,219] Several interrelated factors may underlie this attenuation. First, the compressed pathological timeline of DSAD may leave little temporal window for sex-based modifiers to exert a detectable influence. Second, the intrinsic genetic load conferred by trisomy 21 may saturate the pathological cascade and obscure potential sex effects. Third, the hormonal landscape differs in DS, women with DS undergo early menopause, typically in their early-to-mid 40s,[220] substantially reducing the duration of estrogen-mediated neuroprotection relative to euploid women.[221] If the protective window conferred by estrogen is truncated, the sex-based divergence in WM injury that emerges post-menopausally in the general population may fail to develop. Fourth, the relatively low prevalence of hypertension and dyslipidemia in DS[149,150] reduces the pool of vascular risk factors that typically interact with sex to drive differential WM injury patterns. Finally, gender-related lifestyle exposures are substantially attenuated and more homogeneous in DS, with lower lifetime rates of smoking, alcohol use, and occupational diversity, and with

leisure, employment, and physical activity patterns more strongly shaped by caregiving environments than by individual gendered trajectories.[222]

This differential effect of sex on WM injury in DSAD versus sAD thus offers new insights into the distinct pathogenic mechanisms driving in genetically determined forms of AD, as well as into the conditions under which sex-related biological and gender-related environmental modifiers shape the cerebrovascular contribution to neurodegeneration. Nonetheless, the absence of a detectable main effect of sex does not preclude more subtle interactions with other biological modifiers. Notably, *APOE* ϵ4 has been shown to interact with sex in DS, with female ϵ4 carriers exhibiting an earlier age at AD diagnosis than non-carriers.[218]

5.3.2 The absence of an *APOE* ϵ4 Effect

The *APOE* ϵ4 allele is the strongest genetic risk factor for sAD[46,47] and exerts a robust influence on cerebrovascular pathology, particularly CAA.[223] However, its relationship with WM injury in the aging population and in sAD remains controversial, with some studies suggesting a gene-dose effect on WM damage,[224–228] whereas others reporting no significant effect.[229–231]

In DS, the *APOE* ϵ4 allele has been associated with an earlier age at symptom onset, earlier age at death, and modestly accelerated amyloid and tau accumulation.[62,232] Its impacts on WM injury, however, remains far less clear. Although higher regional WMH volumes in the temporal lobe have been reported in *APOE* ϵ4 carriers,[161] broader assessments of age-residualized WMH[166] and longitudinal annual WMH change[167] have yielded no significant genotype-related differences. Our findings align with this latter body of evidence, as neither WMH volume nor PSMD differed according to *APOE* ϵ4 across the DS lifespan. Several of the mechanisms discussed above in relation to sex, particularly the

compressed pathological timeline, the saturating effect of trisomy 21 and the cerebrovascular profile, may limit the expression of an *APOE* ϵ4 effect on WM lesions in DS.

Importantly, while *APOE* ϵ4 does not appear to drive ischemic WMH or microstructural damage in DS, it has been consistently linked to an increased prevalence of cerebral MB.[163,166] This divergence suggests that the most robust *APOE* ϵ4 vascular phenotype is haemorrhagic rather than diffuse ischemic and microstructural WM injury captures by WMH and PSMD.

5.4 CONVERGENCE BETWEEN WHITE MATTER AND GREY MATTER INJURY

The results across this thesis, encompassing MTL atrophy, and WM damage, converge on the notion that neurodegeneration and SVD in DS are not independent processes but rather the emergent outcome of a tightly interwoven set of mechanisms intrinsic to trisomy 21 (Figure 8). Throughout this section, we present distinct trisomy 21–intrinsic features that likely drive the GM and WM results observed in this thesis: (i) a broad cerebral Aβ amyloidosis spectrum, manifest as both parenchymal AD pathology and vascular deposition (CAA);[51,71,152] (ii) a lifelong, chronic inflammatory phenotype;[233–235] (iii) the emerging concept of an endogenous vascular component arising at least partly independently of amyloid;[236] and (iv) an accelerated brain aging trajectory[237,238].

The aetiology of WM damage in DS is multifactorial and may be driven by several overlapping mechanisms.[236,239] A first contributor is the Wallerian degeneration secondary to cortical tau pathology (Figure 8, Pathway 1 [P1]), whereby disruption of tau-stabilized microtubules triggers axonal degeneration in tracts projecting from affected cortical regions.[240–242] Consistent with this mechanism,

both WMH and PSMD were strongly associated with neurodegenerative markers, such as NfL and GM loss (Study 2 and 4). A second contributor is CAA itself (P2), which compromises microvascular integrity, inducing hypoperfusion, focal ischemia, and microhemorrhagic events that directly injure WM tracts.[127] Supporting this interpretation, we found that individuals harboring MB, a neuroradiological hallmark of CAA, presented with greater WM damage (Study 4).

The spatial topography of WMH offers additional insight into their aetiology. In DS, WMH predominate in the corona radiata (particularly its posterior portion), the posterior radiations, and the splenium, a distribution that closely mirrors the posterior-dominant pattern characteristic of sAD[243] and of CAA.[244] Although recent diagnostic criteria for CAA highlight a multispot WMH pattern,[245] this specific punctate presentation is rarely observed upon visual inspection in individuals with DS. Instead, WMH in the DS brain tend to emerge as confluent, diffuse lesions that extend outward toward the cortex as the disease progresses. This topographical overlap with both sAD and CAA suggests that WM lesions in DS may be driven by the broader cerebral Aβ amyloidosis spectrum rather than by any single pathological entity (P3).

These amyloid pathologies may themselves amplify WM injury by promoting neuroinflammatory responses.[246] Parenchymal Aβ deposition can exacerbate microglial and astrocytic activation (P4), while vascular Aβ accumulation compromises small-vessel endothelium, damages the blood-brain barrier, and further triggers neuroinflammation[247] (P5). In some cases, brain-blood barrier disruption increases permeability, allowing extravasation of interstitial fluid with vasogenic oedema; a mechanism consistent with CAA-related inflammation (CAA-ri).[248] Although this clinical manifestation is rarely observed in DS, cases have been reported, including in our cohort.[249,250]

Superimposed on this secondary inflammatory response, individuals with DS exhibit a unique inflammatory phenotype characterized by lifelong chronic inflammation.[233–235] This phenotype arises from the triplication of chromosome 21, which harbors several immune- and neuroinflammation-related genes, including interferon receptors, which drives enhanced interferon signaling and dysregulated immune cell function.[251,252] Consistent with this genetic predisposition, proteomic studies have demonstrated elevated pro- and anti-inflammatory cytokines in both plasma and brain tissue across the lifespan in DS.[234,246] In parallel, associated microglial activation reaches a dramatic peak in early adulthood[246] and likely interacts with AD and CAA pathologies (P6) to exacerbate the downstream WM damage (P7). Although the exact inflammatory source remains undetermined, inflammatory fluid biomarkers (GFAP and YKL-40) correlated strongly with both WMH and PSMD (Study 2 and 4), supporting a neuroinflammatory contribution to WM injury in DS. The longitudinal shrinkage of WMH (Study 3) further suggests that these lesions do not solely reflect permanent axonal or myelin damage, but may also represent a dynamic component of oedema and reversible neuroinflammatory resolution.

Some authors have also proposed that WM damage in DS reflects an endogenous vascular component intrinsic to trisomy 21 that drives endothelial inflammation (P8), weakens vessel walls in an amyloid-independent manner, and may contribute to downstream tau abnormalities[164,165,236] (P9). Consistent with this view, adults with DS exhibit reduced brain perfusion, prominent in posterior regions, from early ages and already in asymptomatic stages[253] Such vascular injury can, in turn, contribute to tau pathology[254] and further disrupt the cortical networks.[127,255]

The interplay between neuroinflammation and AD pathology may also help explain the biphasic trajectory of cortical thickness and volume in the MTL.

Specifically, in the ERC and PHC, we observed an initial increase in cortical thickness at approximately −20 to −15 estimated years to onset (Study 1). At this age, roughly 30 years old, individuals with DS can already present with Aβ pathology, oxidative damage, and neuroinflammation in these regions[71,83] (P10), suggesting that early inflammatory swelling and glial activation may transiently inflate cortical measurements before being overtaken by neurodegenerative thinning.[256] In addition, the chronic inflammatory state characteristic of DS may further contribute to this apparent thickening (P11). This temporal pattern mirrors the initial cortical thickening previously reported in the preclinical stages of ADAD[257,258] and sAD.[259–261]

Following this early phase, MTL volume and thickness decline progressively with advancing AD clinical stages (P12), beginning years before to symptom onset. Our fluid biomarker analyses showed CSF pTau181 correlated more tightly with MTL atrophy than the Aβ42/Aβ40 ratio, aligning with the broader consensus that tau is the proximate driver of neurodegeneration.[43,44] Moreover, the sequential progression of MTL atrophy, beginning in the ERC before propagating to the hippocampus, closely mirrors the well-established Braak staging of tau deposition in sAD.[71,88,199]

Finally, beyond these core mechanisms, DS is also associated with accelerated brain aging, likely driven by the trisomy 21 specificities. For instance, *SOD1* overexpression induces chronic oxidative stress,[60] while *DYRK1A* triplication impairs neurogenesis and synaptogenesis.[58] This superimposed accelerated aging may interact with the other pathological processes (P13), collectively predisposing the DS brain to premature structural decay.[237,238] In line with this view, every neuroimaging marker assessed throughout this thesis, spanning both GM (P14) and WM (P15), was tightly associated with age and showed greater changes at earlier ages than in euploid controls, with PSMD alterations appearing

up to 15 years before dementia onset and the non-linear MTL volumetric trajectories characteristic of DSAD.

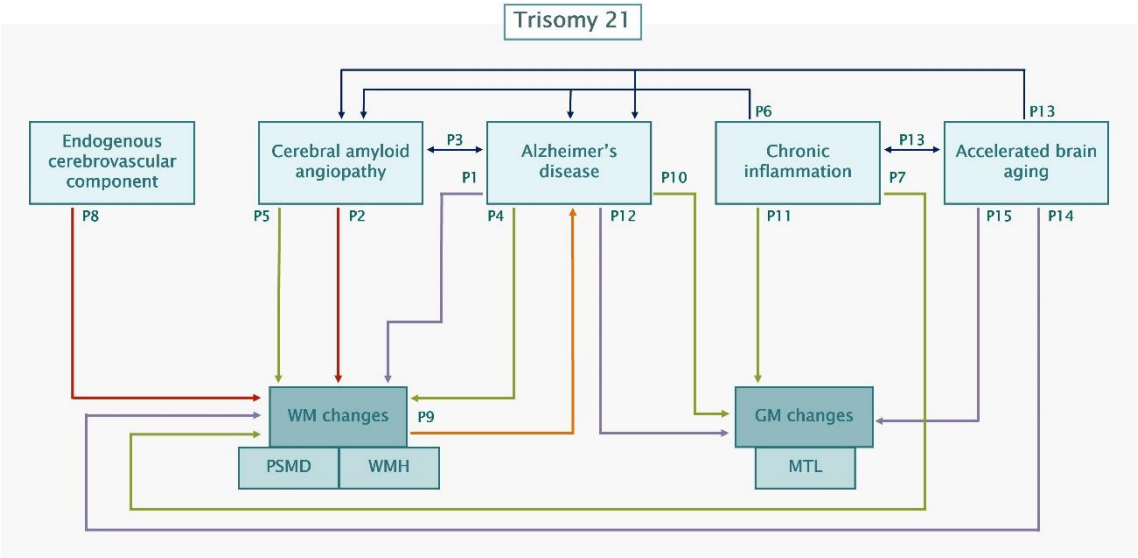

Figure 8. ***Schematic representation of the proposed pathways linking trisomy 21-intrinsic features to downstream brain injury in DS****. Four interrelated mechanisms: chronic neuroinflammation, accelerated aging, cerebral amyloidosis (AD and CAA), and endogenous vascular vulnerability, converge onto two common downstream manifestations: WM changes, captured by WMH and PSMD, and GM changes, reflected by MTL structures (thickness and volume). Pathways: P1) Wallerian degeneration secondary to cortical tau; P2) CAA-driven hypoperfusion; P3) cerebral amyloidosis; P4-P5) parenchymal and vascular Aβ-driven neuroinflammation; P6) interaction between trisomy 21-intrinsic chronic inflammation and AD/CAA pathology; P7) chronic neuroinflammation-driven WM damage; P8) endogenous vascular dysfunction-driven hypoperfusion; P9) vascular contribution to tau pathology through WM tract disruption; P10) early AD- and inflammation-driven cortical thickening; P11) chronic neuroinflammation-driven cortical thickening; P12) AD-driven MTL atrophy; P13) accelerated aging interacting with the other pathological processes; P14, P15) age-driven GM and WM changes.*

5.5 INTEGRATED MODEL IN DOWN SYNDROME-ASSOCIATED ALZHEIMER'S DISEASE

The integration of findings across the four studies of this thesis enables, for the first time, the construction of a putative temporal model describing the emergence of WM and GM imaging biomarkers in the DSAD, anchored to the chronological age and EYO (Figure 9). Positioning these imaging biomarkers alongside the established fluid and molecular trajectory of DSAD situates them

within a biologically window that mirrors the known biomarker cascade of the disease. CSF Aβ42/40 becomes abnormal around the age of 30 (EYO ≈ −23 to -26), followed by plasma NfL and GFAP elevations in the early-to-mid 30s, amyloid PET positivity in the mid-to-late 30s, and CSF pTau181 abnormality around age 38-40 (EYO ≈ −13 to −15), with tau PET positivity closer to symptom onset.[63,83,87,90] This biomarker cascade converges on a stereotyped clinical trajectory, with prodromal AD emerging at a median age of 50-51 years, progression to AD dementia between 53 and 55 years, and death occurring between 57 and 60 years.[51,67,262]

Within this framework, the imaging biomarkers characterised in this thesis define a two- stage trajectory. At the asymptomatic stage, abnormalities in PSMD emerge concurrently with, or shortly before, the rise in CSF pTau181, positioning diffuse microstructural WM injury temporally between amyloid and tau pathology. This early microstructural compromise co-occurs with the earliest changes in the MTL, with atrophy in ERC and posterior hippocampus, suggesting a shared preclinical window in which diffuse WM degeneration and incipient MTL neurodegeneration unfold in parallel. Subsequently, WMH appear in closer temporal proximity to the onset of memory and executive deficits. This later, macrostructural phase of WM injury is temporally coupled with the extension of MTL atrophy into the PHC and Br36, jointly defining an advanced disease stage that precedes, and likely contributes to, the clinical emergence of prodromal AD and dementia. Taken together, this integrative model supports the view that SVD and neurodegeneration in DSAD are temporally convergent processes, in which diffuse microstructural damage precedes macroscopic vascular lesions and parallels the progression of established fluid and molecular biomarkers towards clinical onset. This framework should nonetheless be regarded as hypothesis-

generating rather than confirmatory, and its temporal ordering remain to be validated in longitudinal multimodal cohorts spanning the full DSAD continuum.

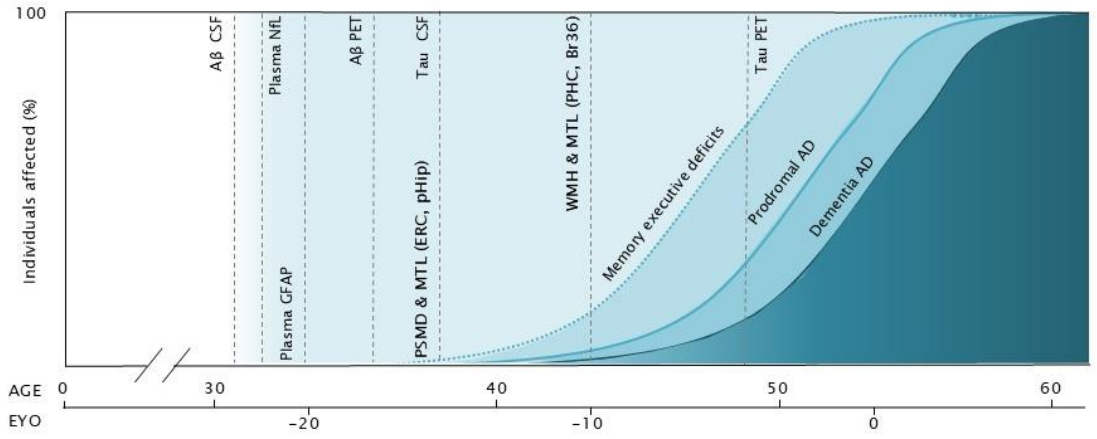

Figure 9. ***Hypothetical integrative model in DSAD.*** *Two-phase trajectory with an early preclinical phase dominated by diffuse microstructural WM damage (PSMD) and emerging MTL atrophy (ERC, posterior hippocampus [pHip]), followed by a later phase characterized by macrostructural WM lesions (WMH), extended MTL atrophy (PHC, Br36), and the subsequent clinical emergence of dementia. Adapted from Fortea et al. (2021).*

5.6 TRANSLATIONAL IMPACT

5.6.1 Research implications

Our findings reinforce the need to prioritize research in DS, a historically underrepresented population in AD research, which, as a genetically determined form of early-onset AD largely free of classical vascular risk factors, offers a unique window into the intrinsic interplay between amyloid pathology, cerebrovascular disease, and neurodegeneration, with implications that extend well beyond DS to our understanding of AD more broadly.

Within this framework, this thesis provides a fundamental conceptual implication for how WM injury is understood within the AD continuum in DS. Rather than representing a late-stage consequence of neurodegeneration or an incidental vascular comorbidity of aging, WM damage emerges as a core and early pathological feature of DSAD, evolving in parallel with, and likely interacting

with, Aβ and tau pathologies across the disease trajectory. This evidence challenges the dichotomy between "pure neurodegenerative" and "pure vascular" contributions in DS, and instead supports a multifactorial pathophysiological framework in which parenchymal and vascular Aβ deposition, neuroinflammation, blood–brain barrier dysfunction, and WM injury converge to shape the clinical expression of DSAD. Reframing WM damage as an intrinsic component of AD has direct consequences for diagnostic criteria, staging models, biomarker selection, and the design of future therapeutic strategies in this genetically determined form of AD.

5.6.2 Clinical implications

The findings of this thesis also challenge the prevailing clinical interpretation of WMH and call for a reconceptualization of SVD in DS. In the general aging population, WMH are commonly considered incidental vascular lesions secondary to aging and cardiovascular risk factors, most notably arterial hypertension, and blood pressure control constitute a preventive strategies against WMH progression.[263] However, adults with DS exhibit a strikingly low prevalence of these classical vascular risk factors,[149] yet display an early emergence of WMH that closely parallels the AD continuum. Although the exact underlying aetiology remains to be fully established, our results indicate that WMH in DS should not be dismissed as age-related or incidental findings, but rather interpreted as potential markers of underlying CAA or AD-related pathophysiology, as well as other T21-intrinsic features. Consequently, conventional antihypertensive strategies are unlikely to meaningfully reduce or slow WMH progression in this population, and alternative, disease-specific preventive approaches will be required.

Beyond this reconceptualization, this thesis offers practical relevance for the early detection of AD in DS. Diagnosing prodromal AD and AD dementia in this population remains a major clinical challenge, as the premorbid ID and coexisting medical comorbidities obscure subtle cognitive decline and delay symptomatic recognition.[51] Our data support a two-stage MRI-based framework to assist clinical staging. In the first stage, atrophy restricted to the hippocampus, particularly its posterior region, and ERC, combined with the early alterations in PSMD, may raise suspicion of underlying AD pathology even in asymptomatic individuals, thereby opening a primary therapeutic window for disease-modifying therapies. In the second stage, the involvement of additional MTL subregions, such as the PHC and Br35, coincides with the transition to the symptomatic phase and represents a secondary therapeutic window. Integrated with fluid biomarkers and clinical assessment, these MRI-derived markers can enhance the prediction of AD clinical status and refine individualized staging in adults with DS.

5.6.3 Implication for design of clinical trials

The advent of anti-amyloid monoclonal antibodies, together with the development of novel disease-modifying agents, has profoundly transformed the therapeutic landscape of AD. Adults with DSAD, however, have been systematically excluded from pivotal clinical trials of anti-amyloid therapies, largely due to concerns about a heightened risk of amyloid-related imaging abnormalities (ARIA). ARIA is a well-recognized side effect of these treatments and may plausibly be exacerbated in DS by the earlier onset, higher prevalence, and greater severity of CAA.[264] Whether this theoretical risk translates into a higher incidence of ARIA in DSAD remains unknown and should be prioritized in future studies. In this context, our results have some implications for the design and interpretation of clinical trials in DSAD.

First, current eligibility criteria for anti-amyloid therapies often exclude participants based on SVD burden. Although specific thresholds vary by drug, these criteria generally consider the number of MB, the presence of macrohemorrhages or superficial siderosis, and the extent of WMH. When applied unmodified to DSAD, such thresholds would exclude a substantial proportion of otherwise eligible individuals, given the early onset and high burden of SVD-related lesions in this population.[161–163,166] Importantly, as discussed in this thesis, WMH in DSAD arise from multiple, partially overlapping mechanisms and cannot be interpreted solely as a marker of SVD. Therefore, their presence cannot be assumed to uniformly reflect susceptibility to ARIA, and their use as an exclusion criterion may risk denying access to potentially beneficial therapies based on a non-specific SVD imaging marker. Of note, the high inter-individual variability and limited predictability of WMH trajectories further constrain their utility as both exclusion criteria and outcome measures in therapeutic trials. A single cross-sectional assessment of elevated WMH burden should not preclude enrolment; rather, reassessment at subsequent visits and integration with complementary biomarkers should be considered before a definitive eligibility decision is made. Similarly, once treatment is initiated, longitudinal changes in WMH volume should be interpreted cautiously and always contextualized with complementary clinical, imaging, and fluid biomarkers, since their unpredictable evolution limits their value. Second, the high prevalence of CAA in DSAD[112,152] underscores the need for sensitive tools to monitor vascular safety during treatment. PSMD may complement conventional MRI-based monitoring of ARIA. As a sensitive vascular safety readout, it may help track treatment-related WM alterations, and contribute to the identification of individuals at elevated risk of ARIA. Finally, the early and progressive involvement of MTL subregions, and the sensitivity of PSMD to

detect preclinical structural alterations, positions these metrics as promising candidate outcome measures for trials aiming to slow neurodegeneration in DSAD. Although longitudinal validation remains necessary, our findings support their potential as biomarkers of early neurodegenerative change.

5.7 LIMITATIONS

It is important to acknowledge the main limitations of this thesis. First, the cross-sectional design of several analyses precludes the establishment of definitive temporal sequences and causal relationships, particularly regarding the interplay between AD pathology, SVD markers (WMH and PSMD), neurodegeneration, and neuroinflammation. While the near-full penetrance and predictable trajectory of AD pathology in the DS population partially mitigates the inherent caveats of cross-sectional observations, longitudinal studies are required to confirm the regional progressive pattern of volume and thickness loss over time, and the temporal sequence between WMH and PSMD. Moreover, our longitudinal analyses for WMH were largely restricted to two MRI timepoints per participant, limiting our ability to model non-linear rates of disease progression or to capture individual-level inflection points. Future studies employing mixed-effects models across longer observation windows and multiple timepoints will be critical to resolve temporal ordering and person-specific and non-linear trajectories.

Second, cohort composition and real-world recruitment constraints introduced inherent limitations. Despite being one of the largest worldwide cohort of adults with DS, our sample sizes were relatively modest and imbalanced across clinical stages, with a relative under-representation of symptomatic DS individuals, spanning both prodromal and dementia stages. This reflects the practical difficulties of MRI tolerability in moderate-to-severe dementia and likely

introduces a survivor bias, whereby individuals with the highest SVD or AD burden are systematically underrepresented. Furthermore, demographic characteristics constrained certain subanalyses; for instance, the low proportion of *APOE* ϵ4 homozygotes precluded the stratification necessary to evaluate gene-dosage effects on neuroimaging markers, and the assessment of sex and *APOE* interaction.

Third, all neuroimaging pipelines and templates applied in this thesis were originally developed for the euploid population and were not specifically optimized for individuals with DS. Although thorough visual control confirmed that segmentation of MTL structures and WMH were correctly performed, with no apparent impact of DS-specific brain anatomy, a reduced sensitivity or potential regional bias cannot be excluded, particularly in small or anatomically complex structures.

Fourth, the absence of neuropathological confirmation limits the biological specificity of MRI-derived findings. While the imaging patterns observed are consistent with established mechanisms related to trisomy 21, such as amyloid overproduction, vascular dysfunction, and neuroinflammation, MRI metrics remain indirect proxies of underlying tissue changes. Without post-mortem validation, the precise substrates of the imaging signatures cannot be definitively determined, and causal inferences regarding the relative contribution of distinct pathological processes remain inherently speculative.

Finally, multicollinearity among fluid biomarkers complicates the interpretation of their associations with MRI-derived measures. The biomarkers examined in this thesis, Aβ42/Aβ40, pTau181, NfL, GFAP and YKL-40, are biologically interrelated and reflect overlapping pathological domains, including amyloid deposition, tau pathology, neurodegeneration, and neuroinflammation.

5.8 FUTURE DIRECTIONS

The findings presented in this thesis open several new perspectives for advancing the characterization of neurodegeneration and SVD in DSAD.

The convergence between WM damage and GM atrophy documented throughout this thesis deserves dedicated mechanistic investigation. To disentangle the complex interplay between amyloid, tau, neuroinflammation, SVD markers, and neurodegeneration, future studies should leverage formal mediation analyses within structural equation modeling frameworks applied to cohorts with longitudinal multimodal data, combining MRI, PET, CSF, plasma and cognitive assessments. These statistical approaches will allow the testing of competing causal hypotheses, including whether Aβ and/or tau mediate the emergence of WM damage, or whether, conversely, WM injury triggers subsequent neurodegenerative cascades. Complementing these cross-sectional causal models, longitudinal designs incorporating repeated assessments of PSMD and WMH across multiple timepoints will be essential to definitively confirm the temporal precedence of diffusion-based WM metrics over conventional FLAIR-derived WMH volumetry, and to consolidate PSMD as a sensitive early marker in DSAD.

The hypothesized role of neuroinflammation as a shared mechanism linking vascular and neurodegenerative pathology in DS also remains to be tested. Future studies incorporating microglial and astrocytic inflammatory PET tracers alongside multimodal MRI will be critical to map the spatial overlap between neuroinflammation, WM damage, and regions of cortical atrophy. Establishing whether neuroinflammation co-localizes with, precedes, or follows structural damage will clarify its mechanistic position within the DSAD cascade and may, in turn, reveal novel therapeutic for disease-modifying intervention.

Finally, a comprehensive comparison between the different genetically determined and sporadic forms of AD, encompassing ADAD, DSAD and early- and late-onset sAD, represents a particularly promising opportunity for elucidating the core pathophysiological mechanisms of the disease. These forms differ substantially in its genetic determinants, age of onset, vascular risk profile, and contribution of co-occurring pathologies. Integrating structural MRI, diffusion metrics, amyloid and tau PET, neuroinflammatory imaging, and fluid biomarkers will enable the delineation of which features constitute the invariant core of AD pathophysiology, and which are modulated by aetiology-specific factors.

6. CONCLUSIONS

The main conclusions of this thesis are:

1. MTL volume and thickness in DS follow a sequential, non-linear pattern of atrophy across EYO, with greater decline at advancing AD clinical stages. The ERC and posterior hippocampus are the earliest regions to decline, followed by the PHC cortex and Br36 at later ages, highlighting MTL as a potential staging biomarker.
2. WMH in adults with DS exhibit a predominantly posterior and periventricular distribution that increases with age and across AD clinical stages. Their associations with fluid biomarkers of AD pathology, neurodegeneration, and neuroinflammation suggest that the emergence of WMH in DSAD reflects the convergent contribution of multiple pathophysiological processes.
3. Longitudinal WMH trajectories are heterogeneous in DS, with a significant group-level decrease over time that is more pronounced at symptomatic stages. These reductions may reflect distinct underlying processes, such as progressive tissue degeneration or resolving neuroinflammation.
4. PSMD increases with age and AD severity in DS, with detectable alterations years before symptom onset. PSMD is strongly associated with NfL and SVD markers, and PSMD abnormalities were more frequent than WMH, positioning PSMD as a sensitive, early biomarker of WM injury in DSAD.

BIBLIOGRAPHY

1. Antonarakis SE, Skotko BG, Rafii MS, et al. Down syndrome. *Nat Rev Dis Prim*. 2020;6(1). doi:10.1038/S41572-019-0143-7

2. Bull MJ. Down Syndrome. Ropper AH, ed. *N Engl J Med*. 2020;382(24):2344-2352. doi:10.1056/NEJMra1706537

3. Esbensen AJ. Health conditions associated with aging and end of life of adults with Down syndrome. *Int Rev Res Ment Retard*. 2010;39(C):107-126. doi:10.1016/S0074-7750(10)39004-5

4. Baksh RA, Pape SE, Chan LF, Aslam AA, Gulliford MC, Strydom A. Multiple morbidity across the lifespan in people with Down syndrome or intellectual disabilities: a population-based cohort study using electronic health records. *Lancet Public Heal*. 2023;8(6):e453-e462. doi:10.1016/S2468-2667(23)00057-9

5. de Graaf G, Buckley F, Dever J, Skotko BG. Estimation of live birth and population prevalence of Down syndrome in nine U.S. states. *Am J Med Genet A*. 2017;173(10):2710-2719. doi:10.1002/AJMG.A.38402

6. Nagaoka SI, Hassold TJ, Hunt PA. Human aneuploidy: mechanisms and new insights into an age-old problem. *Nat Rev Genet*. 2012;13(7):493-504. doi:10.1038/nrg3245

7. Lanzoni M, Kinsner-Ovaskainen A, Morris J, Martin S. EUROCAT : surveillance of congenital anomalies in Europe : epidemiology of Down syndrome, 1990-2014. Published online 2019:12.

8. de Graaf G, Buckley F, Skotko BG. Estimation of the number of people with Down syndrome in Europe. *Eur J Hum Genet*. 2021;29(3):402-410. doi:10.1038/S41431-020-00748-Y

9. Huete García A. Demografía e inclusión social de las personas con síndrome de Down. *Rev Síndrome Down Rev española Investig e Inf sobre el Síndrome Down, ISSN 1132-1911, Vol 33, Nº 129 (Junio), 2016, págs 38-50*. 2016;33(129):38-50. Accessed April 4, 2026. https://dialnet.unirioja.es/servlet/articulo?codigo=5520979&info=resumen&idioma=ENG

10. Papavassiliou P, Charalsawadi C, Rafferty K, Jackson-Cook C. Mosaicism for trisomy 21: a review. *Am J Med Genet A*. 2015;167A(1):26-39. doi:10.1002/AJMG.A.36861

11. Bacalini MG, Gentilini D, Boattini A, et al. Identification of a DNA methylation signature in blood cells from persons with Down Syndrome. *Aging (Albany NY)*. 2015;7(2):82-96. doi:10.18632/aging.100715

12. Gardiner K, Davisson M. The sequence of human chromosome 21 and implications for research into Down syndrome. *Genome Biol*. 2000;1(2):reviews0002.1. doi:10.1186/gb-2000-1-2-reviews0002

13. Wiseman FK, Al-Janabi T, Hardy J, et al. A genetic cause of Alzheimer disease: mechanistic insights from Down syndrome. *Nat Rev Neurosci*. 2015;16(9):564-574. doi:10.1038/NRN3983

14. Schmidt-Sidor B, Wisniewski KE, Shepard TH, Sersen EA. Brain growth in Down syndrome subjects 15 to 22 weeks of gestational age and birth to 60 months. *Clin Neuropathol*. 1990;9(4):181-190. Accessed March 16, 2026. https://europepmc.org/article/med/2146054

15. Guidi S, Ciani E, Bonasoni P, Santini D, Bartesaghi R. Widespread proliferation impairment and hypocellularity in the cerebellum of fetuses with down syndrome. *Brain Pathol*. 2011;21(4):361-373. doi:10.1111/j.1750-3639.2010.00459.x

16. Lott IT, Head E. Dementia in Down syndrome: unique insights for Alzheimer disease research. *Nat Rev Neurol 2019 153*. 2019;15(3):135-147. doi:10.1038/s41582-018-0132-6

17. Neale N, Padilla C, Fonseca LM, Holland T, Zaman S. Neuroimaging and other modalities to assess Alzheimer's disease in Down syndrome. *NeuroImage Clin*. 2018;17:263-271. doi:10.1016/j.nicl.2017.10.022

18. Raz N, Torres IJ, Briggs SD, et al. Selective neuroanatomic abnormalities in Down's syndrome and their cognitive correlates: evidence from MRI morphometry. *Neurology*. 1995;45(2):356-366. doi:10.1212/WNL.45.2.356

19. Lee NR, Adeyemi EI, Lin A, et al. Dissociations in Cortical Morphometry in Youth with Down Syndrome: Evidence for Reduced Surface Area but Increased Thickness. *Cereb Cortex*. 2016;26(7):2982-2990. doi:10.1093/cercor/bhv107

20. Beacher F, Daly E, Simmons A, et al. Brain anatomy and ageing in non-demented adults with Down's syndrome: an in vivo MRI study. *Psychol Med*. 2010;40(4):611-619. doi:10.1017/S0033291709990985

21. Aylward EH, Habbak R, Warren AC, et al. Cerebellar volume in adults with Down syndrome. *Arch Neurol*. 1997;54(2):209-212. doi:10.1001/archneur.1997.00550140077016

22. Pinter JD, Eliez S, Schmitt JE, Capone GT, Reiss AL. Neuroanatomy of Down's syndrome: a high-resolution MRI study. *Am J Psychiatry*. 2001;158(10):1659-1665. doi:10.1176/appi.ajp.158.10.1659

23. Lott IT, Dierssen M. Cognitive deficits and associated neurological complications in individuals with Down's syndrome. *Lancet Neurol*. 2010;9(6):623-633. doi:10.1016/S1474-4422(10)70112-5

24. Pinter JD, Brown WE, Eliez S, Schmitt JE, Capone GT, Reiss AL. Amygdala and hippocampal volumes in children with Down syndrome: a high-resolution MRI study. *Neurology*. 2001;56(7):972-974. doi:10.1212/WNL.56.7.972

25. White NS, Alkire MT, Haier RJ. A voxel-based morphometric study of nondemented adults with Down Syndrome. *Neuroimage*. 2003;20(1):393-403. doi:10.1016/S1053-8119(03)00273-8

26. Stagni F, Giacomini A, Emili M, et al. Subicular hypotrophy in fetuses with Down syndrome and in the Ts65Dn model of Down syndrome. *Brain Pathol*. 2019;29(3):366-379. doi:10.1111/bpa.12663

27. Kesslak JP, Nagata SF, Lott I, Nalcioglu O. Magnetic resonance imaging analysis of age-related changes in the brains of individuals with Down's syndrome. *Neurology*. 1994;44(6):1039-1045. doi:10.1212/wnl.44.6.1039

28. Espallargas I, Capellades J, Haddouche M, Medrano S, Fortea J, Glez-Ortiz S. INVERSIÓN HIPOCAMPAL INCOMPLETA (IHI) EN SUJETOS CON SÍNDROME DE DOWN. *Seram*. Published online November 22, 2018. Accessed April 4, 2026. https://piper.espacio-seram.com/index.php/seram/article/view/2893

29. Bartzokis G, Sultzer D, Lu PH, Nuechterlein KH, Mintz J, Cummings JL. Heterogeneous age-related breakdown of white matter structural integrity: Implications for cortical

"disconnection" in aging and Alzheimer's disease. *Neurobiol Aging*. 2004;25(7):843-851. doi:10.1016/j.neurobiolaging.2003.09.005

30. Powell D, Caban-Holt A, Jicha G, et al. Frontal white matter integrity in adults with Down syndrome with and without dementia. *Neurobiol Aging*. 2014;35(7):1562-1569. doi:10.1016/j.neurobiolaging.2014.01.137

31. 2025 Alzheimer's disease facts and figures. *Alzheimer's Dement*. 2025;21(4):e70235. doi:10.1002/alz.70235

32. World Health Organization (WHO). Accessed March 31, 2026. https://www.who.int/

33. Neurología SE de. No Title. Published online 2025.

34. Scheltens P, De Strooper B, Kivipelto M, et al. Alzheimer's disease. *Lancet*. 2021;397(10284):1577-1590. doi:10.1016/S0140-6736(20)32205-4

35. Dubois B, Hampel H, Feldman HH, et al. Preclinical Alzheimer's disease: Definition, natural history, and diagnostic criteria. *Alzheimers Dement*. 2016;12(3):292-323. doi:10.1016/j.jalz.2016.02.002

36. Dubois B, Villain N, Frisoni GB, et al. Clinical diagnosis of Alzheimer's disease: recommendations of the International Working Group. *Lancet Neurol*. 2021;20(6):484-496. doi:10.1016/S1474-4422(21)00066-1

37. Jack CR, Bennett DA, Blennow K, et al. NIA-AA Research Framework: Toward a biological definition of Alzheimer's disease. *Alzheimer's Dement*. 2018;14(4):535-562. doi:10.1016/J.JALZ.2018.02.018

38. Serrano-Pozo A, Frosch MP, Masliah E, Hyman BT. Neuropathological alterations in Alzheimer disease. *Cold Spring Harb Perspect Med*. 2011;1(1). doi:10.1101/cshperspect.a006189

39. Thal DR, Rüb U, Orantes M, Braak H. Phases of A beta-deposition in the human brain and its relevance for the development of AD. *Neurology*. 2002;58(12):1791-1800. doi:10.1212/WNL.58.12.1791

40. Braak H, Braak E. Neuropathological stageing of Alzheimer-related changes. *Acta Neuropathol*. 1991;82(4):239-259. doi:10.1007/BF00308809

41. Hardy JA, Higgins GA. Alzheimer's disease: the amyloid cascade hypothesis. *Science*. 1992;256(5054):184-185. doi:10.1126/SCIENCE.1566067

42. Biel D, Brendel M, Rubinski A, et al. Tau-PET and in vivo Braak-staging as prognostic markers of future cognitive decline in cognitively normal to demented individuals. *Alzheimers Res Ther*. 2021;13(1). doi:10.1186/S13195-021-00880-X

43. Joie R La, Visani A V., Baker SL, et al. Prospective longitudinal atrophy in Alzheimer's disease correlates with the intensity and topography of baseline tau-PET. *Sci Transl Med*. 2020;12(524). doi:10.1126/SCITRANSLMED.AAU5732

44. Bejanin A, Schonhaut DR, La Joie R, et al. Tau pathology and neurodegeneration contribute to cognitive impairment in Alzheimer's disease. *Brain*. 2017;140(12):3286-3300. doi:10.1093/brain/awx243

45. Long JM, Holtzman DM. Alzheimer Disease: An Update on Pathobiology and Treatment Strategies. *Cell*. 2019;179(2):312-339. doi:10.1016/j.cell.2019.09.001

46. Rabinovici GD. Late-onset Alzheimer Disease. *Continuum (Minneap Minn)*. 2019;25(1):14-33. doi:10.1212/CON.0000000000000700

47. van der Lee SJ, Wolters FJ, Ikram MK, et al. The effect of APOE and other common genetic variants on the onset of Alzheimer's disease and dementia: a community-based cohort study. *Lancet Neurol*. 2018;17(5):434-444. doi:10.1016/S1474-4422(18)30053-X

48. Fortea J, Pegueroles J, Alcolea D, et al. APOE4 homozygozity represents a distinct genetic form of Alzheimer's disease. *Nat Med*. 2024;30(5):1284-1291. doi:10.1038/s41591-024-02931-w

49. Bateman RJ, Xiong C, Benzinger TLS, et al. Clinical and biomarker changes in dominantly inherited Alzheimer's disease. *N Engl J Med*. 2012;367(9):795-804. doi:10.1056/NEJMOA1202753

50. Ryman DC, Acosta-Baena N, Aisen PS, et al. Symptom onset in autosomal dominant Alzheimer disease. *Neurology*. 2014;83(3):253-260. doi:10.1212/WNL.0000000000000596

51. Fortea J, Zaman SH, Hartley S, Rafii MS, Head E, Carmona-Iragui M. Alzheimer's disease associated with Down syndrome: a genetic form of dementia. *Lancet Neurol*. 2021;20(11):930-942. doi:10.1016/S1474-4422(21)00245-3

52. Doran E, Keator D, Head E, et al. Down Syndrome, Partial Trisomy 21, and Absence of Alzheimer's Disease: The Role of APP. *J Alzheimers Dis*. 2017;56(2):459-470. doi:10.3233/JAD-160836

53. Prasher VP, Farrer MJ, Kessling AM, et al. Molecular mapping of Alzheimer-type dementia in Down's syndrome. *Ann Neurol*. 1998;43(3):380-383. doi:10.1002/ana.410430316

54. Dubois B, Villain N, Schneider L, et al. Alzheimer Disease as a Clinical-Biological Construct-An International Working Group Recommendation. *JAMA Neurol*. 2024;81(12):1304-1311. doi:10.1001/JAMANEUROL.2024.3770

55. Jack CR, Andrews JS, Beach TG, et al. Revised criteria for diagnosis and staging of Alzheimer's disease: Alzheimer's Association Workgroup. *Alzheimers Dement*. 2024;20(8):5143-5169. doi:10.1002/ALZ.13859

56. Wiseman FK, Pulford LJ, Barkus C, et al. Trisomy of human chromosome 21 enhances amyloid-β deposition independently of an extra copy of APP. *Brain*. 2018;141(8):2457-2474. doi:10.1093/BRAIN/AWY159

57. Wiseman FK, Alford KA, Tybulewicz VLJ, Fisher EMC. Down syndrome--recent progress and future prospects. *Hum Mol Genet*. 2009;18(R1). doi:10.1093/hmg/ddp010

58. Moreau M, Carmona-Iragui M, Altuna M, et al. DYRK1A and Activity-Dependent Neuroprotective Protein Comparative Diagnosis Interest in Cerebrospinal Fluid and Plasma in the Context of Alzheimer-Related Cognitive Impairment in Down Syndrome Patients. *Biomedicines*. 2022;10(6). doi:10.3390/biomedicines10061380

59. Ballard C, Mobley W, Hardy J, Williams G, Corbett A. Dementia in Down's syndrome. *Lancet Neurol*. 2016;15(6):622-636. doi:10.1016/S1474-4422(16)00063-6

60. Gulesserian T, Seidl R, Hardmeier R, Cairns N, Lubec G. Superoxide dismutase SOD1, encoded on chromosome 21, but not SOD2 is overexpressed in brains of patients with Down syndrome. *J Investig Med*. 2001;49(1):41-46. doi:10.2310/6650.2001.34089

61. Tosh JL, Rhymes ER, Mumford P, et al. Genetic dissection of down syndrome-associated alterations in APP/amyloid-β biology using mouse models. *Sci Rep*. 2021;11(1). doi:10.1038/S41598-021-85062-3

62. Bejanin A, Iulita MF, Vilaplana E, et al. Association of Apolipoprotein E ε4 Allele With Clinical and Multimodal Biomarker Changes of Alzheimer Disease in Adults With Down Syndrome. *JAMA Neurol*. 2021;78(8):937-947. doi:10.1001/JAMANEUROL.2021.1893

63. Boerwinkle AH, Gordon BA, Wisch J, et al. Comparison of amyloid burden in individuals with Down syndrome versus autosomal dominant Alzheimer's disease: a cross-sectional study. *Lancet Neurol*. 2023;22(1):55-65. doi:10.1016/S1474-4422(22)00408-2

64. Lao PJ, Betthauser TJ, Hillmer AT, et al. The effects of normal aging on amyloid-β deposition in nondemented adults with Down syndrome as imaged by carbon 11-labeled Pittsburgh compound B. *Alzheimers Dement*. 2016;12(4):380-390. doi:10.1016/J.JALZ.2015.05.013

65. McCarron M, McCallion P, Reilly E, Dunne P, Carroll R, Mulryan N. A prospective 20-year longitudinal follow-up of dementia in persons with Down syndrome. *J Intellect Disabil Res*. 2017;61(9):843-852. doi:10.1111/JIR.12390

66. Iulita MF, Garzón Chavez D, Klitgaard Christensen M, et al. Association of Alzheimer Disease With Life Expectancy in People With Down Syndrome. *JAMA Netw Open*. 2022;5(5):e2212910-e2212910. doi:10.1001/JAMANETWORKOPEN.2022.12910

67. Sinai A, Mokrysz C, Bernal J, et al. Predictors of Age of Diagnosis and Survival of Alzheimer's Disease in Down Syndrome. *J Alzheimers Dis*. 2018;61(2):717-728. doi:10.3233/JAD-170624

68. Holland AJ, Hon J, Huppert FA, Stevens F. Incidence and course of dementia in people with Down's syndrome: findings from a population-based study. *J Intellect Disabil Res*. 2000;44 (Pt 2)(2):138-146. doi:10.1046/j.1365-2788.2000.00263.x

69. Rodríguez-Baz Í, Benejam B, Morcillo-Nieto AO, et al. Posterior Cortical Atrophy Due to Alzheimer Disease in a Person With Down Syndrome: A Case Report. *Neurology*. 2024;104(1). doi:10.1212/WNL.0000000000210179,

70. Boutoleau-Bretonnière C, Pallardy A. Down syndrome with posterior cortical atrophy. *BMJ Case Rep*. 2018;2018. doi:10.1136/BCR-2017-223108

71. Davidson YS, Robinson A, Prasher VP, Mann DMA. The age of onset and evolution of Braak tangle stage and Thal amyloid pathology of Alzheimer's disease in individuals with Down syndrome. *Acta Neuropathol Commun*. 2018;6(1):56. doi:10.1186/S40478-018-0559-4

72. Mann DMA. The pathological association between down syndrome and Alzheimer disease. *Mech Ageing Dev*. 1988;43(2):99-136. doi:10.1016/0047-6374(88)90041-3

73. Gyure KA, Durham R, Stewart WF, Smialek JE, Troncoso JC. Intraneuronal abeta-amyloid precedes development of amyloid plaques in Down syndrome. *Arch Pathol Lab Med*. 2001;125(4):489-492. doi:10.5858/2001-125-0489-IAAPDO

74. Teller JK, Russo C, DeBusk LM, et al. Presence of soluble amyloid beta-peptide precedes amyloid plaque formation in Down's syndrome. *Nat Med*. 1996;2(1):93-95. doi:10.1038/NM0196-93

75. Lemere CA, Blusztajn JK, Yamaguchi H, Wisniewski T, Saido TC, Selkoe DJ. Sequence of deposition of heterogeneous amyloid β-peptides and APO E in down syndrome: Implications for initial events in amyloid plaque formation. *Neurobiol Dis*. 1996;3(1):16-32. doi:10.1006/nbdi.1996.0003

76. Leverenz JB, Raskind MA. Early amyloid deposition in the medial temporal lobe of young Down syndrome patients: A regional quantitative analysis. *Exp Neurol*. 1998;150(2):296-304. doi:10.1006/exnr.1997.6777

77. Stoltzner SE, Grenfell TJ, Mori C, et al. Temporal accrual of complement proteins in amyloid plaques in Down's syndrome with Alzheimer's disease. *Am J Pathol*. 2000;156(2):489-499. doi:10.1016/S0002-9440(10)64753-0

78. Cenini G, Dowling ALS, Beckett TL, et al. Association between frontal cortex oxidative damage and beta-amyloid as a function of age in Down syndrome. *Biochim Biophys Acta - Mol Basis Dis*. 2012;1822(2):130-138. doi:10.1016/j.bbadis.2011.10.001

79. Nistor M, Don M, Parekh M, et al. Alpha- and beta-secretase activity as a function of age and beta-amyloid in Down syndrome and normal brain. *Neurobiol Aging*. 2007;28(10):1493-1506. doi:10.1016/j.neurobiolaging.2006.06.023

80. Hof PR, Bouras C, Perl DP, Sparks DL, Mehta N, Morrison JH. Age-related distribution of neuropathologic changes in the cerebral cortex of patients with Down's syndrome. Quantitative regional analysis and comparison with Alzheimer's disease. *Arch Neurol*. 1995;52(4):379-391. doi:10.1001/ARCHNEUR.1995.00540280065020

81. Mann DMA, Esiri MM. The pattern of acquisition of plaques and tangles in the brains of patients under 50 years of age with Down's syndrome. *J Neurol Sci*. 1989;89(2-3):169-179. doi:10.1016/0022-510X(89)90019-1

82. Perez SE, Miguel JC, He B, et al. Frontal cortex and striatal cellular and molecular pathobiology in individuals with Down syndrome with and without dementia. *Acta Neuropathol*. 2019;137(3):413-436. doi:10.1007/S00401-019-01965-6

83. Fortea J, Vilaplana E, Carmona-Iragui M, et al. Clinical and biomarker changes of Alzheimer's disease in adults with Down syndrome: a cross-sectional study. *Lancet*. 2020;395(10242):1988-1997. doi:10.1016/S0140-6736(20)30689-9

84. Dekker AD, Fortea J, Blesa R, De Deyn PP. Cerebrospinal fluid biomarkers for Alzheimer's disease in Down syndrome. *Alzheimer's Dement (Amsterdam, Netherlands)*. 2017;8:1-10. doi:10.1016/J.DADM.2017.02.006

85. Fortea J, Carmona-Iragui M, Benejam B, et al. Plasma and CSF biomarkers for the diagnosis of Alzheimer's disease in adults with Down syndrome: a cross-sectional study. *Lancet Neurol*.

2018;17(10):860–869. doi:10.1016/S1474-4422(18)30285-0

86. Henson RL, Doran E, Christian BT, et al. Cerebrospinal fluid biomarkers of Alzheimer's disease in a cohort of adults with Down syndrome. *Alzheimer's Dement (Amsterdam, Netherlands)*. 2020;12(1). doi:10.1002/DAD2.12057

87. Carmona-Iragui M, O'Connor A, Llibre-Guerra J, et al. Clinical and research application of fluid biomarkers in autosomal dominant Alzheimer's disease and Down syndrome. *eBioMedicine*. 2024;108. doi:10.1016/j.ebiom.2024.105327

88. Wisch JK, McKay NS, Boerwinkle AH, et al. Comparison of tau spread in people with Down syndrome versus autosomal-dominant Alzheimer's disease: a cross-sectional study. *Lancet Neurol*. 2024;23(5):500–510. doi:10.1016/S1474-4422(24)00084-X

89. Portelius E, Soininen H, Andreasson U, et al. Exploring Alzheimer molecular pathology in Down's syndrome cerebrospinal fluid. *Neurodegener Dis*. 2014;14(2):98–106. doi:10.1159/000358800

90. Montoliu-Gaya L, Alcolea D, Ashton NJ, et al. Plasma and cerebrospinal fluid glial fibrillary acidic protein levels in adults with Down syndrome: a longitudinal cohort study. *eBioMedicine*. 2023;90. doi:10.1016/j.ebiom.2023.104547

91. Fagan AM, Henson RL, Li Y, et al. Comparison of CSF biomarkers in Down syndrome and autosomal dominant Alzheimer's disease: a cross-sectional study. *Lancet Neurol*. 2021;20(8):615–626. doi:10.1016/S1474-4422(21)00139-3

92. Hendrix JA, Airey DC, Britton A, et al. Cross-Sectional Exploration of Plasma Biomarkers of Alzheimer's Disease in Down Syndrome: Early Data from the Longitudinal Investigation for Enhancing Down Syndrome Research (LIFE-DSR) Study. *J Clin Med*. 2021;10(9). doi:10.3390/jcm10091907

93. Lleó A, Zetterberg H, Pegueroles J, et al. Phosphorylated tau181 in plasma as a potential biomarker for Alzheimer's disease in adults with Down syndrome. *Nat Commun 2021 121*. 2021;12(1):1–8. doi:10.1038/s41467-021-24319-x

94. Huber H, Arranz J, Arslan B, et al. Plasma p-tau217 as a biomarker of Alzheimer's disease pathology in individuals with Down syndrome. *Nat Commun*. 2025;16(1). doi:10.1038/S41467-025-65882-X

95. Carmona-Iragui M, Alcolea D, Barroeta I, et al. Diagnostic and prognostic performance and longitudinal changes in plasma neurofilament light chain concentrations in adults with Down syndrome: a cohort study. *Lancet Neurol*. 2021;20(8):605–614. doi:10.1016/S1474-4422(21)00129-0

96. Wisch JK, Jiao Z, Kennedy JT, et al. Imaging and plasma biomarkers for pathological accumulation in Down syndrome. *Brain*. Published online November 5, 2025. doi:10.1093/brain/awaf418

97. Zammit MD, Laymon CM, Betthauser TJ, et al. Amyloid accumulation in Down syndrome measured with amyloid load. *Alzheimer's Dement (Amsterdam, Netherlands)*. 2020;12(1). doi:10.1002/DAD2.12020

98. Annus T, Wilson LR, Hong YT, et al. The pattern of amyloid accumulation in the brains of adults with Down syndrome. *Alzheimers Dement*. 2016;12(5):538–545. doi:10.1016/J.JALZ.2015.07.490

99. McLachlan M, Bettcher B, McVea A, et al. The striatum is an early, accurate indicator of amyloid burden using [11C]PiB in Down syndrome: comparison of two radiotracers. *medRxiv Prepr Serv Heal Sci*. Published online December 6, 2024. doi:10.1101/2024.12.04.24318526

100. Lao PJ, Handen BL, Betthauser TJ, et al. Longitudinal changes in amyloid positron emission tomography and volumetric magnetic resonance imaging in the nondemented Down syndrome population. *Alzheimer's Dement (Amsterdam, Netherlands)*. 2017;9:1–9. doi:10.1016/j.dadm.2017.05.001

101. Krasny S, Yan C, Hartley SL, et al. Assessing amyloid PET positivity and cognitive function in Down syndrome to guide clinical trials targeting amyloid. *Alzheimers Dement*. 2024;20(8):5570–5577. doi:10.1002/ALZ.14068

102. Zammit MD, Betthauser TJ, McVea AK, et al. Characterizing the emergence of amyloid and tau burden in Down syndrome. *Alzheimers Dement*. 2024;20(1):388–398. doi:10.1002/alz.13444

103. Schworer EK, Zammit MD, Wang J, et al. Timeline to symptomatic Alzheimer's disease in people with Down syndrome as assessed by amyloid-PET and tau-PET: a longitudinal cohort study. *Lancet Neurol*. 2024;23(12):1214–1224. doi:10.1016/S1474-4422(24)00426-5

104. Rafii MS, Lukic AS, Andrews RD, et al. PET Imaging of Tau Pathology and Relationship to Amyloid, Longitudinal MRI, and Cognitive Change in Down Syndrome: Results from the Down Syndrome Biomarker Initiative (DSBI). *J Alzheimers Dis*. 2017;60(2):439–450. doi:10.3233/JAD-170390

105. Rafii MS. Tau PET Imaging for Staging of Alzheimer's Disease in Down Syndrome. *Dev Neurobiol*. 2019;79(7):711–715. doi:10.1002/DNEU.22658

106. Arriola-Infante JE, Morcillo-Nieto AO, Zsadanyi SE, et al. Regional Brain Metabolism across the Alzheimer's Disease Continuum in Down Syndrome. *Ann Neurol*. 2025;98(1):163–173. doi:10.1002/ANA.27226,

107. Lao PJ, Handen BL, Betthauser TJ, et al. Alzheimer-Like Pattern of Hypometabolism Emerges with Elevated Amyloid-β Burden in Down Syndrome. *J Alzheimers Dis*. 2018;61(2):631–644. doi:10.3233/JAD-170720

108. Haier RJ, Alkire MT, White NS, et al. Temporal cortex hypermetabolism in Down syndrome prior to the onset of dementia. *Neurology*. 2003;61(12):1673–1679. doi:10.1212/01.WNL.0000098935.36984.25

109. Verclytte S, Lopes R, Lenfant P, et al. Cerebral Hypoperfusion and Hypometabolism Detected by Arterial Spin Labeling MRI and FDG-PET in Early-Onset Alzheimer's Disease. *J Neuroimaging*. 2016;26(2):207–212. doi:10.1111/jon.12264

110. Zammit MD, Laymon CM, Tudorascu DL, et al. Patterns of glucose hypometabolism in Down syndrome resemble sporadic Alzheimer's disease except for the putamen. *Alzheimer's Dement (Amsterdam, Netherlands)*. 2021;12(1). doi:10.1002/DAD2.12138

111. Teipel SJ, Hampel H. Neuroanatomy of Down syndrome in vivo: a model of preclinical Alzheimer's disease. *Behav Genet*. 2006;36(3):405–415. doi:10.1007/s10519-006-9047-x

112. Carmona-Iragui M, Balasa M, Benejam B, et al. Cerebral

amyloid angiopathy in Down syndrome and sporadic and autosomal-dominant Alzheimer's disease. *Alzheimer's Dement*. 2017;13(11):1251-1260. doi:10.1016/J.JALZ.2017.03.007

113. Aylward EH, Li Q, Honeycutt NA, et al. MRI volumes of the hippocampus and amygdala in adults with Down's syndrome with and without dementia. *Am J Psychiatry*. 1999;156(4):564-568. doi:10.1176/ajp.156.4.564

114. Beacher F, Daly E, Simmons A, et al. Alzheimer's disease and Down's syndrome: an in vivo MRI study. *Psychol Med*. 2009;39(4):675-684. doi:10.1017/S0033291708004054

115. Pearlson GD, Breiter SN, Aylward EH, et al. MRI brain changes in subjects with Down syndrome with and without dementia. *Dev Med Child Neurol*. 1998;40(5):326-334. Accessed March 31, 2026. https://psycnet.apa.org/record/1998-02929-003

116. Pujol J, Fenoll R, Ribas-Vidal N, et al. A longitudinal study of brain anatomy changes preceding dementia in Down syndrome. *NeuroImage Clin*. 2018;18:160-166. doi:10.1016/j.nicl.2018.01.024

117. Prasher V, Cumella S, Natarajan K, Rolfe E, Shah S, Haque MS. Magnetic resonance imaging, Down's syndrome and Alzheimer's disease: research and clinical implications. *J Intellect Disabil Res*. 2003;47(Pt 2):90-100. doi:10.1046/j.1365-2788.2003.00445.x

118. Fenoll R, Pujol J, Esteba-Castillo S, et al. Anomalous White Matter Structure and the Effect of Age in Down Syndrome Patients. *J Alzheimers Dis*. 2017;57(1):61-70. doi:10.3233/JAD-161112

119. Lee NR, Nayak A, Irfanoglu MO, et al. Hypoplasia of cerebellar afferent networks in Down syndrome revealed by DTI-driven tensor based morphometry. *Sci Rep*. 2020;10(1). doi:10.1038/S41598-020-61799-1

120. Romano A, Moraschi M, Cornia R, et al. White matter involvement in young non-demented Down's syndrome subjects: a tract-based spatial statistic analysis. *Neuroradiology*. 2018;60(12):1335-1341. doi:10.1007/S00234-018-2102-5

121. Saini F, Dell'Acqua F, Strydom A. Structural Connectivity in Down Syndrome and Alzheimer's Disease. *Front Neurosci*. 2022;16. doi:10.3389/FNINS.2022.908413

122. Saini F, Ivain P, Idris M, et al. White matter trajectories in Down syndrome and Alzheimer's disease: Insights from diffusion tensor-based morphometry. *Alzheimers Dement*. 2025;21(6). doi:10.1002/ALZ.70382

123. Bazydlo AM, Zammit MD, Wu M, et al. White matter microstructure associations to amyloid burden in adults with Down syndrome. *NeuroImage Clin*. 2022;33. doi:10.1016/j.nicl.2021.102908

124. Rosas HD, Hsu E, Mercaldo ND, et al. Alzheimer-related altered white matter microstructural integrity in Down syndrome: A model for sporadic AD? *Alzheimer's Dement (Amsterdam, Netherlands)*. 2020;12(1). doi:10.1002/DAD2.12040

125. Portegies MLP, Koudstaal PJ, Ikram MA. Cerebrovascular disease. *Handb Clin Neurol*. 2016;138:239-261. doi:10.1016/B978-0-12-802973-2.00014-8

126. Kalaria RN. The pathology and pathophysiology of vascular dementia. *Neuropharmacology*. 2018;134(Pt B):226-239. doi:10.1016/j.neuropharm.2017.12.030

127. ter Telgte A, van Leijsen EMC, Wiegertjes K, Klijn CJM, Tuladhar AM, de Leeuw F-E. Cerebral small vessel disease: from a focal to a global perspective. *Nat Rev Neurol 2018 147*. 2018;14(7):387-398. doi:10.1038/s41582-018-0014-y

128. Pantoni L. Cerebral small vessel disease: from pathogenesis and clinical characteristics to therapeutic challenges. *Lancet Neurol*. 2010;9(7):689-701. doi:10.1016/S1474-4422(10)70104-6

129. Arvanitakis Z, Capuano AW, Leurgans SE, Bennett DA, Schneider JA. Relation of cerebral vessel disease to Alzheimer's disease dementia and cognitive function in elderly people: a cross-sectional study. *Lancet Neurol*. 2016;15(9):934-943. doi:10.1016/S1474-4422(16)30029-1

130. Kapasi A, DeCarli C, Schneider JA. Impact of multiple pathologies on the threshold for clinically overt dementia. *Acta Neuropathol 2017 1342*. 2017;134(2):171-186. doi:10.1007/S00401-017-1717-7

131. Snowdon DA, Greiner LH, Mortimer JA, Riley KP, Greiner PA, Markesbery WR. Brain Infarction and the Clinical Expression of Alzheimer Disease: The Nun Study. *JAMA*. 1997;277(10):813-817. doi:10.1001/jama.1997.03540340047031

132. Blevins BL, Vinters H V., Love S, et al. Brain arteriolosclerosis. *Acta Neuropathol 2020 1411*. 2020;141(1):1-24. doi:10.1007/S00401-020-02235-6

133. Charidimou A, Gang Q, Werring DJ. Sporadic cerebral amyloid angiopathy revisited: recent insights into pathophysiology and clinical spectrum. *J Neurol Neurosurg Psychiatry*. 2012;83(2):124-137. doi:10.1136/JNNP-2011-301308

134. Viswanathan A, Greenberg SM. Cerebral amyloid angiopathy in the elderly. *Ann Neurol*. 2011;70(6):871-880. doi:10.1002/ana.22516

135. Yamada M. Cerebral amyloid angiopathy: emerging concepts. *J stroke*. 2015;17(1):17-30. doi:10.5853/jos.2015.17.1.17

136. Wardlaw JM, Smith EE, Biessels GJ, et al. Neuroimaging standards for research into small vessel disease and its contribution to ageing and neurodegeneration. *Lancet Neurol*. 2013;12(8):822-838. doi:10.1016/S1474-4422(13)70124-8

137. Duering M, Biessels GJ, Brodtmann A, et al. Neuroimaging standards for research into small vessel disease—advances since 2013. *Lancet Neurol*. 2023;22(7):602-618. doi:10.1016/S1474-4422(23)00131-X

138. Baykara E, Gesierich B, Adam R, et al. A Novel Imaging Marker for Small Vessel Disease Based on Skeletonization of White Matter Tracts and Diffusion Histograms. *Ann Neurol*. 2016;80(4):581-592. doi:10.1002/ANA.24758

139. Maillard P, Lu H, Arfanakis K, et al. Instrumental validation of free water, peak-width of skeletonized mean diffusivity, and white matter hyperintensities: MarkVCID neuroimaging kits. *Alzheimer's Dement (Amsterdam, Netherlands)*. 2022;14(1). doi:10.1002/DAD2.12261

140. Liu Y, Braidy N, Poljak A, Chan DKY, Sachdev P. Cerebral small vessel disease and the risk of Alzheimer's disease: A systematic review. *Ageing Res Rev*. 2018;47:41-48. doi:10.1016/J.ARR.2018.06.002

141. Kim HW, Hong J, Jeon JC. Cerebral Small Vessel Disease and Alzheimer's Disease: A Review. *Front Neurol*. 2020;11:927. doi:10.3389/FNEUR.2020.00927/BIBTEX

142. Blevins BL, Vinters H V., Love S, et al. Brain arteriolosclerosis. *Acta Neuropathol*. 2021;141(1). doi:10.1007/S00401-020-02235-6

143. Boyle PA, Yu L, Leurgans SE, et al. Attributable risk of Alzheimer's dementia attributed to age-related neuropathologies. *Ann Neurol*. 2019;85(1):114-124. doi:10.1002/ANA.25380

144. Reijmer YD, Van Veluw SJ, Greenberg SM. Ischemic brain injury in cerebral amyloid angiopathy. *J Cereb Blood Flow Metab*. 2016;36(1):40-54. doi:10.1038/jcbfm.2015.88

145. Jellinger KA. Alzheimer disease and cerebrovascular pathology: an update. *J Neural Transm*. 2002;109(5-6):813-836. doi:10.1007/S007020200068

146. Kalaria RN, Ballard C. Overlap between pathology of Alzheimer disease and vascular dementia. *Alzheimer Dis Assoc Disord*. 1999;13 Suppl 3(SUPPL. 3). doi:10.1097/00002093-199912003-00017

147. Brenowitz WD, Nelson PT, Besser LM, Heller KB, Kukull WA. Cerebral amyloid angiopathy and its co-occurrence with Alzheimer's disease and other cerebrovascular neuropathologic changes. *Neurobiol Aging*. 2015;36(10):2702-2708. doi:10.1016/j.neurobiolaging.2015.06.028

148. Greenberg SM, Bacskai BJ, Hernandez-Guillamon M, Pruzin J, Sperling R, van Veluw SJ. Cerebral amyloid angiopathy and Alzheimer disease — one peptide, two pathways. *Nat Rev Neurol*. 2020;16(1):30-42. doi:10.1038/S41582-019-0281-2,

149. Real De Asua D, Quero M, Moldenhauer F, Suarez C. Clinical profile and main comorbidities of Spanish adults with Down syndrome. *Eur J Intern Med*. 2015;26(6):385-391. doi:10.1016/j.ejim.2015.05.003

150. Draheim CC, Geijer JR, Dengel DR. Comparison of intima-media thickness of the carotid artery and cardiovascular disease risk factors in adults with versus without the Down syndrome. *Am J Cardiol*. 2010;106(10):1512-1516. doi:10.1016/J.AMJCARD.2010.06.079

151. Mills KT, Stefanescu A, He J. The global epidemiology of hypertension. *Nat Rev Nephrol*. 2020;16(4):223. doi:10.1038/S41581-019-0244-2

152. Head E, Phelan MJ, Doran E, et al. Cerebrovascular pathology in Down syndrome and Alzheimer disease. *Acta Neuropathol Commun*. 2017;5(1):93. doi:10.1186/S40478-017-0499-4,

153. Murdoch JC, Rodger JC, Rao SS, Fletcher CD, Dunnigan MG. Down's syndrome: an atheroma-free model? *Br Med J*. 1977;2(6081):226-228. doi:10.1136/BMJ.2.6081.226

154. Korbel JO, Tirosh-Wagner T, Urban AE, et al. The genetic architecture of Down syndrome phenotypes revealed by high-resolution analysis of human segmental trisomies. *Proc Natl Acad Sci U S A*. 2009;106(29):12031-12036. doi:10.1073/pnas.0813248106

155. Mann DMA, Davidson YS, Robinson AC, et al. Patterns and severity of vascular amyloid in Alzheimer's disease associated with duplications and missense mutations in APP gene, Down syndrome and sporadic Alzheimer's disease. *Acta Neuropathol*. 2018;136(4):569-587. doi:10.1007/S00401-018-1866-3/TABLES/3

156. Kasri A, Camporesi E, Gkanatsiou E, et al. Amyloid-β peptide signature associated with cerebral amyloid angiopathy in familial Alzheimer's disease with APPdup and Down syndrome. *Acta Neuropathol*. 2024;148(1). doi:10.1007/S00401-024-02756-4

157. Ikeda SI, Tokuda T, Yanagisawa N, Kametani F, Ohshima T, Allsop D. Variability of beta-amyloid protein deposited lesions in Down's syndrome brains. *Tohoku J Exp Med*. 1994;174(3):189-198. doi:10.1620/TJEM.174.189

158. Lai F, Williams RS. A prospective study of Alzheimer disease in Down syndrome. *Arch Neurol*. 1989;46(8):849-853. doi:10.1001/ARCHNEUR.1989.00520440031017

159. Linn J, Halpin A, Demaerel P, et al. Prevalence of superficial siderosis in patients with cerebral amyloid angiopathy. *Neurology*. 2010;74(17):1346-1350. doi:10.1212/WNL.0B013E3181DAD605

160. Helman AM, Siever M, McCarty KL, et al. Microbleeds and Cerebral Amyloid Angiopathy in the Brains of People with Down Syndrome with Alzheimer's Disease. *J Alzheimer's Dis*. 2019;67(1):103-112. doi:10.3233/JAD-180589,

161. Lao PJ, Gutierrez J, Keator D, et al. Alzheimer-Related Cerebrovascular Disease in Down Syndrome. *Ann Neurol*. 2020;88(6):1165-1177. doi:10.1002/ANA.25905

162. Aranha MR, Montal V, van den Brink H, et al. Cortical microinfarcts in adults with Down syndrome assessed with 3T-MRI. *Alzheimers Dement*. 2024;20(6). doi:10.1002/ALZ.13797

163. Zsadanyi SE, Morcillo-Nieto AO, Aranha MR, et al. Associations of Microbleeds and Their Topography With Imaging and CSF Biomarkers of Alzheimer Pathology in Individuals With Down Syndrome. *Neurology*. 2024;103(4):e209676. doi:10.1212/WNL.0000000000209676

164. Edwards NC, Lao PJ, Alshikho MJ, et al. Cerebrovascular disease is associated with Alzheimer's plasma biomarker concentrations in adults with Down syndrome. *Brain Commun*. 2024;6(5). doi:10.1093/BRAINCOMMS/FCAE331

165. Edwards NC, Lao PJ, Alshikho MJ, et al. Alzheimer's disease diagnostic progression is associated with cerebrovascular disease and neuroinflammation in adults with Down syndrome. *Alzheimers Dement*. 2025;21(10). doi:10.1002/ALZ.70726

166. Lao P, Edwards N, Flores-Aguilar L, et al. Cerebrovascular disease emerges with age and Alzheimer's disease in adults with Down syndrome. *Sci Rep*. 2024;14(1). doi:10.1038/S41598-024-61962-Y,

167. Lao P, Edwards N, Flores-Aguilar L, et al. Longitudinal changes in white matter hyperintensity volume accelerate across the Alzheimer's continuum in adults with Down syndrome. *Alzheimers Dement*. 2025;21(9). doi:10.1002/ALZ.70679

168. Videla L, Benejam B, Barroeta I, et al. The Down Alzheimer Barcelona Neuroimaging Initiative (DABNI) and its contributions to understanding Alzheimer's disease in Down syndrome: A decade of discovery. *Alzheimer's Dement*. 2025;21(6). doi:10.1002/ALZ.70259,

169. Alcolea D, Clarimón J, Carmona-Iragui M, et al. The Sant Pau

Initiative on Neurodegeneration (SPIN) cohort: A data set for biomarker discovery and validation in neurodegenerative disorders. *Alzheimer's Dement Transl Res Clin Interv*. 2019;5:597-609. doi:10.1016/J.TRCI.2019.09.005

170. Esteba-Castillo S, Dalmau-Bueno A, Ribas-Vidal N, Vilá-Alsina M, García Alba J, Novell R. Adaptation and validation of CAMDEX-DS (Cambridge Examination for Mental Disorders of Older People with Down's Syndrome and others with intellectual disabilities) in Spanish population with intellectual disabilities [in Spanish]. *Rev Neurol ISSN 0210-0010, Vol 57, Nº 8, 2013, págs 337-346*. 2013;57(8):337-346. Accessed May 26, 2023. https://dialnet.unirioja.es/servlet/articulo?codigo=4419231&info=resumen&idioma=SPA

171. Devenny DA, Zimmerli EJ, Kittler P, Krinsky-McHale SJ. Cued recall in early-stage dementia in adults with Down's syndrome. *J Intellect Disabil Res*. 2002;46(Pt 6):472-483. doi:10.1046/J.1365-2788.2002.00417.X

172. Regier DA, Kuhl EA, Kupfer DJ. The DSM-5: Classification and criteria changes. *World Psychiatry*. 2013;12(2):92-98. doi:10.1002/WPS.20050

173. Kaufman AS, Calonge Romano I, Cordero Pando A, Kaufman NL. Test breve de inteligencia de Kaufman (K.BIT). *Pearson*. Published online 2011. Accessed June 4, 2025. https://vohaleprofesional.es/tienda/marcas/pearson/k-bit-test-breve-de-inteligencia-de-kaufman

174. Sala I, Illán-Gala I, Alcolea D, et al. Diagnostic and Prognostic Value of the Combination of Two Measures of Verbal Memory in Mild Cognitive Impairment due to Alzheimer's Disease. *J Alzheimers Dis*. 2017;58(3):909-918. doi:10.3233/JAD-170073

175. Albert MS, DeKosky ST, Dickson D, et al. The diagnosis of mild cognitive impairment due to Alzheimer's disease: recommendations from the National Institute on Aging-Alzheimer's Association workgroups on diagnostic guidelines for Alzheimer's disease. *Alzheimers Dement*. 2011;7(3):270-279. doi:10.1016/J.JALZ.2011.03.008

176. McKhann GM, Knopman DS, Chertkow H, et al. The diagnosis of dementia due to Alzheimer's disease: recommendations from the National Institute on Aging-Alzheimer's Association workgroups on diagnostic guidelines for Alzheimer's disease. *Alzheimers Dement*. 2011;7(3):263-269. doi:10.1016/J.JALZ.2011.03.005

177. Alcolea D, Pegueroles J, Muñoz L, et al. Agreement of amyloid PET and CSF biomarkers for Alzheimer's disease on Lumipulse. *Ann Clin Transl Neurol*. 2019;6(9):1815-1824. doi:10.1002/ACN3.50873

178. Gaser C, Dahnke R, Thompson PM, Kurth F, Luders E, Initiative ADN. CAT - A Computational Anatomy Toolbox for the Analysis of Structural MRI Data. *bioRxiv*. Published online June 13, 2022:2022.06.11.495736. doi:10.1101/2022.06.11.495736

179. Jenkinson M, Beckmann CF, Behrens TEJ, Woolrich MW, Smith SM. FSL. *Neuroimage*. 2012;62(2):782-790. doi:10.1016/J.NEUROIMAGE.2011.09.015

180. Garyfallidis E, Brett M, Amirbekian B, et al. Dipy, a library for the analysis of diffusion MRI data. *Front Neuroinform*. 2014;8(FEB):8. doi:10.3389/FNINF.2014.00008

181. Sudre CH, Gomez Anson B, Davagnanam I, et al. Bullseye's representation of cerebral white matter hyperintensities. *J Neuroradiol*. 2018;45(2):114-122. doi:10.1016/J.NEURAD.2017.10.001

182. Jiménez-Balado J, Corlier F, Habeck C, Stern Y, Eich T. Effects of white matter hyperintensities distribution and clustering on late-life cognitive impairment. *Sci Reports 2022 121*. 2022;12(1):1-13. doi:10.1038/s41598-022-06019-8

183. Xie L, Wisse LEM, Pluta J, et al. Automated segmentation of medial temporal lobe subregions on in vivo T1-weighted MRI in early stages of Alzheimer's disease. *Hum Brain Mapp*. 2019;40(12):3431. doi:10.1002/HBM.24607

184. Xie L, Wisse LEM, Das SR, et al. Accounting for the Confound of Meninges in Segmenting Entorhinal and Perirhinal Cortices in T1-Weighted MRI. *Med Image Comput Comput Assist Interv*. 2016;9901:564. doi:10.1007/978-3-319-46723-8_65

185. Yushkevich PA, Xie L, Wisse LE, et al. Mapping Medial Temporal Lobe Longitudinal Change in Preclinical Alzheimer's Disease. *Alzheimer's Dement*. 2023;19(S17):e079381. doi:10.1002/ALZ.079381

186. Yushkevich PA, Ittyerah R, Li Y, et al. Morphometry of medial temporal lobe subregions using high-resolution T2-weighted MRI in ADNI3: Why, how, and what's next? *Alzheimer's Dement*. 2024;20(11):8113-8128. doi:10.1002/ALZ.14161;WEBSITE:WEBSITE:ALZ-JOURNALS;ISSUE:ISSUE:DOI

187. Huntenburg JM, Steele CJ, Bazin PL. Nighres: processing tools for high-resolution neuroimaging. *Gigascience*. 2018;7(7). doi:10.1093/GIGASCIENCE/GIY082

188. Han X, Pham DL, Tosun D, Rettmann ME, Xu C, Prince JL. CRUISE: Cortical reconstruction using implicit surface evolution. *Neuroimage*. 2004;23(3):997-1012. doi:10.1016/j.neuroimage.2004.06.043

189. Canada KL, Saifullah S, Gardner JC, et al. Development and validation of a quality control procedure for automatic segmentation of hippocampal subfields. *Hippocampus*. 2023;33(9):1048-1057. doi:10.1002/HIPO.23552

190. Avants BB, Tustison NJ, Song G, Cook PA, Klein A, Gee JC. A reproducible evaluation of ANTs similarity metric performance in brain image registration. *Neuroimage*. 2011;54(3):2033-2044. doi:10.1016/J.NEUROIMAGE.2010.09.025

191. Schmidt P. Bayesian inference for structured additive regression models for large-scale problems with applications to medical imaging. Published 2017. Accessed April 16, 2022. https://edoc.ub.uni-muenchen.de/20373/

192. Schmidt P, Pongratz V, Küster P, et al. Automated segmentation of changes in FLAIR-hyperintense white matter lesions in multiple sclerosis on serial magnetic resonance imaging. *NeuroImage Clin*. 2019;23:101849. doi:10.1016/J.NICL.2019.101849

193. Yushkevich PA, Piven J, Hazlett HC, et al. User-guided 3D active contour segmentation of anatomical structures: Significantly improved efficiency and reliability. *Neuroimage*. 2006;31(3):1116-1128. doi:10.1016/J.NEUROIMAGE.2006.01.015

194. Vanderstichele HMJ, Janelidze S, Demeyer L, et al. Optimized

Standard Operating Procedures for the Analysis of Cerebrospinal Fluid Aβ42 and the Ratios of Aβ Isoforms Using Low Protein Binding Tubes. *J Alzheimers Dis*. 2016;53(3):1121–1132. doi:10.3233/JAD-160286

195. Del Campo M, Mollenhauer B, Bertolotto A, et al. Recommendations to standardize preanalytical confounding factors in Alzheimer's and Parkinson's disease cerebrospinal fluid biomarkers: an update. *Biomark Med*. 2012;6(4):419–430. doi:10.2217/BMM.12.46

196. Fortin JP, Parker D, Tunç B, et al. Harmonization of multi-site diffusion tensor imaging data. *Neuroimage*. 2017;161:149–170. doi:10.1016/J.NEUROIMAGE.2017.08.047

197. Subirana I, Sanz H, Vila J. Building Bivariate Tables: The compareGroups Package for R. *J Stat Softw*. 2014;57(12):1–16. doi:10.18637/JSS.V057.I12

198. Benejam B, Aranha MR, Videla L, et al. Neural correlates of episodic memory in adults with Down syndrome and Alzheimer's disease. *Alzheimers Res Ther*. 2022;14(1). doi:10.1186/S13195-022-01064-X

199. Braak H, Thal DR, Ghebremedhin E, Del Tredici K. Stages of the pathologic process in Alzheimer disease: age categories from 1 to 100 years. *J Neuropathol Exp Neurol*. 2011;70(11):960–969. doi:10.1097/NEN.0B013E318232A379

200. Kennedy JT, Wisch JK, Boerwinkle AH, et al. Brain volume trajectories in Down syndrome and autosomal dominant Alzheimer's disease. *Alzheimers Dement*. 2026;22(1). doi:10.1002/ALZ.71103

201. De Groot M, Verhaaren BFJ, De Boer R, et al. Changes in normal-appearing white matter precede development of white matter lesions. *Stroke*. 2013;44(4):1037–1042. doi:10.1161/STROKEAHA.112.680223

202. Maillard P, Fletcher E, Harvey D, et al. White Matter Hyperintensity Penumbra. *Stroke*. 2011;42(7):1917–1922. doi:10.1161/STROKEAHA.110.609768

203. Wardlaw JM, Valdés Hernández MC, Muñoz-Maniega S. What are White Matter Hyperintensities Made of?: Relevance to Vascular Cognitive Impairment. *J Am Hear Assoc Cardiovasc Cerebrovasc Dis*. 2015;4(6):001140. doi:10.1161/JAHA.114.001140

204. van Leijsen EMC, de Leeuw FE, Tuladhar AM. Disease progression and regression in sporadic small vessel disease-insights from neuroimaging. *Clin Sci*. 2017;131(12):1191–1206. doi:10.1042/CS20160384,

205. Maillard P, Fletcher E, Lockhart SN, et al. White matter hyperintensities and their penumbra lie along a continuum of injury in the aging brain. *Stroke*. 2014;45(6):1721–1726. doi:10.1161/STROKEAHA.113.004084

206. Van Leijsen EMC, Bergkamp MI, Van Uden IWM, et al. Progression of White Matter Hyperintensities Preceded by Heterogeneous Decline of Microstructural Integrity. *Stroke*. 2018;49(6):1386–1393. doi:10.1161/STROKEAHA.118.020980

207. Ferretti MT, Iulita MF, Cavedo E, et al. Sex differences in Alzheimer disease - the gateway to precision medicine. *Nat Rev Neurol*. 2018;14(8):457–469. doi:10.1038/S41582-018-0032-9

208. Buckley RF, Mormino EC, Rabin JS, et al. Sex Differences in the Association of Global Amyloid and Regional Tau Deposition Measured by Positron Emission Tomography in Clinically Normal Older Adults. *JAMA Neurol*. 2019;76(5):542–551. doi:10.1001/JAMANEUROL.2018.4693

209. Fatemi F, Kantarci K, Graff-Radford J, et al. Sex differences in cerebrovascular pathologies on FLAIR in cognitively unimpaired elderly. *Neurology*. 2018;90(6):e466–e473. doi:10.1212/WNL.0000000000004913;PAGE:STRING:ARTICLE/CHAPTER

210. Sachdev PS, Parslow R, Wen W, Anstey KJ, Easteal S. Sex differences in the causes and consequences of white matter hyperintensities. *Neurobiol Aging*. 2009;30(6):946–956. doi:10.1016/j.neurobiolaging.2007.08.023

211. Peterson A, Sathe A, Zaras D, et al. Sex and APOE ϵ4 allele differences in longitudinal white matter microstructure in multiple cohorts of aging and Alzheimer's disease. *Alzheimers Dement*. 2025;21(1). doi:10.1002/ALZ.14343

212. Cox SR, Ritchie SJ, Tucker-Drob EM, et al. Ageing and brain white matter structure in 3,513 UK Biobank participants. *Nat Commun*. 2016;7. doi:10.1038/NCOMMS13629

213. Beaudet G, Tsuchida A, Petit L, et al. Age-Related Changes of Peak Width Skeletonized Mean Diffusivity (PSMD) Across the Adult Lifespan: A Multi-Cohort Study. *Front psychiatry*. 2020;11. doi:10.3389/FPSYT.2020.00342

214. Arenaza-Urquijo EM, Boyle R, Casaletto K, et al. Sex and gender differences in cognitive resilience to aging and Alzheimer's disease. *Alzheimer's Dement*. 2024;20(8):5695–5719. doi:10.1002/ALZ.13844;WEBSITE:WEBSITE:ALZ-JOURNALS;WGROUP:STRING:PUBLICATION

215. Briceno Silva G, Arvelaez Pascucci J, Karim H, et al. Influence of the Onset of Menopause on the Risk of Developing Alzheimer's Disease. *Cureus*. 2024;16(9). doi:10.7759/CUREUS.69124

216. Mosconi L, Berti V, Quinn C, et al. Sex differences in Alzheimer risk: Brain imaging of endocrine vs chronologic aging. *Neurology*. 2017;89(13):1382–1390. doi:10.1212/WNL.0000000000004425

217. Deming Y, Dumitrescu L, Barnes LL, et al. Sex-specific genetic predictors of Alzheimer's disease biomarkers. *Acta Neuropathol*. 2018;136(6):857–872. doi:10.1007/S00401-018-1881-4

218. Iulita MF, Bejanin A, Vilaplana E, et al. Association of biological sex with clinical outcomes and biomarkers of Alzheimer's disease in adults with Down syndrome. *Brain Commun*. 2023;5(2):14. doi:10.1093/BRAINCOMMS/FCAD074

219. Rozalem Aranha M, Montal V, van den Brink H, et al. Cortical microinfarcts in adults with Down syndrome assessed with 3T-MRI. *Alzheimers Dement*. 2024;20(6):3906–3917. doi:10.1002/ALZ.13797

220. Cosgrave MP, Tyrrell J, McCarron M, Gill M, Lawlor BA. Age at onset of dementia and age of menopause in women with Down's syndrome. *J Intellect Disabil Res*. 1999;43 (Pt 6)(6):461–465. doi:10.1046/J.1365-2788.1999.00192.X

221. Amtul Z, Wang L, Westaway D, Rozmahel RF. Neuroprotective mechanism conferred by 17beta-estradiol on the biochemical basis of Alzheimer's disease. *Neuroscience*. 2010;169(2):781–786. doi:10.1016/j.neuroscience.2010.05.031

222. Schworer EK, Zammit MD, Handen BL, et al. Lifestyle Composite and Resilience to Alzheimer's Disease Pathology in Down Syndrome. *J Appl Res Intellect Disabil*. 2025;38(4):e70109. doi:10.1111/JAR.70109

223. Tai LM, Thomas R, Marottoli FM, et al. The Role of APOE in Cerebrovascular Dysfunction. *Acta Neuropathol*. 2016;131(5):709. doi:10.1007/S00401-016-1547-Z

224. Rojas S, Brugulat-Serrat A, Bargalló N, et al. Higher prevalence of cerebral white matter hyperintensities inhomozygous APOE-ε4 allele carriers aged 45-75: Results from theALFA study. *J Cereb Blood Flow Metab*. 2018;38(2):250. doi:10.1177/0271678X17707397

225. Sudre CH, Cardoso MJ, Frost C, et al. APOE ϵ4 status is associated with white matter hyperintensities volume accumulation rate independent of AD diagnosis. *Neurobiol Aging*. 2017;53:67-75. doi:10.1016/j.neurobiolaging.2017.01.014

226. Operto G, Cacciaglia R, Grau-Rivera O, et al. White matter microstructure is altered in cognitively normal middle-aged APOE-ϵ4 homozygotes. *Alzheimers Res Ther*. 2018;10(1). doi:10.1186/S13195-018-0375-X

227. Heise V, Filippini N, Ebmeier KP, MacKay CE. The APOE ε4 allele modulates brain white matter integrity in healthy adults. *Mol Psychiatry*. 2011;16(9):908-916. doi:10.1038/MP.2010.90

228. Persson J, Lind J, Larsson A, et al. Altered brain white matter integrity in healthy carriers of the APOE epsilon4 allele: a risk for AD? *Neurology*. 2006;66(7):1029-1033. doi:10.1212/01.WNL.0000204180.25361.48

229. Habes M, Erus G, Toledo JB, et al. White matter hyperintensities and imaging patterns of brain ageing in the general population. *Brain*. 2016;139(4):1164. doi:10.1093/BRAIN/AWW008

230. Kumar D, Yatawara C, Wang B, et al. APOE4 and Confluent White Matter Hyperintensities Have a Synergistic Effect on Episodic Memory Impairment in Prodromal Dementia. *J Alzheimer's Dis*. 2022;87(3):1103-1114. doi:10.3233/JAD-215556

231. Slattery CF, Zhang J, Paterson RW, et al. ApoE influences regional white-matter axonal density loss in Alzheimer's disease. *Neurobiol Aging*. 2017;57:8. doi:10.1016/J.NEUROBIOLAGING.2017.04.021

232. Hithersay R, Startin CM, Hamburg S, et al. Association of Dementia With Mortality Among Adults With Down Syndrome Older Than 35 Years. *JAMA Neurol*. 2019;76(2):152-160. doi:10.1001/JAMANEUROL.2018.3616

233. Martini AC, Gross TJ, Head E, Mapstone M. Beyond amyloid: Immune, cerebrovascular, and metabolic contributions to Alzheimer disease in people with Down syndrome. *Neuron*. 2022;110(13):2063-2079. doi:10.1016/j.neuron.2022.04.001

234. Sullivan KD, Evans D, Pandey A, et al. Trisomy 21 causes changes in the circulating proteome indicative of chronic autoinflammation. *Sci Rep*. 2017;7(1). doi:10.1038/S41598-017-13858-3

235. Wilcock DM, Hurban J, Helman AM, et al. Down syndrome individuals with Alzheimer's disease have a distinct neuroinflammatory phenotype compared to sporadic Alzheimer's disease. *Neurobiol Aging*. 2015;36(9):2468-2474. doi:10.1016/J.NEUROBIOLAGING.2015.05.016

236. Brickman AM, Rizvi B. White matter hyperintensities and Alzheimer's disease: An alternative view of an alternative hypothesis. *Alzheimer's Dement*. 2023;19(9):4260-4261. doi:10.1002/ALZ.13371

237. Peng L, Baradar AA, Aguado J, Wolvetang E. Cellular senescence and premature aging in Down Syndrome. *Mech Ageing Dev*. 2023;212. doi:10.1016/J.MAD.2023.111824

238. Horvath S, Garagnani P, Bacalini MG, et al. Accelerated epigenetic aging in Down syndrome. *Aging Cell*. 2015;14(3):491-495. doi:10.1111/ACEL.12325

239. Garnier-Crussard A, Cotton F, Krolak-Salmon P, Chételat G. White matter hyperintensities in Alzheimer's disease: Beyond vascular contribution. *Alzheimer's Dement*. Published online 2023. doi:10.1002/ALZ.13057

240. Bozzali M, Falini A, Franceschi M, et al. White matter damage in Alzheimer's disease assessed in vivo using diffusion tensor magnetic resonance imaging. *J Neurol Neurosurg Psychiatry*. 2002;72(6):742. doi:10.1136/JNNP.72.6.742

241. McAleese KE, Firbank M, Dey M, et al. Cortical tau load is associated with white matter hyperintensities. Published online 2015. doi:10.1186/s40478-015-0240-0

242. McAleese KE, Walker L, Graham S, et al. Parietal white matter lesions in Alzheimer's disease are associated with cortical neurodegenerative pathology, but not with small vessel disease. *Acta Neuropathol*. 2017;134(3):459-473. doi:10.1007/S00401-017-1738-2/FIGURES/5

243. Mayo CD, Garcia-Barrera MA, Mazerolle EL, Ritchie LJ, Fisk JD, Gawryluk JR. Relationship Between DTI Metrics and Cognitive Function in Alzheimer's Disease. *Front Aging Neurosci*. 2019;10(JAN). doi:10.3389/FNAGI.2018.00436

244. Thanprasertsuk S, Martinez-Ramirez S, Pontes-Neto OM, et al. Posterior white matter disease distribution as a predictor of amyloid angiopathy. *Neurology*. 2014;83(9):794-800. doi:10.1212/WNL.0000000000000732

245. Charidimou A, Boulouis G, Frosch MP, et al. The Boston criteria version 2.0 for cerebral amyloid angiopathy: a multicentre, retrospective, MRI-neuropathology diagnostic accuracy study. *Lancet Neurol*. 2022;21(8):714-725. doi:10.1016/S1474-4422(22)00208-3

246. Flores-Aguilar L, Iulita MF, Kovecses O, et al. Evolution of neuroinflammation across the lifespan of individuals with Down syndrome. *Brain*. 2020;143(12):3653-3671. doi:10.1093/BRAIN/AWAA326

247. Grinberg LT, Korczyn AD, Heinsen H. Cerebral amyloid angiopathy impact on endothelium. *Exp Gerontol*. 2012;47(11):838-842. doi:10.1016/j.exger.2012.08.005

248. de Souza A, Tasker K. Inflammatory Cerebral Amyloid Angiopathy: A Broad Clinical Spectrum. *J Clin Neurol*. 2023;19(3):230-241. doi:10.3988/JCN.2022.0493

249. Aranha MR, Fortea J, Carmona-Iragui M. Cerebral Amyloid Angiopathy-Related Inflammation in Down Syndrome-Related Alzheimer Disease. *Neurology*. 2022;98(24):1021-1022. doi:10.1212/WNL.0000000000200704,

250. Fagundes TP, Alves GM, Favaro MG, et al. Probable cerebral amyloid angiopathy - related inflammation in a 32-year-old woman with down syndrome. *Neurogenetics*. 2026;27(1). doi:10.1007/S10048-026-00883-6

251. Sullivan KD, Lewis HC, Hill AA, et al. Trisomy 21 consistently activates the interferon response. *Elife*. 2016;5(JULY). doi:10.7554/ELIFE.16220

252. Araya P, Waugh KA, Sullivan KD, et al. Trisomy 21 dysregulates T cell lineages toward an autoimmunity-prone state associated with interferon hyperactivity. *Proc Natl Acad Sci U S A*. 2019;116(48):24231-24241. doi:10.1073/PNAS.1908129116/-/DCSUPPLEMENTAL

253. Franquesa-Mullerat M, Morcillo-Nieto AO, Arriola-Infante JE, et al. Study of brain perfusion in adults with Down syndrome along the Alzheimer's disease continuum. *Alzheimers Dement*. 2025;21(9). doi:10.1002/ALZ.70581

254. Laing KK, Simoes S, Baena-Caldas GP, et al. Cerebrovascular disease promotes tau pathology in Alzheimer's disease. *Brain Commun*. 2020;2(2). doi:10.1093/BRAINCOMMS/FCAA132

255. Sachdev PS, Zhuang L, Braidy N, Wen W. Is Alzheimer's a disease of the white matter? *Curr Opin Psychiatry*. 2013;26(3):244-251. doi:10.1097/YCO.0B013E32835ED6E8

256. Wisse LEM, La Joie R. Medial temporal lobe structural changes when Down syndrome and Alzheimer's disease collide. *Brain*. 2025;148(7):2235-2237. doi:10.1093/BRAIN/AWAF176

257. Fortea J, Sala-Llonch R, Bartrés-Faz D, et al. Increased cortical thickness and caudate volume precede atrophy in PSEN1 mutation carriers. *J Alzheimers Dis*. 2010;22(3):909-922. doi:10.3233/JAD-2010-100678

258. Montal V, Vilaplana E, Pegueroles J, et al. Biphasic cortical macro- and microstructural changes in autosomal dominant Alzheimer's disease. *Alzheimers Dement*. 2021;17(4):618-628. doi:10.1002/ALZ.12224

259. Chauveau L, Kuhn E, Palix C, et al. Medial Temporal Lobe Subregional Atrophy in Aging and Alzheimer's Disease: A Longitudinal Study. *Front Aging Neurosci*. 2021;13. doi:10.3389/FNAGI.2021.750154/PDF

260. Pegueroles J, Vilaplana E, Montal V, et al. Longitudinal brain structural changes in preclinical Alzheimer's disease. *Alzheimers Dement*. 2017;13(5):499-509. doi:10.1016/J.JALZ.2016.08.010

261. Montal V, Vilaplana E, Alcolea D, et al. Cortical microstructural changes along the Alzheimer's disease continuum. *Alzheimers Dement*. 2018;14(3):340-351. doi:10.1016/J.JALZ.2017.09.013

262. Iulita MF, Diana ;, Chavez G, et al. Association of Alzheimer Disease With Life Expectancy in People With Down Syndrome. *JAMA Netw Open*. 2022;5(5):e2212910-e2212910. doi:10.1001/JAMANETWORKOPEN.2022.12910

263. Prins ND, Scheltens P. White matter hyperintensities, cognitive impairment and dementia: an update. *Nat Rev Neurol 2015 113*. 2015;11(3):157-165. doi:10.1038/nrneurol.2015.10

264. Barroeta I, Videla L, Carmona-Iragui M, Fortea J, Rafii MS. Current advances and unmet needs in Alzheimer's disease trials for individuals with Down syndrome: Navigating new therapeutic frontiers. *Alzheimer's Dement*. 2025;21(6). doi:10.1002/ALZ.70258,

ANNEXES

Supplementary Material

S.1 MRI acquisition parameters

Supplementary Table 1: 3T T1-weighted protocols.

	3T Philips - Achieva (Hospital del Mar – Barcelona, Spain)	**3T Siemens - Prisma fit (Hospital Clinic - Barcelona, Spain)**	
		Protocol 1	Protocol 2
	T1-weighted, n = 290	T1-weighted, n = 67	T1-weighted, n = 40
Echo Time (ms)	3.8	2.98	2.96
Repetition Time (ms)	8.2	2300	2300
Flip Angle	8	9	9
Number of Slices	160	240	208
Slice Thickness (mm)	1	1	1
Field of View (mm²)	256x256	256x256	256x256
Voxel Resolution (mm)	0.94x0.94x1	1x1x1	1x1x1

S.2 Automatic Segmentation of Hippocampal Subfields

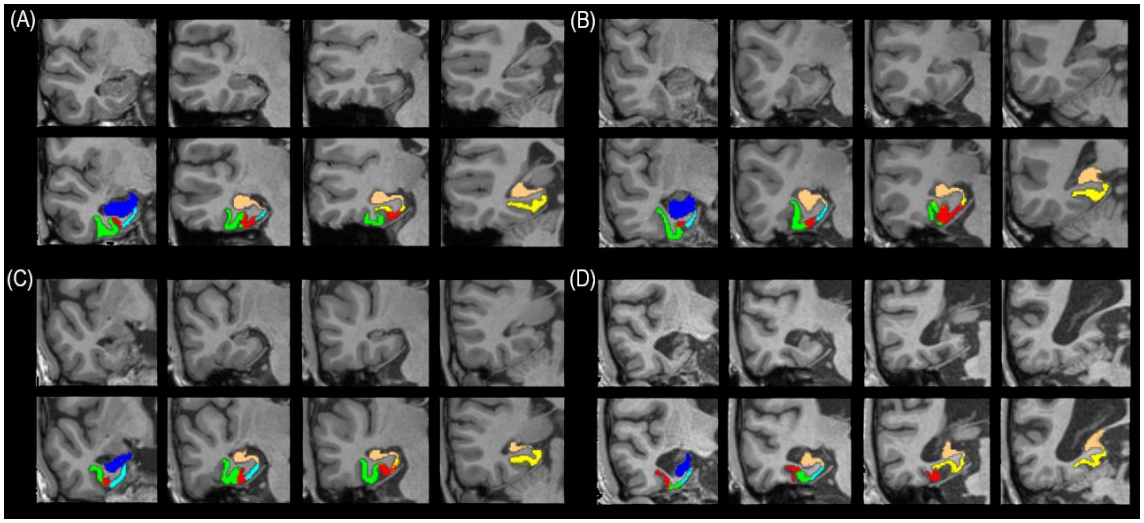

Supplementary Figure 1. Example of Automatic Segmentation of Hippocampal Subfields. Coronal slices ofT1w images of **(A)** 33-year-old HC female and APOE ε4 non-carrier, **(B)** 32-year-old DS male, asymptomatic and APOE ε4 non-carrier, **(C)** 50-year-old DS male, prodromal AD and APOEε4 non-carrier, and **(D)** 57-year-old DS male with AD dementia and APOE ε4 carrier. Colours correspond to the different regions of the medial temporal lobe: dark blue: Anterior Hippocampus, nude: Posterior Hippocampus, yellow: Parahippocampal Cortex, light blue: Entorhinal Cortex, red: Brodmann Area 35, and green: Brodmann Area 36.

S.3 Sample size per genetic and CSF biomarker

Supplementary Table 2: Sample size across Alzheimer's disease clinical diagnosis.

	HC N=138	**aDS N=149**	**pDS N=41**	**dDS N=69**
APOE haplotype	137	143	39	69
CAMCOG-DS	0	119	31	49
CSF biomarkers				
Aβ42/Aβ40	89	78	31	45
pTau181	89	78	31	45
NfL	96	76	29	39

Abbreviations: APOE: apolipoprotein E; CAMCOG-DS: Cambridge Cognitive Examination for Older Adults with Down Syndrome; DS: Down syndrome; aDS: asymptomatic DS; pDS: prodromal DS; dDS: DS with Alzheimer's dementia; HC: Healthy/Euploid Controls; Aβ42/Aβ40: concentration ratio between Amyloid β peptide 1-42 and Amyloid β peptide 1-40 (pg/mL); pTau181: Tau phosphorylated at threonine 181 concentration (pg/mL); NfL: Neurofilament Light chain concentration (pg/mL).

S.4 Medial Temporal Lobe volume/thickness along the Alzheimer's disease clinical continuum

S.4.1 Regional differences

Supplementary Table 3: Regional differences of medial temporal lobe regions across the Alzheimer's disease continuum.

ROI	Comparison	Statistical estimate	p-value	Effect Size
Anterior Hippocampus (vol)	Global	F(3,393) = 79.741	<0.001[a]	
Anterior Hippocampus (vol)	HC vs aDS	-0.866 [-1.160; -0.572]	<0.001[b]	0.919
Anterior Hippocampus (vol)	HC vs pDS	-1.312[-1.755; -0.869]	<0.001[b]	1.269
Anterior Hippocampus (vol)	HC vs dDS	-2.138 [-2.505; -1.771]	<0.001[b]	2.131
Anterior Hippocampus (vol)	aDS vs pDS	-0.446 [-0.885; -0.007]	0.045[b]	0.456
Anterior Hippocampus (vol)	aDS vs dDS	-1.271 [-1.634; -0.909]	<0.001[b]	1.345
Anterior Hippocampus (vol)	pDS vs dDS	-0.826 [-1.317; -0.335]	<0.001[b]	0.796
Posterior Hippocampus (vol)	Global	F(3,393) = 146.162	<0.001[a]	
Posterior Hippocampus (vol)	HC vs aDS	-0.972 [-1.284; -0.66]	<0.001[b]	0.99
Posterior Hippocampus (vol)	HC vs pDS	-2.209 [-2.679; -1.74]	<0.001[b]	1.977
Posterior Hippocampus (vol)	HC vs dDS	-2.961 [-3.35; -2.572]	<0.001[b]	2.87
Posterior Hippocampus (vol)	aDS vs pDS	-1.237 [-1.702; -0.772]	<0.001[b]	1.123
Posterior Hippocampus (vol)	aDS vs dDS	-1.989 [-2.373; -1.605]	<0.001[b]	1.961
Posterior Hippocampus (vol)	pDS vs dDS	-0.752 [-1.272; -0.231]	0.001[b]	0.656
ERC (thick)	Global	F(3,393) = 16.024	<0.001[a]	
ERC (thick)	HC vs aDS	0.871 [0.449; 1.292]	<0.001	-0.681
ERC (thick)	HC vs pDS	0.589 [-0.045; 1.224]	0.08[b]	-0.465
ERC (thick)	HC vs dDS	-0.336 [-0.863; 0.19]	0.352[b]	0.244
ERC (thick)	aDS vs pDS	-0.281 [-0.911; 0.348]	0.657[b]	0.188
ERC (thick)	aDS vs dDS	-1.207 [-1.727; -0.687]	<0.001[b]	0.758
ERC (thick)	pDS vs dDS	-0.926 [-1.63; -0.222]	0.004[b]	0.585
ERC (vol)	Global	F(3,393) = 22.157	<0.001[a]	
ERC (vol)	HC vs aDS	0.653 [0.277; 1.03]	<0.001[b]	-0.576
ERC (vol)	HC vs pDS	0.249 [-0.318; 0.816]	0.669[b]	-0.208
ERC (vol)	HC vs dDS	-0.785 [-1.255; -0.315]	<0.001[b]	0.612
ERC (vol)	aDS vs pDS	-0.404 [-0.966; 0.158]	0.249[b]	0.309
ERC (vol)	aDS vs dDS	-1.438 [-1.902; -0.974]	<0.001[b]	1.035
ERC (vol)	pDS vs dDS	-1.034 [-1.662; -0.405]	<0.001[b]	0.717
PHC (thick)	Global	F(3,393) = 48.565	<0.001[a]	
PHC (thick)	HC vs aDS	1.558 [1.21; 1.905]	<0.001[b]	0.615
PHC (thick)	HC vs pDS	1.398 [0.875; 1.921]	<0.001[b]	0.458

PHC (thick)	HC vs dDS	0.656 [0.223; 1.09]	<0.001[b]	0.264
PHC (thick)	aDS vs pDS	-0.16 [-0.678; 0.359]	0.857[b]	-0.058
PHC (thick)	aDS vs dDS	-0.901 [-1.33; -0.473]	<0.001[b]	-0.311
PHC (thick)	pDS vs dDS	-0.742 [-1.321; -0.162]	0.006[b]	-0.255
PHC (vol)	Global	F(3,393) = 72.857	<0.00 [b]1[a]	
PHC (vol)	HC vs aDS	2.154 [1.767; 2.54]	<0.001[b]	-1.851
PHC (vol)	HC vs pDS	1.713 [1.131; 2.294]	<0.001[b]	-1.49
PHC (vol)	HC vs dDS	0.869 [0.387; 1.351]	<0.001[b]	-0.65
PHC (vol)	aDS vs pDS	-0.441 [-1.017; -0.136]	0.2[b]	0.341
PHC (vol)	aDS vs dDS	-1.284 [-1.76; -0.808]	<0.001[b]	0.877
PHC (vol)	pDS vs dDS	-0.843 [-1.488; -0.199]	0.005[b]	0.58
Br35 (thick)	Global	F(3,393) = 22.404	<0.001[a]	
Br35 (thick)	HC vs aDS	0.963 [0.564; 1.361]	<0.001[b]	-0.889
Br35 (thick)	HC vs pDS	0.6 [0.001; 1.2]	0.049[b]	-0.439
Br35 (thick)	HC vs dDS	-0.405 [-0.903; 0.092]	0.153[b]	0.276
Br35 (thick)	aDS vs pDS	-0.362 [-0.957; 0.232]	0.396[b]	0.253
Br35 (thick)	aDS vs dDS	-1.368 [-1.859; -0.877]	<0.001[b]	0.896
Br35 (thick)	pDS vs dDS	-1.005 [-1.671; -0.341]	<0.001[b]	0-578
Br35 (vol)	Global	F(3,393) = 22.284	<0.001[a]	
Br35 (vol)	HC vs aDS	0.988 [0.601; 1.375]	<0.001[b]	-0.835
Br35 (vol)	HC vs pDS	0.672 [0.089; 1.255]	0.017[b]	-0.517
Br35 (vol)	HC vs dDS	-0.273 [-0.756; 0.210]	0.465[b]	0.223
Br35 (vol)	aDS vs pDS	-0.317 [-0.895; 0.261]	0.492[b]	0.219
Br35 (vol)	aDS vs dDS	-1.261 [-1.738; -0.784]	<0.001[b]	0.916
Br35 (vol)	pDS vs dDS	-0.944 [-1.591; -0.298]	0.001[b]	0.64
Br36 (thick)	Global	F(3,393) = 22.284	<0.001[a]	
Br36 (thick)	HC vs aDS	0.086 [-0.278; 0.45]	0.929[b]	-0.089
Br36 (thick)	HC vs pDS	-0.289 [-0.838; 0.259]	0.525[b]	0.244
Br36 (thick)	HC vs dDS	-1.497 [-1.952; -1.042]	<0.001[b]	1.028
Br36 (thick)	aDS vs pDS	-0.375 [-0.919; 0.168]	0.284[b]	0.323
Br36 (thick)	aDS vs dDS	-1.583 [-2.032; -1.133]	<0.001[b]	1.101
Br36 (thick)	pDS vs dDS	-1.208 [-1.816; -0.599]	<0.001[b]	0.759
Br36 (vol)	Global	F(3,393) = 41.907	<0.001[a]	
Br36 (vol)	HC vs aDS	-0.627 [-0.968; -0.287]	<0.001[b]	0.609
Br36 (vol)	HC vs pDS	-1.174 [-1.687; -0.661]	<0.001[b]	1.022
Br36 (vol)	HC vs dDS	-1.778 [-2.203; -1.352]	<0.001[b]	1.5
Br36 (vol)	aDS vs pDS	-0.546 [-1.055; -0.038]	0.03[b]	0.465
Br36 (vol)	aDS vs dDS	-1.150 [-1.571; -0.730]	<0.001[b]	0.95

Br36 (vol)	pDS vs dDS	-0.604 [-1.173; -0.035]	0.033[b]	0.46

a: Global comparisons were assessed using ANOVA tests followed by b: Tuckey HSD as post hoc analyses. *Abbreviations*: DS: Down syndrome; aDS: asymptomatic DS; pDS: prodromal DS; dDS: DS with Alzheimer's dementia; HC: Healthy/Euploid Controls; Br35: Brodmann Area 35; Br36: Brodmann Area 36; ERC: Entorhinal Cortex; PHC: Parahippocampal Cortex; vol: volume; thick: thickness.

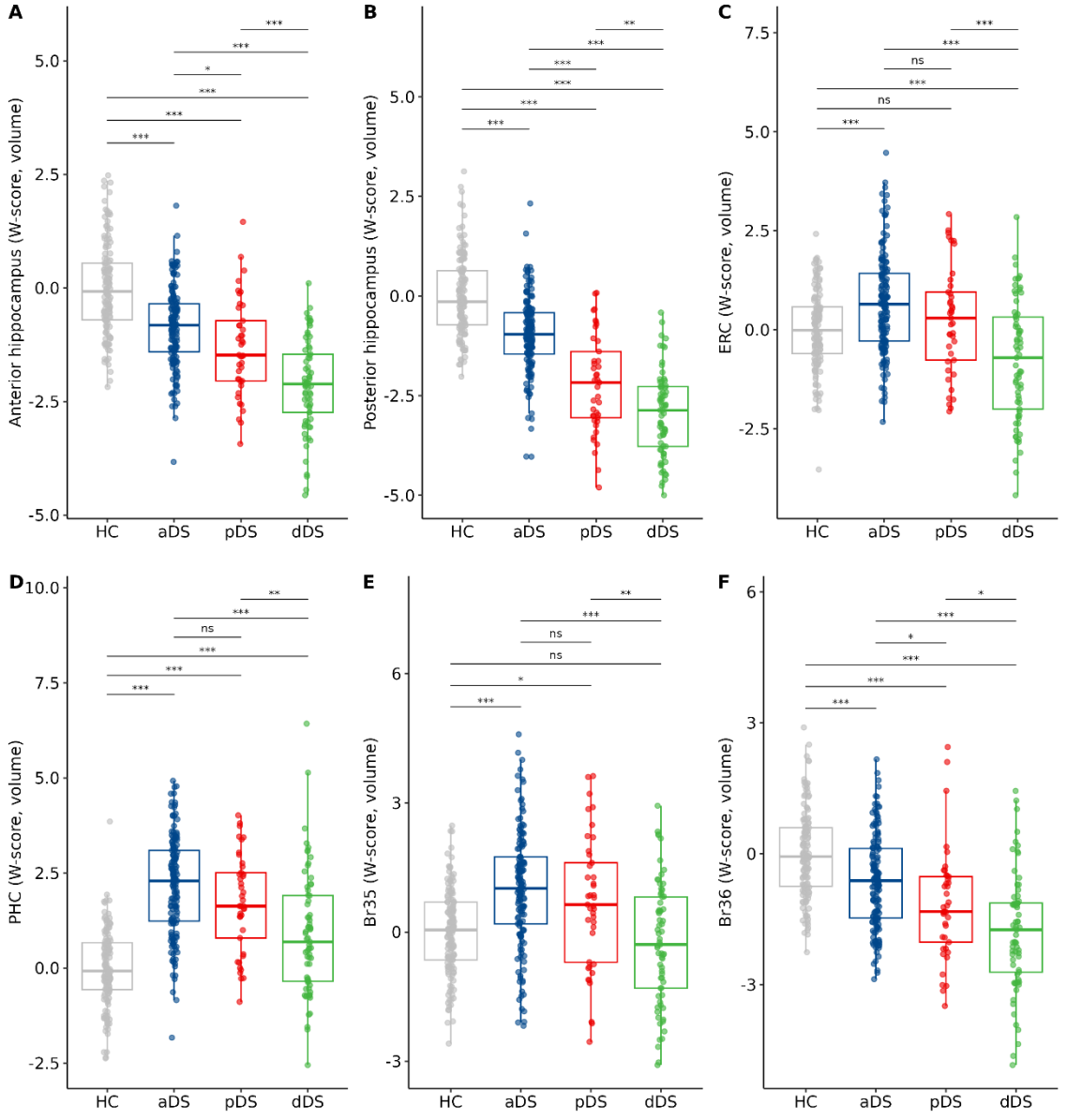

Supplementary Figure 2: Regional volume of medial temporal lobe structures across the Alzheimer's disease continuum.

Boxplots represent the effect of clinical groups on the W-score (age-, sex- and TIV-adjusted volume) of the anterior **(A)** and posterior **(B)** hippocampus, ERC **(C)**, PHC **(D)**, Br35 **(E)**, and Br36 **(F)**. For each boxplot, the box represents the interquartile range, the band represents the median value, and the dots represent individual values. Significance is set at p<0.05 using the Bonferroni correction. *Abbreviations*: ns: no significance; *: p<0.05; **: p<0.01; ***: p<0.001; DS: Down syndrome; aDS: asymptomatic DS; pDS: prodromal DS; dDS: DS with Alzheimer's dementia; HC: Healthy/Euploid Controls; Br35: Brodmann Area 35; Br36: Brodmann Area 36; ERC: Entorhinal Cortex; PHC: Parahippocampal Cortex.

S.5 Medial Temporal Lobe volume changes with EYO

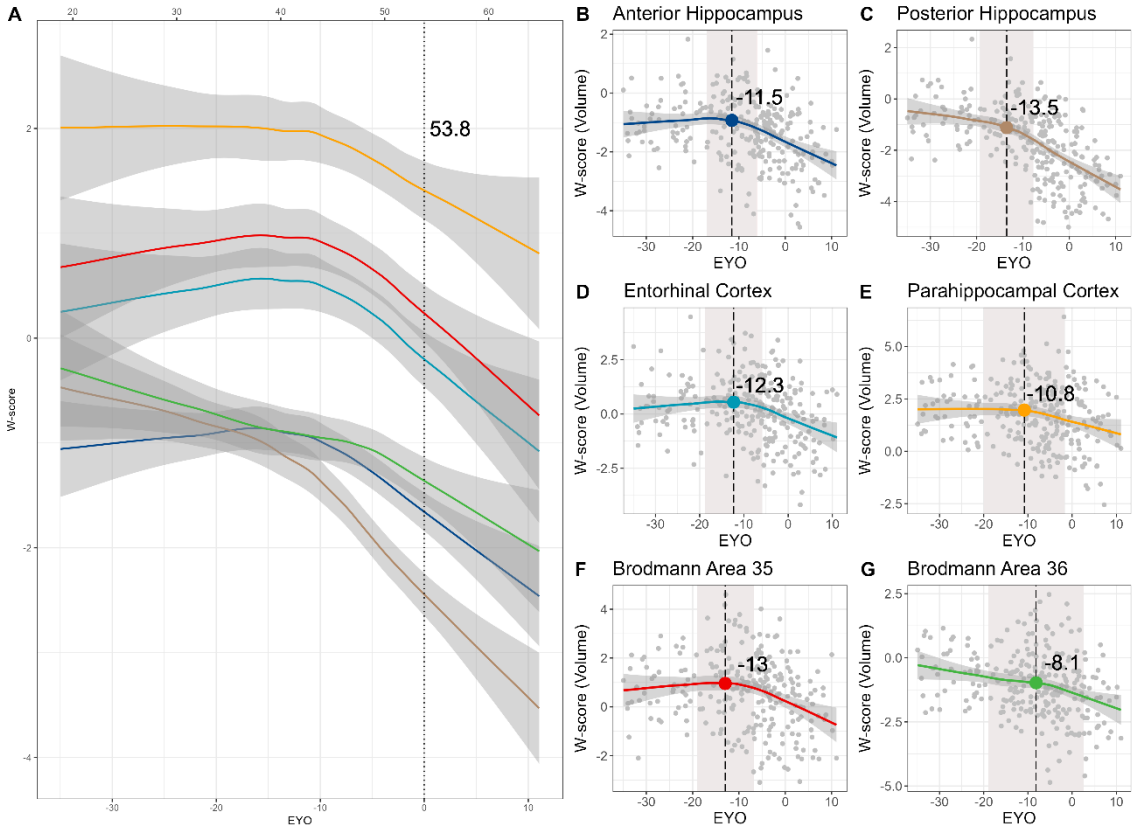

Supplementary Figure 3: Regional volume of medial temporal lobe structures along the estimated age of onset in individuals with Down syndrome.

Line plots represent the relationship between W-scores (age-, sex- and TIV-adjusted volume) of the anterior **(A)** and posterior **(B)** hippocampus, ERC **(C)**, PHC **(D)**, Br35 **(E)**, and Br36 **(F)** against the estimated age of onset (EYO: 53.8 years) of Alzheimer's disease in Down Syndrome. Lines computed using estimated scatterplot smoothing (LOESS) curves. Shaded areas represent the 95% confidence interval. Points represent linear model inflection values, computed against EYO. Colour indicates each region of the medial temporal lobe. *Abbreviations*: EYO: estimated years of onset; DS: Down syndrome; aDS: asymptomatic DS; pDS: prodromal DS; dDS: DS with Alzheimer's dementia; HC: Healthy/Euploid Controls; Br35: Brodmann Area 35; Br36: Brodmann Area 36; ERC: Entorhinal Cortex; PHC: Parahippocampal Cortex.

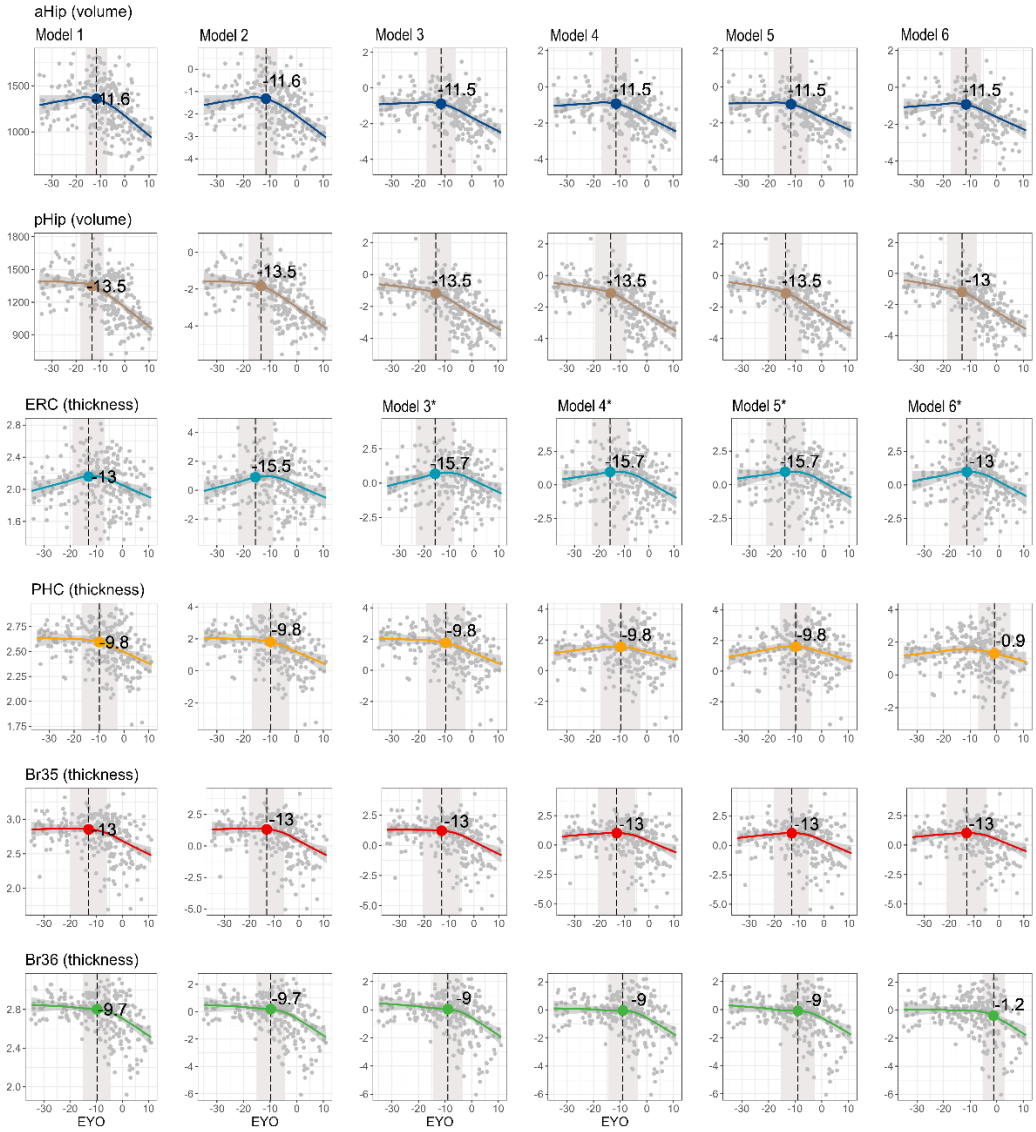

Supplementary Figure 4: Regional volume/cortical thickness of medial temporal lobe structures along the estimated age of onset in individuals with Down syndrome.

Rows represent medial temporal lobe regions while columns show results for six different models applied to analyse the relationship with the estimated age of onset (EYO: 53.8 years) of Alzheimer's disease in Down syndrome. Model 1: raw volume/thickness values extracted from the ASHS segmentation; Model 2: z-scores transformation of the raw values; Model 3: W-score adjusted by sex and ICV; Model 3*: W-scores adjusted by sex; Model 4: W-score adjusted by age, sex and ICV; Model 4*: W-score adjusted by age and sex; Model 5: W-score adjusted by age^2, age, sex and ICV; Model 5*: W-score adjusted by age^2, age and sex; Model 6: W-score adjusted by age, sex, APOEε4 status and ICV; Model 6*: W-score adjusted by age, sex and APOEε4 status. Lines computed using estimated scatterplot smoothing (LOESS) curves. Shaded areas represent the 95% confidence interval. Points represent linear model inflection values, computed against EYO. Colour indicates each region of the medial temporal lobe. *Abbreviations*: EYO: estimated years of onset; DS: Down syndrome; aDS: asymptomatic DS; pDS: prodromal DS; dDS: DS with Alzheimer's dementia; HC: Healthy/Euploid Controls; Br35: Brodmann Area 35; Br36: Brodmann Area 36; ERC: Entorhinal Cortex; PHC: Parahippocampal Cortex; ICV: total intracranial volume (mm^3).

S.6 Relationship of regional volumes with CSF biomarkers of Alzheimer's disease

Supplementary Table 4: Coefficients and p-values of associations between regional volume/thickness of medial temporal lobe structures and CSF AT(N) biomarkers.

	Aβ42/40	pTau181	NfL
aHip (vol)	ρ=0.34; p<0.001	ρ=-0.34; p<0.001	ρ=-0.34; p<0.001
pHip (vol)	ρ=0.55; p<0.001	ρ=0.54; p<0.001	ρ=-0.50; p<0.001
ERC (thick)	ρ=0.13; p=0.112	ρ=-0.17; p=0.034	ρ=-0.16; p=0.058
PHC (thick)	ρ=-0.02; p=0.786	ρ=-0.04; p=0.643	ρ=-0.05; p=0.564
Br35 (thick)	ρ=0.08; p=0.349	ρ=-0.16; p=0.054	ρ=-0.15; p=0.078
Br36 (thick)	ρ=0.14; p=0.075	ρ=-0.15; p=0.057	ρ=-0.23; p=0.006

Abbreviations: aHip: Anterior Hippocampus; pHip: Posterior Hippocampus; ERC: Entorhinal Cortex; PHC: Parahippocampal Cortex; Br35: Brodmann Area 35; Br36: Brodmann Area 36; Aβ42/40: concentration ratio between Amyloid β peptide 1-42 and Amyloid β peptide 1-40 (pg/mL); pTau181: Tau phosphorylated at threonine 181 concentration (pg/mL); NfL: Neurofilament Light chain concentration (pg/mL); vol: volume; thick: thickness.

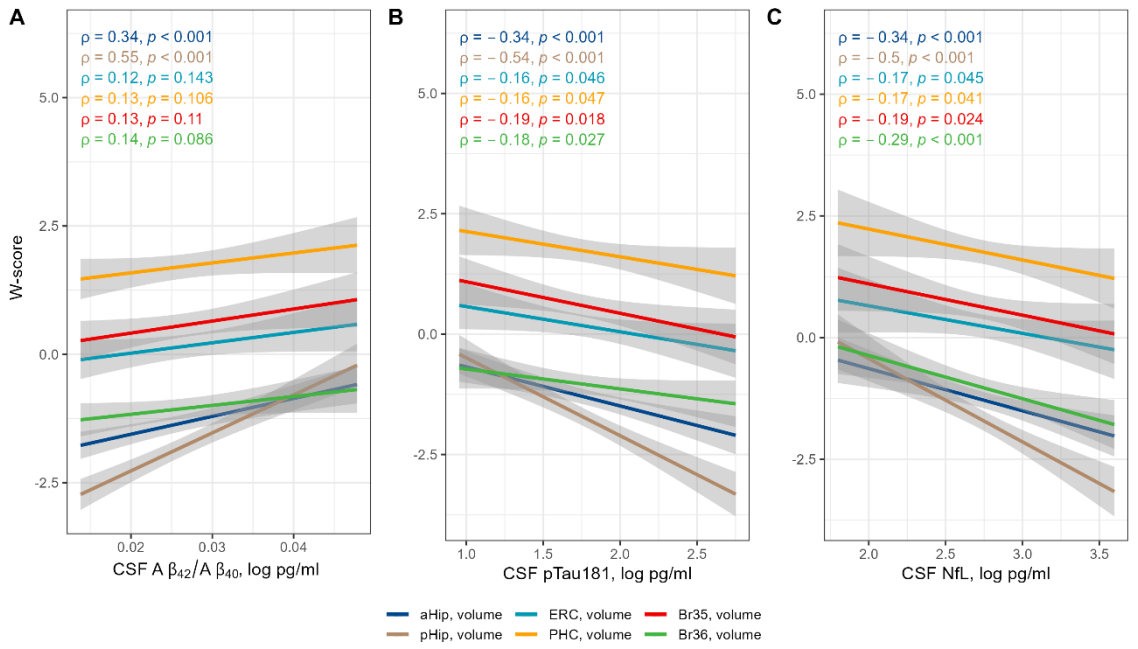

Supplementary Figure 5: Associations between regional volume of medial temporal lobe structures and CSF AT(N) biomarkers.

Correlation between volumes and each corresponding biomarker. Colour indicates each region of the medial temporal lobe. Shaded areas represent 95% confidence interval. *Abbreviations*: ρ: Spearman correlation coefficient; aHip: anterior hippocampus; pHip: posterior hippocampus; ERC: entorhinal cortex; PHC: parahippocampal cortex; Br35: Brodmann area 35; Br36: Brodmann area 36; Aβ42/40: concentration

ratio between Amyloid β peptide 1-42 and Amyloid β peptide 1-40 (pg/mL); pTau181: Tau phosphorylated at threonine 181 concentration (pg/mL); NfL: Neurofilament Light chain concentration (pg/mL). CSF markers are log10 scaled.

S.7 Predicting clinical Alzheimer's disease staging using regional Medial Temporal Lobe volumes/thickness

Supplementary Table 5: Performance of models for the discrimination of asymptomatic from symptomatic individuals with Down syndrome.

Model	**AUC [95%]**
pHip (vol) + PHC (vol) + Age + CSF pTau181	96.35 [93.61; 99.09]
aHip (vol)	74.92 [66.57; 83.26]
pHip (vol)	86.36 [79.99; 92.74]
ERC (thick)	62.70 [53.33; 72.07]
PHC (thick)	58.90 [49.34; 68.47]
Br35 (thick)	66.53 [57.32; 75.74]
Br36 (thick)	67.36 [58.16; 76.55]
CSF Aβ42/Aβ40	90.41 [84.97; 95.85]
CSF pTau181	89.88 [84.68; 95.09]
CSF NfL	88.77 [83.32; 94. 21]

Abbreviations: vol: Volumes; thick: Thickness; aHip: Anterior Hippocampus; pHip: Posterior Hippocampus; ERC: Entorhinal Cortex; PHC: Parahippocampal Cortex; Br35: Brodmann Area 35; Br36: Brodmann Area 36; Aβ42/Aβ40: concentration ratio between Amyloid β peptide 1-42 and Amyloid β peptide 1-40 (pg/mL); pTau181: Tau phosphorylated at threonine 181 concentration (pg/mL); NfL: Neurofilament Light chain concentration (pg/mL). CSF markers are log10 scaled.

Supplementary Table 6: Differences between models for the discrimination of aDS from sDS.

Model 1	**Model 2**	**Estimate (D)**	**p-value**
Model[1]	aHip (vol)	4.848	<0.001
Model[1]	pHip (vol)	2.826	0.005
Model[1]	ERC (thick)	6.720	<0.001
Model[1]	PHC (thick)	7.506	<0.001
Model[1]	Br35 (thick)	6.146	<0.001
Model[1]	Br36 (thick)	6.092	<0.001
Model[1]	CSF Aβ42/Aβ40	1.868	0.062
Model[1]	CSF pTau181	2.155	0.032
Model[1]	CSF NfL	2.440	0.016

*Abbreviation*s: vol: volumes; thick: thickness; Model1: pHip (vol) + PHC (thick) + Age + CSF pTau181; aHip: Anterior Hippocampus; pHip: Posterior Hippocampus; ERC: Entorhinal Cortex; PHC: Parahippocampal Cortex; Br35: Brodmann Area 35; Br36: Brodmann Area 36; Aβ42/Aβ40: concentration ratio between Amyloid β peptide 1-42 and Amyloid β peptide 1-40 (pg/mL); pTau181: Tau phosphorylated at threonine 181 concentration (pg/mL); NfL: Neurofilament Light chain concentration (pg/mL). CSF markers are log10 scaled.

Supplementary Material

S.1 MRI acquisition parameters

***Supplementary Table 1**: 3T T1-weighted and FLAIR acquisition protocols.*

	3T Philips - Achieva (Hospital del Mar – Barcelona, Spain)		**3T Siemens - Prisma fit (Hospital Clinic - Barcelona, Spain)**			
			Protocol 1		Protocol 2	
	T1-weighted	FLAIR	T1-weighted	FLAIR	T1-weighted	FLAIR
Echo Time (ms)	3.8	140	2.98	128	2.96	397
Repetition Time (ms)	8.2	10000	2300	9000	2300	6000
Flip Angle	8	90	9	150	9	120
Number of Slices	160	140	240	45	208	160
Slice Thickness (mm)	1	1	1	1	1	1
Field of View (mm²)	256x256	256x256	256x256	220x220	256x256	256x256
Voxel Resolution (mm)	0.94x0.94x1	0.9x0.9x1	1x1x1	0.9x0.9x3	1x1x1	1x1x1

Abbreviations: FLAIR=Fluid Attenuated Inversion Recovery images.

S.2 White Matter parcellation

S.2.1. White Matter concentric layers

To create an individual map of the white matter (WM) concentric layers, we followed the approach proposed by Jiménez-Balado and colleagues [1] and first computed 2 maps in the native space of the subjects:

- A map representing the distance from each WM voxel to the ventricles. For this, we created a region of interest (ROI) of the lateral and third ventricles using the Hammers atlas [2]. The ROI was multiplied by a mask of cerebrospinal fluid (CSF), using the CSF segmentation from CAT12 (threshold= 0.2). Subsequently, we used the *3dmask_tool* command (from the Analysis of Functional NeuroImages (AFNI) software) to expand the ROI incrementally by 1 mm^3 until the entire WM was covered.
- The second map depicted the distance from WM each voxel to the cortex. For this, we created a ROI of the cortex by adding the cortical ROIs from the Hammers atlas [2]. The ROI was then multiplied by a grey matter mask, resulting in the segmentation of CAT12 (threshold = 0.2). The resulting ROI was expanded by 1 mm^3 increments until covering the entire WM. This consistent expansion ensured a detailed representation of the WM distance from both the ventricles and the cortex.

Then, to compute a normalised distance map for each voxel using the following formula [1]:

$$\frac{Distance\ to\ ventricles_i}{(Distance\ to\ ventricles_i\ +\ Distance\ to\ cortex_i)}$$

The resulting map indicates the distance of each WM voxel to the ventricles, with a value of “0” representing the ventricles and a value of “1” indicating the cortex.

S.2.2. White Matter by lobes

For the lobar regions, we used the anatomical Hammers atlas [2], to label the WM according to the lobes. The corpus callosum was divided into anterior and posterior parts, which were included in the frontal and parietal lobes, respectively. The specific ROIs included for each ROI are as follows:

- Frontal: insula, anterior cingulate gyrus, precentral gyrus, straight gyrus, orbital gyrus, frontal gyrus, subcallosal area, pre-subgenual frontal cortex, and anterior corpus callosum.
- Parietal: posterior cingulate gyrus, angular gyrus, postcentral gyrus, superior parietal gyrus, supramarginal gyrus and posterior corpus callosum.
- Temporal: hippocampus, amygdala, anterior temporal lobe, parahippocampal and ambient gyrus, middle and inferior temporal gyrus, fusiform gyrus, posterior temporal lobes and superior temporal gyrus anterior part.
- Occipital: lingual gyrus, cuneus and lateral remainder occipital lobe.

S.2.3. White Matter parcellation - concentric layers for each lobe

To segment each lobe into 4 concentric layers map of similar volume, we multiplied the normalised distance map by the binary map of the lobe. We then divided the output into four layers, representing specific intervals along the continuum from ventricles to cortex. The first layer comprised voxels with values

greater than 0 and lower or equal to the 25th percentile of the resulting map; the second layer encompassed values greater than the 25th percentile and lower or equal to the 50th percentile; the third layer included values greater than the 50th percentile and lower or equal to the 75th percentile; and the fourth layer consisted of voxels with values greater than the 75th percentile and lower or equal to 1 (Figure S1 C).

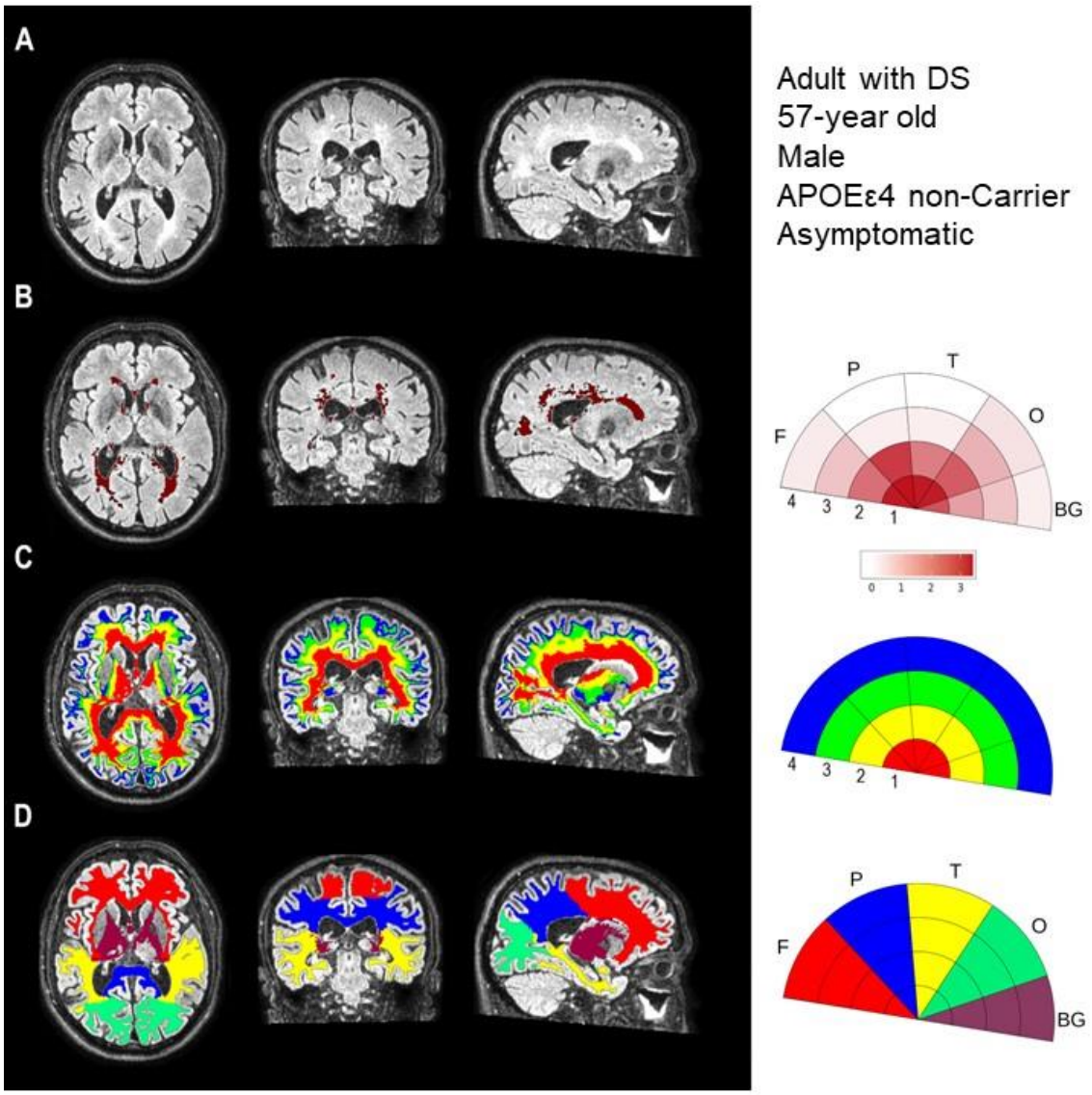

Supplementary Figure 1. *Example of white matter hyperintensity (WMH) segmentation and the bullseye plot representation.*

(A) FLAIR image of a 57-year old DS male, asymptomatic, APOEε4 non-carrier, with ~14000 mm³ of WMHs. (B) WMH segmentation. The WMH segmentation, generated by LPA, is depicted in the left panel. To provide a comprehensive overview of the regional WMH burden, the right panel displays the bullseye plot which integrates both layer and lobar parcellations (total=20 ROIs). Color indicates the WMH volume (log). (C) Concentric layers parcellation. Illustration of the concentric parcellation with four equidistant layers (left panel) and its representation on the bullseye plot (right panel). The layers are named 1 to 4 according to their proximity to the lateral and third ventricles. (D) Lobar parcellations. Illustration of the lobar parcellation (left panel) and its representation on the bullseye plot (right panel). Abbreviation: F: frontal; P: parietal; T: temporal; O: occipital; BG: basal ganglia; 1: first layer; 2: second layer; 3: third layer: 4: fourth layer.

S.3 Association between white matter hyperintensities and age

S.3.1 Regional association

***Supplementary Table 2**: Association between regional white matter hyperintensities and age.*

Diagnosis	Lobe	Layer	rho	p-value
HC	Total	Total	0.36	p<0.001
HC	-	Layer1	0.39	p<0.001
HC	-	Layer2	0.25	p=0.004
HC	-	Layer3	0.21	p=0.018
HC	-	Layer4	0.14	p=0.102
HC	Frontal	-	0.36	p<0.001
HC	Parietal	-	0.31	p<0.001
HC	Temporal	-	0.37	p<0.001
HC	Occipital	-	0.21	p=0.018
HC	Basal Ganglia	-	0.08	p=0.339
HC	Frontal	Layer1	0.35	p<0.001
HC	Frontal	Layer2	0.22	p=0.011
HC	Frontal	Layer3	0.16	p=0.074
HC	Frontal	Layer4	0.09	p=0.305
HC	Parietal	Layer1	0.30	p<0.001
HC	Parietal	Layer2	0.20	p=0.021
HC	Parietal	Layer3	-0.04	p=0.645
HC	Parietal	Layer4	-0.07	p=0.372
HC	Temporal	Layer1	0.36	p<0.001
HC	Temporal	Layer2	0.17	p=0.060
HC	Temporal	Layer3	0.08	p=0.35
HC	Temporal	Layer4	0.10	p=0.24
HC	Basal Ganglia	Layer1	0.08	p=0.338
HC	Basal Ganglia	Layer2	-0.02	p=0.789
HC	Basal Ganglia	Layer3	0.05	p=0.562
HC	Basal Ganglia	Layer4	0.36	p=0.250
DS	Total	Total	0.67	p<0.001
DS	-	Layer1	0.67	p<0.001
DS	-	Layer2	0.60	p<0.001
DS	-	Layer3	0.47	p<0.001

DS	-	Layer 4	0.37	p<0.001
DS	Frontal	-	0.63	p<0.001
DS	Parietal	-	0.63	p<0.001
DS	Temporal	-	0.66	p<0.001
DS	Occipital	-	0.61	p<0.001
DS	Basal Ganglia	-	0.41	p<0.001
DS	Frontal	Layer1	0.62	p<0.001
DS	Frontal	Layer2	0.48	p<0.001
DS	Frontal	Layer3	0.37	p<0.001
DS	Frontal	Layer4	0.34	p<0.001
DS	Parietal	Layer1	0.63	p<0.001
DS	Parietal	Layer2	0.56	p<0.001
DS	Parietal	Layer3	0.40	p<0.001
DS	Parietal	Layer4	0.32	p<0.001
DS	Temporal	Layer1	0.66	p<0.001
DS	Temporal	Layer2	0.53	p<0.001
DS	Temporal	Layer3	0.25	p<0.001
DS	Temporal	Layer4	-0.01	p=0.840
DS	Occipital	Layer1	0.61	p<0.001
DS	Occipital	Layer2	0.52	p<0.001
DS	Occipital	Layer3	0.37	p<0.001
DS	Occipital	Layer4	0.32	p<0.001
DS	Basal Ganglia	Layer1	0.38	p<0.001
DS	Basal Ganglia	Layer2	0.43	p<0.001
DS	Basal Ganglia	Layer3	0.32	p<0.001
DS	Basal Ganglia	Layer4	0.24	p<0.001

Abbreviation: HC: euploid cognitively unimpaired controls; DS: Down Syndrome; rho = Spearman's correlation coefficient.

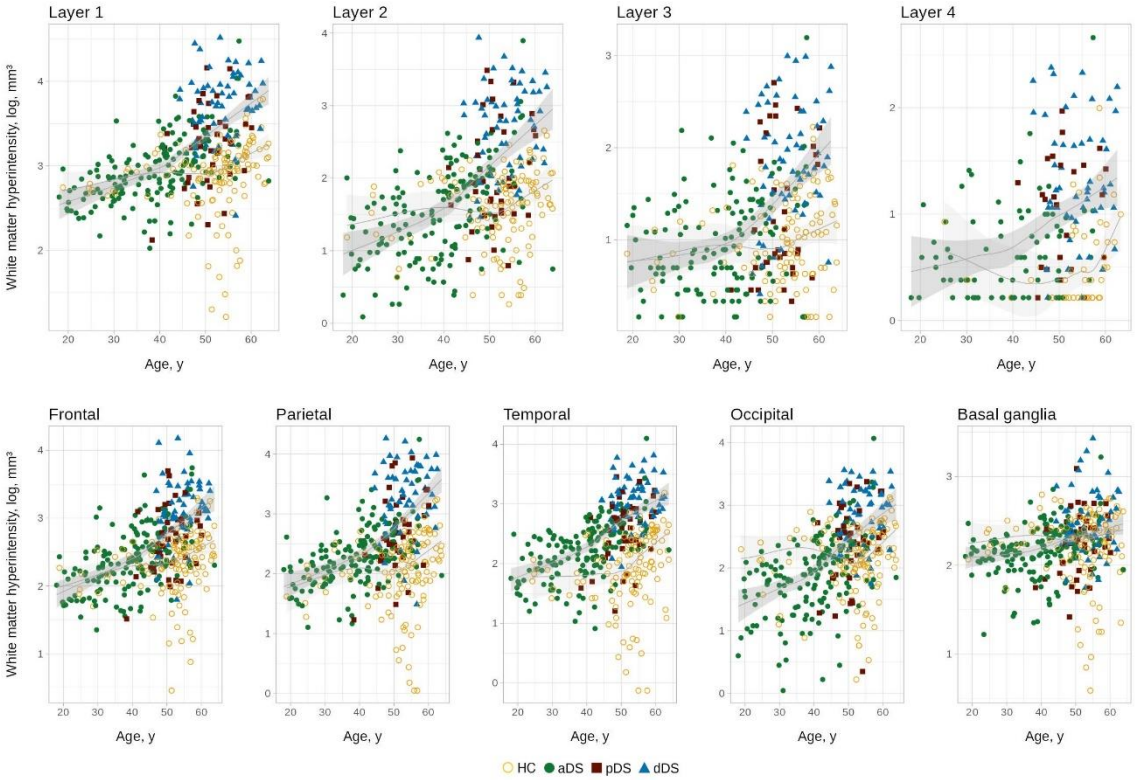

Supplementary Figure 2. *Association between white matter hyperintensities and age in each brain region represented by layers and lobes.*

The points represent individual patients, and the color indicates their clinical diagnosis. Shaded areas represent 95% CI: dark grey represents the age-related change in DS and light grey in the HC group for visual reference. The dashed line indicates when the CI stops overlapping between DS and HC groups. Abbreviation: HC: euploid cognitively unimpaired controls; DS: Down syndrome; aDS: DS asymptomatic; pDS: DS prodromal; dDS: DS with dementia.

S.3.2 Across Sex, *APOE* status and ID levels

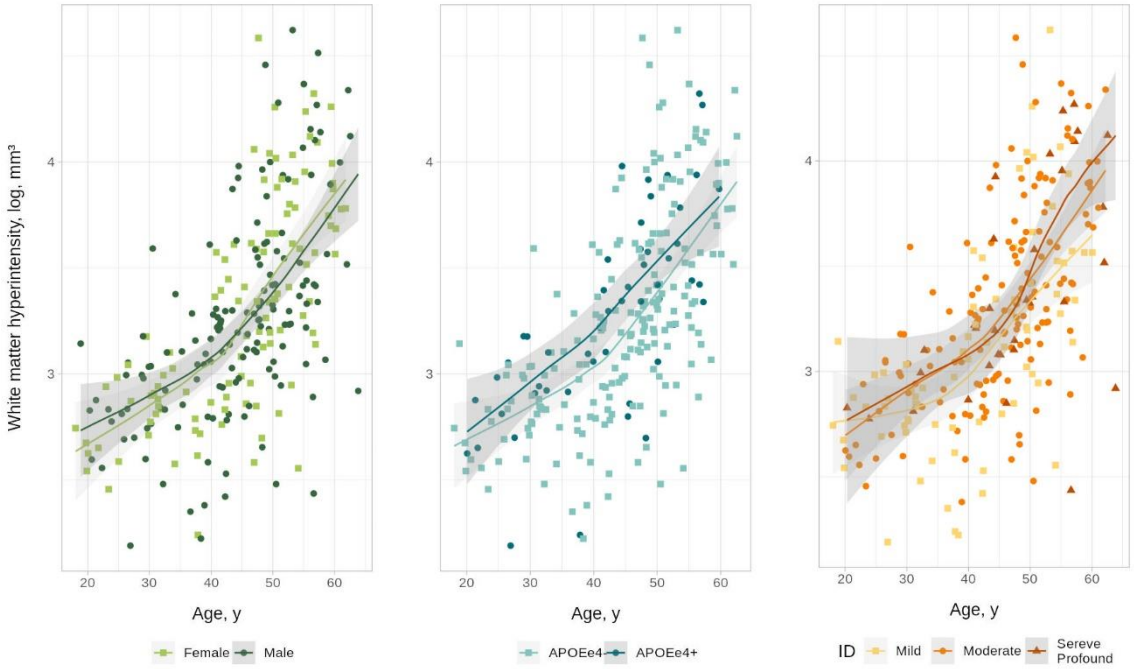

Supplementary Figure 3. *Association between white matter hyperintensity volume and age across sex, APOE status, and intellectual disability levels.*

The points represent individual patients, and the color indicates their sex, APOE status, and level of intellectual disability. Shaded areas represent 95% CI. Abbreviation: ID: intellectual disability.

S.4 Associations between white matter hyperintensity volume and intellectual disability

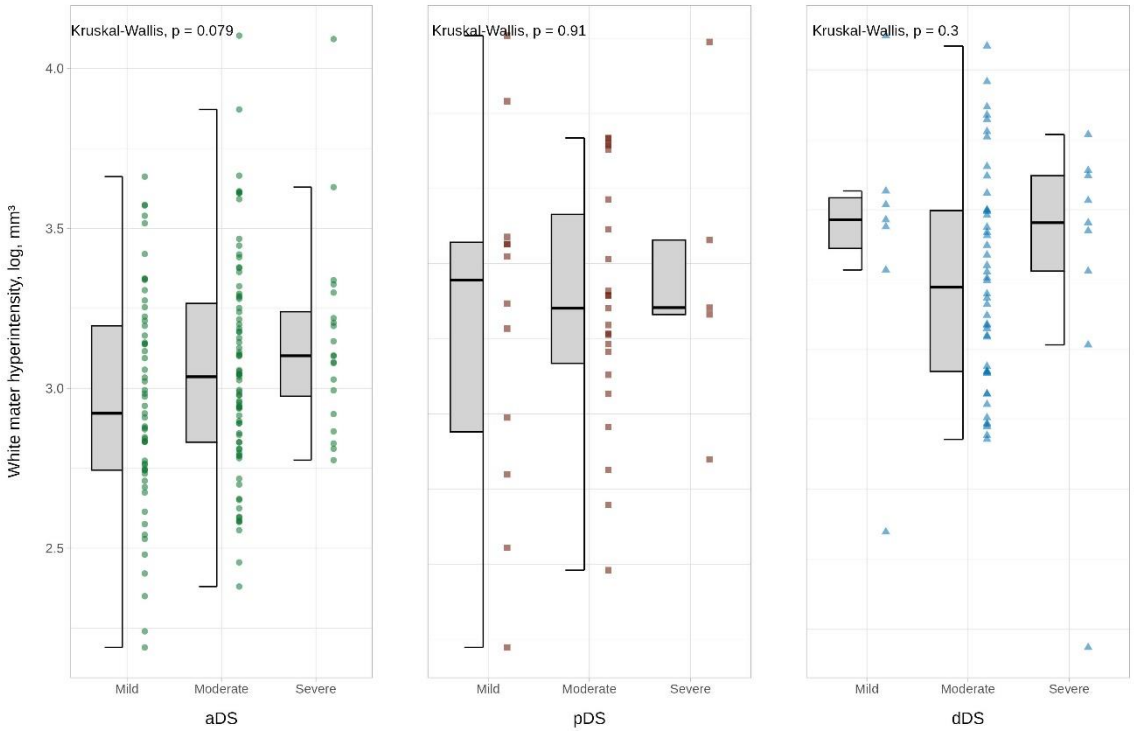

Supplementary Figure 4*. Relationship between white matter hyperintensities and level of intellectual disability across the Alzheimer's disease clinical status.*

Boxplots showing the effect of the intellectual disability level on the distribution of WMH volume within each AD clinical status. The points represent individual patients, and the color indicates clinical diagnosis. Abbreviation: DS: Down syndrome; aDS: DS asymptomatic; pDS: DS prodromal; dDS: DS with dementia.

S.5 Associations between white matter hyperintensity volume and CSF biomarkers

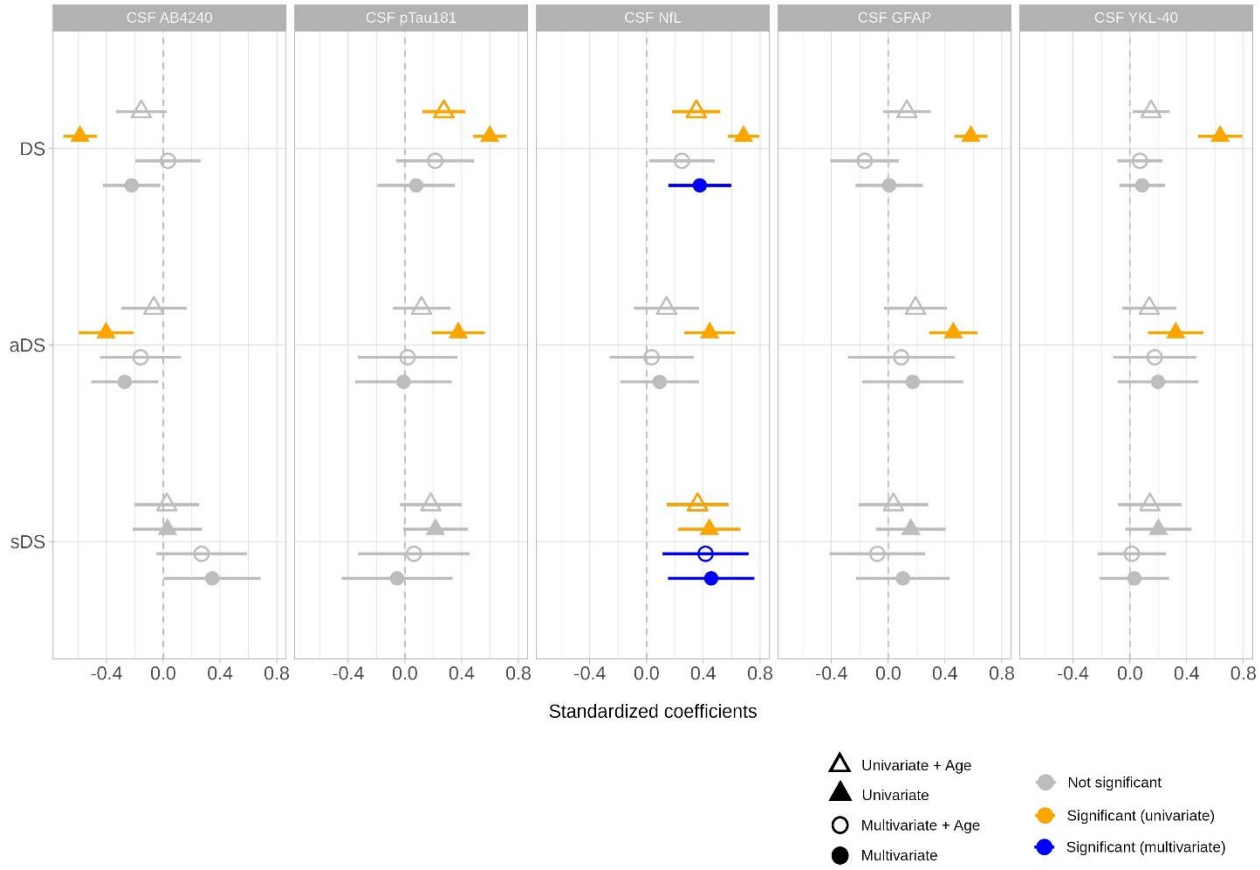

Supplementary Figure 5. Standardized coefficient of univariate and multivariate linear regression models for the WMH volume.

The triangles and circles represent the univariate and multivariate models, respectively, and filled or unfilled shapes indicate whether age is included as a covariate. The lines represent the 95% CI. Grey color indicates non-significant values, while orange color indicates significant values (p<0.01) and blue color after applying Bonferroni correction (α=0.05, p<0.01). Abbreviation: CSF: cerebrospinal fluid; Aβ42/Aβ 40: concentration ratio between amyloid β peptide 1-42 and amyloid β peptide 1-40 (pg/mL); pTau181: tau phosphorylated at threonine 181 concentration (pg/mL); NfL: neurofilament light chain concentration (pg/mL); GFAP: glial fibrillary acidic protein concentration (pg/mL); DS: Down syndrome; aDS: DS asymptomatic; sDS: symptomatic DS.

References:

[1] Jiménez-Balado J, Corlier F, Habeck C, Stern Y, Eich T. Effects of white matter hyperintensities distribution and clustering on late-life cognitive impairment. Sci Reports 2022 121 2022;12:1–13. https://doi.org/10.1038/s41598-022-06019-8.

[2] Hammers A, Allom R, Koepp MJ, Free SL, Myers R, Lemieux L, et al. Three-dimensional maximum probability atlas of the human brain, with particular reference to the temporal lobe. Hum Brain Mapp 2003;19:224–47. https://doi.org/10.1002/HBM.10123.

Supplementary Material

S.1 MRI acquisition parameters

***Table S1**. 3T T1-weighted and FLAIR acquisition protocols.*

	3T Philips - Achieva (Hospital del Mar – Barcelona, Spain)			**3T Siemens - Prisma fit (Hospital Clinic - Barcelona, Spain)**		
	T1w	FLAIR	SWI	T1w	FLAIR	SWI
Echo Time (ms)	3.8	140	24	2.98	128	20
Repetition Time (ms)	8.2	10000	17	2300	9000	26
Flip Angle	8	90	15	9	150	15
Number of Slices	160	140	130	240	45	192
Slice Thickness (mm)	1	1	1	1	3	0.75
Field of View (mm²)	256x256	256x256	512x512	256x256	220x220	240x240
Voxel Resolution (mm)	0.94x0.94x1	0.9x0.9x1	0.45x0.45x1	1x1x1	0.9x0.9x3	0.75x0.75x0.75

Abbreviations: T1w=T1-weighted; FLAIR=Fluid Attenuated Inversion Recovery images; SWI= Susceptibility Weighted Images.

S.2 Population

***Table S2**. Demographic data.*

	aDS	sDS	uDS	
	N=65	N=13	N=2	p-value
Age at baseline, y	39.77 [31.89;44.23]	50.38 [47.67;54.37]	43.71 [39.83;47.59]	0.019
Female	28 (43.08%)	8 (61.54%)	2 (100.00%)	0.151
APOEε4 carriers	11 (22.92%)	3 (33.33%)	0 (0.00%)	0.753
Intellectual disability				0.396
Mild	23 (35.38%)	3 (23.08%)	0 (0.00%)	
Moderate	36 (55.38%)	9 (69.23%)	1 (50.00%)	
Severe/Profound	6 (9.23%)	1 (7.69%)	1 (50.00%)	
Vascular risk factors				
Hypertension	7/65 (10.94%)	1/13 (7.69%)	1/2 (50.00%)	1.000
Dyslipidemia	7/65 (10.94%)	1/13 (7.69%)	1/2 (50.00%)	0.247
Diabetes mellitus	0/64 (0.00%)	2/13 (15.38%)	0/2 (0.00%)	0.052
CAMCOG-DS	78.00 [66.00;85.00]	63.00 [51.00;72.00]	72.00 [72.00;72.00]	0.022
MRI data				
Number of visits 2/3/4	65 (100%) / 16 (24.62%) / 0 (0.00%)	13 (100%) / 1 (7.69%) / 1 (7.69%)	2 (100%) / 2 (100%) / 0 (0.00%)	
Between-visit time delay, y	2.88 [2.22;3.89]	2.23 [2.14; 2.40]	1.75 [1.41; 2.09]	
Duration of the follow-up, y	3.41 [2.46;4.81]	2.31 [2.22; 2.51]	1.75 [1.41; 2.09]	
WMH measures, combat				
WMH at baseline, mm^3	2198.16 [1336.51;4186.58]	6716.15 [4423.17;13162.14]	5366.75 [3150.82;7582.68]	<0.001
Annual WMH change, mm^3/year	-5.39 [-43.75;11.65]	-130.83 [-228.68;-60.19]	-409.33 [-603.86;-214.80]	0.008
Fluid biomarkers, pg/mL				
CSF Aβ42/Aβ40 (N=36/9/0)	0.08 [0.06;0.09]	0.05 [0.04;0.06]		0.003
CSF pTau181 (N=36/9/0)	28.80 [17.28;45.90]	106.90 [88.80;155.00]		0.001
CSF NfL(N=42/9/0)	317.12 [217.78;497.46]	770.00 [645.00;943.90]		0.001
CSF GFAP (N=41/9/0)	2678.84 [1536.17;4049.00]	3078.86 [2910.54;6235.34]		0.063
Plasma GFAP (N=25/9/1)	81.97 [65.22;98.38]	198.42 [155.48;461.94]	158.03 [158.03;158.03]	<0.001
CSF YKL40 (N=42/9/0)	129.07 [70.06;185.04]	223.99 [207.50;284.12]		0.002

S.3 Classification of WMH evolution based on automatic quantification

***Table S3**. Proportion of participants by diagnosis according to the automatic segmentation across both MRI scanners.*

	HC			DS		
	Both	Philips	Siemens	Both	Philips	Siemens
Regression	5 (9.43%)	4 (10.00%)	1 (7.69%)	21 (26.25%)	18 (25.00%)	3 (37.50%)
Stable	35 (66.04%)	25 (62.50%)	10 (76.92%)	53 (66.25%)	49 (68.06%)	4 (50.00%)
Progression	13 (24.53%)	11 (27.50%)	2 (15.38%)	6 (7.50%)	5 (6.94%)	1 (12.50%)

aDS			sDS			uDS		
Both	Philips	Siemens	Both	Philips	Siemens	Both	Philips	Siemens
12 (18.46%)	11 (18.03%)	1 (25.00%)	8 (61.54%)	6 (60.00%)	2 (66.67%)	1 (50.00%)	1 (100.00%)	
48 (73.85%)	46 (75.41%)	2 (50.00%)	4 (30.77%)	3 (30.00%)	1 (33.33%)	1 (50.00%)		1 (100.00%)
5 (7.69%)	4 (6.56%)	1 (25.00%)	1 (7.69%)	1 (10.00%)				

Abbreviation: HC: euploid cognitively unimpaired controls; DS: Down syndrome; aDS: asymptomatic DS; sDS: symptomatic DS; uDS: uncertain DS.

S.4 Effect of AD clinical status on the evolution of WMH

***Table S4**. Effect size of group differences in annual WMH changes.*

Region	Group-comparison	Statistics (z)	p-value	Effect size (r)
HC vs sDS	Total	-3.42	0.002	-0.42
aDS vs sDS	Total	-2.74	0.012	-0.31
HC vs sDS	Frontal	-2.81	0.015	-0.35
aDS vs sDS	Frontal	-2.26	0.048	-0.26
HC vs sDS	Parietal	-5.08	<0.001	-0.63
aDS vs sDS	Parietal	-4.72	<0.001	-0.54
HC vs sDS	Occipital	-3.41	0.002	-0.42
aDS vs sDS	Occipital	-2.83	0.009	-0.32
HC vs sDS	Layer 1	-3.74	<0.001	-0.46
aDS vs sDS	Layer 1	-2.89	0.008	-0.33
HC vs sDS	Layer 2	-2.58	0.03	-0.32

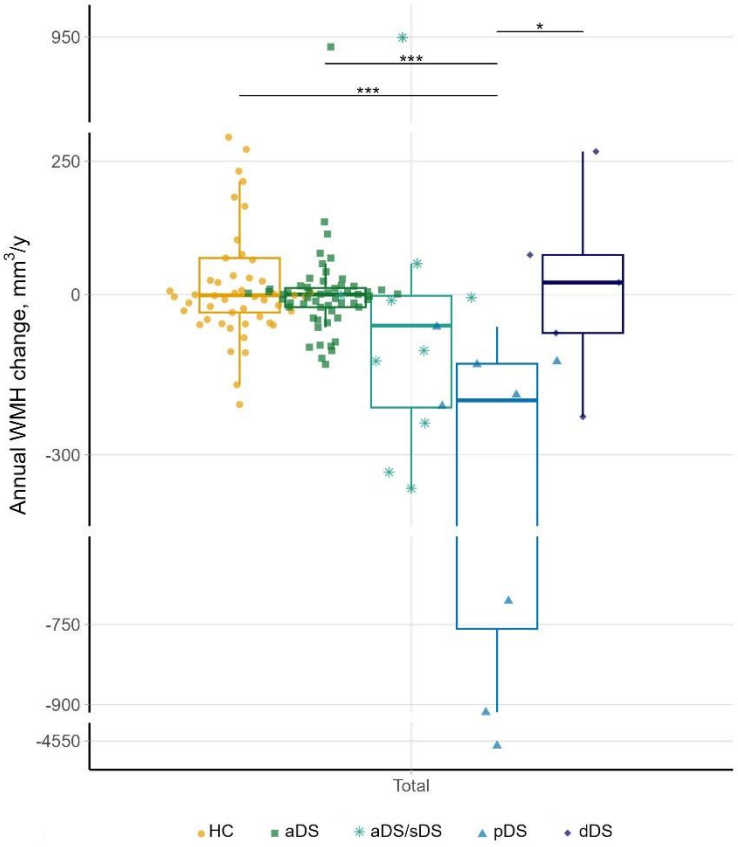

***Figure S1**. Between-group differences for total annual WMH volume changes.*

*The boxplot illustrates WMH volumes across the brain regions. Significant results at p<0.05 using the Holm correction. Abbreviation: ns: no significance; *: p<0.05; **: p<0.01; ***: p<0.001; HC: euploid cognitively unimpaired controls; DS: Down syndrome; aDS: asymptomatic DS; aDS/sDS: asymptomatic DS who progressed to symptomatic DS; pDS: prodromal DS; dDS: DS with AD dementia.*

S.5 Classification of WMH evolution based on automatic quantification and visual assessment

***Table S5**. Proportion of participants by diagnosis according to the visual read across both MRI scanners.*

	HC			DS		
	Both	Philips	Siemens	Both	Philips	Siemens
Regression	12 (22.64%)	10 (25.00%)	2 (15.38%)	18 (22.50%)	16 (20.22%)	2 (25.00%)
Stable	32 (60.38%)	23 (57.50%)	9 (69.24%)	52 (65.00%)	47 (65.28%)	5 (62.50%)
Progression	9 (16.98%)	7 (17.50%)	2 (15.38%)	10 (12.50%)	9 (12.50%)	1 (12.50%)

aDS			sDS			uDS		
Both	Philips	Siemens	Both	Philips	Siemens	Both	Philips	Siemens
12 (16.92%)	11 (18.03%)	1 (25.00%)	5 (38.46%)	4 (40.00%)	1 (33.33%)	1 (50.00%)	1 (100.00%)	
47 (72.31%)	44 (72.13%)	3 (75.00%)	4 (30.77%)	3 (30.00%)	1 (33.33%)	1 (50.00%)		1 (100.00%)
6 (10.77%)	6 (9.84%)		4 (30.77%)	3 (30.00%)	1 (33.33%)			

Abbreviation: HC: euploid cognitively unimpaired controls; DS: Down syndrome; aDS: asymptomatic DS; sDS: symptomatic DS; uDS: uncertain DS.

S.6 Association between annual change in WMH adjusted by WM and demographic, clinical, and genetic data

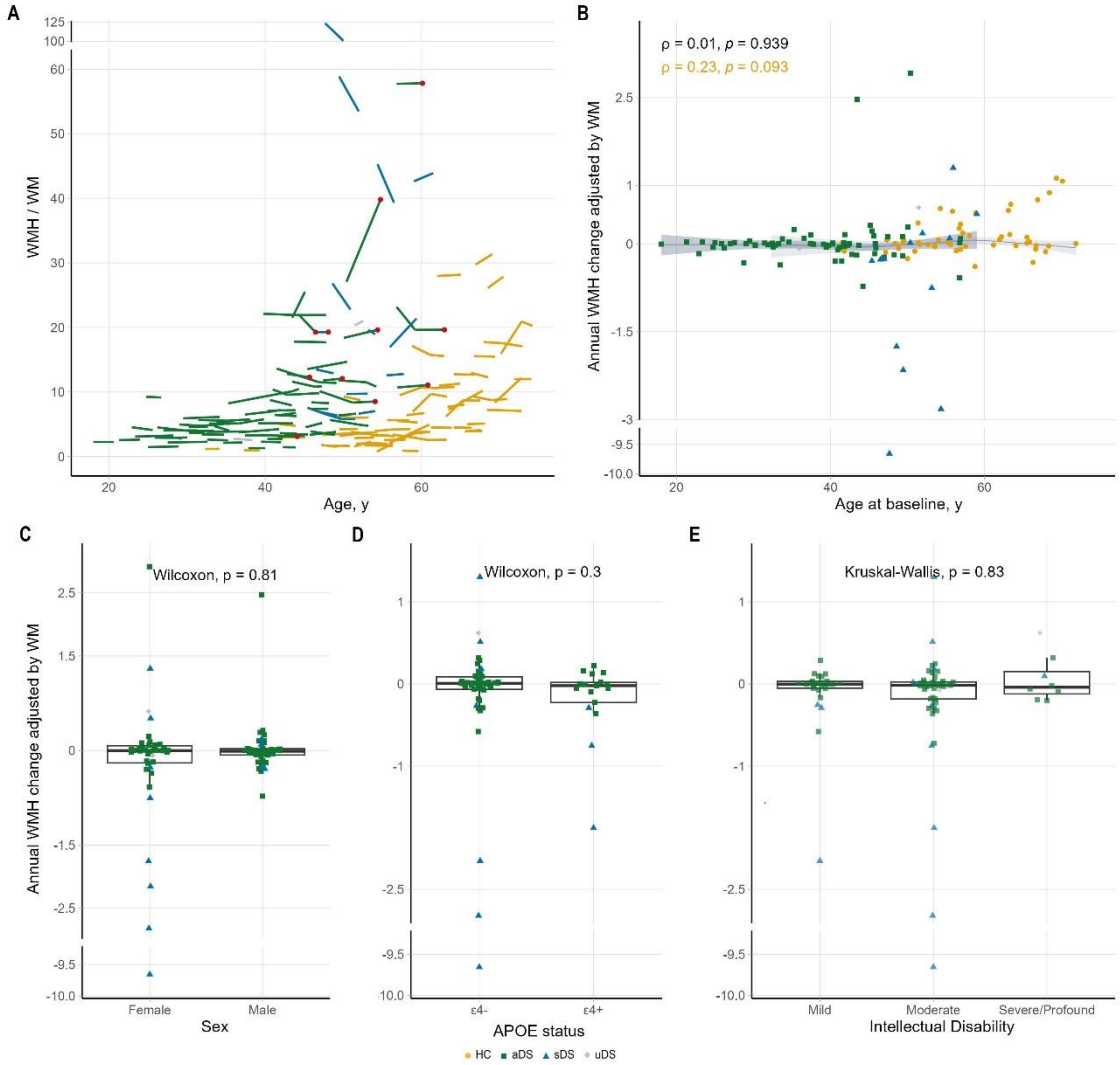

***Figure S2**. Effect of demographic, clinical, and genetic variables on longitudinal WMH adjusted by total WM volume.*

(A) Association between total WMH volume and (B) annual WMH volume with age. The lines/points represent individual participants, with colors indicating their clinical diagnosis. Red points indicate participants who exhibited a clinical change between visits along the AD continuum. Shaded areas represent 95% CI: dark gray represents the age-related change in DS and light gray in the HC group for visual reference. Boxplots showing the effect of (C) sex, (D) APOE genotype and (E) intellectual disability on annual WMH volume changes in DS. Abbreviation: HC: euploid cognitively unimpaired controls; DS: Down syndrome; aDS: DS asymptomatic; sDS: symptomatic DS.

S.7 Effect of AD clinical status on the evolution of WMH adjusted by white matter

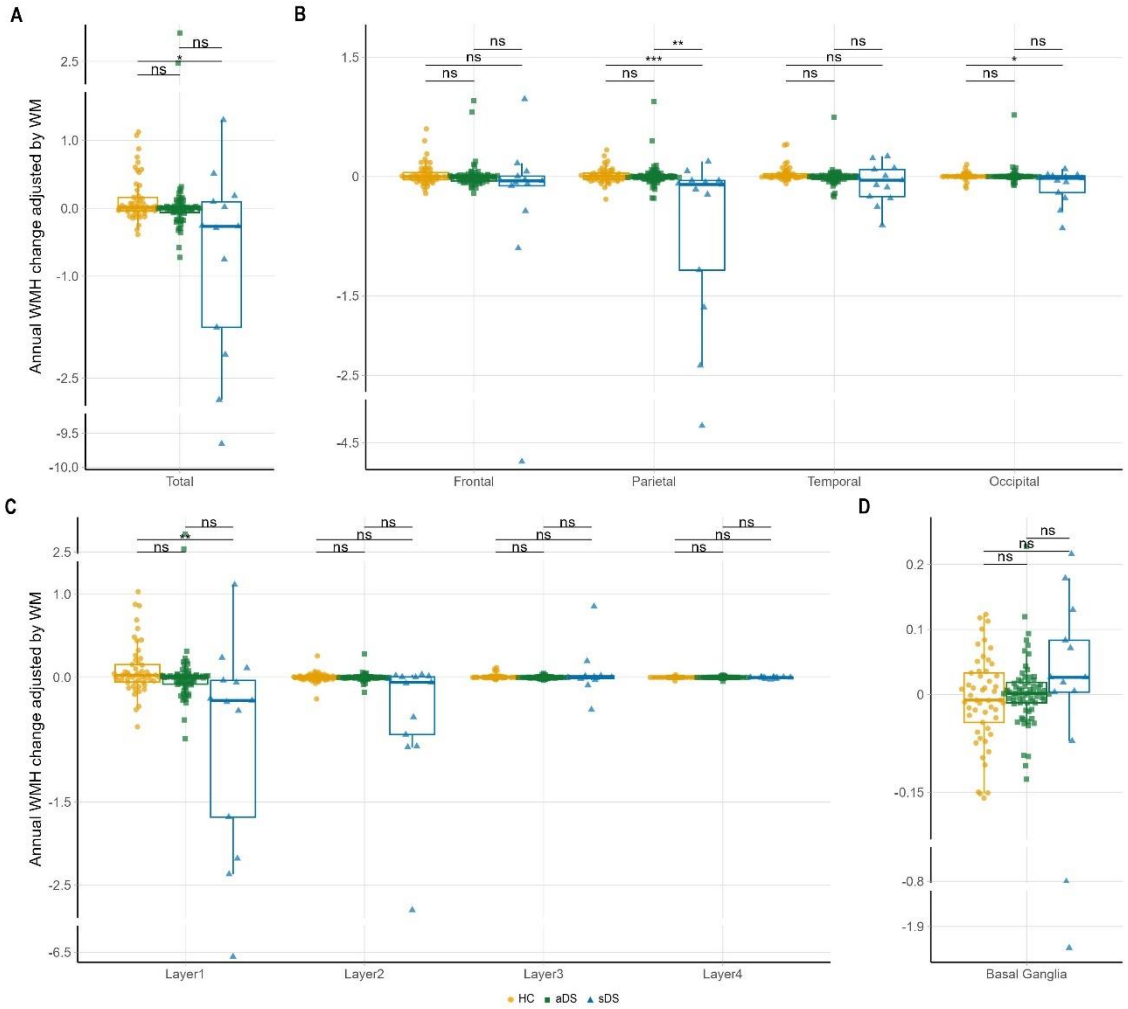

Figure S3. *Between-group differences for total and regional annual WMH volume changes adjusted by total WM volume.*

*(A), (B), (C) and (D) The boxplots illustrate WMH volumes across the brain regions. Significant results at p<0.05 using the Holm correction. Abbreviation: ns: no significance; *: p<0.05; **: p<0.01; ***: p<0.001; HC: euploid cognitively unimpaired controls; DS: Down syndrome; aDS: asymptomatic DS; sDS: symptomatic DS.*

Supplementary Material

Effect of age, sex and APOE status on PSMD in each euploid population

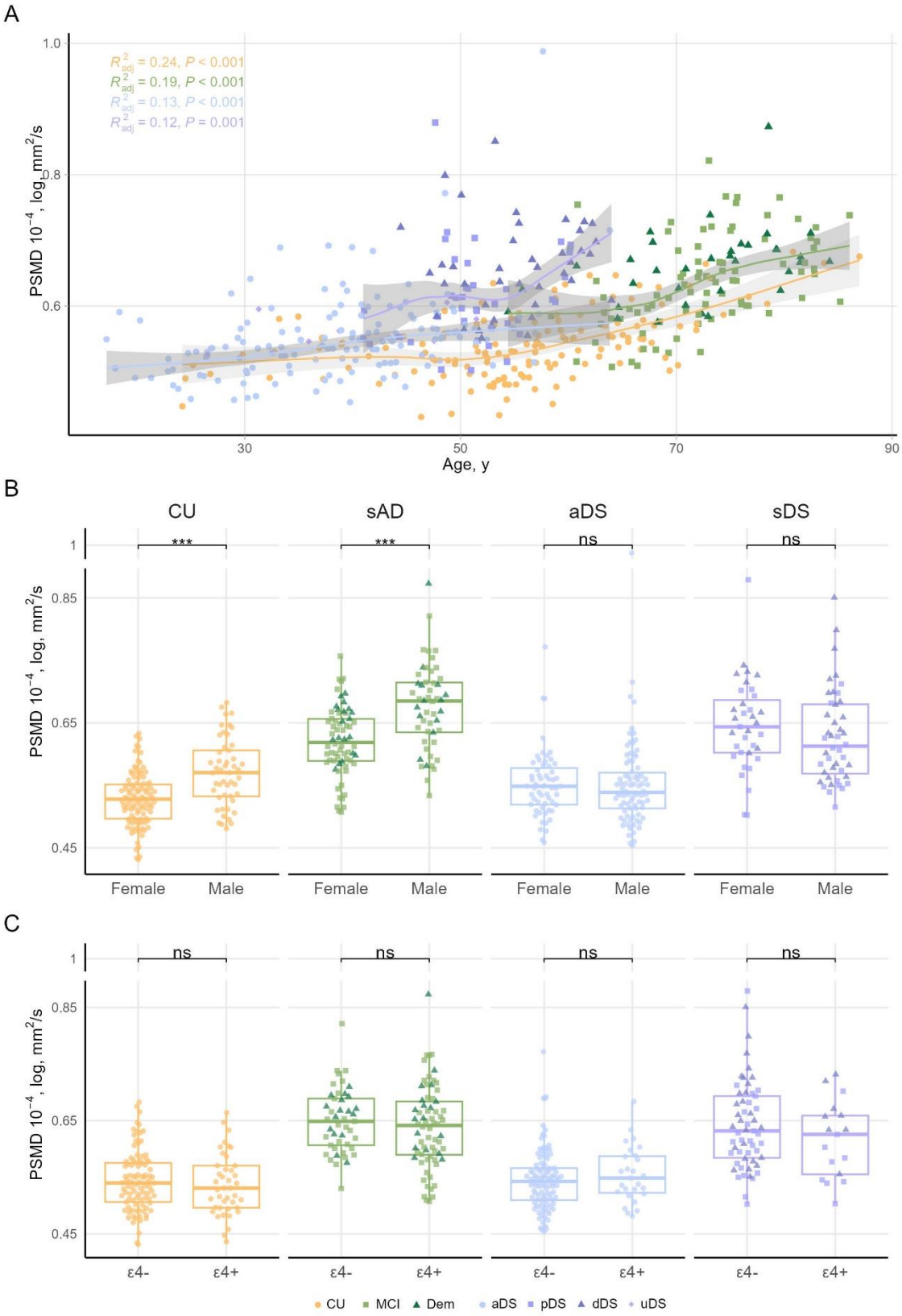

Figure S1. *Effect of age, sex and APOE status on PSMD in CU, sAD, aDS and sDS groups.*

Peak Width of Skeletonized Mean Diffusivity Reveals Early and Multifactorial White Matter Injury Across Sporadic and Down Syndrome–Associated Alzheimer's Disease

Effect of Intellectual Disability levels on PSMD in DS population

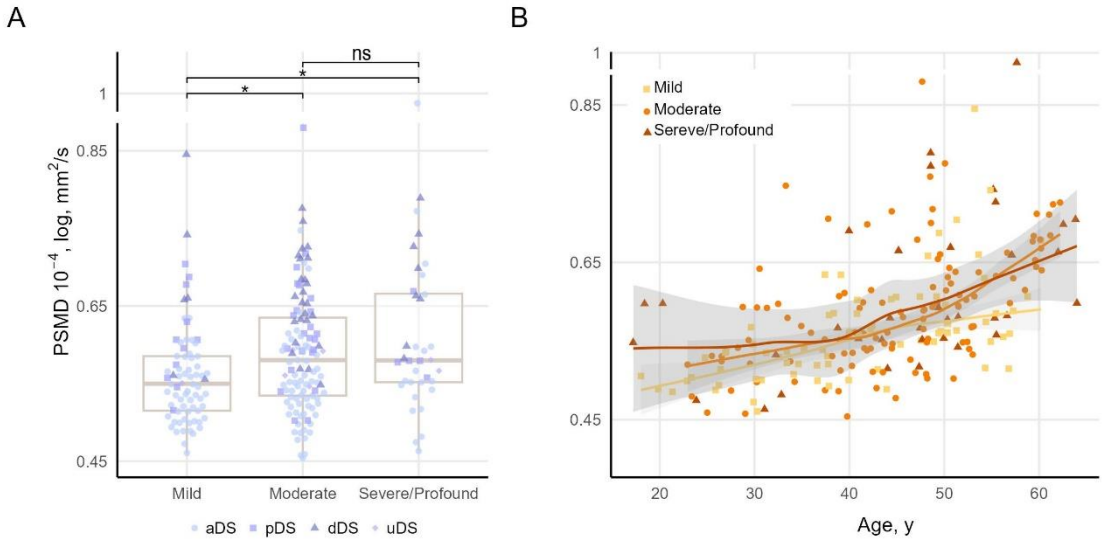

Figure S2. *Effect of Intellectual Disability levels on PSMD in DS population.*

MRI acquisition parameters

***Table S1**. 3T T1w, DWI, FLAIR, and SWI acquisition protocols.*

	3T Philips - Achieva (Hospital del Mar – Barcelona, Spain)			
	Protocol 1			
	T1w	**DWI**	**FLAIR**	**SWI**
Echo Time (ms)	3.8	78	140	24
Repetition Time (ms)	8.2	10800	10000	17
Flip Angle (°)	8	90	90	15
Number of Slices	160	80	140	130
Slice Thickness (mm)	1	2	1	1
Field of View (mm²)	256x256	256x256	256x256	512x512
Voxel Resolution (mm)	0.94x0.94x1	2x2x2	0.9x0.9x1	0.45x0.45x1
b-value		0;100		
N. Directions		32		

	3T (Hospital Clínic– Barcelona, Spain)							
	Protocol 2				Protocol 3			
	T1w	**DWI**	**FLAIR**	**SWI**	**T1w**	**DWI***	**FLAIR**	**SWI**
Echo Time (ms)	2.98	89	128	20	2.96	71	397	20
Repetition Time (ms)	2300	7700	9000	26	2300	3700	6000	26
Flip Angle (°)	9	90	150	15	9	90	120	15
Number of Slices	240	60	45	192	208	60	160	192
Slice Thickness (mm)	1	2	1	0.75	1	2	1	0.75
Field of View (mm²)	256x256	250x250	220x220	240x240	256x256	232x232	256x256	240x240
Voxel Resolution (mm)	1x1x1	2x2x2	0.9x0.9x3	0.75x0.75x0.75	1x1x1	2x2x2	1x1x1	0.75x0.75x0.75
b-value		30				127		
N. Directions		0;1000				0;500;1000; 2000		

Abbreviations: T1w=T1-weighted; DWI=Diffusion Weighted Imaging; FLAIR=Fluid Attenuated Inversion Recovery images; SWI= Susceptibility Weighted Images.

**Multishell acquisition*

Population

***Table S2**. Demographic data.*

	Euploid population			Down syndrome population				
	CU	MCI	AD dementia	aDS	pDS	dDS	uDS	p-value
	N = 150	N=84	N=34	N=141	N=39	N=40	N=8	
Age, y	56.35 [51.08;63.27]	72.60 [68.17;75.73]	73.18 [67.90;78.51]	39.46 [30.73;44.93]	50.98 [48.98;54.28]	55.29 [51.39;59.63]	41.66 [34.78;47.86]	<0.001
Female	101 (67.33%)	49 (58.33%)	19 (55.88%)	59 (41.84%)	20 (51.28%)	15 (37.50%)	5 (62.50%	0.030
APOEε4 carriers	41/134 (30.60%)	50/79 (63.29%)	18/34 (52.94%)	27/131 (20.61%)	9/38 (23.68%)	8/36 (22.22%)	1/7 (14.29%)	0.313
Intellectual disability								
Mild				56 (40.00%)	11 (28.21%)	6 (15.38%)	1 (14.29%)	
Moderate				63 (45.00%)	23 (58.97%)	25 (64.10%)	4 (57.14%)	
Severe				21 (15.00%)	5 (12.82%)	8 (20.51%)	2 (28.57%)	
Vascular risk factors								
Hypertension	16/78 (20.51%)	21/38 (55.26%)	11/22 (50.00%)	2/140 (1.43%)	0/36 (0.00%)	2/38 (5.26%)	1/7 (14.29%)	0.431
Dyslipidemia	25/78 (32.05%)	24/38 (63.16%)	9/22 (40.91%)	23/138 (16.67%)	7/36 (19.44%)	9/37 (24.32%)	2 (28.57%)	0.583
Diabetes mellitus	3/78 (3.85%)	4/37 (10.81%)	1/21 (4.76%)	4/140 (2.86%)	3/36 (8.33%)	3/38 (7.89%)	0/7 (0.00%)	0.261
Cognitive scores								
MMSE	29.00 [29.00;30.00]	26.00 [24.50;27.50]	21.00 [18.00;24.00]					<0.001
CAMCOG-DS				79.00 [68.00;84.00]	64.00 [59.00;77.00]	44.50 [30.25;54.50]	62.00 [50.00;72.00]	<0.001
MRI protocol (1/2/3)	103 (68.67%) / 21 (14.00%) / 26 (17.33%)	66 (78.57%) / 6 (7.14%) / 12 (14.29%)	21 (61.76%) /4 (11.76%) / 9 (26.48%)	94 (66.67%) / 23 (16.31%) / 24 (17.02%)	23 (58.97%) / 9 (23.08%) / 7 (17.95%)	20 (50.00%) / 10 (25.00%) / 10 (25.00%)	2 (25.00%) /3 (37.50%) /3 (37.50%)	
CSF biomarkers								
Aβ42/Aβ40 (N=102/65/29/9/30/26/2)	0.10 [0.10;0.11]	0.04 [0.04;0.05]	0.04 [0.04;0.05]	0.08 [0.07;0.10]	0.05 [0.04;0.06]	0.04 [0.04;0.05]	0.08 [0.07;0.08]	<0.001
pTau181 (N=102/65/29/9/30/26/2)	32.70 [26.95;42.38]	106.65 [84.38;155.45]	104.50 [77.70;136.80]	27.90 [16.00;48.10]	88.35 [46.30;142.23]	148.65 [89.78;197.75]	22.50 [16.40;28.60]	<0.001
NfL (N=128/61/22/75/27/22/2)	369.05 [307.20;496.92]	938.15 [820.05;1263.60]	1274.95 [839.16;1443.67]	338.51 [218.75;458.75]	732.65 [590.58;774.75]	1250.38 [774.31;1790.79]	252.85 [228.68;277.02]	<0.001
GFAP (N=45/41/9/63/26/20/1)	3019.55 [1510.64;5335.14]	10620.81 [6113.58;15076.20]	7877.87 [5385.11;12293.95]	2553.76 [1541.05;4001.81]	4672.26 [3254.56;5961.02]	6572.28 [5131.96;9760.33]	2293.52 [2293.52;2293.52]	<0.001
YKL40 (N=140/59/20/75/27/22/2)	176.97 [134.78;223.54]	289.70 [258.66;332.14]	333.50 [278.76;362.25]	122.50 [81.58;177.00]	214.43 [149.60;284.43]	239.38 [201.66;296.56]	99.34 [74.67;124.01]	<0.001

Abbreviations: Aβ42/Aβ40, concentration ratio between amyloid beta peptide 1-42 and amyloid beta peptide 1-40 (pg/mL); AD, Alzheimer's disease; aDS, asymptomatic Down syndrome; APOE, apolipoprotein E; CAMCOG-DS, Cambridge Cognitive Examination for Older Adults with Down Syndrome; CSF, cerebrospinal fluid; sDS, symptomatic Down syndrome; DS, Down syndrome; GFAP, glial fibrillary acidic protein concentration (pg/mL); CU, euploid cognitively unimpaired controls; IQR, interquartile range; MMSE, Mini-Mental State Examination; NfL, neurofilament light chain concentration (pg/mL); pTau181, tau phosphorylated at threonine 181 concentration (pg/mL); uDS, Down syndrome with an uncertain diagnosis of neurodegenerative disease, YKL-40, chitinase 3-like 1; MCI, mild cognitive impairment.

Associations between PSMD and CSF biomarkers

***Table S3**. Robust linear regression analyses of PSMD versus CSF biomarkers.*

Diagnostic group	CSF biomarker	β	CI	R^2	p-value (unadjusted)	FDR
CU	Aβ42/Aβ40	-0.22	[-0.43,-0.02]	0.04	0.03	**0.05**
CU	pTau181	0.26	[0.05,0.46]	0.05	0.01	**0.02**
CU	NfL	0.39	[0.22,0.56]	0.14	<0.001	**<0.001**
CU	YKL-40	0.30	[0.13,0.47]	0.08	0.001	**0.001**
CU	GFAP	0.12	[-0.21,0.44]	-0.01	0.47	0.65
sAD	Aβ42/Aβ40	0.06	[-0.14,0.25]	-0.01	0.57	0.67
sAD	pTau181	-0.24	[-0.43,-0.05]	0.05	0.01	**0.03**
sAD	NfL	0.26	[0.03,0.48]	0.05	0.03	**0.04**
sAD	YKL-40	0.11	[-0.13,0.35]	0.00	0.37	0.47
sAD	GFAP	0.17	[-0.11,0.46]	0.01	0.23	0.32
DS	Aβ42/Aβ40	-0.46	[-0.60,-0.32]	0.24	<0.001	**<0.001**
DS	pTau181	0.39	[0.23,0.54]	0.16	<0.001	**<0.001**
DS	NfL	0.59	[0.46,0.73]	0.38	<0.001	**<0.001**
DS	YKL-40	0.35	[0.20,0.50]	0.13	<0.001	**<0.001**
DS	GFAP	0.46	[0.30,0.62]	0.22	<0.001	**<0.001**
aDS	Aβ42/Aβ40	-0.22	[-0.43,-0.02]	0.05	0.03	0.07
aDS	pTau181	0.02	[-0.20,0.23]	-0.01	0.88	0.91
aDS	NfL	0.31	[0.13,0.49]	0.12	0.001	**0.007**
aDS	YKL-40	0.09	[-0.09,0.28]	0.00	0.32	0.61
aDS	GFAP	0.25	[0.08,0.42]	0.10	0.005	**0.03**
sDS	Aβ42/Aβ40	0.02	[-0.23,0.27]	-0.02	0.89	0.99
sDS	pTau181	0.09	[-0.16,0.34]	-0.01	0.48	0.56
sDS	NfL	0.46	[0.21,0.70]	0.21	<0.001	**0.001**
sDS	YKL-40	0.09	[-0.19,0.37]	-0.01	0.52	0.47
sDS	GFAP	0.32	[0.04,0.60]	0.09	0.009	**0.02**

Abbreviations: Aβ42/Aβ40, concentration ratio between amyloid beta peptide 1-42 and amyloid beta peptide 1-40 (pg/mL); AD, Alzheimer's disease; aDS, asymptomatic Down syndrome; CSF, cerebrospinal fluid; sDS, symptomatic Down syndrome; DS, Down syndrome; GFAP, glial fibrillary acidic protein concentration (pg/mL); CU, euploid cognitively unimpaired controls; CI, confidence interval; NfL, neurofilament light chain concentration (pg/mL); pTau181, tau phosphorylated at threonine 181 concentration (pg/mL); YKL-40, chitinase 3-like 1.

***Table S4**. Elastic net regression models.*

Diagnostic group	CSF biomarker	Coefficient	Bootstrap	R^2	MSE
CU	Aβ42/Aβ40	0.00	0.44	0.20	0.80
	pTau181	-0.13	**0.70**		
	NfL	0.27	**0.94**		
	YKL-40	0.32	**0.94**		
	GFAP	0.00	0.56		
sAD	Aβ42/Aβ40	0.00	0.51	0.03	0.97
	pTau181	0.00	0.55		
	NfL	0.16	**0.93**		
	YKL-40	0.00	0.55		
	GFAP	0.00	0.51		
DS	Aβ42/Aβ40	-0.36	**1.00**	0.35	0.65
	pTau181	-0.20	**0.86**		
	NfL	0.63	**1.00**		
	YKL-40	-0.36	**0.95**		
	GFAP	0.16	**0.86**		
aDS	Aβ42/Aβ40	-0.43	**0.91**	0.02	0.98
	pTau181	-0.46	**0.83**		
	NfL	0.29	**0.71**		
	YKL-40	-0.17	0.58		
	GFAP	0.20	**0.74**		
sDS	Aβ42/Aβ40	0.05	0.62	0.15	0.85
	pTau181	-0.21	**0.74**		
	NfL	0.69	**1.00**		
	YKL-40	-0.19	**0.74**		
	GFAP	0.03	0.67		

Abbreviations: Aβ42/Aβ40, concentration ratio between amyloid beta peptide 1-42 and amyloid beta peptide 1-40 (pg/mL); sAD, sporadic Alzheimer's disease; aDS, asymptomatic Down syndrome; CSF, cerebrospinal fluid; sDS, symptomatic Down syndrome; DS, Down syndrome; GFAP, glial fibrillary acidic protein concentration (pg/mL); CU, euploid cognitively unimpaired controls; CI, confidence interval; NfL, neurofilament light chain concentration (pg/mL); pTau181, tau phosphorylated at threonine 181 concentration (pg/mL); YKL-40, chitinase 3-like 1.

PSMD and WMH status

***Table S5**. Proportion of euploid individuals across alternative thresholds.*

Threshold	PSMD+WMH-	PSMD-WMH+	χ^2	p-value
mean + 1 SD	7.38%	6.15%	0.12	0.72
mean + 1.5 SD	5.74%	5.74%	0	1
mean + 2 SD	6,15%	9.02%	0.97	0.32
mean + 2.5 SD	3.69%	8.61%	4.03	0.04
mean + 3 SD	3.28%	6.57%	0.64	0.15

***Table S6**. Proportion of individuals with DS across alternative thresholds.*

Threshold	PSMD+WMH-	PSMD-WMH+	χ^2	p-value
mean + 1 SD	16.76%	3.24%	15.57	<0.001
mean + 1.5 SD	10.27%	1.62%	10.23	0.001
mean + 2 SD	8.65%	1.62%	7.58	0.006
mean + 2.5 SD	10.27%	2.16%	8.52	0.004
mean + 3 SD	7.03%	2.70%	2.72	0.09

ANNEX 5. ADDITIONAL PUBLICATIONS

List of additional publications of the candidate that are not included in the Thesis. These papers are the result of collaborative work with other projects during the time of the Thesis:

- Sara E Zsadanyi, Alejandra O. Morcillo-Nieto, Mateus R Aranha, Irina Aragón, José E Arriola-Infante, Lídia Vaqué-Alcázar, Victor Montal, Jordi Pegueroles, Javier Arranz, Íñigo Rodríguez-Baz, Lucia M Blesa, Laura Videla, Isabel Barroeta, Laura Del Hoyo Soriano, Bessy Benejam, Susana Fernández, Aida S Hernandez, Nuria Bargallo, Sofía González-Ortiz, Sandra Giménez, Daniel Alcolea, Olivia Belbin, Alberto Lleó, Juan Fortea, Maria Carmona-Iragui, Alexandre Bejanin. (2024). Associations of Microbleeds and Their Topography With Imaging and CSF Biomarkers of Alzheimer Pathology in Individuals With Down Syndrome. *Neurology*. 27;103(4):e209676. doi: 10.1212/WNL.0000000000209676. IF(2024)=8.5 (D1).
- José Enrique Arriola-Infante, Alejandra O. Morcillo-Nieto, Sara E Zsadanyi, María Franquesa-Mullerat, Lídia Vaqué-Alcázar, Mateus Rozalem-Aranha, Javier Arranz, Íñigo Rodríguez-Baz, Lucia Maure-Blesa, Laura Videla, Isabel Barroeta, Laura Del Hoyo Soriano, Bessy Benejam, Susana Fernández, Aida Sanjuan-Hernández, Sandra Giménez, Daniel Alcolea, Olivia Belbin, Albert Flotats, Valle Camacho, Alberto Lleó, María Carmona-Iragui, Juan Fortea, Alexandre Bejanin. (2025). Regional Brain Metabolism across the Alzheimer's Disease Continuum in Down Syndrome. *Ann Neurol*. 98(1):163-173. doi: 10.1002/ana.27226. IF(2024)=7.7 (D1).
- Maria Franquesa-Mullerat, Alejandra O. Morcillo-Nieto, José Enrique Arriola-Infante, Sara E Zsadanyi, Lídia Vaqué-Alcázar, Mateus Rozalem-Aranha, Javier Arranz, Íñigo Rodríguez-Baz, Lucia Maure-Blesa, Laura Videla, Isabel Barroeta, Laura Del Hoyo Soriano, Bessy Benejam, Susana Fernández, Aida Sanjuan Hernandez, Sandra Giménez, Daniel Alcolea, Olivia Belbin, Alberto Lleó, María Carmona-Iragui, Juan Fortea, Alexandre Bejanin. (2025). Study of brain perfusion in adults with Down syndrome along the Alzheimer's disease continuum. *Alzheimer's Dement*. 21(9):e70581. doi: 10.1002/alz.70581. IF(2024)=11.7 (D1).
- Íñigo Rodríguez-Baz, Bessy Benejam, Alejandra O. Morcillo-Nieto, Lídia Vaqué-Alcázar, José Enrique Arriola-Infante, Valle Camacho, Mateus Rozalem Aranha, Maria Carmona-Iragui, Laura Videla, Isabel Barroeta,

Susana Fernández, Sara E Zsadanyi, Sandra Giménez, Javier Arranz, Lucia Maure Blesa, Daniel Alcolea, Alberto Lleó, Alexandre Bejanin, Juan Fortea. (2025). Posterior Cortical Atrophy Due to Alzheimer Disease in a Person With Down Syndrome: A Case Report. *Neurology*. 14;104(1):e210179. doi: 10.1212/WNL.0000000000210179. IF(2024)=8.5 (D1).

- Lídia Vaqué-Alcázar, Laura Videla, Bessy Benejam, Laura Del Hoyo Soriano, Isabel Barroeta, Susana Fernandez, Íñigo Rodríguez-Baz, José Enrique Arriola-Infante, Javier Arranz, Lucía Maure Blesa, Aida Sanjuan-Hernández, Alejandra O. Morcillo-Nieto, Alexandre Bejanin, Eider M Arenaza-Urquijo, Alberto Lleó, David Bartrés-Faz, Maria Carmona-Iragui, Juan Fortea. (2025). Generational effects in Down syndrome: Enriched environment enhances functionality without reducing Alzheimer's disease risk. *Alzheimer's Dement*. 21(10):e70447. doi: 10.1002/alz.70447. IF(2024)=11.7 (D1)
- Alexander Maximilian Bernhardt, Íñigo Rodríguez-Baz, Iban Aldecoa, Javier Arranz, José Enrique Arriola-Infante, Lucia Maure-Blesa, Maria Carmona-Iragui, Sebastian Longen, Svenja Verena Trossbach, Armin Giese, Torsten Matthias, Bessy Benejam, Laura Videla, Laura Del Hoyo Soriano, Isabel Barroeta, Aída Sanjuan, Susana Fernández, Lídia Vaqué-Alcázar, Mateus Rozalem Aranha, Alejandra O. Morcillo-Nieto, Georg Nübling, Olivia Wagemann, Anna Stockbauer, Mireia Tondo, Alexandre Bejanin, Alberto Lleó, Daniel Alcolea, Laura Molina-Porcel, Juan Fortea, Johannes Levin. (2025). Alpha-synuclein co-pathology in Down syndrome-associated Alzheimer's disease. *Alzheimer's Dement*. 21(6):e70342. doi: 10.1002/alz.70342. IF(2024)=11.7 (D1)
- Neus Falgàs, Lucia Maure-Blesa, Beau Ances, Lisi Flores-Aguilar, Sigan Hartley, Jason Hassenstab, M Florencia Iulita, Matthew Janicki, Katherine Koenig, Patrick Lao, Johannes Levin, Eric McDade, Laurent Meijer, Michael S Rafii, Heather M Snyder, Raquel Sánchez-Valle, Juan Fortea; DSAD-ADAD conference group; Jose Arriola Infante, Mirea Balasa, Isabel Barroeta, Nicolas Barthelemy R, Alexandre Bejanin, Bessy Benejam, Beatriz Bosch, Angela Bradshaw, Maria Carmona-Iragui, Ann Cohen, Aina Comas Albertí, Lajos Csincsik, A Claudio Cuello, Laura Del Hoyo Soriano, Janna Dijkstra, Natalie Edwards, Sandra Giménez, Fernando Gonzalez-Ortiz, Brian Gordon, Sara Gutiérrez Fernández, Benjamin Handen, Charlotte Jacob, Erik Johnson, Charlotte Johansson, Albert Lladó, Alberto Lleó, Samuel Morabito, Alejandra O. Morcillo-Nieto, Laia Montoliu-Gaya, Michael Okafor, Agnes Pérez-Millan,

Marie Claude Potier, John Ringman, Íñigo Rodríguez-Baz, Eric Rubenstein, Natalie S Ryan, André Strydom, Lidia Vaqué-Alcázar, Lisa Vermunt, Laura Videla Toro, Shahid Zaman. (2025). Genetically determined Alzheimer's disease research advances: The Down Syndrome & Autosomal Dominant Alzheimer's Disease 2024 Conference. *Alzheimer's Dement*. 21(7):e70309. doi: 10.1002/alz.70309. IF(2024)=11.7 (D1)

- Laura Videla, Bessy Benejam, Isabel Barroeta, Susana Fernandez, Miren Altuna, Javier Arranz, Íñigo Rodríguez-Baz, José Enrique Arriola-Infante, Lucía Maure-Blesa, Laura Del Hoyo Soriano, Ignacio Illán-Gala, Teresa Estellés, Aida Sanjuan, Lídia Vaqué-Alcázar, Mateus Rozalem Aranha, Alejandra O. Morcillo-Nieto, Sarah Erzsebet Zsadanyi, Maria Franquesa-Mullerat, Sílvia Valldeneu, María Belén Sánchez-Saudinós, Concepción Padilla, Mireia Carreras, Oriol Lorente, Natalia Valle-Tamayo, Érika Sánchez-Aced, Oriol Dols-Icardo, Sònia Sirisi, Laia Muñoz, Soraya Torres, Shaima El Bounasr El Bennadi, Oriol Sánchez, Diana Garzón, Laia Ribas, Sumia Elbachiri, Cecilia Mota, Mireia Tondo, Valle Camacho, Sandra Giménez, Constance Delaby, Olivia Belbin, María Florencia Iulita, Víctor Montal, Jordi Pegueroles, Eduard Vilaplana, Jordi Clarimón, Sofía González-Ortiz, Laura Molina-Porcel, Iban Aldecoa, Daniel Alcolea, Alexandre Bejanin, Sebastià Videla, Rafael Blesa, Alberto Lleó, María Carmona-Iragui, Juan Fortea. (2025). The Down Alzheimer Barcelona Neuroimaging Initiative (DABNI) and its contributions to understanding Alzheimer's disease in Down syndrome: A decade of discovery. *Alzheimer's Dement*. 21(6):e70259. doi: 10.1002/alz.70259. IF(2024)=11.7 (D1).
- Sandra Giménez, Lídia Vaqué-Alcázar, Nuole Zhu, Bessy Benejam, Javier Arranz, Lucia Maure-Blesa, Laura Videla, Maria Carmona-Iragui, Isabel Barroeta, Anne-Sophie Rebillat, Íñigo Rodríguez-Baz, Alexandre Bejanin, José Enrique Arriola-Infante, Ana Bueno, Susana Fernandez, Laia Ribas, Sara E Zsadanyi, Alejandra O. Morcillo-Nieto, Daniel Alcolea, Christos Panagiotis Lisgaras, Esther Blessing, Ricardo S Osorio, Alberto Lleó, Juan Fortea. (2025). Impact of Alzheimer's disease on sleep in adults with Down syndrome. *Alzheimer's Dement*. 21(7):e70400. doi: 10.1002/alz.70400. IF(2024)=11.7 (D1).
- Jesús Garcia Castro, Sara Rubio-Guerra, Kaitlin B Casaletto, Judit Selma González, Molly Memel, Lídia Vaqué-Alcázar, Alejandra O. Morcillo-Nieto, José Arriola-Infante, Oriol Dols-Icardo, Alexandre Bejanin, Olivia Belbin, Juan

Fortea, Daniel Alcolea, Maria Carmona-Iragui, Isabel Barroeta, Miguel Santos-Santos, María Belen Sánchez Saudinós, Isabel Sala Matavera, Hilary W Heuer, Leah K Forsberg, Kejal Kantarci, Adam M Staffaroni, Carmela Tartaglia, Katherine P Rankin, Brad Boeve, Adam Boxer, Howard J Rosen, Alberto Lleó, Ignacio Illán-Gala; ALLFTD Consortium. (2025). Sex differences in the executive and behavioral reserve of autosomal dominant frontotemporal dementia. *Alzheimer's Dement*. 21(4):e70070. doi: 10.1002/alz.70070. IF(2024)=11.7 (D1).

- Jesús Garcia Castro, Sara Rubio-Guerra, Kaitlin B Casaletto, Judit Selma González, Molly Memel, Lídia Vaqué-Alcázar, Alejandra O. Morcillo-Nieto, José Arriola-Infante, Oriol Dols-Icardo, Alexandre Bejanin, Olivia Belbin, Juan Fortea, Daniel Alcolea, Maria Carmona-Iragui, Isabel Barroeta, Miguel Santos-Santos, María Belen Sánchez Saudinós, Isabel Sala Matavera, Hilary W Heuer, Leah K Forsberg, Kejal Kantarci, Adam M Staffaroni, Carmela Tartaglia, Katherine P Rankin, Brad Boeve, Adam Boxer, Howard J Rosen, Alberto Lleó, Ignacio Illán-Gala; ALLFTD Consortium. (2026) Potential role of MRI to optimize clinical trial design for progressive supranuclear palsy and corticobasal degeneration. *J Prev Alzheimer's Dis*. 13(3):100486. doi: 10.1016/j.tjpad.2026.100486. IF(2024)=7.8 (D1).

ANNEX 6. PRESENTATIONS AT CONFERENCES

Oral presentations

- Alejandra O. Morcillo-Nieto, Mateus Rozalem-Aranha, José Enrique Arriola-Infante, Maria Franquesa-Mullerat, Sara E. Zsadanyi, Lídia Vaqué-Alcázar, José Allende Parra, Zili Zhao, Javier Arranz, Íñigo Rodríguez-Baz, Lucia Maure-Blesa, Laura Videla, Isabel Barroeta, Laura Del Hoyo Soriano, Bessy Benejam, Susana Fernández, Aida Sanjuan Hernandez, Sandra Giménez, Daniel Alcolea, Olivia Belbin, Alberto Lleó, María Carmona-Iragui, Juan Fortea, and Alexandre Bejanin. Dinámica de las hiperintensidades de la sustancia blanca en adultos con síndrome de Down: reevaluando su etiología. 19/11/2025. LXXVII Reunión Anual de la Sociedad Española de Neurología, Sevilla, Spain.

- Alejandra O. Morcillo-Nieto, José Enrique Arriola-Infante, Maria Franquesa-Mullerat, Sara E. Zsadanyi, Lídia Vaqué-Alcázar, Mateus Rozalem-Aranha, José Allende, Zili Zhao, Javier Arranz, Íñigo Rodríguez-Baz, Lucia Maure-Blesa, Laura Videla, Isabel Barroeta, Laura Del Hoyo Soriano, Bessy Benejam, Susana Fernández, Aida Sanjuan Hernandez, Sandra Giménez, Daniel Alcolea, Olivia Belbin, Alberto Lleó, María Carmona-Iragui, Juan Fortea, and Alexandre Bejanin. PSMD as a Promising Biomarker for Early Identification of White Matter Integrity Changes in Down Syndrome. 23/05/2025. DSAD-ADAD International Conference, Barcelona, Spain. Awarded
- José Enrique Arriola-Infante, Alejandra O. Morcillo-Nieto (Presenter), Sara E. Zsadanyi, María Franquesa-Mullerat, Lidia Vaqué-Alcázar, Mateus Rozalem Aranha, Javier Arranz, Íñigo Rodriguez-Baz, Lucia Maure Blesa, Laura Videla, Isabel Barroeta, Laura Del Hoyo, Bessy Benejam, Susana Fernández, Aida Sanjuan Hernandez, Nuole Zhu, Jesus García-Castro, Sara Rubio-Guerra, Eleva Vera-Campuzano, Judit Selma-González, Sandra Giménez, Daniel Alcolea, Olivia Belbin, Valle Camacho, Alberto Lleó, María Carmona-Iragui, Juan Fortea, Alexandre Bejanin. Patrón de metabolismo cerebral en el continuum de la enfermedad de Alzheimer en el síndrome de Down. 19/11/2024. LXXVI Reunión Anual de la Sociedad Española de Neurología, Valencia, Spain. Awarded
- Alejandra O. Morcillo-Nieto, Benjamin J. Buehner, Sara E. Zsadanyi, Mateus Rozalem Aranha, José Enrique Arriola-Infante, Lidia Vaqué-Alcázar, María Franquesa-Mullerat, Javier Arranz, Íñigo Rodriguez-Baz, Lucia Maure Blesa, Laura Videla, Isabel Barroeta, Laura Del Hoyo, Bessy Benejam, Susana Fernández, Aida Sanjuan Hernandez, Nuria Bargalló, Sofía González-Ortiz, Sandra Giménez, Robin de Flores, Daniel Alcolea, Olivia Belbin, Alberto Lleó, Maria Carmona-Iragui, Juan Fortea, Alexandre Bejanin. Medial Temporal Lobe Volumes as Biomarkers for Early Alzheimer's Detection in in Down Syndrome. 11/04/2024. DSAD-ADAD International Conference, Barcelona, Spain.

Poster presentations

- Alejandra O. Morcillo-Nieto, Mateus Rozalem-Aranha, José Enrique Arriola-Infante, Maria Franquesa-Mullerat, Sara E. Zsadanyi, Lídia Vaqué-Alcázar, José Allende Parra, Zili Zhao, Javier Arranz, Íñigo Rodríguez-Baz, Lucia Maure-Blesa, Laura Videla, Isabel Barroeta, Laura Del Hoyo Soriano, Bessy

Benejam, Susana Fernández, Aida Sanjuan Hernandez, Sandra Giménez, Daniel Alcolea, Olivia Belbin, Alberto Lleó, María Carmona-Iragui, Juan Fortea, and Alexandre Bejanin. Longitudinal White Matter Hyperintensities in Down's Syndrome. 27/07/2025 - 31/07/2025. Alzheimer's Association International Conference (AAIC 2025) and preconference Alzheimer's Imaging Consortium (AIC). Toronto, Canada.

- Alejandra O. Morcillo-Nieto, Maria Franquesa-Mullerat, José Enrique Arriola-Infante, Sara E. Zsadanyi, Lídia Vaqué-Alcázar, Mateus Rozalem-Aranha, Javier Arranz, Íñigo Rodríguez-Baz, Lucia Maure-Blesa, Laura Videla, Isabel Barroeta, Laura Del Hoyo Soriano, Bessy Benejam, Susana Fernández, Aida Sanjuan Hernandez, Sandra Giménez, Daniel Alcolea, Olivia Belbin, Alberto Lleó, María Carmona-Iragui, Juan Fortea, and Alexandre Bejanin. Early Detection of White Matter Integrity Changes in Down Syndrome: The Promise of PSMD as a Sensitive Biomarker. 27/07/2025 - 31/07/2025. Alzheimer's Association International Conference (AAIC 2025) and preconference Alzheimer's Imaging Consortium (AIC). Toronto, Canada.
- Alejandra O. Morcillo-Nieto, Mateus Rozalem-Aranha, José Enrique Arriola-Infante, Maria Franquesa-Mullerat, Sara E. Zsadanyi, Lídia Vaqué-Alcázar, José Allende Parra, Zili Zhao, Javier Arranz, Íñigo Rodríguez-Baz, Lucia Maure-Blesa, Laura Videla, Isabel Barroeta, Laura Del Hoyo Soriano, Bessy Benejam, Susana Fernández, Aida Sanjuan Hernandez, Sandra Giménez, Daniel Alcolea, Olivia Belbin, Alberto Lleó, María Carmona-Iragui, Juan Fortea, and Alexandre Bejanin. Unraveling the Evolution of White Matter Hyperintensities Associated with Alzheimer's Disease in Down Syndrome. 23/05/2025. DSAD-ADAD International Conference. Barcelona, Spain.
- Alejandra O. Morcillo-Nieto, Benjamin J. Buehner, Sara E. Zsadanyi, Mateus Rozalem Aranha, José Enrique Arriola-Infante, Lidia Vaqué-Alcázar, Javier Arranz, Íñigo Rodriguez-Baz, Lucia Maure Blesa, Laura Videla, Isabel Barroeta, Laura Del Hoyo, Bessy Benejam, Susana Fernández, Aida Sanjuan Hernandez, Nuria Bargalló, Sofía González-Ortiz, Sandra Giménez, Robin deFlores, Daniel Alcolea, Olivia Belbin, Alberto Lleó, Maria Carmona-Iragui, Juan Fortea, Alexandre Bejanin - Medial Temporal Lobe Volumes in Down Syndrome Along the Alzheimer's Disease Continuum. 05/06/2024 - 08/06/2024. 5th International Conference of the Trisomy 21 Research Society (T21RS). Rome, Italy.

- Alejandra O. Morcillo-Nieto, Sara E. Zsadanyi, Víctor Montal, Mateus Rozalem Aranha, Jordi Pegueroles, Lídia Vaqué-Alcázar, Bessy Benejam, Laura Videla, Isabel Barroeta, Susana Fernandez, Sandra Giménez, Sofía González-Ortiz, Nuria Bargalló, Laia Ribas, Javier Arranz, Olivia Belbin, Daniel Alcolea,Rafael Blesa, Alberto Lleó, Maria Carmona-Iragui, Juan Fortea, Alexandre Bejanin. Longitudinal white matter hyperintensities in Down's syndrome. 16/7/2023-20/7/2023. Alzheimer's Association International Conference (AAIC 2023). Amsterdam, Netherlands.